COPPER(I) AND SILVER(I) COMPLEXES OF OLEFINS, ALKYNES, AND CYCLOPROPENES AND THEIR APPLICATIONS

by

ANURAG NOONIKARA POYIL

Presented to the Faculty of the Graduate School of

The University of Texas at Arlington in Partial Fulfillment

of the Requirements

for the degree of

DOCTOR OF PHILOSOPHY

THE UNIVERSITY OF TEXAS AT ARLINGTON

May 2022

To my mother and my father for their sacrifices to support my dreams

Acknowledgements

I would like to acknowledge and express my deepest appreciation to my supervising professor Dr. Rasika Dias. This dissertation would not have been possible without his constant support, invaluable advice, insightful discussions, endless patience, and financial support. I would also like to thank my dissertation committee, Dr. Carl Lovely and Dr. Kayunta Johnson-Winters for their indispensable suggestions and feedback.

I extend my sincere appreciation to Dr. Alejandro Bugarin for his support and motivation during the initial days of my graduate studies. I am extremely grateful to present and past members of the Dias group and past members of the Bugarin group for their help and support – Dr. Devaborniny Parasar, Dr. Monika Patterson, Adway Zacharias, Brandon Watson, Dr. Mukundam Vanga, Vo Phan, Deepika Karade, Quynh Le, Dr. Enrique Barragan, Olatunji Ojo, and Alena Denisenko. I am thankful to all my collaborators for their help and contribution to finishing my research works. I would like to additionally thank the faculty members and staff of the Department of chemistry and Biochemistry. I would like to thank Dr. Brian Edwards for the technical support and for patiently teaching the NMR techniques. I am thankful to Jill Howard and Debbie Cooke for the administrative support and Beth Klimek for the stockroom support.

I would like to thank my undergraduate advisers, Dr. Subhajit Bandyopadhyay and Dr. Tarakranjan Gupta for their great guidance and motivation. I am thankful to my friends who enriched my life with their gracious presence- Sidharth Thankappan, Limi Thomas, Akhil Das, Amal Thomas, Bahir AbdhulGhani, Sethu Bhattathiri, Jacob Cyril, and Roshan George.

Finally, I am eternally grateful to my family. I express my sincere gratitude to my girlfriend, Athma Praveen, my parents Chandran Noonikara Poyil and Usha Vadakkumpat, my sister, Anusha Noonikara Poyil, brother-in-Law, Praveen Das, nephew, Anirudh, niece, Aradhya for their sacrifices to support me, and my dreams with unconditional love, never-ending emotional support, and consistent encouragement. I am forever grateful and lucky to be with such a wonderful family.

April 14, 2022

Abstract

COPPER(I) AND SILVER(I) COMPLEXES OF OLEFINS, ALKYNES, AND CYCLOPROPENES AND THEIR APPLICATIONS

Anurag Noonikara Poyil, Ph.D.

The University of Texas at Arlington, 2022

Supervising Professor: H. V. Rasika Dias

Poly(pyrazolyl)borates are very popular ligands in organometallic chemistry due to their attractive properties. It is easy to modify the steric and electronic properties of these ligands by changing the pyrazolyl substituents. Fluorinated tris(pyrazolyl)borates are used to stabilize many reactive metal ions. The metal complexes of them are used for multiple applications. These ligands are extensively used to isolate and stabilize many coinage metal complexes (Cu, Ag, and Au). We have synthesized comparably less explored fluorinated bis(pyrazolyl)borate ligands and utilized them to isolate several π-ligands (olefin, alkyne, and cyclopropene) complexes of copper(I) and silver(I).

Chapter 2 of this research work focuses on ethylene/ethane separation technology and the development of novel pentafluorosulfanyl supported bis(pyrazolyl)borate ligands. The copper(I) bis(pyrazolyl)borate trimer, $\{[H_2B(3,5\text{-}(CF_3)_2Pz)_2]Cu\}_3$, reversibly coordinate ethylene and forms $[H_2B(3,5\text{-}(CF_3)_2Pz)_2]Cu(C_2H_4)$. We have studied the chemistry of this transformation both in the solution and solid phase and also how efficiently it can separate ethylene from a mixture of ethylene and ethane. The second part

of this chapter focuses on the development of a novel pentafluorosulfanyl supported bis(pyrazolyl)borate ligand, $[Ph_2B(3\text{-}(SF_5))Pz)_2]^-$. We have synthesized copper(I) and silver(I) ethylene complexes using this ligand and compared it to the metal complexes of the CF_3 analog $[Ph_2B(3\text{-}(CF_3)Pz)_2]^-$ in a structure and bonding study and also as a catalyst in cyclopropanation reactions.

Chapter 3 discusses the synthesis and characterization of several copper(I) and silver(I) alkyne complexes including the rare complexes with acetylene. We have compared the ligand and metal effect on acetylene complexes using various characterization methods such as NMR, Raman, XRD, etc. We have also performed computational studies to support our experimental results. We have utilized one of our copper(I) complexes as a catalyst for the azide-alkyne cycloaddition reaction of various alkynes including acetylene.

Chapter 4 describes the synthesis and isolation of novel copper(I) bis(pyrazolyl)borate cyclopropene complexes. These cyclopropane complexes are the first examples of copper(I) η^2-cyclopropene complexes. The studies show how the backbonding due to metal coordination effects ring angle and bond lengths of highly strained cyclopropenes. We have shown a copper(I) catalyzed method to synthesize cyclopropenes from alkynes using ethyl diazoacetate.

Table of Contents

List of Figures

List of Tables

Chapter 1

Introduction

1.1 Poly(pyrazolyl)borates

Poly(pyrazolyl)borates are a very useful set of ligands known in coordination chemistry since their introduction in 1966 by S. Trofimenko.[1] It has been reported that di-, tri-, tetra(pyrazolyl)borates can be obtained by heating an alkali metal borohydride with pyrazole by maintaining the temperature around 110, 180, and >210 ºC, respectively. The bidentate $[R_2B(Pz)_2]^-$ and tridentate $[RB(Pz)_3]^-$ have been compared to β-diketonates and cyclopentadienyl ligands, respectively. This comparison is based on properties such as the same electron donation, coordination sites occupied, and charge, but they have different symmetry, substitutable position, etc. A boat-shaped six-membered ring ($RR'B(\mu\text{-}Pz)_2M$) is the fundamental feature in all poly(pyrazolyl)borates (figure 1.1). The poly(pyrazolyl)borates are known as 'scorponates' ever since Trofimenko named them because of the closest analogy in features; "this creature grabs its prey with two identical claws (Pz_2) and then may proceed to sting it with the sharp point of the curving tail (pseudoaxial R')" (figure 1.1).[2]

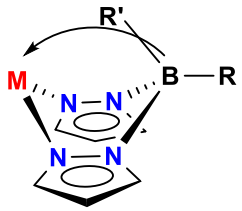

Figure 1. 1. A representation of poly(pyrazolyl)borate

These scoripionate ligands can be further categorized into "homoscorpionates" where the pseudoaxial R' group is Pz and "heteroscopionates" where R' is anything but Pz but it can be a different substituted Pz group and the latter being still an underdeveloped set of ligands even though there are many substitutions possible.

The popularity of poly(pyrazolyl)borates is mainly because of the easiness of tuning electronic and steric properties by varying the number and nature of the substituents on the pyrazole. The 'first-generation' tris(pyrazolyl)borates falls in the category $[HB(Pz)_3]^-$ and $[HB(3,5\text{-}(R',R'')Pz)_3]^-$ (Figure 1.2). They often tend to form octahedral ML_2 complexes with first-row transition metals. The 'second-generation' tris(pyrazolyl)borates were introduced in 1986 to overcome this problem (Figure 1.3).[3] $[HB(3\text{-}(R)Pz)_3]^-$ with bulky alkyl (eg: *t*-Bu) or aryl (eg: Ph) group as R solves the issue of bis-chelate formation and dimerization and tends to form ML(X) complexes. The 'third-generation' poly(pyrazolyl)borates are the ligands specifically functionalized at the non-coordinating 'back' position of the boron (Figure 1.4). These types of ligands are used to make multi-metallic complexes.[4]

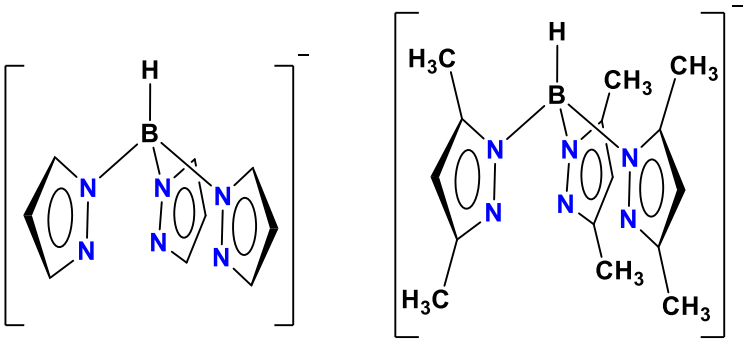

Figure 1. 2. Examples of first-generation homoscorpionates

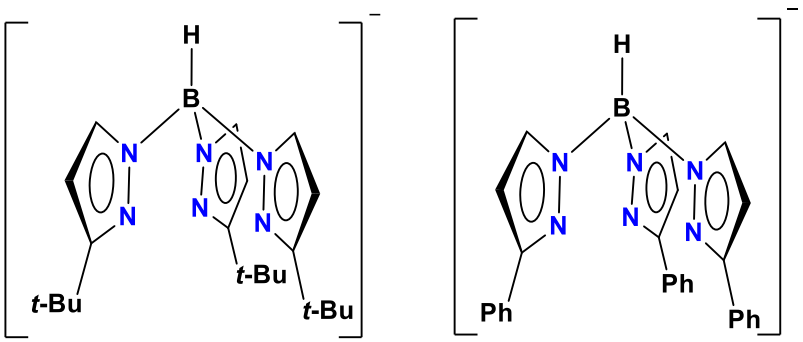

Figure 1. 3. Examples of second-generation homoscorpionates

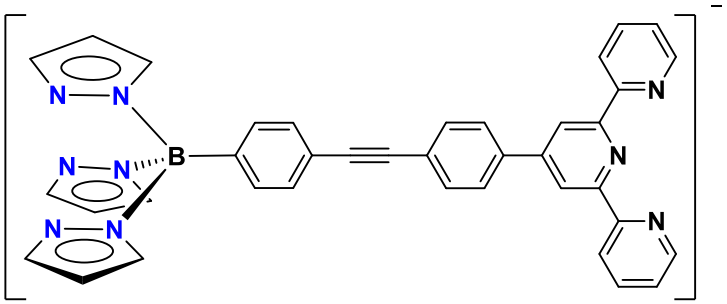

Figure 1. 4. Example of third generation homoscorpionates

1.2 Applications of Poly(pyrazolyl)borates

Trofimenko explored the coordination chemistry of poly(pyrazolyl)borates with first-row transition metal salts and had his hands-on making more than 100 of those. He preferred to make those while others explored the chemistry that can be done with them, he said, "I consider myself a gunsmith rather than a hunter".[5] The poly(pyrazolyl)borates are used for multiple applications such as catalysis, enzyme modeling, metal deposition, metal extraction, etc.[6, 7]

One of the initial uses of these ligands was in bioinorganic chemistry for modeling studies, particularly for enzymes in which metal is coordinated to three imidazolyl nitrogen atoms from the amino acid histidine.[6]

Tris(pyrazolyl)borates were used for this purpose. [HB(3,5-$(CH_3)_2Pz)_3$]Cu(C_2H_4) (**1**) was used to demonstrate the ethylene binding site in plants that contains a copper(I) cofactor.[8] There are several other examples of modeling studies with various metals such as Zn, V, Mo, Mn, Fe, Ni, W, Mo, etc.[6]

Poly(pyrazolyl)borate metal complexes are an excellent catalyst for several important chemical transformations. [HB(3,5-$(CF_3)_2Pz)_3$]Cu(C_2H_4) (**2**) catalyzes aziridination of a variety of olefins into *N*-tosyl aziridines with *N*-tosyl phenyliodinane.[9] [HB(3,4,5-$(Br)_3Pz)_3$]Cu(NCMe) (**3**) is a good catalyst for C-H bond activation of alkanes using ethyl diazoacetate.[10] It has been shown that cyclopropanation of various olefins using ethyl diazoacetate using different copper(I) tris(pyrazolyl)borates. The copper(I) complex of the bulky tris(pyrazolyl)borate, [HB(3,5-$(Mes)_2Pz)_3$]$^-$ (**4**) gives a higher cis isomer yield due to the bulkiness caused by mesityl groups.[11] [MeB(3-$(Mes)Pz)_3$]CuCl (**5**) is an excellent catalyst to polymerize aniline dimer to emeraldine base. There are several other tris(pyrazolyl)borate metal catalysts for polymerization, oxidation, C-H activation, etc.[6, 7]

1.3 Fluorinated Poly(pyrazolyl)borates

Fluorinated tris(pyrazolyl)borates can be synthesized using an alkali metal borohydride and a little more than three equivalent of fluorinated pyrazole were used to make hydridotris(pyrazolyl)borates (Figure 1.5).[12] The B-H free tris(pyrazolyl)borates are also reported which were synthesized using alkyl or aryl borohydride (RBH_3Li) and fluorinated pyrazole (Figure 1.6). The synthesis of fluorinated tris(pyrazolyl)borates requires a lower temperature compared to

the non-fluorinated analogs since the acidic fluorinated pyrazole reacts readily with borohydride salts.

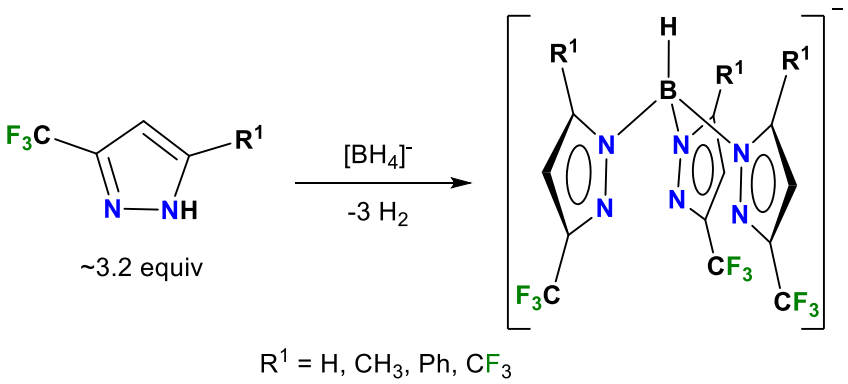

Figure 1. 5. Synthesis of fluorinated hydridotris(pyrazolyl)borates.

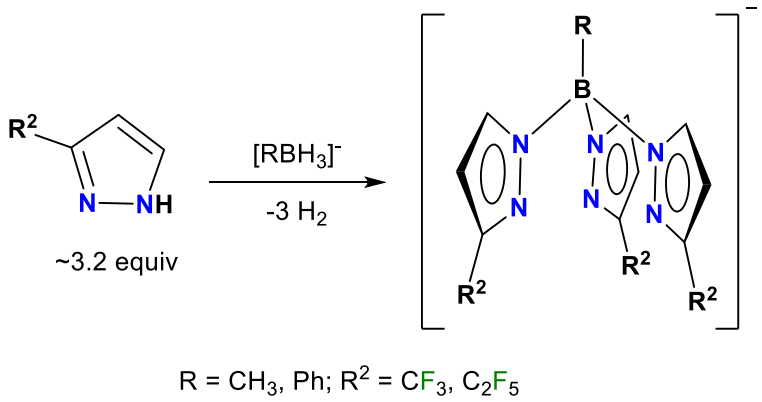

Figure 1. 6. Synthesis of fluorinated B-H substituted tris(pyrazolyl)borates.

The fluorinated bis(pyrazolyl)borates (heteroscorpionates) are less explored compared to fluorinated tris(pyrazolyl)borates (homoscorpionates). The bis(pyrazolyl)borates $[H_2B(3,5\text{-}(CF_3)_2Pz)_2]^-$ and $[H_2B(3\text{-}(CF_3)_2Pz)_2]^-$ were synthesized from borohydride salt and respective pyrazole (~2.0 equiv.) at 110-120 ºC in toluene (Figure 1.7).[13, 14]The B-H substituted fluorinated

bis(pyrazolyl)borates were unknown to the best of our knowledge until we reported it recently (more details in chapter 2.2).

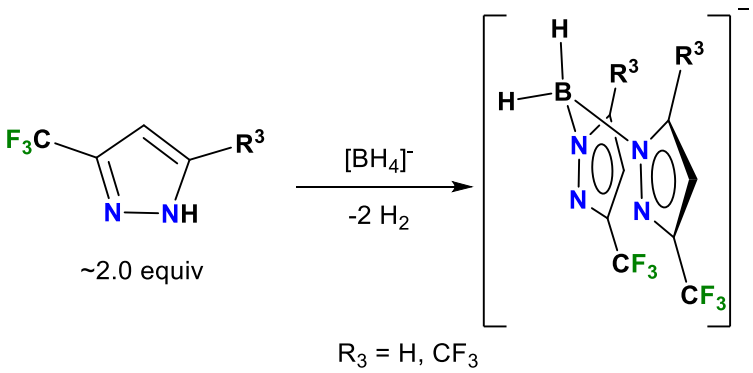

Figure 1. 7. Synthesis of fluorinated bis(pyrazolyl)borates.

Poly(pyrazolyl)borates having fluorocarbon substituents are sterically similar but electronically very different compared to their hydrocarbon counterparts. The cone angle data provide information about steric properties of tris(pyrazolyl)borates, and it is important to note that cone angles depend not only on the ligand but also on the metal-N bond length. Tris(pyrazolyl)borates bearing bulkier substitutes tend to have larger cone angles (Figure 1.8). A study on estimated/calculated cone angles of thallium[6] and tri(carbonyl)rhenium[15] tris(pyrazolyl)borates shows that the steric effects of $[HB(3,5\text{-}(CF_3)_2Pz)_3]^-$ are similar to $[HB(3,5\text{-}(CH_3)_2Pz)_3]^-$ rather than $[HB(3,5\text{-}(i\text{-}Pr)_2Pz)_3]^-$ although the CF_3 group is closer in size to *i*-Pr group.[16]

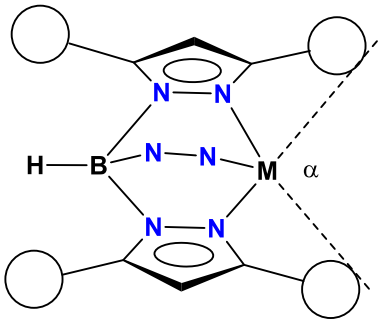

Figure 1. 8. Side view of Tris(pyrazolyl)borate showing cone angle = (360-α).

However, electronically $[HB(3,5\text{-}(CF_3)_2Pz)_3]^-$ and $[HB(3,5\text{-}(CH_3)_2Pz)_3]^-$ are very different. The IR stretching frequency of the carbonyl group (ν_{CO}) in metal-carbonyl complexes is a convenient way to understand the electronic properties of ligands. For instance, $[HB(3,5\text{-}(CF_3)_2Pz)_3]Cu(CO)$ (**6**)[17] shows carbonyl stretching at 2137 cm^{-1} whereas in its hydrocarbon version, $[HB(3,5\text{-}(CH_3)_2Pz)_3]Cu(CO)$ (**7**),[18] ν_{CO} appears at 2066 cm^{-1}. The IR stretching frequency of free CO is at 2143 cm^{1}. The small reduction in IR stretching frequency in fluorinated complex relative to free CO shows that it is a weak donor compared to the non-fluorinated complex. The difference in IR stretching frequency of fluorinated and non-fluorinated is large (77 cm^{-1}), which implies that they are significantly different electronically. The copper complexes of $[HB(3,5\text{-}(CF_3)_2Pz)_3]^-$ also show relatively high oxidation potentials, therefore harder to oxidize.[19]

Fluorinated hydridotris(pyrazolyl)borates and dihydridobis(pyrazolyl)borates have less reducing B-H groups and have weakly donating nitrogen sites.[20] These characteristics help to isolate and stabilize many reactive metals complexes which would not have been achieved with nonfluorinated ligands. For example, $[HB(3,5\text{-}(CF_3)_2Pz)_3]Au(C_2H_4)$ (**8**)[21] is one of the first reported thermally stable

neutral gold(I)-ethylene complexes. The fluorinated poly(pyrazolyl)borates confer air and thermal stability to the metal complexes. [HB(3,5-$(CH_3)_2Pz)_3$]Cu(C_2H_4) (**1**)[8] is an air-sensitive copper(I) complex where as its fluorinated counterpart [HB(3,5-$(CF_3)_2Pz)_3$]Cu(C_2H_4) (**2**)[9] is an air-stable complex and can be handled open to air for a long time without any decomposition. Some of the metal complexes supported by fluorinated poly(pyrazolyl)borates are better catalysts than non-fluorinated analogs. For instance, [HB(3,5-$(CF_3)_2Pz)_3$]Ag(THF) (**9**) catalyzed the reaction of ethyl diazoacetate with chloroform to give ethyl 2,3,3-trichloropropanoate in 60% yield whereas the non-fluorinated analog, [HB(3,5-$(CH_3)_2Pz)_3$]Ag(THF) (**10**) remained inactive (Figure 1.9).[22] Majority of the copper(I) catalysts supported by non-fluorinated poly(pyrazolyl)borates are air-sensitive and either difficult to prepare or must be prepared in situ whereas the fluorinated poly(pyrazolyl)borate copper(I) catalysts are stable and easy to handle.[9, 23]

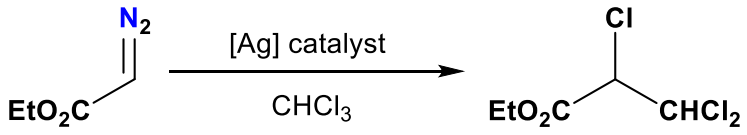

Sl. No.	Catalyst	yield
1	[HB(3,5-$(CF_3)Pz)_3$]Ag(THF) (**9**)	60%
2	[HB(3,5-$(CH_3)Pz)_3$]Ag(THF) (**10**)	0%

Figure 1. 9. Activation of C-Cl bond using Ag catalyst

Our group (Dias group) has significantly contributed to the synthesis and applications of coinage metal (Cu, Ag, Au) complexes, especially supported by

the fluorinated poly(pyrazolyl)borates.[20, 24, 25] For example, the structurally authenticated ethylene adducts of copper, [HB(3,5-$(CF_3)_2Pz)_3$]Cu(C_2H_4) (**1**),[9] silver, [HB(3,5-$(CF_3)_2Pz)_3$]Ag(C_2H_4) (**11**),[26] gold, [HB(3,5-$(CF_3)_2Pz)_3$]Au(C_2H_4) (**8**)[21] involve use of fluorinated tris(pyrazolyl)borates.

The π ligands are important in coordination chemistry. Since the discovery of Zeise's platinum-ethylene complex K[$PtCl_3(C_2H_4)$].H_2O (**12**) in 1827,[27] numerous attempts were made to capture and understand the chemistry of π complexes of coinage metal (Cu, Ag, Au) ions. The π-ligands coordinate to the metal center in a manner consistent with the Dewar-Chatt-Duncanson model,[28, 29] Figure 1.6, illustrated for an olefin which states that the olefin donates electron density from its filled π-orbitals to empty d-orbitals of metal and the metal donates electrons from its filled d-orbitals into the empty π^*-orbital of olefin. This causes a reduction in C-C bond order, leading to an elongated C-C bond distance, hence lowering its vibrational frequency.

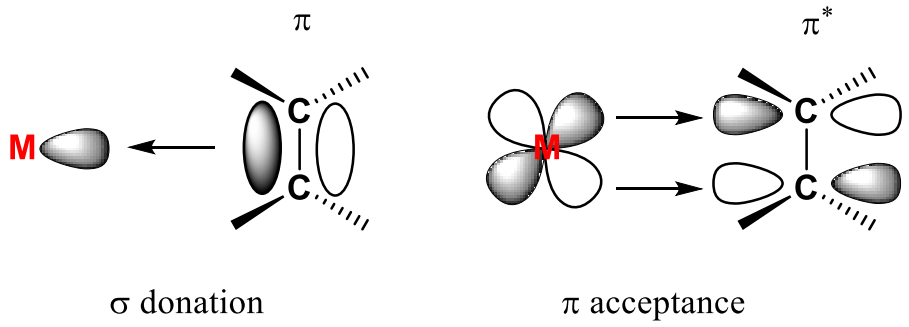

Figure 1. 10. Dewar-Chatt-Duncanson Model

Copper and silver salts are involved in many chemical processes of olefines and alkynes. For example, ethylene is an important plant hormone and the ethylene receptor site in the plant is a copper center.[30] Copper is involved in

many olefin transformations such as cyclopropanation,[31, 32, 33] aziridinations,[34] etc. Copper and silver salts are used for olefin-paraffin separations. Partial oxidation of ethylene to ethylene oxide is a major industrial process and silver is the catalyst of choice.[35-37] Copper and silver salts are also used as a catalyst for alkyne transformations such as cyclopropenation,[38, 39]triazole synthesis,[40] coupling reactions (cross coupling and glacier coupling),[41, 42] carboxylation,[42], etc. Silver salts with Pd are used for hydrogenation of acetylene.[43]

Considering all the advantages of fluorinated poly(pyrazolates)borates, we set to expand the work done on coinage metal (Cu and Ag) complexes of π-ligands. As mentioned earlier, if Trofimenko was a gunsmith, we have worked on making new varieties of guns by developing new fluorinated bis(pyrazolyl)borates which are underdeveloped compared to tris(pyrazolyl)borates and using them to hunt various preys which include ethylene, acetylene, and cyclopropene. In chapter 2, the synthesis of $[H_2B(3,5\text{-}(CF_3)_2Pz)_2]Cu(C_2H_4)$ (**13**) and its utility in ethylene-ethane separation is discussed. This is the first example of a poly(pyrazolyl)borate used for olefin-paraffin separation. The second part of this chapter contains the synthesis of novel bis(pyrazolyl)borate, $[Ph_2B(3\text{-}(SF_5)_2Pz)_2]^-$, and the use of this ligand to make Cu(I) and Ag(I) ethylene complexes. The third chapter contains the synthesis of several copper(I) and silver(I) complexes of acetylene supported by fluorinated bis and tris(pyrazolyl)borates and non-fluorinated bis(pyrazolyl)methane. We have discussed the ligand and metal effects of metal-acetylene bonding. We have also shown a copper(I) catalyzed azide-alkyne cycloaddition method to synthesize several triazoles from various alkynes including acetylene. We have shown the synthesis of new copper-

cyclopropene complexes in chapter 4. Copper-cyclopropene complexes are not known until our recent report even though copper plays different roles in cyclopropene chemistry. We are also showing a copper(I) catalyzed cylopropenation of various alkynes using ethyl diazoacetate. Further details about this research work can be found in the related chapters herein.

Chapter 2

Ethylene Complexes of Copper(I) and Silver(I) and Their Applications

Part 2.1 A Molecular Compound for Highly Selective Purification of Ethylene

Anurag Noonikara Poyil, Hui Cui, Andrey Yakovenko, Peter W. Stephens, Rui-Biao Lin, Bin Wang, Banglin Chen, and H. V. Rasika Dias

(Part of this work has been published in *Angew. Chem. Int. Ed.* **2021**, *60*, 1-6)[44]

2.1.1 Abstract

Purification of C_2H_4 from an C_2H_4/C_2H_6 mixture is one of the most challenging separation processes, which is achieved mainly through energy-intensive, cryogenic distillation in industry. Sustainable, non-distillation methods are highly desired as alternatives. We discovered that the fluorinated bis(pyrazolyl)borate ligand supported copper(I) complex $\{[H_2B(3,5\text{-}(CF_3)_2Pz)_2]Cu\}_3$ has features very desirable in an olefin-paraffin separation material. It binds ethylene exclusively over ethane generating $[H_2B(3,5\text{-}(CF_3)_2Pz)_2]Cu(C_2H_4)$. This molecular compound exhibits extremely high and record IAST C_2H_4/C_2H_6 gas separation selectivity, affording high purity (> 99.5%) ethylene that can be readily desorbed from separation columns. *In-situ* PXRD provides a "live" picture of the reversible conversion between $[H_2B(3,5\text{-}(CF_3)_2Pz)_2]Cu(C_2H_4)$ and the ethylene free sorbent in the solid-state, driven by the presence or removal of C_2H_4. Molecular structures of trinuclear $\{[H_2B(3,5\text{-}(CF_3)_2Pz)_2]Cu\}_3$ and mononuclear $[H_2B(3,5\text{-}(CF_3)_2Pz)_2]Cu(C_2H_4)$ are also presented.

2.1.2 Introduction

Ethylene, the largest-volume organic product of the chemical industry, is produced mainly by the steam-cracking of petroleum feedstocks. This process results in a mixture of gaseous hydrocarbons that includes ethylene (C_2H_4) and ethane (C_2H_6). Industrial purification of ethylene from ethane is achieved by highly energy consuming, cryogenic distillation which requires distillation columns with over 100 trays operating at temperatures around -25 °C and

pressures >2000 kPa due to similarities in volatility.[45, 46] There have been extensive research endeavours to pursue materials for the cost- and energy-efficient separation of ethylene purification over the past half-decade but without significant progress. The emergence of porous metal-organic framework materials (MOFs) has primarily provided a promising option for this very challenging and immensely important industrial gas separations given the fact that the pores of MOFs can be readily tuned for the sieving separations and functionalized for the specific recognition of one gas molecule over another one.[47, 48] In fact, we and other groups have successfully targeted several high-performance MOF materials for the ethylene purification over the past several years.[49-56] Here we describe the use of a molecular compound based on copper and a popular ligand class very effectively and repeatedly to provide high-purity ethylene from ethylene-ethane mixtures.

Ethylene is also a vital plant hormone with many roles in growth and development including seed germination, fruit ripening, and senescence.[57] Studies on ethylene receptor ETR1 indicate that copper is the cofactor in this protein, which binds ethylene quite tightly (K_d = 2.4 x 10^{-9} M and a half-life for ethylene dissociation of 12.5 h).[30, 58, 59] Poly(pyrazolyl)borates, often referred to as scorpionates,[60] are a useful family of ligands for many applications including modelling ethylene receptor site of plants and obtaining isolable copper-ethylene complexes such as the tris(pyrazolyl)borate [HB(3,5-$(CH_3)_2Pz)_3$]Cu(C_2H_4) (**1**).[8, 24] In contrast to most copper(I) ethylene complexes which are quite air sensitive and labile,[61, 62] the fluorinated analog, [HB(3,5-$(CF_3)_2Pz)_3$]Cu(C_2H_4) (**2**) is a thermally stable solid and quite resistant to O_2, and the loss of coordinated ethylene.[9]

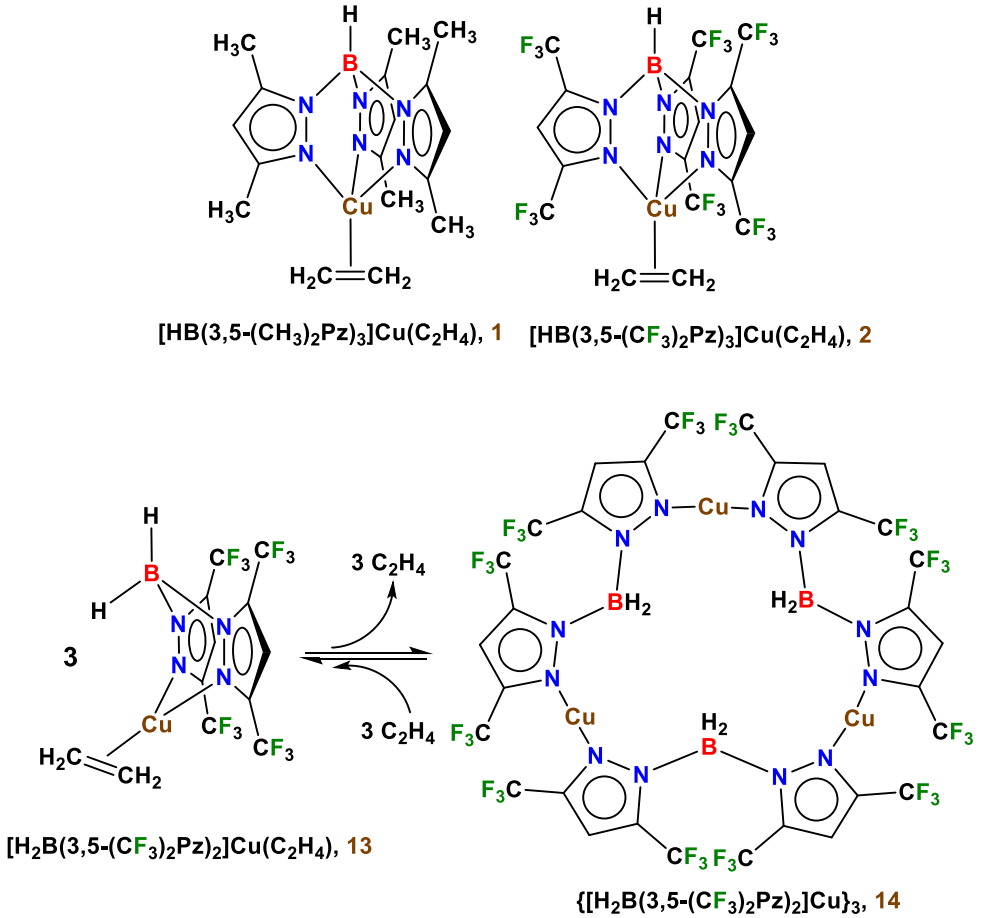

Figure 2.1. 1. Copper(I) ethylene complexes [HB(3,5-(CH$_3$)2Pz)$_3$]Cu(C$_2$H$_4$) (**1**) and [HB(3,5-(CF$_3$)$_2$Pz)$_3$]Cu(C$_2$H$_4$) (**2**) supported by scorpionates, as well as reversible structural rearrangement of [H$_2$B(3,5-(CF$_3$)$_2$Pz)$_2$]Cu(C$_2$H$_4$) (**13**) and {[H$_2$B(3,5-(CF$_3$)$_2$Pz)$_2$]Cu}$_3$ (**14**) driven by C$_2$H$_4$ removal and sorption in solution.

Considering the current interest in non-porous materials that can facilitate ethylene-ethane separation without the need for cryogenic distillation,[63-65] and inspired by the copper-based ethylene receptor in plants, we set out to develop molecules that *reversibly bind ethylene* using scorpionates. Although the tris(pyrazolyl)borate [HB(3,5-(CF$_3$)$_2$Pz)$_3$]Cu(C$_2$H$_4$) (**2**) is too inert for this purpose, we discovered that the fluorinated bis(pyrazolyl)borate [H$_2$B(3,5-

$(CF_3)_2Pz)_2]Cu(C_2H_4)$ (**13**) (based on a ligand that is missing a pyrazolyl arm from **2**, Figure 2.1.1) has exceptional features for effective ethylene-ethane separation.

2.1.3 Results and Discussions

Our work that led to this discovery started with solution studies of copper(I) scorpionates. Treatment of $[H_2B(3,5\text{-}(CF_3)_2Pz)_2]Cu(NCMe)$ (**15**)[66] with ethylene in dichloromethane at room temperature led to the displacement of acetonitrile ligand from copper and the formation of copper(I) ethylene complex $[H_2B(3,5\text{-}(CF_3)_2Pz)_2]Cu(C_2H_4)$ (**13**) in 92% isolated yield (Figure 2.1.2). It is a colorless, thermally stable solid that can be handled in air for hours without decomposition. The ethylene protons of **13** in the ^1H NMR spectrum appear at δ 4.69 ppm. This points to an intermediate level of olefinic proton shielding relative to those of **1** (δ 4.41 ppm) and **2** (δ 4.96 ppm). The presence of additional ethylene leads to separate broad signals of free and coordinated ethylene indicating associative olefin exchange. In contrast, coordinatively saturated complex **2** does not exchange with free ethylene at room temperature. The $^{13}C\{^1H\}$ NMR spectrum of $[H_2B(3,5\text{-}(CF_3)_2Pz)_2]Cu(C_2H_4)$ (**13**) in $CDCl_3$ shows a peak at δ 86.6 ppm corresponding to the carbons of the copper bound ethylene moiety, which is an upfield shift (of 36.5 ppm) compared to the corresponding resonance of the free C_2H_4, δ 123.1 ppm. The $\bar{\upsilon}$(C=C) of solid **13** was observed at 1539 cm^{-1} in the Raman spectrum. For comparison, free ethylene exhibits the C=C stretch coupled with the CH_2 scissoring vibrations at 1623 cm^{-1}.[67] Molecular structure of **13** was unambiguously established by single-crystal X-ray diffraction (Figure 2.1.3). It is a three-coordinate copper

complex with an η^2-bound C_2H_4 moiety. The bis(pyrazolyl)borate ligand adopts the familiar boat conformation.

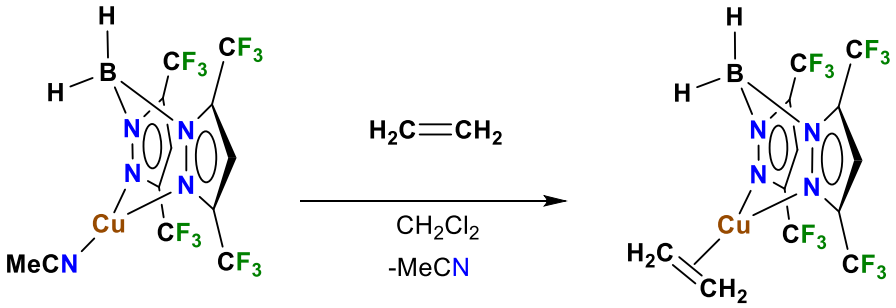

Figure 2.1. 2. Synthesis of $[H_2B(3,5\text{-}(CF_3)_2Pz)_2]Cu(C_2H_4)$ (**13**)

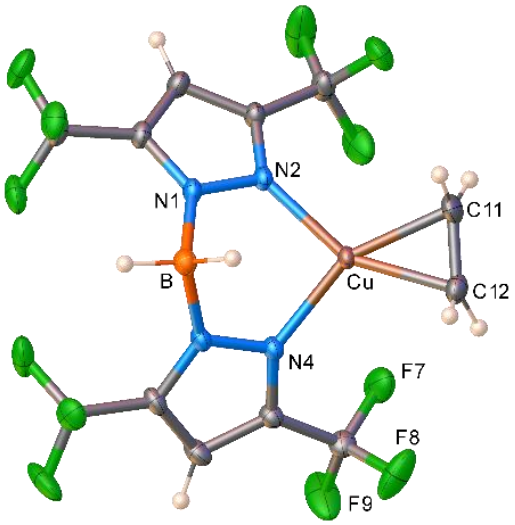

Figure 2.1. 3. Molecular structures of $[H_2B(3,5\text{-}(CF_3)_2Pz)_2]Cu(C_2H_4)$ (**13**). Selected bond distances (Å) and angles (°) for $[H_2B(3,5\text{-}(CF_3)_2Pz)_2]Cu(C_2H_4)$: Cu-N2 1.9873(13), Cu-N4 1.9885(12), Cu-C11 2.0184(16), Cu-C12 2.0182(16), C11-C12 1.360(3), Cu•••B 2.9823(19), N2-Cu-N4 93.28(5), C12-Cu-C11 39.38(7).

Notably, it is possible to remove the coordinated C_2H_4 from solid **13** using reduced pressure with mild heat (~40 °C) or by refluxing a solution of **13** in

hexanes. The resulting ethylene-free product, which crystallizes as {[H_2B(3,5-$(CF_3)_2Pz)_2$]Cu}$_3$ (**14**) in hexane, converts readily back to **3** upon treatment with C_2H_4 (1 atm) in solution or solid state as confirmed by NMR spectroscopy (Figure 2.1.1). The molecular structure of {[H_2B(3,5-$(CF_3)_2Pz)_2$]Cu}$_3$ (**14**) was established by X-ray crystallography (Figure 2.1.4). It is a quite interesting, trinuclear species with a metallacrown (18-MC-3) structure,[68] featuring bridging bis(pyrazolyl)borates. We are unaware of any such structures involving bis(pyrazolyl)borate ligands.[69] Compound {[H_2B(3,5-$(CF_3)_2Pz)_2$]Cu}$_3$ (**14**) sits on a two-fold rotation axis. Two-coordinate copper sites adopt a linear geometry.

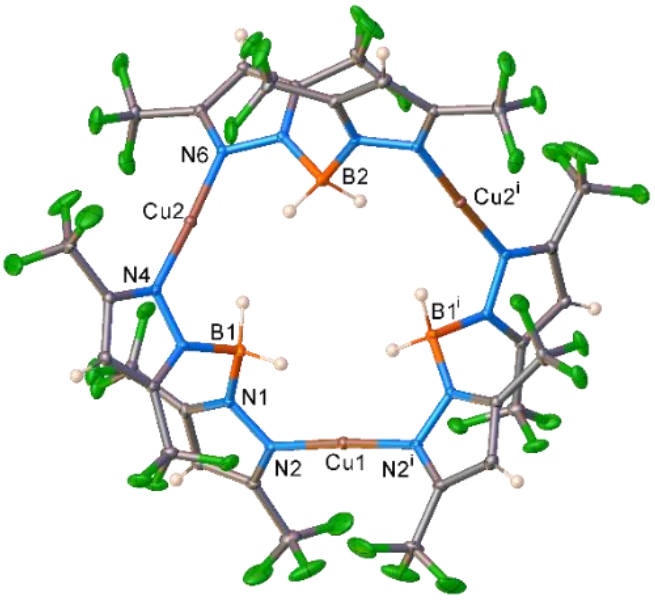

Figure 2.1. 4. Molecular structures of {[H_2B(3,5-$(CF_3)_2Pz)_2$]Cu}$_3$ (**14**). Selected bond distances (Å) and angles (°) for {[H_2B(3,5-$(CF_3)_2Pz)_2$]Cu}$_3$: Cu1-N2 1.8900(17), Cu1-N2^i 1.8900(17), Cu2-N4 1.8955(17), Cu2-N6 1.8942(17); N2-Cu1-N2^i 176.32(10), N6-Cu2-N4 177.46(7), Cu1•••B2 5.767(3), Cu1•••Cu2 5.8570(6); Cu2•••Cu2^i 5.8836(6).

Remarkably, the ethylene-driven transformation of copper(I) sorbent to mononuclear $[H_2B(3,5\text{-}(CF_3)_2Pz)_2]Cu(C_2H_4)$ also occurs in dense crystalline materials in the *solid-state*. To confirm this, we performed *in-situ* PXRD measurements at 17-BM beamline at the Advanced Photon Source, Argonne National Laboratory. It is possible to remove ethylene from $[H_2B(3,5\text{-}(CF_3)_2Pz)_2]Cu(C_2H_4)$ in a flow of helium under gentle heating, and generate the ethylene free copper sorbent (Figure 2.1.5) consistent with the observations noted above and the isotherm work noted below. This material under an ethylene flow at 100 kPa (1 bar) and 295 K, converts almost instantly to ethylene complex $[H_2B(3,5\text{-}(CF_3)_2Pz)_2]Cu(C_2H_4)$ as evident from *in-situ* PXRD (Figure 2.1.5).

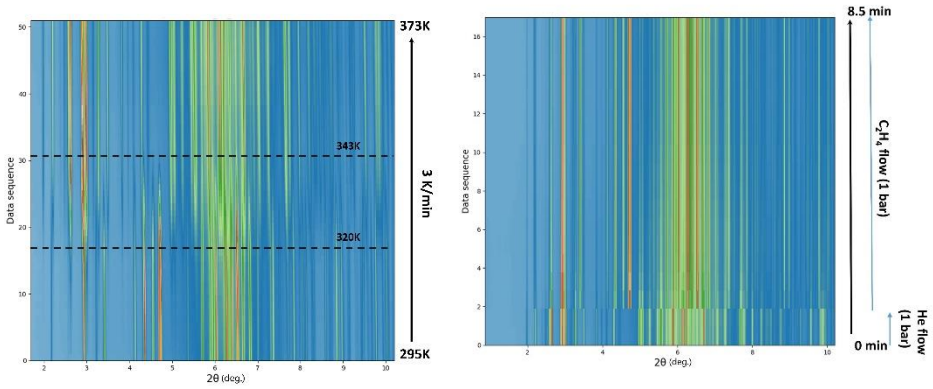

Figure 2.1. 5. Left side image: Top view of the powder diffraction patterns as $[H_2B(3,5\text{-}(CF_3)_2Pz)_2]Cu(C_2H_4)$ (**13**) converts to the ethylene free sorbent under slow heating and a He flow. The bottom section of the figure shows the powder diffraction pattern of pure $[H_2B(3,5\text{-}(CF_3)_2Pz)_2]Cu(C_2H_4)$. The top section of the figure shows the powder diffraction pattern for the ethylene free copper complex. Right side image: Top view of the powder diffraction patterns for the ethylene loading experiment of the in-situ generated sorbent. This shows the

rapid conversion to the $[H_2B(3,5\text{-}(CF_3)_2Pz)_2]Cu(C_2H_4)$ complex as soon as ethylene was introduced.

In addition to the quite interesting fundamental chemistry described above, we discovered that this system can be utilized very effectively, and repeatedly (i.e., recyclable) for the ethylene-ethane separation. To evaluate the adsorptive separation of C_2H_4 and C_2H_6 on $\{[H_2B(3,5\text{-}(CF_3)_2Pz)_2]Cu\}_3$, single-component adsorption isotherms of the two gases were collected at 298 K. It was shown that the adsorption isotherm for C_2H_4 on $\{[H_2B(3,5\text{-}(CF_3)_2Pz)_2]Cu\}_3$ exhibited a very steep slope at relatively low pressure, indicating a strong affinity of $\{[H_2B(3,5\text{-}(CF_3)_2Pz)_2]Cu\}_3$ towards C_2H_4 molecules (Figures 2.1.6a). At 298 K and 100 kPa (1 bar), the C_2H_4 uptake by $\{[H_2B(3,5\text{-}(CF_3)_2Pz)_2]Cu\}_3$ reaches 39.4 $cm^3\ g^{-1}$ (71.2 $cm^3\ cm^{-3}$, 1.8 mmol g^{-1}, 33 mmol cm^{-3}; ~87% conversion based on available copper sites), which is slightly lower than those of the top-performing MOF UTSA-280 (2.5 mmol g^{-1}, 3.9 mmol cm^{-3});[56] in contrast, $\{[H_2B(3,5\text{-}(CF_3)_2Pz)_2]Cu\}_3$ adsorbs a negligible amount of C_2H_6 (0.8 $cm^3\ g^{-1}$) under the same conditions. From the measured isotherms, a *record high* C_2H_4/C_2H_6 ideal absorbed solution theory (IAST) selectivity at 298 K and 100 kPa, exceeding 1.7×10^7, can be estimated. The Cu(I) sites in $\{[H_2B(3,5\text{-}(CF_3)_2Pz)_2]Cu\}_3$ exclusively bind ethylene over ethane; while those reported porous materials simultaneously adsorb both ethylene and ethane through the pores that have a certain degree of sieving effects, thus the IAST C_2H_4/C_2H_6 separation selectivity is significantly higher than those reported,[56] FeMOF-74 (13.6),[70] NOTT-300 (48.7),[51] PAF-1-SO_3Ag (27),[52] CuI@UiO-66-$(COOH)_2$ (80.8),[71] Co-gallate (52),[72] HOF-4a (14).[73] A comparison with the best reported porous material UTSA-280 (> 10000)[56] is shown in Figure 2.1.6b.

In a typical ethylene production process based on the cracking of heavier hydrocarbon fractions followed by dehydrogenation reactions, the observed conversion yields are only around 50-60%.[74] Thus, the separation of C_2H_4 from the C_2H_4/C_2H_6 mixture is an essential process before further utilization. To evaluate the performance of $\{[H_2B(3,5\text{-}(CF_3)_2Pz)_2]Cu\}_3$ in an adsorptive dynamic separation process, breakthrough experiments were performed, in which an equimolar C_2H_4/C_2H_6 mixture flowed over a packed column of the activated $\{[H_2B(3,5\text{-}(CF_3)_2Pz)_2]Cu\}_3$ solid with a rate of 2 mL min^{-1} at 298 K (Figure 2.1.6c).

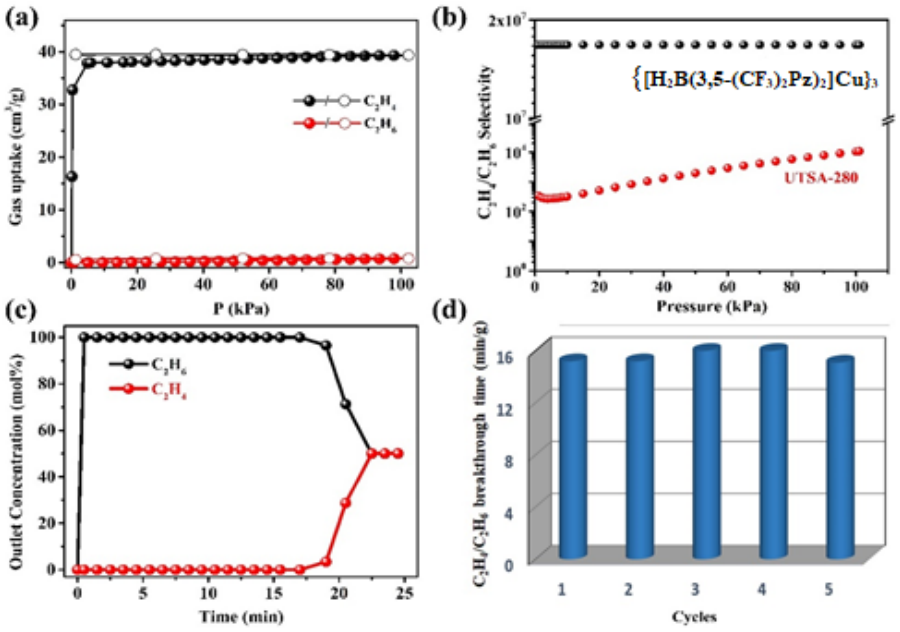

Figure 2.1. 6. (a) Single-component sorption isotherms of ethylene (black), ethane (red) at 298 K for $\{[H_2B(3,5\text{-}(CF_3)_2Pz)_2]Cu\}_3$; (b) Qualitative comparison of IAST adsorption selectivities of $\{[H_2B(3,5\text{-}(CF_3)_2Pz)_2]Cu\}_3$ with the benchmark porous material UTSA-280 for an equimolar ethylene/ethane mixture at 298 K; (c) breakthrough curves of $\{[H_2B(3,5\text{-}(CF_3)_2Pz)_2]Cu\}_3$ for an equimolar binary mixture of C_2H_4/C_2H_6 (50/50 v/v) at 298 K and 100 kPa (1

bar); (d) The recyclability of $\{[H_2B(3,5\text{-}(CF_3)_2Pz)_2]Cu\}_3$ in multiple breakthrough experiments under the same condition.

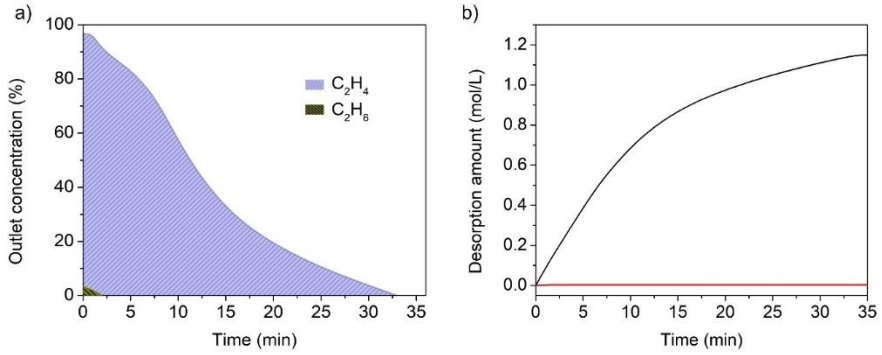

Figure 2.1. 7. a) Concentration curve of the desorbed C_2H_4 from during the regeneration process; b) desorption curve for an equimolar mixture of ethylene and ethane. Color scheme: black: ethylene; red: ethane.

As expected, a clean separation of the C_2H_4/C_2H_6 mixture was achieved: C_2H_6 was first to elute through the bed, and this outlet gas quickly reached pure ethane grade with no detectable C_2H_4, which then results in an elute of high concentration of C_2H_4 that was >99.5 % pure (Figure 2.1.6c), better than the benchmark C_2H_4-selective MOF UTSA-280 (99.2%).[56] Note that the latter is the highest ethylene purity ever reported thus far from the direct release of the breakthrough beds among any porous materials. The purity can be even higher up to the polymer-grade (>99.7%) C_2H_4 if helium purge was applied before generating C_2H_4.[49] The solid adsorbent retained C_2H_4 for an adequate time before its breakthrough. Therefore, C_2H_6 can be removed from C_2H_4 with no loss of valuable C_2H_4, which is in line with the sorption experiments. Moreover, the regeneration of $\{[H_2B(3,5\text{-}(CF_3)_2Pz)_2]Cu\}_3$ in a vacuum oven at 313 K

revealed that the adsorbed gas could be completely recovered within 24 h (Figure 2.1.6d). The amount of C_2H_4 enriched from the thermal regeneration of the adsorbent is 1.15 mol L^{-1} (Figure 2.1.7).[21-22]

2.1.4 Summary

In summary, we have uncovered a remarkably effective, molecular compound $\{[H_2B(3,5\text{-}(CF_3)_2Pz)_2]Cu\}_3$ for C_2H_4/C_2H_6 separation. We have also investigated the ethylene uptake by $\{[H_2B(3,5\text{-}(CF_3)_2Pz)_2]Cu\}_3$ and removal from $[H_2B(3,5\text{-}(CF_3)_2Pz)_2]Cu(C_2H_4)$ in solution, as well as in the solid-state. Complete characterization of these interesting molecular species including their crystal structures has been achieved. Furthermore, *in-situ* PXRD provides a complete "live" picture of the solid-state process that also retains the precursor and product crystallinity and undergoes fast and complete and reversible conversion between the copper based sorbent and $[H_2B(3,5\text{-}(CF_3)_2Pz)_2]Cu(C_2H_4)$ driven by the presence or removal of C_2H_4. The accessible Cu(I) sites within this molecular compound have enabled it to exclusively bind ethylene over ethane, so this molecular compound exhibits extremely high and record IAST C_2H_4/C_2H_6 gas separation selectivity. The superior ethylene separation and purification performance of this molecular compound have been further confirmed by the breakthrough experiments in which ethylene of a purity level of over 99.5% can be readily desorbed from the separation columns. Such sorbents could not only aid the large-scale ethylene purification processes, but also enable the recovery of olefins from small-volume hydrocarbon sources such as refinery off-gases (typically from fluid catalytic cracker units), waste hydrocarbon streams from poly-olefin processes,

and vents from polymer storage facilities. We are currently developing additional molecular compounds based on this discovery for the effective separation of ethylene as well as larger olefins from their saturated counterparts.

Part 2.2 When SF_5 Outplays CF_3: Effects of Pentafluorosulfanyl Decorated Scorpionates on Copper and Silver

Anurag Noonikara Poyil, Alvaro Muñoz-Castro, Andrii Boretskyi, Pavel Mykhailiuk and H. V. Rasika Dias

(Part of this work has been published in *Chem. Sci.* **2021**, *12*, 14618-146623)[75]

2.2.1 Abstract

Polyfluorinated, electron-withdrawing, and sterically demanding supporting ligands are of significant value in chemistry. Here we report the assembly and use of a bis(pyrazolyl)borate, $[Ph_2B(3\text{-}(SF_5)Pz)_2]^-$ that combines all such features, and involves underutilized pentafluorosulfanyl substituents. The ethylene and carbonyl chemistry of copper(I) or silver(I) supported by $[Ph_2B(3\text{-}(SF_5)Pz)_2]^-$, a comparison to the trifluoromethylated counterparts involving $[Ph_2B(3\text{-}(CF_3)Pz)_2]^-$, as well as copper catalyzed cyclopropanation of styrene with ethyl diazoacetate and CF_3CHN_2 are presented. The results from cyclopropanation show that SF_5 groups dramatically improved the yields and stereoselectivity compared to the CF_3.

2.2.2 Introduction

Substituents are the key to modulating the chemical and physical properties of molecules, including those of metal complexes and catalysts. The number of electron-withdrawing substituents that can be utilized for this purpose that are also relatively inert and practical, however, are quite limited. Fluorinated substituents such as the trifluoromethyl (CF_3) group are especially useful in this regard as they often drastically alter the properties of a molecule compared to their hydrocarbon counterparts.[76-81] The pentafluorosulfanyl (SF_5) is a noticeably underutilized fluorinated substituent compared to the CF_3 group in chemistry.[82, 83] It is, however, gaining increasing attention due to its unique and attractive properties including large size (marginally smaller than a *tert*-butyl group), strong electron-withdrawing capabilities, high lipophilicity and excellent

chemical and thermal stability, and showing great promise in agrochemical, medicinal and materials chemistry applications.[82-90] Furthermore, molecules with pentafluorosulfanyl groups are also becoming more accessible via effective and convenient routes.[91-95]

The metal complexes featuring SF_5 groups are quite limited,[84, 96-98] although it was a substituent first introduced in 1960.[99] Promising outcomes noted in recent reports suggest that pentafluorosulfanyl moiety merits more closer scrutiny and wider utility. For example, recent work by Mecking and co-workers illustrated the benefits of SF_5 over CF_3 groups on Ni(II) salicylaldiminato complexes in ethylene polymerization catalysis (to get more linear and higher molecular weight polymers),[96] as well as on tetraphenylborate ions in Ni(II) mediated butadiene polymerizations.[100] In addition, SF_5 group has been utilized in luminescent transition metal complexes to minimize the aggregation in the solid-state, improve the solubility, and alter the emission features such as blue shifting of the phosphorescent emissions more significantly relatively to CF_3 bearing analogs.[83, 84, 101-105]

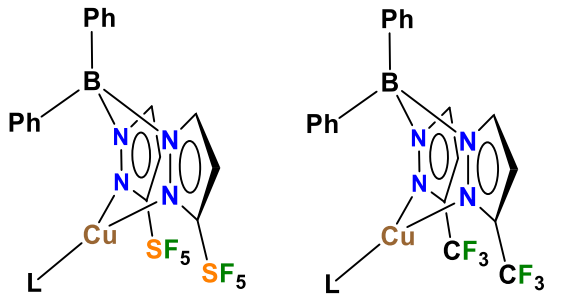

$[Ph_2B(3\text{-}(SF_5)Pz)_2]CuL$ $[Ph_2B(3\text{-}(CF_3)Pz)_2]CuL$

L = C_2H_4 (**23**), CO (**24**) L = C_2H_4 (**27**), CO (**28**)

Figure 2.2. 1. Bis(pyrazolyl)boratocopper(I) complexes decorated with pentafluorosulfanyl (SF_5) and trifluoromethyl (CF_3) groups.

Poly(pyrazolyl)borates, commonly referred to as scorpionates,[60, 106] are a very valuable class of ligands in coordination chemistry and catalysis, and form complexes with most metals of the periodic table. Here we report the first metal scorpionates decorated with pentafluorosulfanyl groups. In particular, we describe the synthesis of $[Ph_2B(3\text{-}(SF_5)Pz)_2]^-$ and the effects of this ligand support on copper(I) and silver(I) as reflected in the structures and bonding of ethylene and CO (with copper) complexes (which represent two classes of organometallic complexes with significant fundamental and practical significance),[24] and catalytic alkene cyclopropanation, as well as a direct comparison to the related trifluoromethylated analogs (Figure 2.2.1). It is also notable that there is only an isolated example of a copper complex involving a 4-$SF_5C_6H_4$-substituted ligand to our knowledge,[107] whereas CF_3-bearing ligands with copper and silver are more common and valued in many applications.[24, 63, 64, 108-110]

2.2.3 Results and Discussions

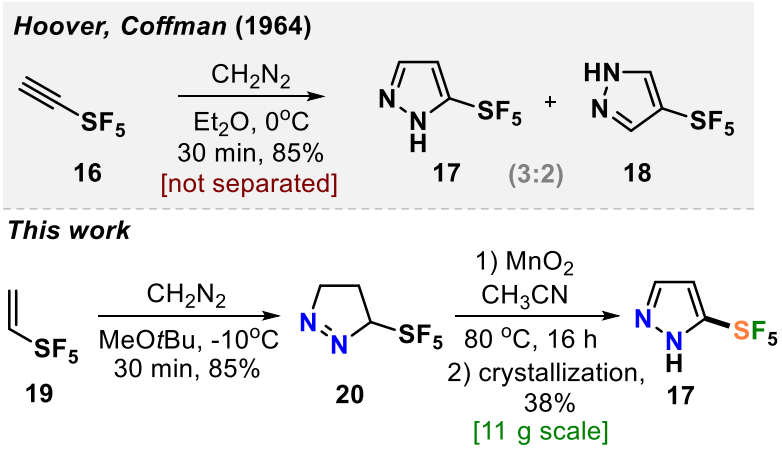

Figure 2.2. 2. Synthesis of SF_5-pyrazole **17.**

The SF_5-pyrazole (**17**) is unknown in the literature in the individual form. However, it was mentioned before in one manuscript. In 1964, Hoover and Coffman, reported that a reaction of alkyne **2** with diazomethane in diethyl ether at 0 ^oC led to the formation of a mixture of isomeric products **17** and **18** (3:2) (Figure 2.2.2).[111] The authors also mentioned that: "*these pyrazoles were not separated*." Therefore, we needed to develop a robust practical protocol for pyrazole **17**. After some optimization, we found that the reaction of alkene **19** with diazomethane at -10 ^oC gave pyrazoline **20** in 85% yield. Oxidation of the latter with MnO_2 followed by crystallization of the resulting material from hexane gave the needed compound SF_5-pyrazole (**17**) in 38% yield. This product was obtained in 11 g scale in one run (Figure 2.2.2).

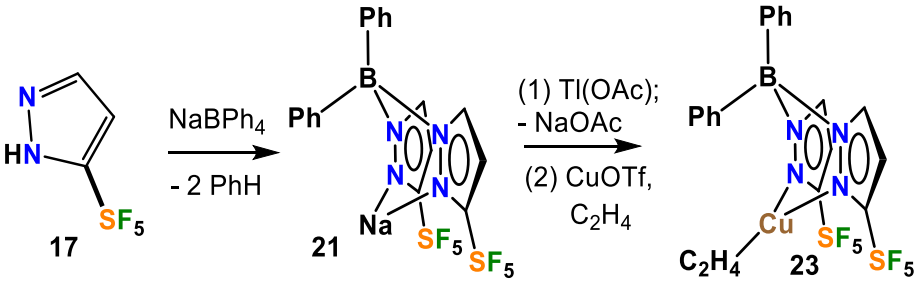

Figure 2.2. 3. Synthesis of $[Ph_2B(3\text{-}(SF_5)Pz)_2]Cu(C_2H_4)$.

The fluorinated bis(pyrazolyl)borate $[Ph_2B(3\text{-}(SF_5)Pz)_2]^-$ ligand possessing SF_5 groups at the pyrazolyl ring 3-positions was prepared by a reaction of SF_5-pyrazole (**1**) with $NaBPh_4$ via a benzene elimination pathway (Figure 2.2.3). This resulting sodium salt was converted to $[Ph_2B(3\text{-}(SF_5)Pz)_2]Tl$ (**22**) through metathesis using TlOAc, and utilized in the synthesis of $[Ph_2B(3\text{-}(SF_5)Pz)_2]Cu(C_2H_4)$ (**23**) by treating with CuOTf and ethylene (Figure 2.2.3). The related copper-ethylene, complex $[Ph_2B(3\text{-}$

$(CF_3)Pz)_2]Cu(C_2H_4)$ (**27**) was also synthesized for comparison. They are colorless crystalline solids, and stable to loss of ethylene in a nitrogen atmosphere at room temperature. The ^{19}F NMR spectra of the two adducts are very different due to the unique square pyramidal arrangement of fluorine atoms in SF_5 moieties vs trigonal pyramidal array in CF_3 groups, leading to a doublet and pentet in the former and a singlet in the latter.

The ethylene ^{13}C NMR signal in $[Ph_2B(3\text{-}(SF_5)Pz)_2]Cu(C_2H_4)$ and $[Ph_2B(3\text{-}(CF_3)Pz)_2]Cu(C_2H_4)$ were observed at δ = 86.4 and 82.7 ppm, respectively. This resonance in $[Ph_2B(3\text{-}(CF_3)Pz)_2]Cu(C_2H_4)$ was observed at δ 82.7 ppm, which is an even larger upfield shift from the free C_2H_4 (δ 123.1 ppm) signal. Larger upfield shift of the metal bound ethylene ^{13}C resonance from the free C_2H_4 (δ 123.1 ppm) signal has been attributed to the increased shielding resulting from metal-to-ethylene π-back-donation.[25, 112, 113] Thus $[Ph_2B(3\text{-}(SF_5)Pz)_2]Cu(C_2H_4)$, with a smaller shift points to relatively lower Cu$\rightarrow$ethylene π-backbonding. This is reasonable considering the presence of more electron withdrawing SF_5 groups (with an estimated electronegativity of 3.65 vs 3.36, and Hammett substituent constant s_m of 0.61 vs 0.43 for SF_5 vs CF_3)[82, 83, 114] on the scorpionate ligand backbone of this copper complex. For comparison, three coordinate $[t\text{-}Bu_2P(NSiMe_3)_2]Cu(C_2H_4)$ (**31**) with a more strongly backbonding copper site displays its ethylene carbon shift at δ 73.0 ppm.[62] The ^{13}C NMR data are particularly useful for such bonding analysis since they are less affected by the ring current effects.

The ethylene protons of $[Ph_2B(3\text{-}(R)Pz)_2]Cu(C_2H_4)$ (R = $-SF_5$, $-CF_3$) in the ^1H NMR spectrum appear at δ 3.72 and 3.69 ppm, respectively. These protons are most likely affected by the ring currents of flanking phenyl groups

sitting over ethylene moieties (see molecular structures below). The presence of additional ethylene in $CDCl_3$ solutions at room temperature leads to separate broad signals of free and coordinated ethylene in $[Ph_2B(3\text{-}(CF_3)Pz)_2]Cu(C_2H_4)$ whereas these signals remain sharp for the $-SF_5$ analog, suggesting a quite rapid associative olefin exchange only in the former at room temperature on the NMR time scale.

Molecular structure of $[Ph_2B(3\text{-}(R)Pz)_2]Cu(C_2H_4)$ (R = SF_5, CF_3) were unambiguously established by single-crystal X-ray diffraction (Figure 2.2.4). Compound $[Ph_2B(3\text{-}(SF_5)Pz)_2]Cu(C_2H_4)$ crystallizes with two chemical identical but crystallographically distinct molecules in the asymmetric unit. Selected bond distance and angles are given in Table 2.2.1. They are three-coordinate, trigonal planar copper complexes with an η^2-bound C_2H_4 moieties. The bis(pyrazolyl)borate ligands coordinate to copper in κ^2 fashion via nitrogen atoms of two pyrazolyl arms and adopt a boat configuration. One of the phenyl groups on boron sits above the ethylene group. Most of the key features are similar between the two adducts, although the $[Ph_2B(3\text{-}(SF_5)Pz)_2]Cu(C_2H_4)$ has slightly longer Cu-C and Cu-N distances compared to those of the CF_3 analog. This could be a result of either greater steric demand or more weakly donating nature of scorpionate in $[Ph_2B(3\text{-}(SF_5)Pz)_2]Cu(C_2H_4)$.

Analysis of the topographic steric maps of the two metal complexes using SambVca[115] and the X-ray crystallographic data indicate percent buried volumes of 69.9% and 64.0% for $[Ph_2B(3\text{-}(SF_5)Pz)_2]Cu(C_2H_4)$ and $[Ph_2B(3\text{-}(CF_3)Pz)_2]Cu(C_2H_4)$, respectively (Figure 2.2.5), clearly indicating more protected copper sites in the former as a result of having sterically more demanding SF_5 groups at the periphery of the coordination pocket. Sluggish

ethylene exchange in $[Ph_2B(3\text{-}(SF_5)Pz)_2]Cu(C_2H_4)$ noted above is probably a result of having greater steric protection at the copper site of this $-SF_5$ bearing molecule.

Table 2.2. 1. Selected bond distances (Å) and angles (º) of copper(I) complexes. Data for the second molecule in the asymmetric unit in *italics*.

Parameter	$[Ph_2B(3\text{-}(SF_5)Pz)_2]Cu(C_2H_4)$	$[Ph_2B(3\text{-}CF_3)Pz)_2]Cu(C_2H_4)$	$[Ph_2B(3\text{-}SF_5)Pz_2]Cu(CO)$	$[Ph_2B(3\text{-}CF_3)Pz)_2]Cu(CO)$
C=C	1.369(2) *1.353(2)*	1.3750(17)	-	-
C≡O	-	-	1.120(2) *1.121(2)*	1.119(2)
Cu-C	2.0199(13) 2.0225(13) *2.0307(14)* *2.0230(15)*	2.0123(11) 2.0184(11)	1.803(2) *1.807(2)*	1.8028(16)
Cu••C(Phenyl)	2.875 *2.723*	2.957	2.643 *2.510*	2.778
Cu-N	1.9937(10) 1.9870(10) *1.9980(10)* *2.0075(11)*	1.9745(8) 1.9795(8)	2.0054(15) 1.9910(15) *2.0154(15)* *2.0094(16)*	1.9871(11) 1.9838(10)
N-Cu-N	93.05(4) *92.30(4)*	95.12(3)	92.50(6) *91.24(6)*	93.92(4)
C-Cu-C	39.59(6) *39.00(6)*	39.89(5)	-	-
Cu-C-O	-	-	179.3(2) *172.2(2)*	176.4(2)
N-Cu-C	-	-	134.34(8) 131.12(8) *130.38(8)* *138.06(8)*	137.21(6) 128.47(6)
Σ angles at Cu	359.42 *360.00*	359.98	357.96 *359.68*	359.61

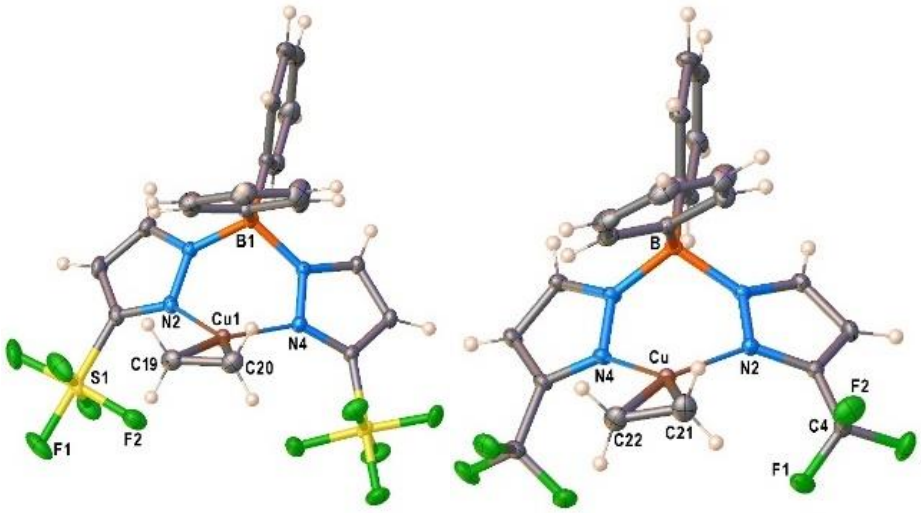

Figure 2.2. 4. Molecular structures of $[Ph_2B(3\text{-}(SF_5)Pz)_2]Cu(C_2H_4)$ (**23**) and $[Ph_2B(3\text{-}(CF_3)Pz)_2]Cu(C_2H_4)$ (**27**), from left to right.

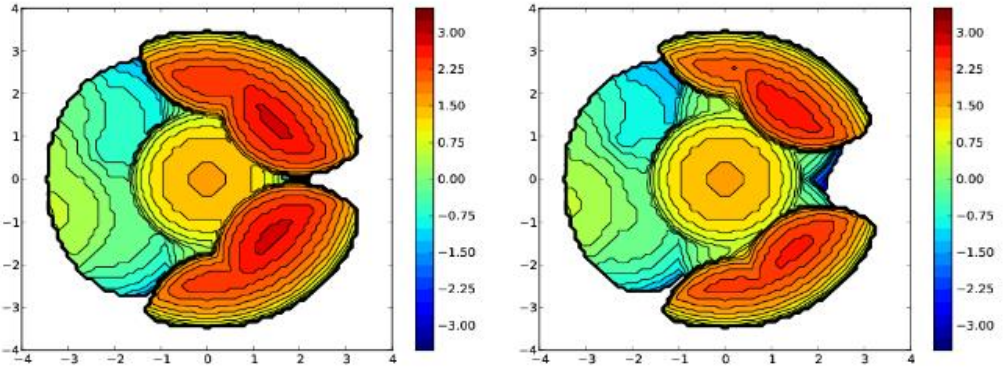

Figure 2.2. 5. Steric maps of $[Ph_2B(3\text{-}(SF_5)Pz)_2]Cu$ (left) and $[Ph_2B(3\text{-}(CF_3)Pz)_2]Cu$ (right) moieties based on the calculations using SambVca tool and X-ray data from the ethylene complexes $[Ph_2B(3\text{-}(SF_5)Pz)_2]Cu(C_2H_4)$ and $[Ph_2B(3\text{-}(CF_3)Pz)_2]Cu(C_2H_4)$. The resulting %buried volume values are 69.9% (average for the two molecules in the asymmetric unit) and 64.0%, respectively.

We have also investigated alkene-copper(I) bonding of $[Ph_2B(3\text{-}(SF_5)Pz)\}_2]Cu(C_2H_4)$, $[Ph_2B(3\text{-}(CF_3)Pz)_2]Cu(C_2H_4)$, and the hypothetical $[Ph_2B(3\text{-}(CH_3)Pz)_2]Cu(C_2H_4)$ via density functional calculations. The

calculated interaction energy (ΔE_{int}) between the ethylene and Cu(I) center remains similar, ranging from -44.9, -45.9, to -45.2 kcal·mol^{-1} (Table 2.2.2), respectively, which is further dissected in different contributions within the Ziegler-Rauk energy decomposition analysis (EDA).[116, 117] It shows that these interactions are primarily electrostatic in nature for all three [Ph_2B(3-(R)Pz)$_2$]Cu(C_2H_4) complexes as evident from ΔE_{elstat} of about ~60%, with the remainder consists of ~36% orbital contributions (ΔE_{orb}) and ~4% dispersion-type interactions (ΔE_{disp}). The ΔE_{orb} of [Ph_2B(3-(SF_5)Pz)}$_2$]Cu(C_2H_4) composed of σ-donation and π-backdonation ascribed to the π_1-C_2H_4 → Cu and π_2*-C_2H_4 ← Cu (Figure 5.2.2.2) in a 29.9% and 54.9% contribution, respectively, which is similar in trend but shows a gradual decrease and an increase in the two components going from -SF_5 to the -CF_3 and -CH_3 analogs, culminating in 24.5% and 63.7%, s/p-contributions in the most electron rich scorpionate ligand analog [Ph_2B(3-(CH_3)Pz)$_2$]Cu(C_2H_4). These interactions cause a more red-shifted $\bar{\upsilon}$(C=C) as evident from the computed values of 1516.3, 1513.5 and 1509.3 cm^{-1}, for [Ph_2B(3-(R)Pz)$_2$]Cu(C_2H_4) (R = -SF_5, -CF_3, -CH_3, respectively). These numbers follow the order of Hammett substituent constant s_m/s_p (0.61/0.68, 0.43/0.54, and -0.07/-0.17 for -SF_5, -CF_3, -CH_3, respectively),[82, 83, 114] and are inversely related to the the π_2*-C_2H_4 ← Cu backbonding contribution (Table 2.2.2). This trend is also consistent with computed proton affinities of the [Ph_2B(3-(R)Pz)$_2$]$^-$ ligands (and therefore, the donor features of the scorpionate nitrogen sites; see Figure 5.2.2.2), and indicate that [Ph_2B(3-(SF_5)Pz)$_2$]Cu(C_2H_4) features the most weakly donating scorpionate and least backbonding copper site in this series.

Table 2.2. 2. Energy decomposition analyses for the C_2H_4-Cu interaction for different $[Ph_2B(3\text{-}(R)Pz)_2]Cu(C_2H_4)$ complexes, with R= -SF_5, -CF_3, and -CH_3. Values in kcal·mol^{-1}. In addition, π-backbonding and σ-donation components are given as π_2^*-C_2H_4 ← Cu and π_1-C_2H_4 → Cu, respectively. Calculated $\bar{\upsilon}$(C=C) (in cm^{-1}) values are also given.

Parameter	$[Ph_2B(3\text{-}(SF_5)Pz)_2]Cu(C_2H_4)$ (**23**)		$[Ph_2B(3\text{-}(CF_3)Pz)_2]Cu(C_2H_4)$ (**27**)		$[Ph_2B(3\text{-}(CH_3)Pz)_2]Cu(C_2H_4)$ (**32**)	
ΔE_{int}	-44.9		-45.9		-45.2	
ΔE_{Pauli}	114.0		112.5		125.4	
ΔE_{disp}	-6.5	4.1%[a]	-5.6	3.5%[a]	-5.3	3.1%[a]
ΔE_{elstat}	-95.2	59.9%[a]	-95.0	59.9%[a]	-102.1	59.9%[a]
ΔE_{orb}	-57.2	36.0%[a]	-57.9	36.6%[a]	-63.2	37.1%[a]
π_1-C_2H_4 → Cu	-17.1	29.9%[b]	-16.5	28.5%[b]	-15.5	24.5%[b]
π_2^*-C_2H_4 ← Cu	-31.4	54.9%[b]	-33.5	57.9%[b]	-40.2	63.7%[b]
ΔE_{orb}^{rest}	-8.7		-7.8		-7.5	
$\bar{\upsilon}$(C=C) Calc.	1516.3		1513.5		1509.3	

[a]Percentage contribution to the total attractive interactions ΔE_{elstat}+ ΔE_{orb} + ΔE_{disp}. [b]Percentage contribution to the total orbital interactions ΔE_{orb}.

Some reactivities and catalytic features of $[Ph_2B(3\text{-}(SF_5)Pz)_2]Cu(C_2H_4)$, $[Ph_2B(3\text{-}(CF_3)Pz)_2]Cu(C_2H_4)$ have also been investigated. Upon treatment with CO in CH_2Cl_2, both adducts afford the corresponding copper carbonyl complexes. They do not lose CO under reduced pressure. The CO stretching frequencies of $[Ph_2B(3\text{-}(SF_5)Pz)_2]Cu(CO)$ and $[Ph_2B(3\text{-}(CF_3)Pz)_2]Cu(CO)$ were observed at 2121 and 2117 cm^{-1}, respectively. For comparison, the $\bar{\upsilon}$(CO) for the highly fluorinated $[H_2B(3,5\text{-}(CF_3)_2Pz)_2]Cu(CO)$ (**33**)[118] and relatively electron rich $[(Ph_3B)CH(3,5\text{-}(CH_3)_2Pz)_2]Cu(CO)$ (**34**)[119] appear at 2127 and 2092 cm^{-1}, respectively. These data indicate that $[Ph_2B(3\text{-}(SF_5)Pz)_2]Cu(CO)$ has a notably Lewis acidic copper site, and a relatively weakly donating supporting scorpionate, consistent with the observed carbon chemical shifts and DFT analysis of the corresponding ethylene complex. DFT calculations show that the Cu-CO interaction is slightly less favorable than Cu-C_2H_4 (Table 2.2.1) in the corresponding $[Ph_2B(3\text{-}(R)Pz)_2]Cu(CO)$ (ΔE_{int}= -39.9 (R = SF_5), -39.8 (R = CF_3), and -40.9 kcal·mol^{-1} (for hypothetical R = CH_3)), suggesting a kinetic control of the ethylene replacement. Bonding features vary along the R = $–SF_5$, -CF_3, and $–CH_3$ series, with the lowest $2\pi^*\leftarrow$Cu backbonding observed for $[Ph_2B(3\text{-}(SF_5)Pz)_2]Cu(CO)$, leading to the calculated $\bar{\upsilon}$(CO) of 2110, 2099, and 2080 cm^{-1}, respectively.

Molecular structures of $[Ph_2B(3\text{-}(SF_5)Pz)_2]Cu(CO)$, $[Ph_2B(3\text{-}(CF_3)Pz)_2]Cu(CO)$ are illustrated in Figure 2.2.6. There are two chemically identical molecules of $[Ph_2B(3\text{-}(SF_5)Pz)_2]Cu(CO)$ in its asymmetric unit. Selected bond distances and angles are presented in Table 2.2.1. The Cu-CO moieties are essentially linear. The scorpionate coordinates to the metal ion in κ^2 fashion and adopts a boat configuration. One of the phenyl groups on boron

sits above the copper center. The metal to *ipso*-carbon distances are 2.58 and 2.78 Å in $[Ph_2B(3\text{-}(R)Pz)_2]Cu(C_2H_4)$ (R = $-SF_5$, $-CF_3$), respectively. These separations are within the sum of van der Waals radii of Cu and C (3.10 Å). However, these contacts do not appear to be significant enough to distort the coordination geometry at the metal center because these molecules feature trigonal planar metal sites as evident from the sum of angles at the metal center (~360°). Furthermore, the $\bar{\upsilon}$(CO) values suggest that the copper sites remain quite Lewis acidic despite the close approach of the phenyl groups. Note that three-coordinate, trigonal planar copper carbonyls are very limited.[120-123]

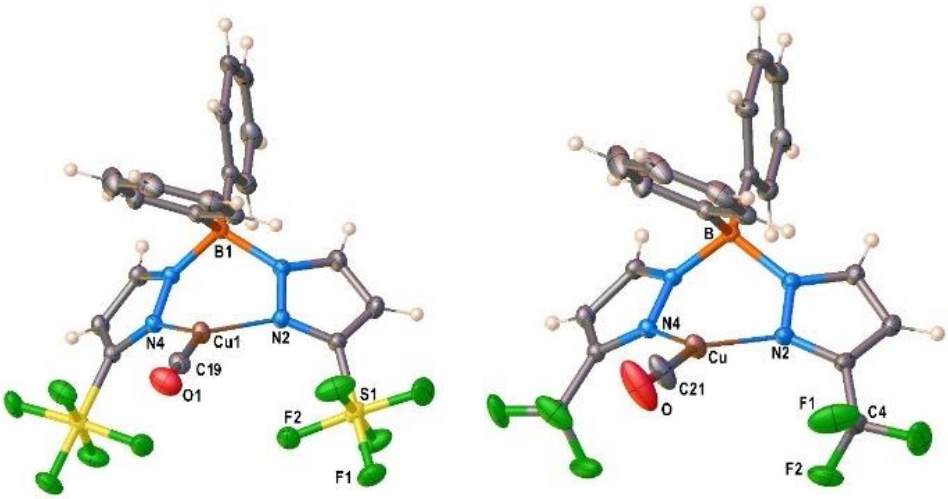

Figure 2.2. 6. Molecular structures of $[Ph_2B(3\text{-}(SF_5)Pz)_2]Cu(CO)$ (**24**) and $[Ph_2B(3\text{-}(CF_3)Pz)_2]Cu(CO)$ (**28**), from left to right.

Analysis of the topographic steric maps of the two metal complexes using SambVca[115] and the X-ray crystallographic data indicate percent buried volumes ($\%V_{bur}$) of 72.8% and 66.3% for $[Ph_2B(3\text{-}(SF_5)Pz)_2]Cu(CO)$ and $[Ph_2B(3\text{-}(CF_3)Pz)_2]Cu(CO)$, respectively clearly indicting more protected copper sites in the former as a result of having sterically more demanding SF_5

groups at the periphery of the coordination pocket (Figure 2.2.7). These percent buried volume values are larger than those observed for the related ethylene analogs (described above), indicating the adaptability of the scorpionate to accommodate organometallic fragments of different sizes.

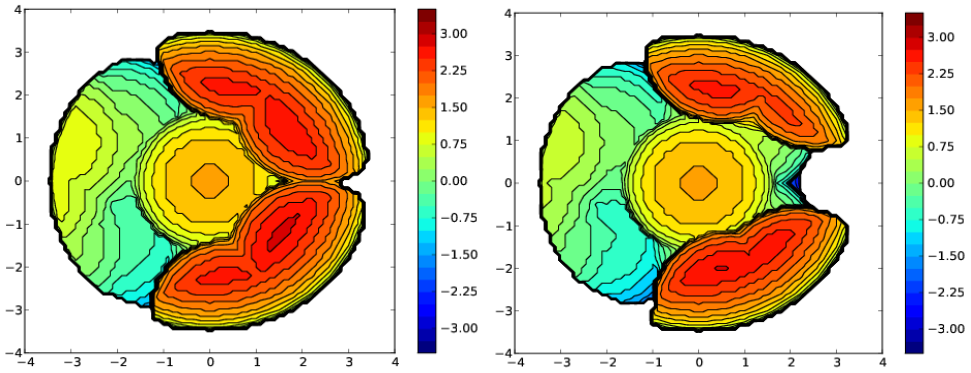

Figure 2.2. 7. Steric maps of $[Ph_2B(3\text{-}(SF_5)Pz)_2]Cu$ and $[Ph_2B(3\text{-}(CF_3)Pz)_2]Cu$ (from left to right) based on the calculations using SambVca tool and the X-ray data from carbonyl complexes, $[Ph_2B(3\text{-}(SF_5)Pz)_2]Cu(CO)$ and $[Ph_2B(3\text{-}(CF_3)Pz)_2]Cu(CO)$. The resulting % buried volume values are 72.9% (average for the two molecules in the asymmetric unit) and 66.3%, respectively.

We have also investigated the catalytic potential of $[Ph_2B(3\text{-}(R)Pz)_2]Cu(C_2H_4)$ (R = $-SF_5$, $-CF_3$) in cyclopropanation via a carbene transfer process. It was found that on reaction of styrene with ethyl diazoacetate (EDA), both copper(I) complexes serve as carbene transfer agents providing the expected cyclopropane as a diastereomeric mixture (Table 22.3). However, $[Ph_2B(3\text{-}(SF_5)Pz)_2]Cu(C_2H_4)$ gave dramatically higher cyclopropane product yields (99% vs 62%) and greater *cis*-selectivity (3:2 vs 1:1) compared to the $-CF_3$ substituted analog (Table 2.2.3).

Table 2.2. 3. Cyclopropanation of styrene with N_2CHCO_2Et (EDA) and CF_3CHN_2.

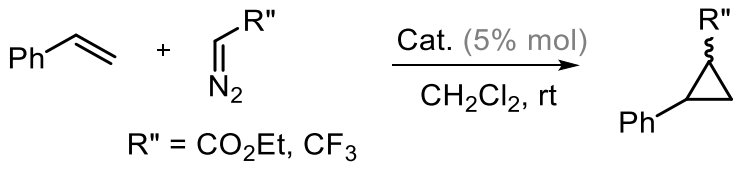

Catalyst	*Carbene source*	*Yield*	*Cis/Trans*
$[Ph_2B(3\text{-}(CF_3)Pz)_2]Cu(C_2H_4)$	$N_2CH(CO_2Et)$	62%	48:52
$[Ph_2B(3\text{-}(\mathbf{SF_5})Pz)_2]Cu(C_2H_4)$	$N_2CH(CO_2Et)$	**99%**	**61:39**
$[Ph_2B(3\text{-}(CF_3)Pz)_2]Cu(C_2H_4)$	N_2CHCF_3	70%	44:56
$[Ph_2B(3\text{-}(\mathbf{SF_5})Pz)_2]Cu(C_2H_4)$	N_2CHCF_3	**83%**	**25:75**

These results are consistent with the previous reports by Perez and co-workers involving tris(pyrazolyl)boratocopper complexes and EDA, which indicate that the higher *cis*-selectivities are associated with bulkier supporting ligands.[124] Interestingly, when CF_3CHN_2 was used as the carbene source,[125] $[Ph_2B(3\text{-}(SF_5)Pz)_2]Cu(C_2H_4)$ again gave notably higher product yields than the $[Ph_2B(3\text{-}(CF_3)Pz)_2]Cu(C_2H_4)$ catalyzed process, but this time, the *trans*-isomer was the major product. It is also known that the *cis*-isomer is the kinetic product while the *trans*-isomer is the thermodynamically favored product.[124] Therefore, it is possible that the greater steric bulk of the diazo reagent CF_3CHN_2 (compared to EDA) favors the latter, causing this interesting reversal in diastereoselectivity. Indeed, Doyle et al has observed high *trans*-selective cyclopropanations in rhodium chemistry with bulky diazo reagents.[31, 126]

The $[Ph_2B(3\text{-}(SF_5)Pz)_2]Ag(C_2H_4)$ (**29**) was synthesized by reacting $[Ph_2B(3\text{-}(SF_5)Pz)_2]Tl$ with Ag(OTf) and ethylene in dichloromethane (Figure

2.2.8). The related silver-ethylene, complex $[Ph_2B(3\text{-}(CF_3)Pz)_2]Ag(C_2H_4)$ was also synthesized for a comparison in a similar way. The ethylene ^{13}C NMR signal in $[Ph_2B(3\text{-}(SF_5)Pz)_2]Ag(C_2H_4)$ and $[Ph_2B(3\text{-}(CF_3)Pz)_2]Ag(C_2H_4)$ (**30**) were observed at δ = 103.8 and 101.8 ppm, respectively. These shifts are not as large as observed in the copper-ethylene analogs which makes sense because silver is a weakly donating metal.

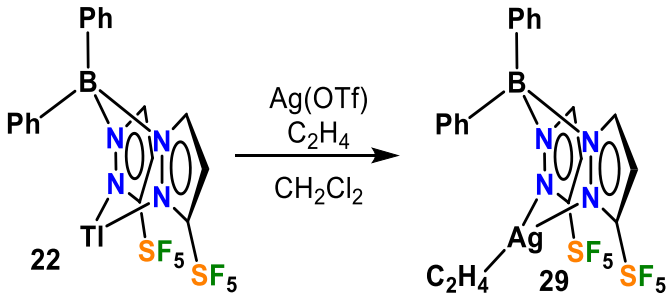

Figure 2.2. 8. Synthesis of $[Ph_2B(3\text{-}(SF_5)Pz)_2]Ag(C_2H_4)$ (**29**).

The ethylene protons of $[Ph_2B(3\text{-}(R)Pz)_2]Ag(C_2H_4)$ (R = $-SF_5$, $-CF_3$) in the ^1H NMR spectrum appear at δ 4.73 and 4.67 ppm, respectively. These protons are most likely affected by the ring currents of flanking phenyl groups sitting over ethylene moieties (see molecular structures below).

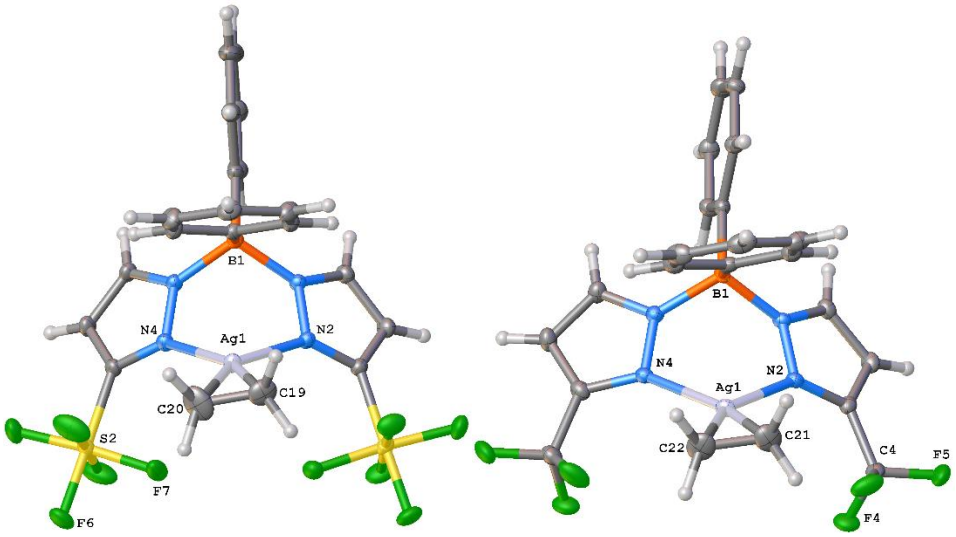

Figure 2.2. 9. Molecular structures of $[Ph_2B(3\text{-}(SF_5)Pz)_2]Ag(C_2H_4)$ (**29**) and $[Ph_2B(3\text{-}(CF_3)Pz)_2]Ag(C_2H_4)$ (**30**), from left to right.

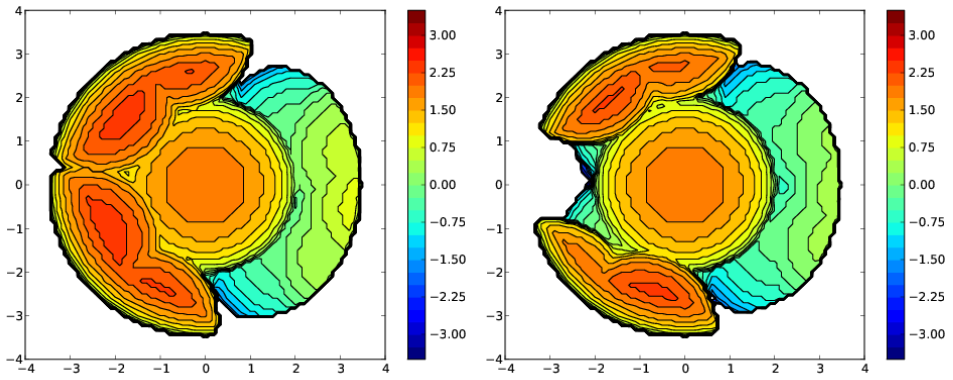

Figure 2.2. 10. Steric maps of $[Ph_2B(3\text{-}(SF_5)Pz)_2]Ag$ and $[Ph_2B(3\text{-}(CF_3)Pz)_2]Ag$ (from left to right) based on the calculations using SambVca tool and the X-ray data from carbonyl complexes, [Ph2B(3-(SF5)Pz)2]Ag(C_2H_4) and [Ph2B(3-(CF3)Pz)2]Ag(C_2H_4). The resulting % buried volume values are 71.2% (average for the two molecules in the asymmetric unit) and 65.1% (average for the three molecules in the asymmetric unit), respectively.

Molecular structure of $[Ph_2B(3\text{-}(R)Pz)_2]Ag(C_2H_4)$ (R = SF_5, CF_3) were unambiguously established by single-crystal X-ray diffraction (Figure 2.2.9). Compound $[Ph_2B(3\text{-}(SF_5)Pz)_2]Ag(C_2H_4)$ crystallizes with two chemically identical but crystallographically distinct molecules in the asymmetric unit whereas $Ph_2B(3\text{-}(CF_3)Pz)_2]Ag(C_2H_4)$ crystallizes with three chemically identical but crystallographically distinct molecules in the asymmetric unit. They are three-coordinate, trigonal planar silver complexes with an η^2-bound C_2H_4 moieties. The bis(pyrazolyl)borate ligands coordinate to silver in κ^2 fashion via nitrogen atoms of two pyrazolyl arms and adopt a boat configuration. One of the phenyl groups on boron sits above the ethylene group.

Analysis of the topographic steric maps of the two metal complexes using SambVca[115] and the X-ray crystallographic data indicate percent buried volumes ($\%V_{bur}$) of 71.2% and 65.1% for $[Ph_2B(3\text{-}(SF_5)Pz)_2]Ag(C_2H_4)$ and $[Ph_2B(3\text{-}(CF_3)Pz)_2]Ag(C_2H_4)$, respectively clearly indicting more protected silver sites in the former as a result of having sterically more demanding SF_5 groups at the periphery of the coordination pocket (Figure 2.2.10). These percent buried volume values are slightly larger than those observed for the related copper-ethylene analogs (described above), because of the larger size of silver atom relative to copper atom.

2.2.4 Summary

Overall, we have described the preparation and characterization of the first pentafluorosulfanyl decorated scorpionate $[Ph_2B(3\text{-}(SF_5)Pz)_2]^-$ and some of its copper chemistry, as well as a new, regioselective route to SF_5-pyrazole. The $[Ph_2B(3\text{-}(SF_5)Pz)_2]^-$ is a more sterically demanding and weakly donating ligand compared to the $[Ph_2B(3\text{-}(CF_3)Pz)_2]^-$, as evident from the silver ethylene,

copper ethylene and carbonyl chemistry and computational analysis. Moreover, the $[Ph_2B(3\text{-}(SF_5)Pz)_2]Cu(C_2H_4)$ (**23**) complex displays significantly better efficacy in cyclopropanation of styrene with EDA and CF_3CHN_2 compared to that of $[Ph_2B(3\text{-}(SF_5)Pz)_2]Cu(C_2H_4)$. Fluorinated ligands are important as they often provide metal complexes with certain beneficial features relative to the non-fluorinated, hydrocarbon group bearing ligands. Given the common appearance of CF_3-ligands in various areas of chemistry,[81] we believe that with this work, the SF_5-analogues will also become popular. Further studies on metal complexes supported by SF_5 containing ligands and practical approaches to other SF_5-heterocycles are currently underway.

Chapter 3

Acetylene and Other Alkyne Complexes of Copper(I) and Silver(I) and their Application

Part 3.1 Terminal and Internal Alkyne Complexes and Azide-Alkyne Cycloaddition Chemistry of Copper(I) Supported by a Fluorinated Bis(pyrazolyl)borate

Anurag Noonikara Poyil, Alvaro Muñoz-Castro, and H. V. Rasika Dias

(Part of this work has published in *Molecule*, **2022**, *27*, 16)[127]

3.1.1 Abstract

Copper plays an important role in alkyne coordination chemistry and transformations. This report describes the isolation and full characterization of a thermally stable, copper(I) acetylene complex using a highly fluorinated bis(pyrazolyl)borate ligand support. Details of the related copper(I) complex of $HC{\equiv}CSiMe_3$ are also reported. They are three-coordinate copper complexes featuring η^2-bound alkynes. Raman data show significant red-shifts in C≡C stretch of $[H_2B(3,5\text{-}(CF_3)_2Pz)_2]Cu(C_2H_2)$ and $[H_2B(3,5\text{-}(CF_3)_2Pz)_2]Cu(HC{\equiv}CSiMe_3)$ relative to those of the corresponding alkynes. Computational analysis using DFT indicates that the Cu(I) alkyne interaction in these molecules is primarily of the electrostatic character. The π-backbonding is the larger component of the orbital contribution to the interaction. The dinuclear complexes such as $Cu_2(\mu\text{-}[3,5\text{-}(CF_3)_2Pz])_2(C_2H_2)_2$ display similar Cu-alkyne bonding features. The mononuclear $[H_2B(3,5\text{-}(CF_3)_2Pz)_2]Cu(NCMe)$ complex catalyzes [3+2] cycloadditions between tolyl azide and a variety of alkynes including acetylene. It is comparatively less effective than the related trinuclear copper catalyst $\{\mu\text{-}[3,5\text{-}(CF_3)_2Pz]Cu\}_3$ involving bridging pyrazolates.

3.1.2 Introduction

Copper is an important metal in alkyne chemistry. It mediates a number of transformations of acetylene as well as larger alkynes including cycloaddition chemistry,[128-132] cyclopropenation,[38, 109, 133] partial hydrogenation,[134, 135] hetero atom-hydrogen bond additions,[71, 136-140] C_{sp}-H bond functionalizations, and alkyne coupling processes.[141-150] Copper catalyzed azide-alkyne cycloaddition (CuAAC) is perhaps the most popular among the different reaction types due to

its virtues of mild reaction conditions, high yields, and regioselectivity, with a major impact on organic and materials chemistry to chemical-biology applications.[129, 132, 151-156] Copper based materials are also useful for the separation of acetylene from CO_2 and acetylene storage.[157-161] Copper alkyne or alkynide complexes[162] are believed to be key intermediates in many of these reactions. Copper alkynes are used as precursors for the copper deposition as well.[163-165]

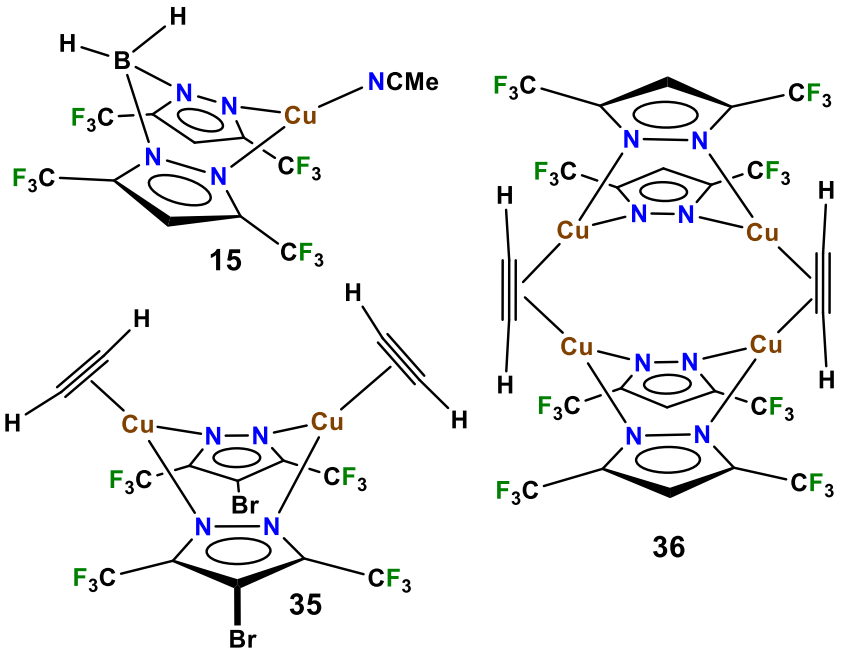

Figure 3.1. 1. $[H_2B(3,5\text{-}(CF_3)_2Pz)_2]Cu(NCMe)$ (**15**) and a selected group of structurally characterized copper complexes of acetylene, $Cu_2(\mu\text{-}[4\text{-}Br\text{-}3,5\text{-}(CF_3)_2Pz])_2(C_2H_2)_2$ (**35**) and $Cu_4(\mu\text{-}[3,5\text{-}(CF_3)_2Pz])_4(\eta\text{-}C_2H_2)_2$ (**36**)

Over the past few years, we have been working on the coordination chemistry and transformations of alkynes involving copper. For example, we demonstrated that the trinuclear copper(I) pyrazolate $\{\mu\text{-}[3,5\text{-}(CF_3)_2Pz]Cu\}_3$[166] is an effective catalyst for facile azide-alkyne cycloaddition leading to 1,2,3-

triazoles, alkyne C(sp)-H bond carboxylation with CO_2, and S-H addition to alkyne moiety.[167] Some of the alkyne complexes of copper pyrazolates show interesting luminescence.[168] We also discovered that the mononuclear, bis(pyrazolyl)borate $[H_2B(3,5\text{-}(CF_3)_2Pz)_2]Cu(NCMe)$ (Pz = pyrazolyl; Figure 3.1.1, **15**) is an excellent mediator of cyclopropenation chemistry of alkynes with ethyl diazoacetate.[109]

In this work, we describe the use of $[H_2B(3,5\text{-}(CF_3)_2Pz)_2]Cu(NCMe)$ as a catalyst in azide-alkyne cycloaddition chemistry between *p*-tolylazide and several alkynes including acetylene and trimethylsilylacetylene. We also describe the isolation of an acetylene complex as well as larger alkyne complexes involving the copper bis(pyrazolyl)borate moiety $[H_2B(3,5\text{-}(CF_3)_2Pz)_2]Cu$. Such compounds are of current interest,[162, 169, 170] and allow a comparison of mono-nuclear copper bis(pyrazolyl)borates to dinuclear copper(I) pyrazolates (e.g. $[H_2B(3,5\text{-}(CF_3)_2Pz)_2]Cu(C_2H_2)$ (**37**) and $Cu_2(\mu\text{-}[4\text{-}Br\text{-}3,5\text{-}(CF_3)_2Pz])_2(C_2H_2)_2$ (**35**)). It is also noteworthy that despite the long history of copper(I)-acetylene chemistry,[171, 172] copper(I) acetylene complexes with detailed structural and spectroscopic data are surprisingly scarce. For example, apart from the dinuclear and tetranuclear copper complexes **2** and $Cu_4(\mu\text{-}[3,5\text{-}(CF_3)_2Pz])_4(\mu\text{-}C_2H_2)_2$ (**36**) reported by us recently[167] structurally authenticated copper-HC≡CH complexes are limited to $[Cu\{NH(Py)_2\}(C_2H_2)]BF_4$ (**39**) and $[Cu(phen)(C_2H_2)]ClO_4$ (**40**) with $Cu(\eta^2\text{-}HC{\equiv}CH)$ moieties,[173, 174] and polymeric or octanuclear, chloride bridged copper(I) adducts containing $\mu_2\text{-}\eta^2,\eta^2\text{-}(HC{\equiv}CH)$ moieties.[175-177]

3.1.3 Results and Discussions

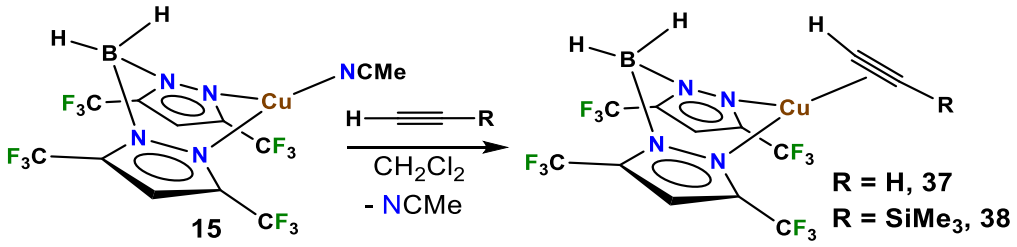

Figure 3.1. 2. Synthesis of $[H_2B(3,5\text{-}(CF_3)_2Pz)_2]Cu(C_2H_2)$ (**37**) and $[H_2B(3,5\text{-}(CF_3)_2Pz)_2]Cu(HC{\equiv}CSiMe_3)$ (**38**) from $[H_2B(3,5\text{-}(CF_3)_2Pz)_2]Cu(NCMe)$ (**15**) and the corresponding alkyne.

The bis(pyrazolyl)borate copper(I) complex $[H_2B(3,5\text{-}(CF_3)_2Pz)_2]Cu(NCMe)$[66] reacts with purified acetylene (~1 atm)[178, 179] in CH_2Cl_2, affording $[H_2B(3,5\text{-}(CF_3)_2Pz)_2]Cu(C_2H_2)$ (**37**) as a white solid in >90% yield (Figure 3.2.2), which is quite amenable to detailed spectroscopic and structural studies. The room temperature ^1H NMR spectrum of **37** in $CDCl_3$ displayed the acetylenic proton resonances at δ 4.70 ppm. That is a significant downfield shift relative to the corresponding signal of the free acetylene (δ 2.01 ppm).[180] The ^{13}C resonance of the acetylenic carbons appears at δ 80.2 ppm, which is a downfield shift of 7.0 ppm relative to that of the free acetylene (δ 73.2 ppm).[180] The $\bar{\upsilon}_{C\equiv C}$ band of solid **37** in the Raman spectrum was observed at 1819 cm^{-1}, representing a 155 cm^{-1} red shift relative to the corresponding stretching frequency of the free C_2H_2 (1974 cm^{-1}).[181] This red shift is not as high as that observed for $Cu_4(\mu\text{-}[3,5\text{-}(CF_3)_2Pz])_4(\mu\text{-}C_2H_2)_2$ (**36** with $\bar{\upsilon}_{C\equiv C}$ of 1638 cm^{-1}) containing a $\mu_2\text{-}\eta^2,\eta^2\text{-}(HC{\equiv}CH)$ (which is a formally 4e-donor, bridging acetylene). Table 3.1.1 shows available, albeit limited, ^1H and ^{13}C NMR data

and C≡C stretch of structurally characterized copper complexes featuring a formally 2e-donor η^2-(HC≡CH). $[H_2B(3,5\text{-}(CF_3)_2Pz)_2]Cu(C_2H_2)$ (**37**) shows the smallest downfield shift of the acetylenic NMR signal, and red-shift of C≡C stretching frequency relative to that of the free C_2H_2 among these (although the differences are minor), suggesting relatively weaker σ/π-interaction between the copper(I) and acetylene ligand in terms of the Dewar-Chatt-Duncanson picture.[28, 29] A rare, well-authenticated silver(I)-acetylene complex, $[HB(3,5\text{-}(CF_3)_2Pz)_3]Ag(C_2H_2)$ (**41**) is also available for a comparison (although it has a *tris(pyrazolyl)borate* (not bis(pyrazolyl)borate) ligand support).[26] It is a system that features relatively low M→alkyne backbonding. The acetylenic ^1H signal of this silver(I) complex has been observed at δ 3.48 ppm, which is an even smaller downfield shift from the free acetylene resonance (δ 2.01 ppm), compared to that observed for $[H_2B(3,5\text{-}(CF_3)_2Pz)_2]Cu(C_2H_2)$ (**37**). Interestingly, alkyne resonance of $[HB(3,5\text{-}(CF_3)_2Pz)_3]Ag(C_2H_2)$ in ^{13}C NMR appears at δ 66.3 ppm.

Overall, acetylenic ^1H and ^{13}C resonance of d-block metal complexes bearing 2e-donor, η^2-acetylene ligands has been observed (keeping in mind that η^2-acetylene can also serve as a formally 4e-donor moiety) at quite a wide chemical shift range.[182] For example, NMR spectra of Ru(II) complex $[Cp^*Ru(C_2H_2)(PEt_3)_2][BPh_4]$ (**42**)[183] and Ni(0) complex $(Ph_3P)_2Ni(C_2H_2)$ (**43**)[184] display their signals for the metal bound C_2H_2 in ^1H and ^{13}C at δ 4.38, 66.14 ppm and δ 6.41, 122 ppm, respectively. The latter nickel complex is expected to display more pronounced M→alkyne backbonding than in **4**. For

comparison, protons of the *bridging* acetylene group of $Cu_4(\mu\text{-}[3,5\text{-}(CF_3)_2Pz])_4(\eta\text{-}C_2H_2)_2$ (**36**) have been observed at δ 6.16 ppm.[167]

Table 3.1. 1. Selected bond distances (Å) and angles (º) for $[H_2B(3,5\text{-}(CF_3)_2Pz)_2]Cu(C_2H_2)$ (**37**), $Cu_2(\mu\text{-}[4\text{-}Br\text{-}3,5\text{-}(CF_3)_2Pz])_2(C_2H_2)_2$ (**35**), $[Cu\{NH(Py)_2\}(C_2H_2)]BF_4$ (**39**) and $[Cu(phen)(C_2H_2)]ClO_4$ (**40**). Specific bond distances and angles of 4 are presented in CIF and Supporting Information section. Data collection temperatures are in Kelvin. Free acetylene C≡C distance, C≡C stretching frequency, ^1H and ^{13}C chemical shifts are 1.2033(2) Å (gas phase) and 1.193(6) Å (neutron diffraction – less accurate),[181, 185] 1974 cm^{-1}, 2.01 ppm, and 73.2 ppm,[180] respectively.

Complex\ Parameter	**37**	**35**	$[Cu\{NH(Py)_2\}(HC\equiv CH)]BF_4$ (**39**)	$[Cu(phen)(HC\equiv CH)]ClO_4$ (**40**)
Temp.	100	100	173	283-303
Cu-C	1.972(3) 1.973(3)	1.966(3) 1.974(3)	1.971(3) 1.971(3)	1.930(5) 1.961(5)
C≡C	1.225(5)	1.227(4)	1.188(11)	1.190(7)
Cu-N	1.981(3) 1.981(3)	1.9697(18) 1.9742(18)	1.968(3) 1.968(3)	1.979(4) 1.978(4)
C-Cu-C	36.17(14)	36.29(11)	35.1(3)	35.6(2)
N-Cu-N	96.63(10)	98.94(8)	96.8(2)	84.9(2)
$\bar{\upsilon}$(C≡C)	1819	1811	1795	1800
^1H	4.40	4.75	5.21	-
^{13}C	80.2	-	-	-
ref	*This work*	*167*	*186*	*174*

The X-ray crystal structure of $[H_2B(3,5\text{-}(CF_3)_2Pz)_2]Cu(C_2H_2)$ (**37**) is illustrated in Figure 3.1.3. It is a three coordinate, trigonal planar copper-acetylene complex. The acetylene ligand is oriented parallel to the NCuN plane so as to maximize back-bonding interactions.[187] Selected bond distances and angles of **37** and copper complexes featuring 2e-donor, η^2-acetylene ligand in the literature are given in Table 3.1.1. The key parameters involving the CuC_2 core are remarkably similar between these molecules. This suggests that cationic copper species $[Cu\{NH(Py)_2\}(C_2H_2)]BF_4$ and $[Cu(phen)(C_2H_2)]ClO_4$ featuring relatively electron-rich supporting ligands and neutral copper complexes **37** and **36** involving weakly donating fluorinated ligands have similar effects on the Cu-C_2H_2 alkyne moiety, or produce effects that are not large enough to be parsed out by routine X-ray crystallography. They both show slightly elongated C≡C bonds relative to the free acetylene (1.181(7) Å)[188] but these changes are overshadowed by the somewhat high esd associated with bond distance measurements.

In addition to acetylene, we also tested the use of $HC{\equiv}CSiMe_3$ as a substrate in CuACC chemistry. Considering that structurally authenticated metal complexes of η^2-$HC{\equiv}CSiMe_3$ are rare (a search of Cambridge Structural Database[69] disclosed only three such examples involving transition metal ions),[189-191] and unknown for copper to our knowledge,[69] we also synthesized $[H_2B(3,5\text{-}(CF_3)_2Pz)_2]Cu(HC{\equiv}CSiMe_3)$ (**38**) for a detailed study. Treatment of $[H_2B(3,5\text{-}(CF_3)_2Pz)_2]Cu(NCMe)$ with $HC{\equiv}CSiMe_3$ in CH_2Cl_2 led to **38** in 91% yield (Figure 3.1.2). It is a white solid and was characterized by NMR and Raman spectroscopy and X-ray crystallography. The $\bar{\upsilon}_{C\equiv C}$ band of solid **5** in the

Raman spectrum was observed at 1870 cm^{-1}, which is a 237 cm^{-1} red shift relative to the corresponding stretching frequency of the free $HC{\equiv}CSiMe_3$ (2107 cm^{-1}). This $\bar{\upsilon}(C{\equiv}C)$ is similar to that reported for $[HC\{C(CF_3)CO\}_2]Cu(HC{\equiv}CSiMe_3)$ (**44**).[165] This suggests the presence of an η^2-$HC{\equiv}CSiMe_3$ bound alkyne moiety on copper(I).[168, 169]

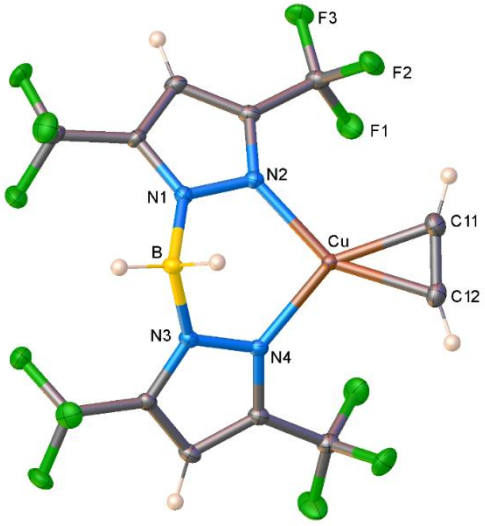

Figure 3.1. 3. Molecular structure of $[H_2B(3,5\text{-}(CF_3)_2Pz)_2]Cu(C_2H_2)$ (**37**); ORTEP view with 50% probability ellipsoids are shown. Selected bond distances (Å) and angles (º): Cu-N2 1.981(3), Cu-N4 1.981(3), Cu-C11 1.972(3), Cu-C12 1.973(3), C11-C12 1.225(5), B-N1 1.570(4), B-N3 1.569(4), Cu•••B 3.046, C11-Cu-C12 36.17(14), N2-Cu-N4 96.63(10), N4-Cu-C12 113.19(13), N2-Cu-C11 114.01(13), N1-B-N3 107.6(2).

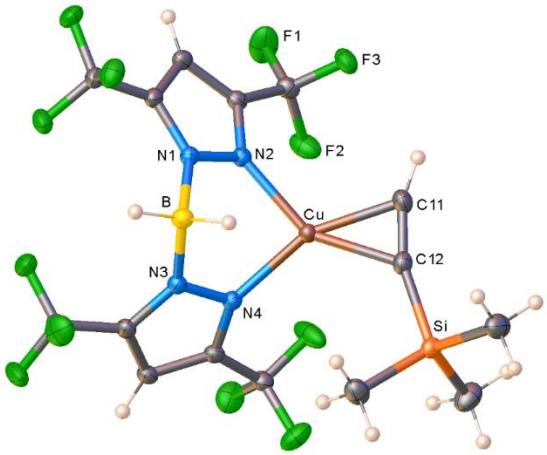

Figure 3.1. 4. Molecular structure of $[H_2B(3,5\text{-}(CF_3)_2Pz)_2]Cu(HC{\equiv}CSiMe_3)$ (**38**); ORTEP view with 50% probability ellipsoids are shown. Selected bond distances (Å) and angles (º): Cu-N2 1.9857(9), Cu-N4 1.9845(9), Cu-C11 1.9600(12), Cu-C12 1.9957(11), C11-C12 1.2343(17), B-N1 1.5778(15), B-N3 1.5737(16), C12-Si 1.8713(12), Cu•••B 2.964, C11-Cu-C12 36.35(5), N2-Cu-N4 90.59(4), N4-Cu-C12 120.05(4), N2-Cu-C11 112.92(5), N1-B-N3 106.41(9), C11-C12-Si 160.64(11).

X-ray crystal structure of $[H_2B(3,5\text{-}(CF_3)_2Pz)_2]Cu(HC{\equiv}CSiMe_3)$ (**38**) is depicted in Figure 3.1.4. It is a monomeric, trigonal planar copper complex with an η^2-$HC{\equiv}CSiMe_3$ bound alkyne moiety. The $HC{\equiv}CSiMe_3$ is bonded slightly asymmetrically as evident from the marginally longer Cu-C12, which is a carbon atom with the larger, silyl group. The alkyne group shows a significant deviation from the ideal 180° as evident from C≡C-Si angle, 160.64(11)°. This is about 19° bending back of the alkyne group due to the metal ion coordination. As noted above, there are no structural data on related copper η^2-$HC{\equiv}CSiMe_3$ complexes for comparisons. The

$Cp_2Nb(H)(HC{\equiv}CSiMe_3)$ (**45**)[189] and (NMe-Paa)W(CO)F($HC{\equiv}CSiMe_3$) (**46**) (based on a κ^3-[C,N,N'] chelator NMe-Paa = 2-(2-dimethylaminoethyl)methylaminomethylphenyl)[191] complexes are known and display significantly smaller C≡C-Si angles of 141.7(5)° and 138.1(1)° (or much larger deviation from linearity), which points to stronger metal-alkyne σ/π-bonding in these W(II) and Nb(III) complexes, in terms of the Dewar-Chatt-Duncanson model.[28, 29]

Compounds $[H_2B(3,5\text{-}(CF_3)_2Pz)_2]Cu(C_2H_2)$ (**37**) and $Cu_2(\mu\text{-}[4\text{-}Br\text{-}3,5\text{-}(CF_3)_2Pz])_2(C_2H_2)_2$ (**35**) (note: non-brominated, $Cu_2(\mu\text{-}[3,5\text{-}(CF_3)_2Pz])_2(C_2H_2)_2$ analog has been observed but not isolated) allow us to compare the effects of replacing a $[H_2B]^+$ with a $[(alkyne)Cu]^+$ moiety in these systems. Although structural features of N_2CuC_2 core are very comparable (Table 3.1.1), ^1H and Raman spectroscopic data of the alkyne group suggest that the copper site in the mononuclear **37** is slightly more Lewis acidic than that of dinuclear **36**, despite having a 4-bromo pyrazolate in the latter. Table 5.3.1.1 shows two additional sets of molecules, more closely related to each other; $[H_2B(3,5\text{-}(CF_3)_2Pz)_2]Cu(EtC{\equiv}CEt)$ (**47**)[109] and $Cu_2(\mu\text{-}[3,5\text{-}(CF_3)_2Pz])_2(EtC{\equiv}CEt)_2$ (**48**)[168] as well as $[H_2B(3,5\text{-}(CF_3)_2Pz)_2]Cu(HC{\equiv}CPh)$ (**49**)[66] and $Cu_2(\mu\text{-}[3,5\text{-}(CF_3)_2Pz])_2(HC{\equiv}CPh)_2$ (**50**).[167] To facilitate this analysis, the X-ray crystal structure of $[H_2B(3,5\text{-}(CF_3)_2Pz)_2]Cu(EtC{\equiv}CEt)$ was also investigated and the details are included in the chapter 5.[109] A comparison of mononuclear bis(pyrazolyl)borate systems to the corresponding dinuclear pyrazolate systems show very similar metrical parameters involving the N_2CuC_2 cores, except for N-Cu-N angles, which are smaller for the bis(pyrazolyl)borate copper

complexes. Closer analysis indicates that this is not because of noticeably longer Cu-N distances in bis(pyrazolyl)borate copper systems but due to their more folded CuN_4B cores (compared to the flatter CuN_4C rings in the related dinuclear pyrazolates). This is evident from the separation of the pyrazolyl ring carbons at 4-positions (e.g., Pz-C4•••Pz-C4 distance of $[H_2B(3,5\text{-}(CF_3)_2Pz)_2]Cu(EtC{\equiv}CEt)$ (**47**) and $Cu_2(\mu\text{-}[3,5\text{-}(CF_3)_2Pz])_2(EtC{\equiv}CEt)_2$ (**48**) is 6.18 and 6.38 Å).

Further analysis of the alkyne-copper(I) interaction is performed using density functional calculations (Table 3.1.2) to understand the variations between the mononuclear and dinuclear species as well as the copper and different alkynes. The overall interaction energy (ΔE_{int}) between the alkyne and copper(I) center for mononuclear species $[H_2B(3,5\text{-}(CF_3)_2Pz)_2]Cu(C_2H_2)$ (**37**), $[H_2B(3,5\text{-}(CF_3)_2Pz)_2]Cu(EtC{\equiv}CEt)$ (**47**), and $[H_2B(3,5\text{-}(CF_3)_2Pz)_2]Cu(PhC{\equiv}CH)$ (**49**) is -46.8, -51.5, and -49.4 $kcal{\cdot}mol^{-1}$, respectively, which is further dissected in different contributions within the Ziegler-Rauk energy decomposition analysis (EDA).[116, 117] In this framework, the interaction energy (ΔE_{int}) exhibits a larger electrostatic character (ΔE_{elstat}) of about ~60% of the stabilizing terms, whereas the orbital contribution to the interaction is about ~35% (ΔE_{orb}), with the remaining ~5% attributable to dispersion-type contributions (ΔE_{disp}). The ΔE_{orb} involves both π-backdonation and σ-donation, which contributes 57.2% and 26.3% to the bonding stabilization of **37**. The π-backbonding contribution in EtC≡CEt and PhC≡CH counterparts is similar to that of **37** (Figure 3.1.4). For the dinuclear species, $Cu_2(\mu\text{-}[3,5\text{-}(CF_3)_2Pz])_2(C_2H_2)_2$ (**51**), $Cu_2(\mu\text{-}[3,5\text{-}(CF_3)_2Pz])_2(EtC{\equiv}CEt)_2$ (**48**), and $Cu_2(\mu$-

[3,5-$(CF_3)_2$Pz])$_2$(HC≡CPh)$_2$ (**50**), the Cu-alkyne interaction energy (ΔE_{int}) amounts to -43.8, -49.4 and -47.8 kcal·mol^{-1}, respectively. These values are slightly lower than the somewhat related mononuclear, bis(pyrazolyl)borate species. They, however, involve similar bonding characteristics. The structurally characterized, brominated species Cu_2(μ-[4-Br-3,5-$(CF_3)_2$Pz])$_2$(C_2H_2)$_2$ (**35**) with an Cu-alkyne interaction energy of -42.9 kcal·mol^{-1}, shows a slight destabilization in comparison to Cu_2(μ-[3,5-$(CF_3)_2$Pz])$_2$(C_2H_2)$_2$ (**51**).

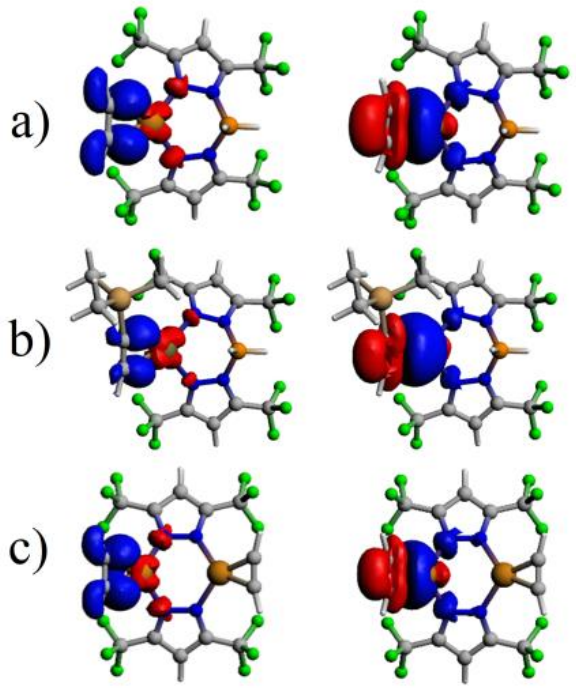

Figure 3.1. 5. Representative deformation densities accounting for the π-backbonding (left) and σ-donation (right) contribution to the bonding scheme in the formation of alkyl copper complexes (from top to bottom) for a) [H_2B(3,5-$(CF_3)_2$Pz)$_2$]Cu(C_2H_2) (**37**), b) [H_2B(3,5-$(CF_3)_2$Pz)$_2$]Cu(HC≡CSiMe_3) (**38**) and c) the dinuclear Cu_2(μ-[3,5-$(CF_3)_2$Pz])$_2$(C_2H_2)$_2$ (**51**). Charge flow from red to blue.

Table 3.1. 2. Energy decomposition analysis of the interaction energy in mononuclear and dinuclear Cu(I) species. Values in kcal.mol^{-1}. Vibrational frequencies in cm^{-1}.

Mononuclear, bis(pyrazolyl)borate copper complexes, L = [$H_2B(3,5\text{-}(CF_3)_2Pz)_2$]; L' = [$H_2B(4\text{-}Br\text{-}3,5\text{-}(CF_3)_2Pz)_2$]										
	LCu(HC≡CH), 37		**LCu(EtC≡CEt), 47**		**LCu(PhC≡CH), 49**		**LCu(HC≡CSiMe$_3$), 38**		**L'Cu(HC≡CH)**	
ΔE_{Pauli}	121.8		131.0		124.8		123.6		119.9	
ΔE_{Elstat}	-100.4	59.5 %	-112.6	61.7 %	-102.3	58.8 %	-103.7	59.0 %	-99.1	59.5%
ΔE_{orb}	-62.2	36.9 %	-59.9	32.8 %	-61.8	35.5 %	-60.3	34.3 %	-61.5	36.9%
ΔE_{Disp}	-6.0	3.6%	-10.0	5.5%	-10.0	5.7%	-11.7	6.7%	-6.0	3.6 %
ΔE_{int}	-46.8		-51.5		-49.4		-52.1		-46.7	
π→Cu	-35.6	57.2 %	-31.0	51.8 %	-33.8	54.6 %	-31.5	52.2 %	-34.8	56.5%
σ←Cu	-16.3	26.3 %	-17.5	29.2 %	-16.6	26.9 %	-16.7	27.7 %	-16.5	26.8%
$\nu_{C\equiv C,}$ Calc. (Exp.)	1817 (1819)		2056 (2064)		1954 (1927)		1870 (1870)		1818	

Dinuclear, copper pyrazolate complexes								
	$Cu_2(\mu\text{-}[3,5\text{-}(CF_3)_2Pz])_2(HC\equiv CH)_2$, **51**		$Cu_2(\mu\text{-}[3,5\text{-}(CF_3)_2Pz])_2(EtC\equiv CEt)_2$, **48**		$Cu_2(\mu\text{-}[3,5\text{-}(CF_3)_2Pz])_2(PhC\equiv CH)_2$, **50**		$Cu_2(\mu\text{-}[4\text{-}Br\text{-}3,5\text{-}(CF_3)_2Pz])_2(HC\equiv CH)_2$, **35**	
ΔE_{Pauli}	128.0		143.2		142.0		124.6	
ΔE_{Elstat}	-102.7	59.8 %	-118.2	61.3%	-109.8	57.8 %	-99.9	59.6 %
ΔE_{orb}	-62.8	36.5 %	-62.2	32.3%	-65.6	34.5 %	-61.5	36.7 %
ΔE_{Disp}	-6.3	3.7%	-12.2	6.3%	-14.5	7.6%	-6.1	3.7%
ΔE_{int}	-43.8		-49.4		-47.8		-42.9	
π→Cu	-35.8	57.0 %	-32.3	52.0%	-35.7	54.5 %	-34.8	56.6 %
σ←Cu	-16.7	26.5 %	-17.9	28.7%	-17.0	25.9 %	-16.6	27.1 %
$\nu_{C\equiv C,}$ Calc. (Exp.)	1814		2055 (2066)		1950		1813 (1811)	

We also probed the effect of different substituents on the alkyne moieties by including a phenyl and silyl group –SiMe$_3$ (Table 3.1.2). In [$H_2B(3,5\text{-}(CF_3)_2Pz)_2$]Cu(PhC≡CH) (**49**) and [$H_2B(3,5\text{-}(CF_3)_2Pz)_2$]Cu(HC≡CSiMe$_3$) (**38**),

the Cu-alkyne stabilization increases slightly due to a small increase of the electrostatic character in comparison to the HC≡CH counterpart (**37**). Moreover, if the silicon atom in the silyl derivative is replaced by a carbon atom, i.e. $–CMe_3$, the stabilization is further improved with an increase in electrostatic contribution. The computational analysis of the Ni(0) complex $(Ph_3P)_2Ni(C_2H_2)$[184] was also performed for a comparison. As expected, it shows a significantly more stabilized Ni-(C_2H_2) bond (ΔE_{int} = -75.9 kcal·mol^{-1}) owing to the increase of both electrostatic and orbital stabilizations, as given by a pronounced M→alkyne backbonding which amounts to -77.6 versus -35.6 kcal·mol^{-1} in **37**, which is consistent with the trends of red-shift of the C≡C stretching frequency (or the weakening of the C≡C bond).

Considering the importance and interest on copper catalyzed azide-alkyne cycloaddition (CuAAC) as well as rich alkyne chemistry of "$[H_2B(3,5\text{-}(CF_3)_2Pz)_2]Cu$" moiety, we also set out to explore the use of fluorinated bis(pyrazolyl)borate copper(I) complex $[H_2B(3,5\text{-}(CF_3)_2Pz)_2]Cu(NCMe)$ as a catalyst in cycloaddition of organic azides with terminal alkynes. We also compare the effectiveness of $[H_2B(3,5\text{-}(CF_3)_2Pz)_2]Cu(NCMe)$ with the trinuclear copper(I) pyrazolate $\{\mu\text{-}[3,5\text{-}(CF_3)_2Pz]Cu\}_3$[166] which was found to be quite an effective catalyst for these reactions.[167, 192] The Huisgen 1,3-dipolar cycloaddition[193] of organic azides and alkyne received significant attention ever since Sharpless[129] and Meldal[128] independently developed a copper(I) catalyzed reaction. Multidentate nitrogen ligands such as poly(pyrazolyl)borate ligands are known for stabilizing different metal ions including Cu(I).[24, 60] Ruthenium(II) tris(pyrazolyl)borates are reported to catalyze cycloaddition of

organic azides and alkyne.[194] There are however very few reports on copper(I) tris(pyrazolyl)borate catalyzed azide-alkyne cycloaddition even though they are known to catalyze several reactions such as cyclopropanation, cyclopropenation, nitrene transfer reactions, etc.[195] One of the reports concerns the synthesis of N-sulfonyl-1,2,3-triazoles from N-sulfonyl azides and alkynes.[196] That report shows copper(I) supported by tris(pyrazolyl)methanes providing better yields than the tris(pyrazolyl)borate based catalysts. More recent work by Stiriba and co-workers described the use of bis- and tris(pyrazolyl)boratocopper(I) systems to mediate reactions between phenyl- and alkyl-azides with different alkynes to produce 1,4-disubstituted 1,2,3-triazole derivatives moderate to excellent yields.[197]

Table 3.1. 3. Azide-alkyne cycloaddition mediated by the mononuclear bis(pyrazolyl)borate $[H_2B(3,5\text{-}(CF_3)_2Pz)_2]Cu(NCMe)$ (**15**) and the trinuclear copper(I) pyrazolate $\{\mu\text{-}[3,5\text{-}(CF_3)_2Pz]Cu\}_3$ (**52**). Method I and Method II are described in the experimental section.

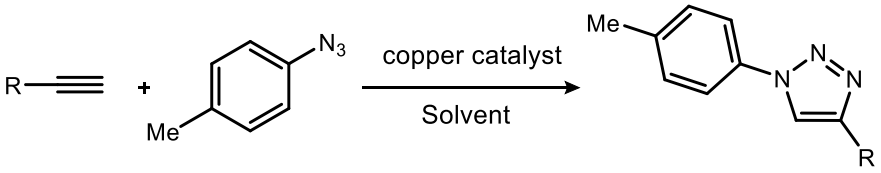

Product No	Alkyne	Yield (%) $[H_2B(3,5\text{-}(CF_3)_2Pz)_2]Cu(NCMe)$ catalyst		Yield (%) $\{\mu\text{-}[3,5\text{-}(CF_3)_2Pz]Cu\}_3$ catalyst
		Method I	Method II	Method III
53	HC≡CH	-	80	99
54	*n*-PrC≡CH	99	85	99
55	*n*-BuC≡CH	99	89	99
56	*n*-C_8H_{17}C≡CH	99	91	99
57	PhC≡CH	99	84	99
58	Me_3SiC≡CH	99	56	10

Table 3.1.3 summarizes the results of azide-alkyne cycloaddition mediated by the mononuclear $[H_2B(3,5\text{-}(CF_3)_2Pz)_2]Cu(NCMe)$ (**15**) and the trinuclear copper(I) pyrazolate $\{\mu\text{-}[3,5\text{-}(CF_3)_2Pz]Cu\}_3$ (**52**). A reaction of *p*-tolylazide with different terminal alkynes using 1 mol% of catalyst **15** at 110 ºC in toluene gives a very high yield for all substrates. The control reaction of *p*-tolyl azide with phenylacetylene without catalyst at the same temperature gives a lower (64%) yield. Thus, the temperature alone drives some of these processes albeit less effectively. We then tested the chemistry using a lower temperature but using a higher catalyst load. The use of 10 mol% compound **15** in EtOH at 40 ºC gives triazoles in moderate to excellent yield including a rare CuACC reaction involving the acetylene gas. The control reaction without the catalyst for these conditions gives <1% triazole (reaction of phenylacetylene and *p*-tolylazide). We compared these results to the corresponding $\{\mu\text{-}[3,5\text{-}(CF_3)_2Pz]Cu\}_3$ mediated chemistry using 1 mol% catalyst, at room temperature in dichloromethane. This trinuclear catalyst catalyzed alkyne-azide cycloadditions very effectively under milder conditions and generated products in high yield for all substrates except for trimethylsilylacetylene. It is noteworthy that all reactions (except 110 ºC reactions) are done in a vial using normal solvents and without using any inert atmosphere. Although we have not probed the mechanistic details, recent work by Larinov and coworkers on $\{\mu\text{-}[3,5\text{-}(CF_3)_2Pz]Cu\}_3$ and Stiriba and co-workers on poly(pyrazolyl)borate copper catalyzed cycloadditions suggest different mechanisms, most notably involving tetranuclear and dinuclear intermediates, respectively for the two systems.[197, 198] Better activity of the trinuclear $\{\mu\text{-}[3,5\text{-}(CF_3)_2Pz]Cu\}_3$ over mononuclear $[H_2B(3,5\text{-}(CF_3)_2Pz)_2]Cu(NCMe)$ in copper catalyzed azide-alkyne

cycloaddition suggests that these reactions involve multicenter catalytic intermediates, consistent with proposed mechanisms,[155] and having pre-assembled copper sites with bridging ligands is an advantage.[199]

3.1.5 Summary

In summary, we report the isolation and characterization of $[H_2B(3,5\text{-}(CF_3)_2Pz)_2]Cu(C_2H_2)$ and $[H_2B(3,5\text{-}(CF_3)_2Pz)_2]Cu(HC{\equiv}CSiMe_3)$ supported by a highly fluorinated bis(pyrazolyl)borate ligand. They feature three-coordinate, trigonal planar copper sites in the solid state and exhibit a significant reduction in $\bar{\upsilon}_{C\equiv C}$ value relative to the corresponding free alkyne C≡C stretch. Computational analysis of these molecules and several other related compounds using DFT indicates that the Cu(I)-alkyne interaction in these copper complexes is primarily of the electrostatic character. Furthermore, despite the presence of a highly fluorinated ligand in $[H_2B(3,5\text{-}(CF_3)_2Pz)_2]Cu(C_2H_2)$ and $[H_2B(3,5\text{-}(CF_3)_2Pz)_2]Cu(HC{\equiv}CSiMe_3)$, the Cu→alkyne p-backbonding component is much larger than the alkyne→Cu s-bonding interaction. However, the backbonding is not as high as that computed for $(Ph_3P)_2Ni(C_2H_2)$. The mononuclear and dinuclear complexes such as $[H_2B(3,5\text{-}(CF_3)_2Pz)_2]Cu(C_2H_2)$ and $Cu_2(\mu\text{-}[3,5\text{-}(CF_3)_2Pz])_2(C_2H_2)_2$ display similar Cu-alkyne bonding features. The bis(pyrazolyl)borate complex $[H_2B(3,5\text{-}(CF_3)_2Pz)_2]Cu(NCMe)$ catalyzes [3+2] cycloaddition chemistry between tolyl azide and a variety of alkynes including acetylene to produce 1,2,3-triazoles. It is, however, comparatively less effective than the related trinuclear copper catalyst $\{\mu\text{-}[3,5\text{-}(CF_3)_2Pz]Cu\}_3$ involving bridging pyrazolates. We are presently exploring the metal mediated

alkene and alkyne chemistry supported by these and other fluorinated ligands.[44, 75]

`

Part 3.2 Isolable Acetylene Complexes of Copper and Silver

Anurag Noonikara Poyil, Shawn G. Ridlen, Israel Fernández and H. V. Rasika Dias

`

3.2.1 Abstract

Copper and silver play important roles in acetylene transformations but isolable molecules with acetylene bonded to Cu(I) and Ag(I) ions are sparse. This report describes the stabilization of π-acetylene complexes of such metal ions supported by fluorinated and non-fluorinated, pyrazole-based chelators. These Cu(I) and Ag(I) complexes were formed readily in solutions under an atmosphere of excess acetylene and the appropriate ligand supported metal precursor and could be isolated as crystalline solids, enabling complete characterization using multiple tools including X-ray crystallography. Molecules that display κ^2- or κ^3-ligand coordination modes and trigonal planar or tetrahedral metal centers have been observed. Different trends in coordination shifts of the acetylenic carbon resonance were revealed by ^{13}C NMR spectroscopy for the Cu(I) and Ag(I) complexes. The reduction in acetylene $\bar{\upsilon}_{C\equiv C}$ due to metal ion coordination is relatively large for copper adducts. Computational tools were also used to quantitatively understand in detail the bonding situation in these species. It is found that the interaction between the transition metal fragment and the acetylene ligand is significantly stronger in the copper complexes, which is consistent with the experimental findings.

3.2.2 Introduction

Acetylene (C_2H_2) is a useful building block in organic and industrial chemistry.[43, 200, 201] It is usually obtained from coal via a process involving calcium carbide (which is different from the petroleum-based, other important C2-feedstock, ethylene).[201, 202] However, compared to ethylene, the applications involving acetylene are somewhat challenging due to its fire and explosion

`

risks, especially under high-pressure conditions and in purified form.[201] Furthermore, additional care must be taken when certain metals such as copper and silver are involved because they are known to form explosive acetylides and carbides with acetylene.[43, 203] Nevertheless, transition metals, including copper and silver, have been utilized successfully in many acetylene transformations.[43, 200, 204] Selective semi-hydrogenation of acetylene in ethylene-rich gas streams to produce ethylene is one such application with great industrial importance, as it serves as an effective method to remove acetylene impurities in ethylene feedstocks. Silver-modified palladium is the most commonly used catalyst for this purpose.[205-208] Various other silver and copper containing materials and copper complexes are also known to facilitate this process.[205, 209-212] Silver mediated addition[213] and carboxylation[214] reactions of acetylene and the involvement in acetylene sensing[215] have been reported. Copper and/or copper salts also play diverse roles in acetylene chemistry as in the ethynylation (e.g., in the 1,4-butynedione synthesis), hydrochlorination, carbonylation, cross-couplings, and azide-alkyne cycloaddition reactions, as well as vinylacetylene and cuprene synthesis.[43, 167, 200] Acetylene has also been separated very effectively from CO_2 using copper containing materials.[216] The metal carbide formations noted above could be considered as "C-H activation" processes.[217] Although limitations must be considered, the advancements stated herein show that copper and silver play an integral role in the acetylene chemistry.

`

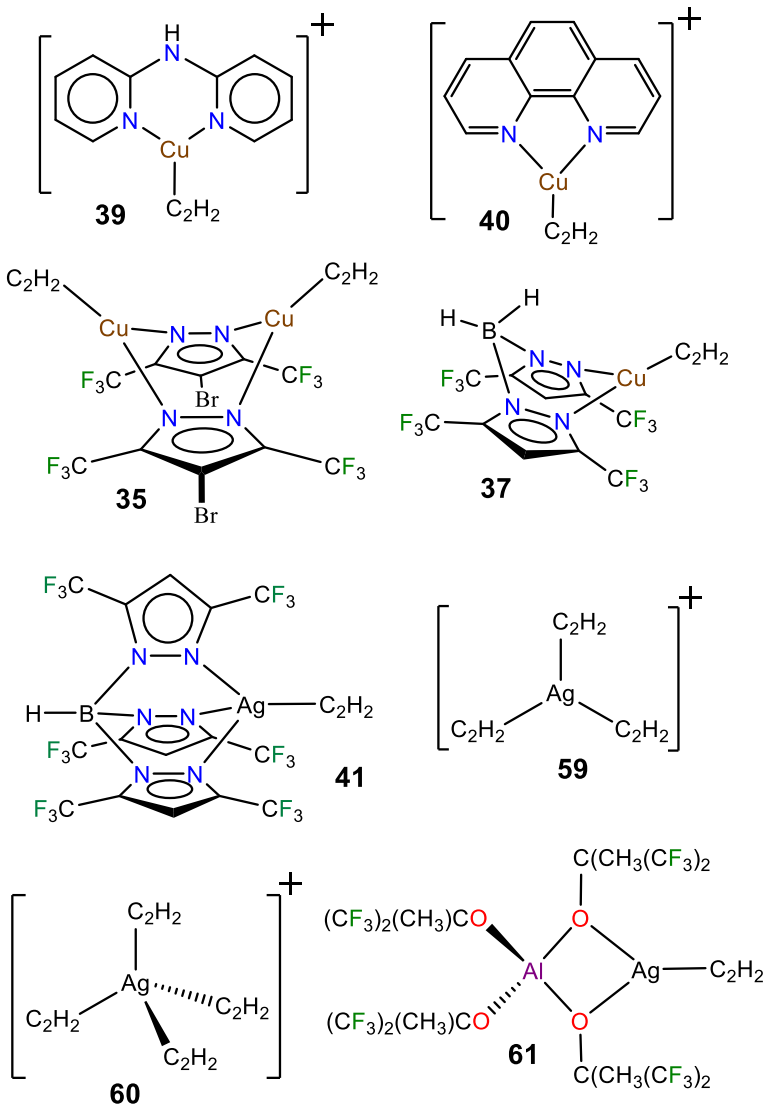

Figure 3.2. 1. Diagram showing the structures of well-characterized copper(I) and silver(I) complexes containing h2-bound acetylene. Counterions of the reported 39 and 40 are $[BF_4]$-, $[ClO_4]$-, and for 59 and 60 is $[Al(OC(CF_3)_3)_4]$-, respectively. Those ions have been omitted for clarity.

The fundamental chemistry such as structures and bonding of π-acetylene complexes of copper and silver are of significant interest because they provide useful information for the design and development of processes for separation,[218-220] activation, and utilization of this important C2-feedstock

`

chemical.[43, 200, 201] However, despite over a 100 year history of coinage metal (Cu, Ag, Au) chemistry of acetylene[221, 222] and the current importance,[43, 204] well-characterized molecules featuring terminal Cu(η^2-HC≡CH) and Ag(η^2-HC≡CH) bonds are still very limited. For example, a search of the Cambridge Structural Database[223] revealed only four copper complexes, [Cu{NH(Py)$_2$}(C$_2$H$_2$)][BF$_4$] (**1**[BF$_4$]),[8] [Cu(phen)(C$_2$H$_2$)][ClO$_4$] (**2**[ClO$_4$]),[174] Cu$_2$(μ-[4-Br-3,5-(CF$_3$)$_2$Pz])$_2$(C$_2$H$_2$)$_2$ (**35**),[167] and [H$_2$B(3,5-(CF$_3$)$_2$Pz)$_2$]Cu(C$_2$H$_2$) (**37**),[127] and four silver complexes [HB(3,5-(CF$_3$)$_2$Pz)$_3$]Ag(C$_2$H$_2$) (**41**),[26] [Ag(C$_2$H$_2$)$_3$][Al(OC(CF$_3$)$_3$)$_4$] (**59**[Al(OC(CF$_3$)$_3$)$_4$]),[224] [Ag(C$_2$H$_2$)$_4$][Al(OC(CF$_3$)$_3$)$_4$] (**60**[Al(OC(CF$_3$)$_3$)$_4$]),[224] and [Al(OC(CH$_3$)(CF$_3$)$_2$)$_4$]Ag(C$_2$H$_2$) (**61**)[224] containing terminal M(η^2-HC≡CH) bonds (Figure 3.2.1, M = Cu, Ag). It is also noteworthy that these few isolable species differ in terms of charge, coordination number and/or supporting ligands, and therefore are of limited use for comparisons. Even the gas-phase studies of Cu and Ag acetylene species are quite limited.[225-228] This scarcity is perhaps due to challenges such as facile loss of coordinated acetylene, metal acetylide and carbide formation, and the potential safety hazards associated with this work.[203]

Considering the importance of copper and silver in acetylene chemistry, we set out to uncover and characterize a group of molecules suitable for detailed comparisons and analysis. Herein we report the successful stabilization of several π-acetylene complexes of copper(I) and silver(I) and their spectroscopic features and X-ray crystal structures (Figure 3.2.2). Furthermore, in this work, we demonstrate the utility of bis- and tris(pyrazolyl)borate ligands, [Ph$_2$B(3-

`

$(CF_3)Pz)_2]^-$, $[HB(3,5\text{-}(CF_3)_2Pz)_3]^-$, and $[HB(3\text{-}(CF_3),5\text{-}(Ph)Pz)_2]^-$ to stabilize neutral, and bis(pyrazolyl)methane $H_2C(3,5\text{-}(CH_3)_2Pz)_2$ to isolate cationic, copper and silver acetylene complexes. A complete, comparative analysis of the bonding situation of these metal-acetylene complexes using density functional theory (DFT) calculations is also presented.

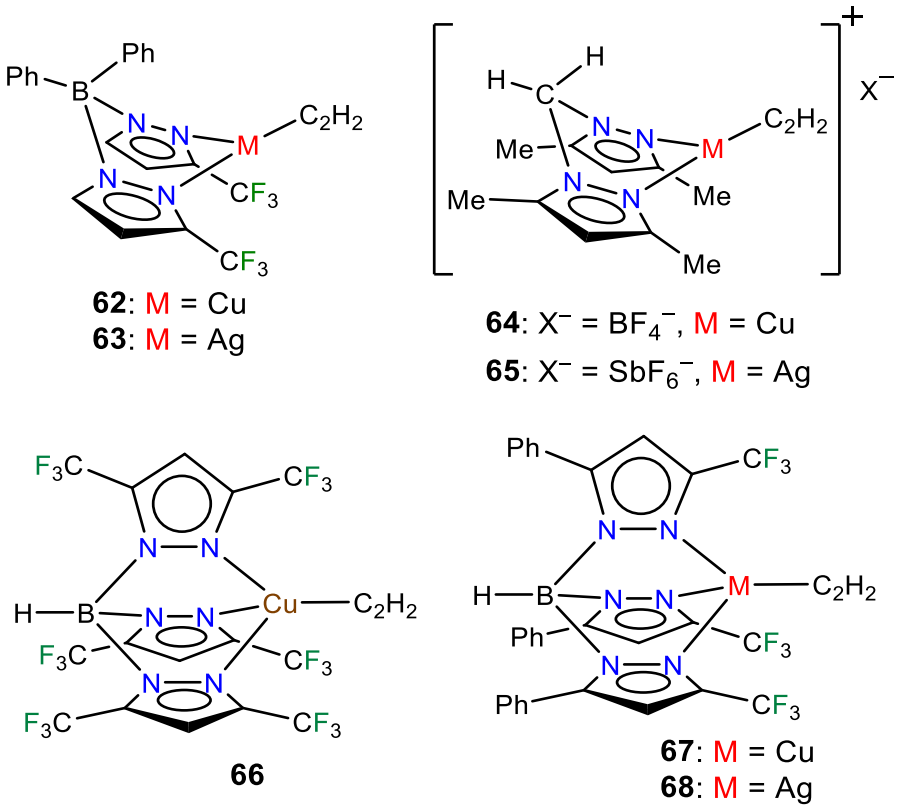

Figure 3.2. 2. Structures of stabilized p-acetylene complexes of copper(I) and silver(I) described in this work.

3.2.3 Results and Discussions

Fluorinated scorpionates[60, 106] have been quite useful in producing isolable molecules of reactive and/or labile organometallic fragments, including ethylene complexes of coinage metal ions.[24, 75, 109, 229, 230] Thus, we turned to the same family of supporting ligands as the starting point for this challenging

`

endeavor to stabilize molecules with Cu(η^2-HC≡CH) and Ag(η^2-HC≡CH) bonds. Indeed, the fluorinated bis(pyrazolyl)borate copper(I) complex [$Ph_2B(3\text{-}(CF_3)Pz)_2$]Cu($C_2H_4$) (**27**)[75] undergoes displacement reaction quite readily with purified acetylene (~1 atm)[178, 179] in CH_2Cl_2, affording [$Ph_2B(3\text{-}(CF_3)Pz)_2$]Cu($C_2H_2$) (**62**) as a white solid in 98% yield (Scheme 3.2.1). The room temperature ^{1}H NMR spectrum of **62** in $CDCl_3$ exhibited the acetylenic proton resonance at δ 4.22 ppm which is a significant downfield shift relative to the corresponding signal of the free acetylene (δ 1.91 ppm). The ^{13}C NMR data shows a downfield shift of 6.7 ppm for the copper-bound acetylenic carbon atoms (δ 78.7 ppm) relative to that of free acetylene (δ 72.0 ppm). The $\bar{\upsilon}_{C\equiv C}$ band of solid **62** in the Raman spectrum was observed at 1807 cm^{-1}, representing a redshift (167 cm^{-1} shift to a lower wavenumber) relative to the corresponding stretching frequency of the free acetylene (1974 cm^{-1}).[181]

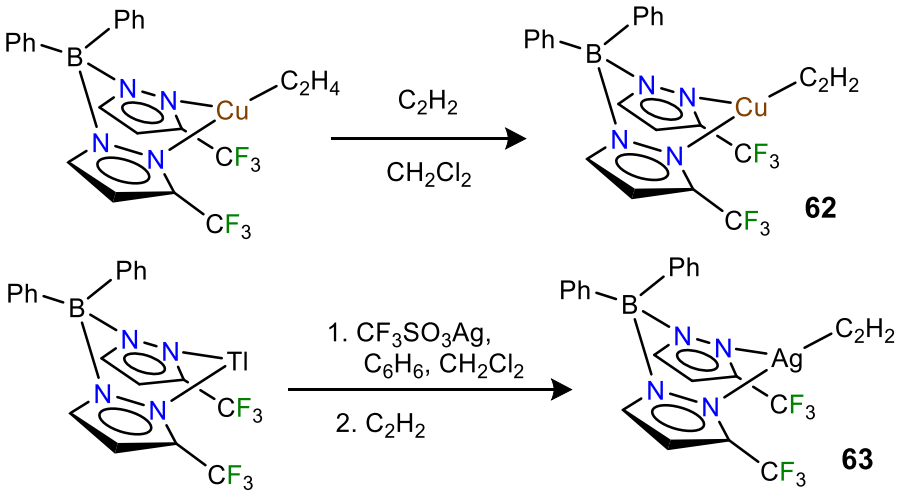

Figure 3.2. 3. Structures and synthetic routes to bis(pyrazolyl)borate complexes [$Ph_2B(3\text{-}(CF_3)Pz)_2$]Cu($C_2H_2$) (**62**), [$Ph_2B(3\text{-}(CF_3)Pz)_2$]Ag($C_2H_2$) (**63**)

`

The related silver(I) complex $[Ph_2B(3\text{-}(CF_3)Pz)_2]Ag(C_2H_2)$ (**63**) has been synthesized from $[Ph_2B(3\text{-}(CF_3)Pz)_2]Tl$,[75] silver triflate and purified C_2H_2 (~1 atm) and isolated as a white powder in 52% yield. Unlike the copper analog, the acetylene dissociates easily under reduced pressure from solid samples of **63** at room temperature. The ^1H NMR data of **63** in $CDCl_3$ displayed the resonance of acetylenic protons at δ 2.13 ppm, which compared to **62**, is a much smaller downfield shift from the free acetylene signal. The resonance of acetylenic carbons of **63** in ^{13}C NMR appears at δ 70.9 ppm, which in contrast to its copper counterpart, is an upfield shift from the free acetylene carbon resonance (δ 72.0 ppm). The room temperature NMR spectroscopic data of **62** and **63** suggest that in both complexes, the acetylene moiety stays coordinated to the metal site in solution, but in the latter, acetylene dissociated species is also observable.

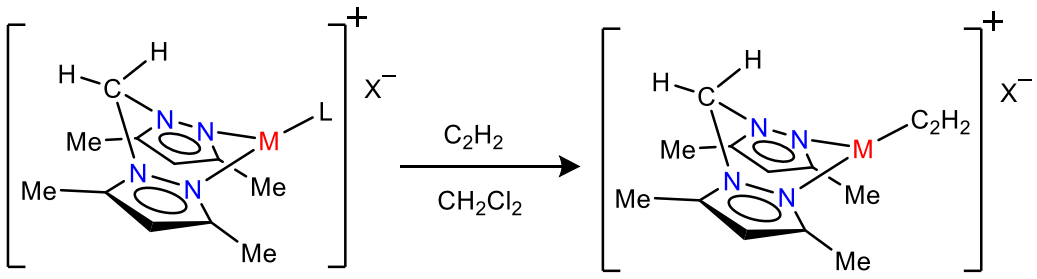

Figure 3.2. 4. Structures and synthetic routes to bis(pyrazolyl)methane complexes $[\{H_2C(3,5\text{-}(CH_3)_2Pz)_2\}Cu(C_2H_2)][BF_4]$ (**64**) and $[\{H_2C(3,5\text{-}(CH_3)_2Pz)_2\}Ag(C_2H_2)][SbF_6]$ (**65**)

`

The cationic, bis(pyrazolyl)methane copper(I) complex [{$H_2C(3,5\text{-}(CH_3)_2Pz)_2$}$Cu(C_2H_2)$][$BF_4$] (**64**) was obtained as a white solid in 97% yield by treating the copper(I) acetonitrile complex [{$H_2C(3,5\text{-}(CH_3)_2Pz)_2$}$Cu(CH_3CN)$][$BF_4$] (**69**)[229] with purified acetylene in CH_2Cl_2 (Scheme 3.2.2). The acetylenic protons appeared at δ 5.14 ppm in ^{1}H NMR spectrum of **64** in $(CD_3)_2CO$, showing a significant downfield shift relative to the corresponding resonance of the free acetylene. This also indicates that the acetylene on [{$H_2C(3,5\text{-}(CH_3)_2Pz)_2$}$Cu$]$^+$ does not get displaced by acetone. The $\bar{\upsilon}_{C\equiv C}$ band in Raman spectrum appears at 1812 cm^{-1}, indicating a 162 cm^{-1} redshift relative to free acetylene, which is very similar to that observed with the neutral, yet fluorinated ligand supported copper adduct **62**.

The bis(pyrazolyl)methane silver(I) complex [{$H_2C(3,5\text{-}(CH_3)_2Pz)_2$}$Ag(C_2H_2)$][$SbF_6$] (**65**) was synthesized from [{$H_2C(3,5\text{-}(CH_3)_2Pz)_2$}$Ag(C_2H_4)$][$SbF_6$] (**70**)[229] by displacing ethylene with acetylene in CH_2Cl_2 and isolated in 93% yield as a white powder. Like **63**, this cationic silver complex **65** also loses acetylene under reduced pressure at room temperature. The ^{1}H and ^{13}C NMR chemical shift values of the acetylenic moiety of **65** are similar to those observed with the neutral silver(I) acetylene complex **63**.

`

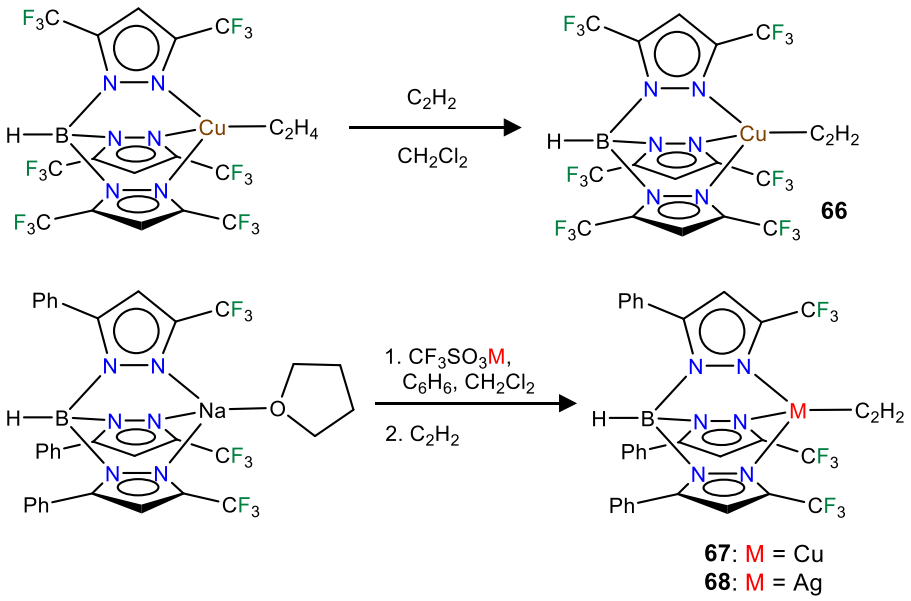

Figure 3.2. 5. Structures and synthetic routes to tris(pyrazolyl)borato copper and silver complexes, $[HB(3,5\text{-}(CF_3)_2Pz)_3]Cu(C_2H_2)$ (**66**), $[HB(3\text{-}(CF_3),5\text{-}(Ph)Pz)_3]Cu(C_2H_2)$ (**67**) and $[HB(3\text{-}(CF_3),5\text{-}(Ph)Pz)_3]Ag(C_2H_2)$ (**68**).

In addition to the 3-coordinate species described above, we also wanted to develop molecules using tridentate chelators to isolate 4-coordinate molecules and probe their chemistry. As apparent from the list of molecules illustrated in Figure 3.1.1, such species are the minority. The $[HB(3,5\text{-}(CF_3)_2Pz)_3]Cu(C_2H_2)$ (**66**) supported by a highly fluorinated tris(pyrazolyl)borate was obtained in essentially quantitative yield from the corresponding ethylene complex $[HB(3,5\text{-}(CF_3)_2Pz)_3]Cu(C_2H_4)$ (**2**)[9] (Scheme 3.2.3). It is the copper analog of the silver- η^2-acetylene complex $[HB(3,5\text{-}(CF_3)_2Pz)_3]Ag(C_2H_2)$ (**41**).[26] The ^1H and ^{13}C NMR spectra of **66** show notable downfield shifts for the resonance of acetylenic protons (δ 4.50) and carbons (δ 75.8 ppm) respectively, relative to corresponding resonances of the free acetylene. The Raman spectrum of $[HB(3,5\text{-}(CF_3)_2Pz)_3]Cu(C_2H_2)$ (**66**) shows

`

$\bar{\upsilon}_{C\equiv C}$ band at 1845 cm^{-1}, representing a redshift of 129 cm^{-1} relative to that of free acetylene. We have also synthesized copper(I) and silver(I) complexes supported by a relatively less fluorinated tris(pyrazolyl)borate, [HB(3-(CF_3),5-(Ph)Pz)$_2$]Cu(C_2H_2) (**67**) and [HB(3-(CF_3),5-(Ph)Pz)$_2$]Ag(C_2H_2) (**68**) starting from the ligand sodium salt [HB(3-(CF_3),5-(Ph)Pz)$_2$]Na(THF) (**71**)[120] and the corresponding metal triflate and acetylene (Scheme 3.2.3), and isolated as solids in 69% and 71% yield, respectively. Molecular pairs such as **66**, **67** and **41**, **68** serve as ideal systems to investigate ligand effects on spectroscopic and structural features of the M(η^2-HC≡CH) group.

Some properties of these acetylene complexes deserve comment. Copper complexes **62, 64, 66,** and **67** are fairly thermally stable solids under an inert or acetylene atmosphere. These copper complexes do not lose acetylene under reduced pressure at room temperature. Compound **64** gets oxidized easily upon exposure to air and turns green. Dichloromethane solution of **62** and acetone solution of **64** turn to green color immediately upon exposure to air. Silver complexes **65** and **68** are stable under acetylene atmosphere. They however tend to lose acetylene under reduced pressure. Solid samples of compound **63** turn to brown color even at -20 °C under acetylene or nitrogen atmosphere. Dichloromethane solution of compound **63** also turns to brown color slowly and loses acetylene at room temperature.

`

Table 3.2. 1. Selected peaks from ^{1}H, ^{13}C NMR and Vibrational Spectra for copper(I) and silver(I) complexes and the chemical shift (Δδ) from free acetylene (Δδ = δ (metal complex) – δ (free acetylene) and $\Delta\bar{\upsilon}_{C\equiv C} = \bar{\upsilon}_{C\equiv C}$ (metal complex) - $\bar{\upsilon}_{C\equiv C}$ (free acetylene))

Compound	**Raman/IR (cm^{-1}) (C≡C)**	**$\Delta\bar{\upsilon}_{C\equiv C}$ (cm^{-1})**	**^{1}H NMR (ppm) ($C_2\underline{H}_2$)**	**Δδ (ppm)**	**$^{13}C\{^{1}H\}$ NMR (ppm) (C≡C)**	**Δδ (ppm)**	**Reference**
$[Ph_2B(3\text{-}(CF_3)Pz)_2]Cu(C_2H_2)$ (**62**)	1807	-167	4.22	2.31	78.7	6.7	This work
$[HB(3\text{-}(CF_3),5\text{-}(Ph)Pz)_3]Cu(C_2H_2)$ (**67**)	1829	-145	4.66	2.75	76.5	4.5	This work
$[HB(3,5\text{-}(CF_3)_2Pz)_3]Cu(C_2H_2)$ (**66**)	1845	-129	4.50	2.59	75.8	3.8	This work
$[\{H_2C(3,5\text{-}(CH_3)_2Pz)_2\}Cu(C_2H_2)][BF_4]$ (**64**)	1812	-162	5.14[a]	2.73	79.5[a]	5.9	This work
$[H_2B(3,5\text{-}(CF_3)_2Pz)_2]Cu(C_2H_2)$ (**37**)	1819	-155	4.70	2.79	80.2	8.2	127
$Cu_2(\mu\text{-}[4\text{-}Br\text{-}3,5\text{-}(CF_3)_2Pz])_2(C_2H_2)_2$ (**3**)	1811	-163	4.75[b,d]	2.95	-	-	167
$[Cu\{NH(Py)_2\}(C_2H_2)][BF_4]$ (**39**$[BF_4]$)	1795	-179	5.59[a]	3.18	-	-	186
$[Cu(phen)(C_2H_2)][ClO_4]$ (**40**$[ClO_4]$)	1800	-174	-	-	-	-	174
$Cu_4(\mu\text{-}[3,5\text{-}(CF_3)_2Pz])_4(\mu\text{-}C_2H_2)_2$[c]	*1638*	*-336*	*6.16*	*4.25*	*79.2*	*7.2*	*167*
$[Ph_2B(3\text{-}(CF_3)Pz)_2]Ag(C_2H_2)$ (**63**)	-	-	2.13	0.22	70.9	-1.1	This work
$[HB(3\text{-}(CF_3),5\text{-}(Ph)Pz)_3]Ag(C_2H_2)$ (**68**)	1895	-79	3.59[b]	1.79	66.7[b]	-5.2	This work
$[HB(3,5\text{-}(CF_3)_2Pz)_3]Ag(C_2H_2)$ (**41**)	-	-	3.48	1.57	66.3	-5.6	26
$[\{H_2C(3,5\text{-}(CH_3)_2Pz)_2\}Ag(C_2H_2)][SbF_6]$ (**65**)	-	-	2.25[b]	0.45	71.7[b]	-0.2	This work
$[Al(OC(CH_3)(CF_3)_2)_4]Ag(C_2H_2)$ (**59**)	1914	-60	3.03[b]	1.23	69.7[b]	-2.3	224
$[Ag(C_2H_2)_3][Al(OC(CF_3)_3)_4]$ (**60**$[Al(OC(CF_3)_3)_4]$)	1925	-49	2.87[b]	1.07	72.8[b]	0.9	224
$[Ag(C_2H_2)_4][Al(OC(CF_3)_3)_4]$ (**61**$[Al(OC(CF_3)_3)_4]$)	1940	-34	2.66[b]	0.86	72.7[b]	0.8	224
Free C_2H_2	1974	0	1.91 ($CDCl_3$) 2.41 ($(CD_3)_2CO$) 1.80 (CD_2Cl_2)	0	72.0 ($CDCl_3$) 73.6 ($(CD_3)_2CO$) 71.9 (CD_2Cl_2)	0	This work, 181, 224

Some NMR data in solvents other than $CDCl_3$, [a]$(CD_3)_2CO$, [b]CD_2Cl_2; [c]A copper complex featuring a bridging acetylene ligand (serving as a formally 4e-donor) for comparisons.
[d]NMR data collected at -70 ºC

`

Table 3.2.1 shows available, albeit limited, key ^{1}H and ^{13}C NMR data and C≡C stretch of structurally characterized copper and silver complexes and those of the newly synthesized complexes **62-68**. A copper complex $Cu_4(\mu$-[3,5-$(CF_3)_2Pz])_4(\mu$-HC≡CH$)_2$ (**36**) containing a μ_2-η^2,η^2-(HC≡CH) (which is a bridging acetylene)[167] has also been included for comparisons. The Raman and IR data of the η^2-(HC≡CH) copper(I) complexes show a reduction of C≡C stretch by over >100 cm^{-1} with an average reduction of 160 cm^{-1} relative to that of the free acetylene stretch observed at 1974 cm^{-1}. This implies a weakening of the C≡C bond due to σ/π-interaction between copper(I) and acetylene (both components reduce the CC bond order) in terms of the Dewar-Chatt-Duncanson picture.[28, 29] However, the reduction in wavenumber is not as high as that observed with $Cu_4(\mu$-[3,5-$(CF_3)_2Pz])_4(\mu$-HC≡CH$)_2$ containing a bridging acetylene, which is understandable. Furthermore, ligand effects on $\bar{\upsilon}_{C\equiv C}$ are also apparent from some related complexes in which weakly donating ligand support on copper(I) produces molecules that display relatively higher HC≡CH stretch, e.g., **62** and **37** or **67** and **66**. Compared to Cu(I), the effect of Ag(I) on η^2-(HC≡CH) is relatively smaller as evident from a significantly smaller reduction (average 60 cm^{-1} reduction from the corresponding stretch of the free C_2H_2). This is in agreement with silver(I) being a weaker s-bonding and p-backbonding metal ion compared to copper(I) atom (e.g., $d^{10}\rightarrow d^{10}s^1$ electron affinities of Cu(I) and Ag(I) ions are 7.72 and 7.57 eV, in terms of energy released, respectively, and $d^{10}\rightarrow d^9p^1$ promotional energies of Cu(I) and Ag(I) are 8.25 and 9.94 eV, respectively).[231] A much more detailed analysis of metal-acetylene bonding using DFT is also given below.

`

The ^{1}H NMR spectra of copper(I) complexes in general show a larger downfield shift (shift towards typical alkene region) of acetylenic proton signal from the free acetylene resonance, whereas the silver analog shows only a smaller congruent shift. The ^{13}C NMR resonances of the copper(I) and silver(I) coordinated acetylene carbons are interesting in that they show shifts in opposite directions from that of free acetylene carbon signal. Note also that, some other d-block metal-acetylene complexes show a much larger downfield shift in acetylenic proton and carbon signals. For example, $(Ph_3P)_2Ni(HC{\equiv}CH)$[182, 184] involving the significantly better backbonding Ni(0) displays its signals for the nickel-bound η^2-(HC≡CH) in ^{1}H and ^{13}C NMR spectra at δ 6.41, 122 ppm, respectively.

The copper and silver acetylene complexes, $[Ph_2B(3\text{-}(CF_3)Pz)_2]Cu(C_2H_2)$ and $[Ph_2B(3\text{-}(CF_3)Pz)_2]Ag(C_2H_2)$ afforded excellent single crystals and were characterized by X-ray crystallography. Figure 3.2.3 depicts the molecular structures of these molecules. They are three-coordinate, trigonal planar metal complexes with κ^2-bound $[Ph_2B(3\text{-}(CF_3)Pz)_2]^-$ ligands. The acetylene ligand coordinates to the metal in a familiar η^2-fashion. The $M(NN)_2B$ core (M = Cu, Ag) adopts a boat conformation.

`

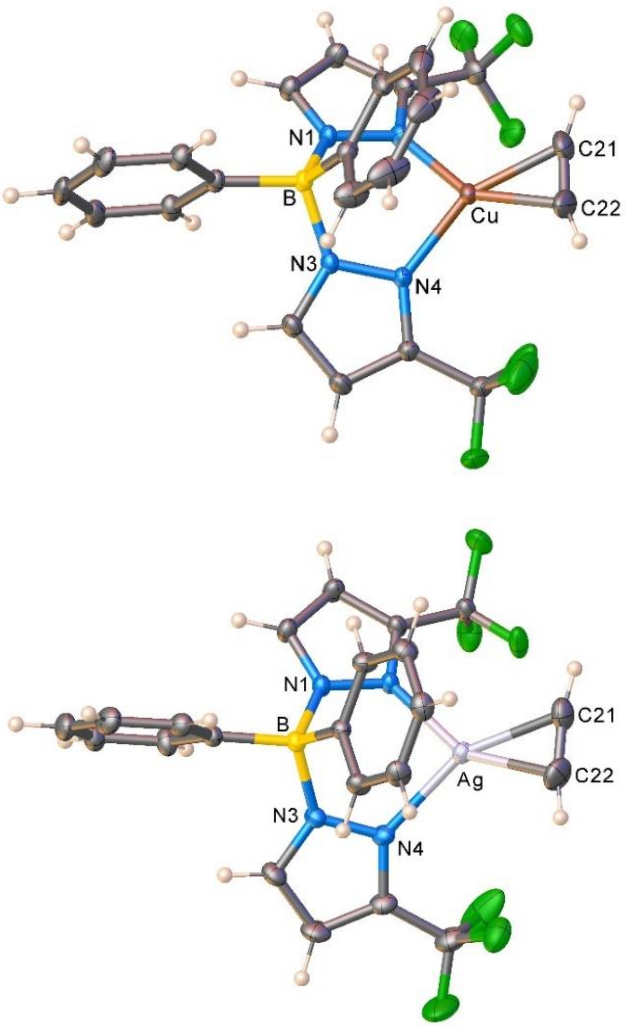

Figure 3.2. 6. Molecular structures of $[Ph_2B(3\text{-}(CF_3)Pz)_2]Cu(C_2H_2)$ (**62**) and $[Ph_2B(3\text{-}(CF_3)Pz)_2]Ag(C_2H_2)$ (**63**)

`

Table 3.2. 2. Selected bond lengths and angles of three-coordinate copper and silver acetylene complexes and those of several related ethylene complexes for comparisons. The CC distance of free acetylene is 1.20286(3) Å based on gas-phase experimental data[232] and 1.193(6) Å from neutron diffraction data on solid acetylene.[185] The CC distance of free ethylene for comparison is 1.3305(10) Å from gas phase data and 1.313 Å from X-ray data.[233, 234]

Compound	**π-CC (Å)**	**C-M-C (°)**	**N-M-N (°)**	**M-N (Å)**	**C-M (Å)**	**CN at M[a]**	**Ref.**
[$Ph_2B(3\text{-}(CF_3)Pz)_2$]Cu($C_2H_2$) (**62**)	1.217(3)	36.17(8)	95.51(4)	1.9714(10), 1.9697(10)	1.9629(14), 1.9567(15)	3	This work
[{$H_2C(3,5\text{-}(CH_3)_2Pz)_2$}Cu($C_2H_2$)][$BF_4$] (**64**)	1.203(4)	35.55(13)	97.14(9)	1.978(2), 1.977(2)	1.970(3), 1.971(3)	3	This work
[$Ph_2B(3\text{-}(CF_3)Pz)_2$]Ag($C_2H_2$) (**63**)	1.193(3)	30.63(8)	82.76(5)	2.2665(12), 2.2415(14)	2.2653(19), 2.2531(19)	3	This work
[{$H_2C(3,5\text{-}(CH_3)_2Pz)_2$}Ag($C_2H_2$)][$SbF_6$] (**65**)	1.203(5)	31.10(14)	88.66(9)	2.220(2), 2.235(2)	2.251(3), 2.237(4)	3	This work
[$HB(3,5\text{-}(CF_3)_2Pz)_3$]Cu($C_2H_2$) (**66**)	1.134(7)	33.16(19)	90.17(10), 88.25(7), 88.25(7)	2.0466(17), 2.0466(17), 2.179(3)	1.986(3), 1.986(3),	4	This work
[$HB(3,5\text{-}(CF_3)_2Pz)_3$]Ag($C_2H_2$) (**41**)	1.143(14)	28.9(4)	80.99(11), 80.99(11), 81.1(2)	2.293(4), 2.347(3), 2.364(4)	2.293(4), 2.293(4)	4	[26]
[$Ph_2B(3\text{-}(CF_3)Pz)_2$]Cu($C_2H_4$)[b]	1.369(2); 1.353(2)	39.59(6); 39.00(6)	93.05(4); 92.30(4)	1.9937(10), 1.9870(10); 1.9980(10), 2.0075(10)	2.0199(13), 2.0225(13); 2.0307(14), 2.0230(15)	3	[75]
[{$H_2C(3,5\text{-}(CH_3)_2Pz)_2$}Cu($C_2H_4$)][*n*-$BuBF_3$]	1.361(2)	39.44(6)	94.45(4)	1.9885(11), 1.9896(11)	2.0153(13), 2.0181(13)	3	[229]
[{$H_2C(3,5\text{-}(CH_3)_2Pz)_2$}Ag($C_2H_4$)][$SbF_6$]	1.350(5)	34.96(12)	88.96(9)	2.223(2), 2.232(2)	2.243(3), 2.253(3)	3	[229]
[{$H_2C(3,5\text{-}(CF_3)_2Pz)_2$}Ag($C_2H_4$)][$SbF_6$][b]	1.340(4); 1.340(4)	33.67(11); 33.69(11)	86.44(6); 86.49(6)	2.3306(18), 2.3328(18); 2.3330(18), 2.3293(18)	2.309(3), 2.319(3); 2.312(3), 2.313(3)	3	[229]

[a] coordination number at M
[b] Two molecules in the asymmetric unit

`

Table 3.2.2 summarizes selected structural parameters. These molecules feature flanking phenyl group above the metal-acetylene moiety with closest M••C(phenyl) separations of 3.01 and 2.88 Å in the Cu and Ag complex, respectively. Although these atoms are within the Bondi's van der Waals separation distances of 3.10 and 3.42 Å (or 4.15 and 4.30 Å proposed by Alvarez)[235] for Cu••C and Ag••C,[236] any interactions present between the metal and phenyl group do not affect the trigonal planar geometry at the metal (see also the computational section, below).

As evident from the data presented in Table 3.2.2, Cu-N and Cu-C distances are shorter than the related separations involving silver, which is expected as Ag is the largest metal of the coinage metal triad.[237, 238] Consequently, the C-Cu-C and N-Cu-N angles are significantly larger than those parameters involving silver. The acetylene ligands are essentially coplanar with the N-M-N plane (M = Cu, Ag; silver complex shows the larger twist angle of 3° but it is still minor). This parallel orientation of NMN and CMC planes is the best for maximizing metal-(η^2-ligand) back-bonding interactions, rather than the orthogonal conformation.[187]

We have also characterized the cationic acetylene complexes [{$H_2C(3,5\text{-}(CH_3)_2Pz)_2$}$Cu(C_2H_2)$][$BF_4$] (**64**) and [{$H_2C(3,5\text{-}(CH_3)_2Pz)_2$}$Ag(C_2H_2)$][$SbF_6$] (**65**) involving a bis(pyrazolyl)methane ligand support using X-ray crystallography. The molecular structures are illustrated in Figure 3.2.4. Selected bond distances and angles are given in Table 3.2.2. The $H_2C(3,5\text{-}(CH_3)_2Pz)_2$ ligand coordinates in κ^2-fashion while the acetylene ligand shows η^2-bonding with the metal sites. The $M(NN)_2C$ core of the bis(pyrazolyl)methane ligand adopts a flat boat conformation, and the

`

difference between bis(pyrazolyl)borate and bis(pyrazolyl)methane backbone shapes reported in this manuscript are reflected in the larger MN•••NM separation of the pyrazolyl groups of the latter. Also, unlike **62** and **63**, C-M-C and N-M-N planes of **64** and **65** deviate somewhat from co-planarity with the copper and silver adducts showing 8.8° and 11.9° inter-planar twist angles. This perhaps indicates a weakened M-acetylene backbonding in the cationic systems **64** and **65** over the neutral **62** and **63**. Crystal packing diagrams indicate that one of the fluorine atoms of $[BF_4]^-$ in $[\{H_2C(3,5\text{-}(CH_3)_2Pz)_2\}Cu(C_2H_2)][BF_4]$ sits near Cu at 2.8842(12) Å, while two fluorine atoms of two different $[SbF_6]^-$ counter-ions are closer (3.364(4), 3.439(3) Å) to the silver center of $[\{H_2C(3,5\text{-}(CH_3)_2Pz)_2\}Ag(C_2H_2)][SbF_6]$. These separations are at or longer than the Bondi's van der Waals contact separation of F with Cu (2.87 Å) and Ag (3.19 Å), and do not distort the trigonal planar geometry at copper and silver, as evident from the sum of angles at M (M = Cu, Ag) of 360°.

Interestingly, metrical parameters such Cu-N and Cu-C distances and N-Cu-N and C-Cu-C angles involving the copper center are quite similar between the cationic $[\{H_2C(3,5\text{-}(CH_3)_2Pz)_2\}Cu(C_2H_2)][BF_4]$ and the neutral complexes $[Ph_2B(3\text{-}(CF_3)Pz)_2]Cu(C_2H_2)$. The $[\{H_2C(3,5\text{-}(CH_3)_2Pz)_2\}Ag(C_2H_2)][SbF_6]$ and $[Ph_2B(3\text{-}(CF_3)Pz)_2]Ag(C_2H_2)$ also show analogous features at silver. The anionic but weakly coordinating ligand $[Ph_2B(3\text{-}(CF_3)Pz)_2]^-$ therefore appears to produce the same net result as the neutral and electron-rich $H_2C(3,5\text{-}(CH_3)_2Pz)_2$ on the bond distances and angles associated with copper(I) or silver(I).

`

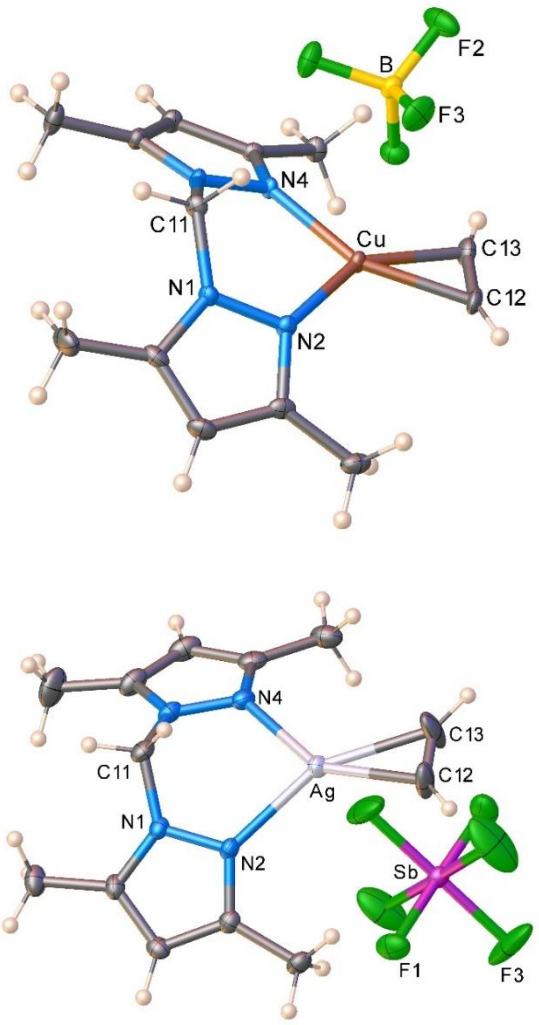

Figure 3.2. 7. Molecular structures of [{$H_2C(3,5\text{-}(CH_3)_2Pz)_2$}$Cu(C_2H_2)$][$BF_4$] (**64**) and [{$H_2C(3,5\text{-}(CH_3)_2Pz)_2$}$Ag(C_2H_2)$][$SbF_6$] (**65**)

We also managed to characterize [$HB(3,5\text{-}(CF_3)_2Pz)_3$]$Cu(C_2H_2)$ (**66**) that has a highly fluorinated tris(pyrazolyl)borate supporting ligand, [$HB(3,5\text{-}(CF_3)_2Pz)_3$]$^-$ using single-crystal X-ray crystallography (Figure 3.2.5). Interestingly, [$HB(3,5\text{-}(CF_3)_2Pz)_3$]$Cu(C_2H_2)$ is the first four-coordinate, Cu(η^2-HC≡CH) complex with structural data reported so far. It has a tetrahedral metal site. The copper atom and the centroid of the acetylene group sit on a crystallographic mirror plane. Basic structural features are similar between

`

these copper(I) complexes and the analogous $[HB(3,5\text{-}(CF_3)_2Pz)_3]Ag(C_2H_2)$ (**41**), but as expected **66** has relatively shorter M-N and M-C distances relative to those of **5** with the larger metal ion.

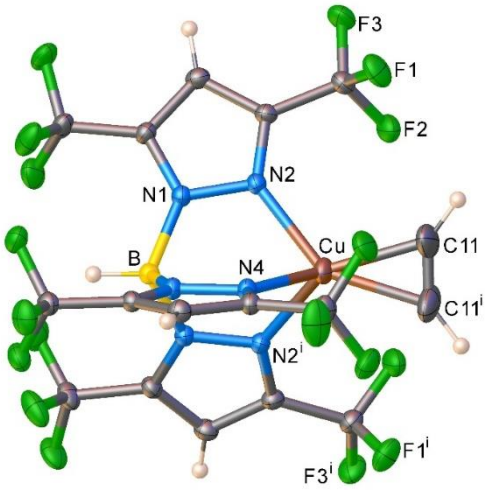

Figure 3.2. 8. Molecular structure of $[HB(3,5\text{-}(CF_3)_2Pz)_3]Cu(C_2H_2)$ (**66**).

The molecular structures of $[HB(3\text{-}(CF_3),5\text{-}(Ph)Pz)_3]Cu(C_2H_2)$ (**67**) and $[HB(3\text{-}(CF_3),5\text{-}(Ph)Pz)_3]Ag(C_2H_2)$ (**68**) have also been investigated using X-ray crystallography. Unfortunately, the M(η^2-HC≡CH) moieties of these molecules suffer significant positional disorder and therefore are not suitable for the analysis of metrical parameters. We have also observed a similar disorder in copper and silver ethylene complexes of the analogous tripodal scorpionates.[9, 239] These molecules possess pockets that allow significant degrees of free motion for the small π-ligands bonded to the metal sites. Nevertheless, basic structural features and atom connectivities of **67** and **68** are clear and indicate the presence of η^2-(HC≡CH) moieties, consistent with the spectroscopic data, and tetrahedral metal sites.

`

As noted above, X-ray crystallographic data on a limited number of copper(I) and silver(I) acetylene complexes are available for comparison. The C≡C bond distance of those compounds and the five uncovered in this work (Table 3.2.2) range from 1.092(7) Å in **7**[Al(OC(CF_3)$_3$)$_4$][224] to 1.227(4) Å in Cu_2(μ-[4-Br-3,5-(CF_3)$_2$Pz])$_2$(C_2H_2)$_2$ (**35**).[167] The C≡C bond distance of Cu(I) and Ag(I) bound acetylene complexes is expected to be longer than that of the free acetylene (which is 1.20286(3) Å based on gas-phase experimental data[232] and 1.193(6) Å from neutron diffraction data on solid acetylene),[185] as both the s-donation and p-backdonation interactions between the metal and acetylene causes a reduction in CC bond-order, and a lengthening of the C≡C bond distance than that of the free acetylene. The Raman and IR data (Table 3.2.1) also support this expectation. However, most of the metal bound C≡C bond distances of these silver and copper acetylene complexes resulting from X-ray crystallographic studies (Table 3.2.2) are lower than that of the free ligand. As Krossing, Scherer and co-workers have pointed out, this apparent contradiction is a result of systematic errors associated with the measurement.[224] In small molecules involving multiple covalent bonds between light atoms, libration effects, incomplete deconvolution of thermal smearing, and anisotropy of the electron density tend to produce bond distances that are too short. Furthermore, most of these C≡C bond distance changes as a result of Ag(I) and Cu(I) coordination are also expected to be small and they are often overshadowed by the relatively high estimated standard deviations (esds) associated with the measurement and are not significantly different at the 3σ limit of estimated standard deviations. Therefore, acetylene C≡C bond distances based solely on

`

routine X-ray crystallography are not suitable for discussions of metal-ligand bonding in most Cu(I) and Ag(I) complexes, and to parse out the metal and supporting ligand effects on the acetylene moiety. Similar issues have been noted also with ethylene complexes, especially involving silver(I).[25, 240]

Table 3.2.2 also includes structural data on a select group of Cu(I) and Ag(I) η^2-ethylene complexes. With the availability of the analogous acetylene complexes, it is now possible to make a meaningful comparison between the two families. As expected, and despite the issues noted above with CC bond distances based on routine crystallography, the metal-bound acetylene bond distances are significantly shorter than the related ethylene bond lengths. The Cu-C and Cu-N bond distances are also shorter in the copper(I) acetylene complexes compared to their ethylene analogs. Interestingly, however, Ag-N and Ag-C distances are essentially the same between the two families. It would be interesting to see if this difference holds true also for a larger dataset.

Density Functional Theory (DFT) calculations at the relativistic ZORA-BP86-D3/TZ2P level (see computational details in the Supporting Information) were carried out to understand the chemical bonding between the scorpionate-M moieties and acetylene in the above-described LM-(C_2H_2) complexes (L = supporting ligand; M = Cu, Ag). To this end, the combination of the Energy Decomposition Analysis (EDA) and the Natural Orbitals for Chemical Valence (NOCV) methods was applied to gain a detailed quantitative insight into the interaction between the LM and C_2H_2 fragments. From the data in Table 3, it becomes clear that in all cases the main contribution to the interaction between the LM and C_2H_2 fragments comes from the electrostatic attractions (measured

`

by the ΔE_{elstat} term), which represents ca. 60% to the total attractive contribution. This indicates that the nature of the LM-acetylene bond is markedly ionic. Despite that, the orbital interactions (measured by the ΔE_{orb} term) are also significant as they contribute ca. 35-40% to the total interaction energy. At variance, the interactions coming from dispersion forces are much less important in the description of the bonding (< 5%) and can be considered negligible.

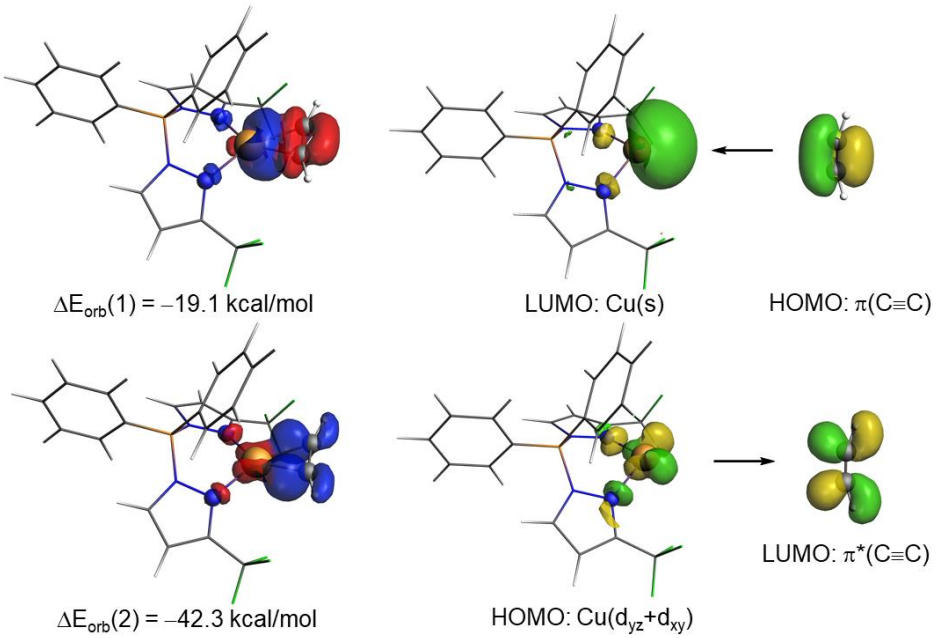

Figure 3.2. 9. Deformation densities and the associated molecular orbitals of the dominant orbital interactions $\Delta E_{orb}(1)$ and $\Delta E_{orb}(2)$ in complex $[Ph_2B(3\text{-}(CF_3)Pz)_2]Cu(C_2H_2)$ (**62**). The color code used to represent the flow of charge is red→blue.

`

Table 3.2. 3. Results of the EDA-NOCV calculations (ZORA-BP86-D3/TZ2P//RI-BP86-D3/def2-TZVPP level, in kcal/mol) on Cu(I)- and Ag(I)-(C_2H_2) complexes using LM and C_2H_2 as fragments (L = supporting ligand).

Compound	**DE_{int}**	**DE_{Pauli}**	**DE_{elstat}**[a]	**DE_{orb}**[a]	**DE_{orb}(1)**	**DE_{orb}(2)**	**DE_{rest}**	**DE_{disp}**[a]
[$H_2B(3,5\text{-}(CF_3)_2Pz)_2$]Cu($C_2H_2$) (**37**)	-55.2	133.9	-109.5 (57.9%)	-73.4 (38.8%)	-19.5	-41.9	-12.0	-6.2 (3.3 %)
[$H_2B(3,5\text{-}(CF_3)_2Pz)_2$]Ag($C_2H_2$) (**37-Ag**)	-32.8	115.1	-93.7 (63.3%)	-50.5 (34.1%)	-16.4	-27.5	-6.6	-3.8 (2.6 %)
[$H_2B(3,5\text{-}(CH_3)_2Pz)_2$]Cu($C_2H_2$) (**37'**)	-56.5	152.3	-119.9 (57.4%)	-83.3 (39.9%)	-18.4	-53.5	-11.4	-5.6 (2.7 %)
[$H_2B(3,5\text{-}(CH_3)_2Pz)_2$]Ag($C_2H_2$) (**37-Ag'**)	-37.1	131.7	-104.0 (61.6%)	-61.8 (36.6%)	-16.8	-35.7	-9.3	-3.0 (1.8 %)
[$Ph_2B(3\text{-}(CF_3)Pz)_2$]Cu($C_2H_2$) (**62**)	-55.3	136.0	-110.4 (57.7%)	-73.4 (38.4%)	-19.1	-42.3	-12.0	-7.5 (3.9 %)
[$Ph_2B(3\text{-}(CF_3)Pz)_2$]Ag($C_2H_2$) (**63**)	-35.9	119.9	-96.8 (62.1%)	-54.7 (35.1%)	-17.1	-28.2	-9.4	-4.3 (2.8 %)
[{$H_2C(3,5\text{-}(CH_3)_2Pz)_2$}Cu($C_2H_2$)]$^+$ (**64+**)	-57.2	131.6	-108.4 (57.4%)	-75.2 (39.8%)	-20.4	-42.4	-12.4	-5.3 (2.8 %)
[{$H_2C(3,5\text{-}(CH_3)_2Pz)_2$}Ag($C_2H_2$)]$^+$ (**65+**)	-37.0	111.6	-91.6 (61.6%)	-54.1 (36.4%)	-18.9	-25.8	-9.4	-2.9 (2.0 %)
[$HB(3,5\text{-}(CF_3)_2Pz)_3$]Cu($C_2H_2$) (6**6**)	-48.6	124.6	-100.1 (57.8%)	-64.7 (37.4%)	-18.6	-35.5	-10.6	-8.4 (4.8 %)
[$HB(3,5\text{-}(CF_3)_2Pz)_3$]Ag($C_2H_2$) (**41**)	-30.9	104.7	-84.3 (62.2%)	-46.4 (34.2%)	-16.6	-21.2	-8.8	-4.9 (3.6 %)
[$HB(3\text{-}(CF_3),5\text{-}(Ph)Pz)_3$]Cu($C_2H_2$) (**67**)	-48.6	127.6	-102.0 (57.9%)	-66.1 (37.5%)	-18.0	-37.5	-10.6	-8.1 (4.6 %)
[$HB(3\text{-}(CF_3),5\text{-}(Ph)Pz)_3$]Ag($C_2H_2$) (**68**)	-30.8	109.0	-87.1 (62.3%)	-48.0 (34.3%)	-16.1	-23.4	-8.5	-4.7 (3.4 %)
[Cu(C_2H_2)]$^+$ (**72+**)	-64.7	92.1	-86.8 (55.3%)	-68.4 (43.6%)	-20.7	-30.9		-1.7 (1.1 %)
[Ag(C_2H_2)]$^+$ (**73+**)	-39.8	68.6	-63.2 (58.3%)	-44.5 (41.1%)	-9.4	-25.1		-0.7 (0.6 %)

[a] The percentage values within parenthesis give the contribution to the total attractive interactions, $\Delta E_{elstat} + \Delta E_{orb} + \Delta E_{disp}$

`

The NOCV extension of the EDA method allows us to not only identify but also quantify the main orbital interactions contributing to the total DE_{orb} term. According to the NOCV method, two main donor-acceptor orbital interactions dominate the orbital interactions in these acetylene complexes. On one hand, the s-donation from the doubly-occupied π(C≡C) molecular orbital of the acetylene ligand to the empty s atomic orbital of the transition metal (denoted as $\Delta E_{orb}(1)$) and, on the other hand, the backdonation from a doubly-occupied d atomic orbital of the transition metal to the vacant π*(C≡C) molecular orbital of acetylene (denoted as $\Delta E_{orb}(2)$, see Figure 3.2.9 for complex **62**). Interestingly, our NOCV calculations indicate that, in all cases, the backdonation from the transition metal fragment is significantly stronger (ca. twice as strong) than the donation from the acetylene ligand ($\Delta E_{orb}(2) > \Delta E_{orb}(1)$), regardless of the transition metal and the supporting ligand. In addition, our EDA-NOCV calculations confirm that both orbital interactions are stronger (in particular, the LM→ π*(C≡C) backdonation) in the Cu(I)-complexes as compared to their Ag(I)-analogs, which is in agreement the above-commented weaker σ-bonding and π-backbonding ability of Ag(I) as compared to copper(I).[231] Despite that, the bonding situation in these acetylene complexes can be safely described in terms of the Dewar-Chatt-Duncanson model involving two donor-acceptor interactions (s-donation from the acetylene ligand and π-backdonation from the transition metal fragment).

Interesting trends emerge from a closer inspection of the data gathered in Table 3.2.3. First, when comparing the copper complexes with their silver counterparts, it is found that, regardless of the supporting ligand, the interaction

`

between the transition metal fragment and the acetylene ligand is clearly stronger in the corresponding copper complexes ($\Delta\Delta E_{int}$ ~ 20 kcal/mol). This is consistent with above-commented higher NMR-downfield shifts (or redshifts of the C≡C stretch), with respect to free acetylene, observed experimentally for the copper complexes. According to the data in Table 3.2.3, the enhanced interaction in the copper(I) complexes is the result of an enhancement of all the main attractive interactions (ΔE_{elstat}, ΔE_{orb} and $\Delta E_{orb}(2)$) as compared to the corresponding silver(I) complexes. This finding suggests that the observed experimental shifts of these mono-acetylene complexes are closely related to the computed interaction energies (as well as their main energy contributors). To our delight, we found that indeed good linear correlations are obtained when plotting these experimental values versus not only the computed total interaction energies (ΔE_{int}) but also their main EDA-NOCV contributors (see Figure 6 for the linear relationships involving the ^{13}C-NMR shifts, Dd). From the data in Figure 6, there appears to exist a limit defining the observed shift in the ^{13}C-NMR spectra with respect to free acetylene: while complexes having a LM-(C_2H_2) interaction $DE_{int} \geq$ -40 kcal/mol lead to a positive (i.e., downfield) shift with respect to free acetylene (Dd > 0 ppm), complexes exhibiting lower LM-(C_2H_2) interaction energies provoke the opposite (i.e., upfield shift) effect ($\Delta\delta$ < 0 ppm).

`

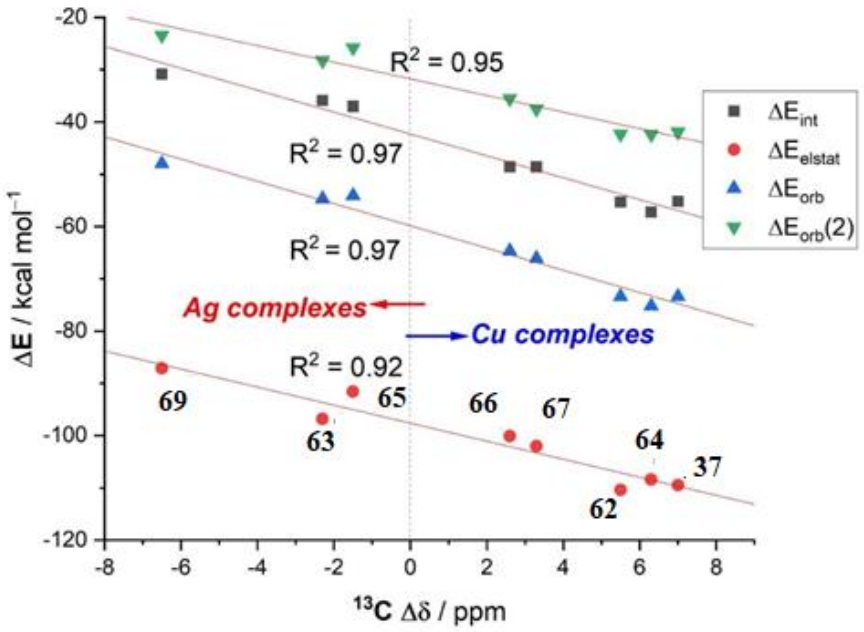

Figure 3.2. 10. Correlations between the experimental ^{13}C-NMR shifts of the acetylene carbon atom in LM-(C_2H_2) complexes with respect to free acetylene ($\Delta\delta$) versus the computed EDA-NOCV energy terms.

Data in Table 3 also indicates that the nature of the supporting ligand also affects the LM-(C_2H_2) interaction. Regardless of the involved transition metal, it is found that complexes having a bidentate bis(pyrazolyl)borate/methane supporting ligand (complexes **37**, **37-Ag**, **62**, **63**, **64+**, **65+**) exhibit stronger LM-(C_2H_2) interactions than the analogous systems having a tridentate tris(pyrazolyl)borate ligand (complexes **41**, **66**, **67**, **68**). For instance, when comparing bidentate complexes **37** or **37-Ag** with their tridentate counterparts **66** or **41**, it becomes clear that the weaker interaction computed for the latter complexes finds its origin in the lower electrostatic and orbital (mainly the LM→ π^*(C≡C) backdonation, $\Delta E_{orb}(2)$) interactions computed for these species. Therefore, it can be concluded that supporting ligands having a lower

`

number of donor sites lead to stronger LM-(C_2H_2) interactions. This is also supported by the calculations on the naked $[Cu(C_2H_2)]^+$ and $[Ag(C_2H_2)]^+$ cations, which exhibit the highest ΔE_{int} values of their corresponding series (see Table 3.2.3). Furthermore, it is found that the replacement of bidentate fluorinated bis(pyrazolyl)borate ligand (which is anionic) by the analogous non-fluorinated and neutral bis(pyrazolyl)methane ligand provokes an almost negligible effect on the LM-(C_2H_2) interaction (e.g., compare **37** and **64+** or **37-Ag** and **65+**).

We have also examined the C≡C bond distance and the C≡C stretching frequency of the copper(I) and silver(I) complexes, computationally. The expected changes to the CC distance are especially useful considering the challenges associated with measuring this parameter precisely noted above. Table 3.2.4 shows the computed C≡C distances and the corresponding stretching frequencies for the considered Cu(I) and Ag(I)-complexes. From the data in Table 3.2.4, it becomes evident that, in all cases, the Cu(I)-complexes exhibit longer C≡C distances than their corresponding Ag(I)-analogs, which is translated into a higher redshift of the C≡C stretching frequency. This is therefore fully consistent with the experimental findings and with the higher LM-(C_2H_2) interaction energies computed for the Cu(I)-complexes as compared to their Ag(I)-congeners (see above). For this reason, it is not surprising that a very good linear correlation was found when plotting the computed distances vs the shift in the ν(C≡C) stretching mode with respect to free acetylene (correlation coefficient of 0.98, see Figure 3.2.7). In addition, data presented in

`

Table **3**.2.4 show that fluorinated substituents on the supporting ligand L have a noticeable effect on ν(C≡C) (see for example **37** vs **37'**; **37-Ag** vs **37-Ag'**).

Table 3.2. 4. Computed C≡C bond lengths and corresponding stretching frequencies in the Cu(I)- and Ag(I)-scorpionate complexes. All data have been computed at the RI-BP86/def2-TZVPP level. $\Delta\bar{\upsilon}_{C\equiv C} = \bar{\upsilon}_{C\equiv C}$ (metal complex) - $\bar{\upsilon}_{C\equiv C}$ (free acetylene)

Compound	**r (C≡C) / Å**	**$\bar{\upsilon}_{C\equiv C}$ / cm^{-1}**	**$\Delta\bar{\upsilon}_{C\equiv C}$ / cm^{-1}**
[$H_2B(3,5\text{-}(CF_3)_2Pz)_2$]Cu($C_2H_2$) (**37**)	1.247	1811	-196
[$H_2B(3,5\text{-}(CF_3)_2Pz)_2$]Ag($C_2H_2$) (**37-Ag**)	1.240	1835	-172
[$H_2B(3,5\text{-}(CH_3)_2Pz)_2$]Cu($C_2H_2$) (**37'**)	1.255	1778	-229
[$H_2B(3,5\text{-}(CH_3)_2Pz)_2$]Ag($C_2H_2$) (**37-Ag'**)	1.248	1798	-209
[$Ph_2B(3\text{-}(CF_3)Pz)_2$]Cu($C_2H_2$) (**62**)	1.248	1808	-199
[$Ph_2B(3\text{-}(CF_3)Pz)_2$]Ag($C_2H_2$) (**63**)	1.242	1829	-178
[{$H_2C(3,5\text{-}(CH_3)_2Pz)_2$}Cu($C_2H_2$)]$^+$ (**64+**)	1.249	1806	-201
[{$H_2C(3,5\text{-}(CH_3)_2Pz)_2$}Ag($C_2H_2$)]$^+$ (**65+**)	1.240	1836	-171
[$HB(3,5\text{-}(CF_3)_2Pz)_3$]Cu($C_2H_2$) (**66**)	1.241	1841	-166
[$HB(3,5\text{-}(CF_3)_2Pz)_3$]Ag($C_2H_2$) (**41**)	1.235	1861	-146
[$HB(3\text{-}(CF_3),5\text{-}(Ph)Pz)_3$]Cu($C_2H_2$) (**67**)	1.242	1833	-174
[$HB(3\text{-}(CF_3),5\text{-}(Ph)Pz)_3$]Ag($C_2H_2$) (**68**)	1.237	1852	-155

`

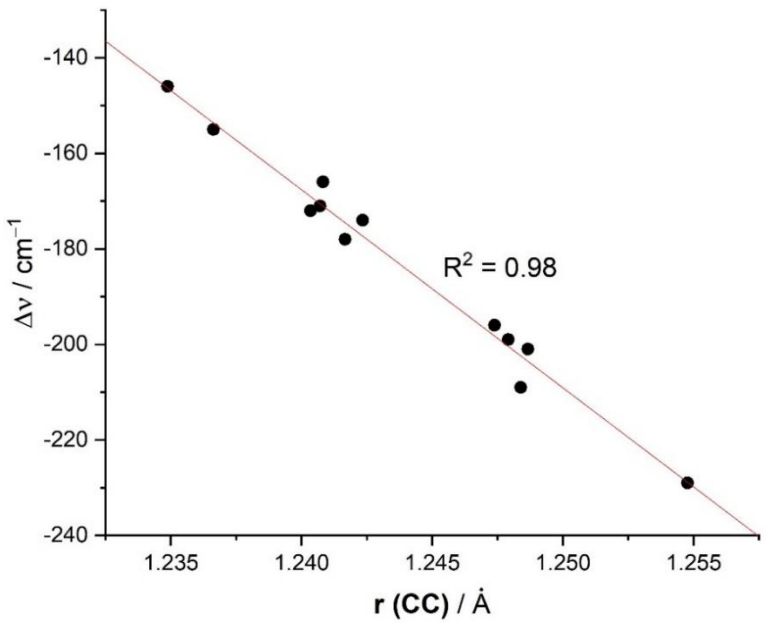

Figure 3.2. 11. Plot of the computed C≡C bond distances versus the shift of the ν(C≡C) stretching frequency (with respect to free acetylene).

Finally, we were curious to analyze the nature of the weak yet noticeable interaction between one of the phenyl groups attached to the boron atom and the transition metal in complexes **62** and **63** (see above). The NCIPLOT[241] method clearly confirms the occurrence of a significant noncovalent attractive interaction (greenish surface in Figure 8) between this aryl group and the transition metal. According to the Natural Orbital Bond (NBO)[242] method, this stabilizing noncovalent interaction finds its origin in the donation of electron density from the closest π(C=C) molecular orbital of the phenyl group to the vacant s atomic orbital of the transition metal (associated stabilizing energy, $\Delta E^{(2)}$ = -1.2 and -1.1 kcal/mol, for complexes **62** and **63**, respectively).

`

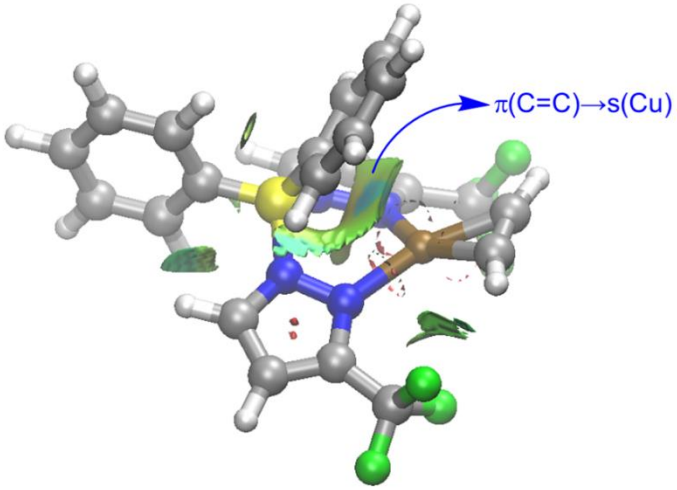

Figure 3.2. 12. Contour plots of the reduced density gradient isosurfaces (density cutoff of 0.04 a.u.) for complex **62** The green surfaces indicate attractive noncovalent interactions.

3.2.4 Summary

In summary, we have presented the isolation and complete characterization of several new acetylene adducts of Cu(I) and Ag(I) supported by $[Ph_2B(3\text{-}(CF_3)Pz)_2]^-$, $[HB(3,5\text{-}(CF_3)_2Pz)_3]^-$, $[HB(3\text{-}(CF_3),5\text{-}(Ph)Pz)_2]^-$, and bis(pyrazolyl)methane $H_2C(3,5\text{-}(CH_3)_2Pz)_2$, as well as details on their ^{1}H, ^{13}C, and ^{19}F NMR spectroscopy, Raman spectroscopy, and X-ray crystallography. According to our DFT calculations, the bonding situation in these complexes can be described in terms of the traditional Dewar-Chatt-Duncanson involving two donor-acceptor interactions, namely s-donation from the acetylene ligand to the transition metal and σ-backdonation from the transition metal fragment to the π*(C≡C) molecular orbital of acetylene (the latter being markedly stronger than the former). Interestingly, the copper complexes exhibit a downfield shift for acetylenic carbons in their ^{13}C NMR spectra and a more notable reduction in $\bar{\upsilon}_{C\equiv C}$ relative to the free acetylene. This can be ascribed to

`

a stronger interaction between the transition metal fragment and the acetylene ligand in the Cu(I)-complexes than that in their Ag(I)-counterparts as confirmed by our EDA-NOCV calculations ($\Delta\Delta E_{int}$ ~ 20 kcal/mol). Furthermore, it is found that while the replacement of bidentate fluorinated bis(pyrazolyl)borate ligand by the analogous non-fluorinated bis(pyrazolyl)methane ligand provokes an almost negligible effect on the LM-(C_2H_2) interaction, the related tridentate tris(pyrazolyl)borate supporting ligand weakens the LM-(C_2H_2) interaction, which is reflected into less significant NMR/Raman shifts. Molecules presented herein represent the largest collection of isolable copper(I) and silver(I) complexes featuring the terminal, η^2-HC≡CH ligand. We believe that the contents of the present work contribute significantly to the development of acetylene chemistry.

`

Chapter 4

Isolable Copper(I) η^2-Cyclopropene Complexes

Anurag Noonikara Poyil, Shawn G. Ridlen, H. V. Rasika Dias

(Part of this work has been published in *Inorg. Chem.* **2020**, *59*, 17860-17865)[109]

`

4.1 Abstract

Treatment of bis(pyrazolyl)borate ligand supported [$H_2B(3,5\text{-}(CF_3)_2Pz)_2$]Cu(NCMe) with 1,2,3-trisubstituted cyclopropenes produced thermally stable copper(I) η^2-cyclopropene complexes amenable to detailed solution and solid-state analysis. The [$H_2B(3,5\text{-}(CF_3)_2Pz)_2$]Cu(NCMe) also catalyzed [2+1]-cycloaddition chemistry of terminal and internal alkynes with ethyl diazoacetate affording cyclopropenes, including those used as ligands in this work. The tris(pyrazolyl)borate [$H_2B(3,5\text{-}(CF_3)_2Pz)_2$]Cu(NCMe) is a competent catalyst for this process as well. The treatment of [$HB(3,5\text{-}(CF_3)_2Pz)_3$]Cu with ethyl 2,3-diethylcycloprop-2-enecarboxylate substrate gave an O-bonded rather than a η^2-cyclopropene copper complex.

4.2 Introduction

Cyclopropenes are highly strained, small carbocyclic alkenes with a long history.[243] They have been investigated extensively during past decades and found to be impactful in multiple fields ranging from organic synthesis,[134, 244-246] materials chemistry,[134, 247, 248] horticulture,[249, 250] biochemistry and natural product chemistry to the bioorthogonal labelling reactions.[251, 252] For example, cyclopropenes are energy packed organic synthones (with strain energy of over 200 kJ mol^{-1})[253] that undergo reactions such as addition, substitution, isomerization, and metatheses often not seen in the related non-strained olefins.[134, 244, 245] 1-Methyl cyclopropene is an economically important ethylene antagonist utilized widely to prolong the shelf-life of fruits, vegetables, and cut flowers.[249, 250] Cyclopropenes are popular mini-tags in chemical biology to label biomolecules in live cells.[251, 254, 255]

`

In comparison to the diverse uses of cyclopropenes, synthetic routes to cyclopropenes are relatively limited. The metal catalyzed [2+1] cycloaddition of diazoalkanes with alkyne substrates is perhaps the most promising and leading route. Catalysts based on metals such as rhodium,[256-258] copper,[38, 133, 259-262] silver,[39, 133] cobalt[263] and a few others[264-266] are useful for this purpose with even heme proteins and metal foils entering the fray in the search for better catalysts.[133, 267] Metals also play a key role in cyclopropene utilizations as a synthone in organic chemistry, which either proceed with the preservation or opening of the three-membered carbocyclic ring.[245, 246, 268] Although the commonly invoked intermediates in quite a few of these metal mediated processes are metal-cyclopropene complexes,[244, 245] many of them are too reactive for direct investigations, and therefore reliable structural or spectroscopic information have been extremely limited.[245, 246, 268] Most notably, despite the multiple roles copper play in cyclopropene chemistry from the synthesis,[38, 133, 246, 259-262, 269] ring opening chemistry,[245, 270-273] carbometallations,[268, 274] to being the target of ethylene antagonists (because of the ethylene binding copper-cofactor in plants),[58, 249, 275] there are no structurally authenticated η^2-cyclopropene complexes of copper to date.[69] Herein we report the isolation and complete characterization of three copper(I) η^2-cyclopropene complexes, as well as a useful copper mediated route to cyclopropenes.

`

4.3 Results and Discussions

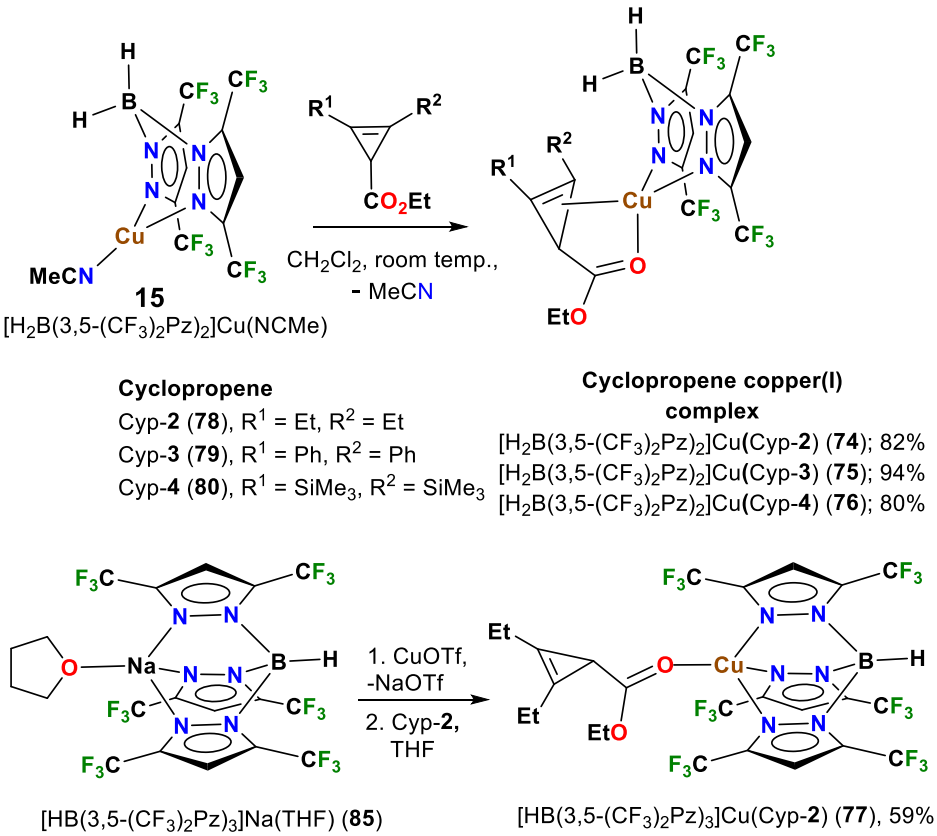

Figure 4. 1. Synthesis of copper(I) cyclopropene complexes

Treatment of $[H_2B(3,5\text{-}(CF_3)_2Pz)_2]Cu(NCMe)$ (**15**)[66] with cyclopropene Cyp-**2** (**78**) in dichloromethane at room temperature led to the displacement of acetonitrile ligand from copper and the formation of copper η^2-cyclopropene complex $[H_2B(3,5\text{-}(CF_3)_2Pz)_2]Cu(Cyp\text{-}2)$ (**74**) in 82% isolated yield (Figure 4.1). It is a colorless, thermally stable solid that can be handled in air for short periods without decomposition. The room temperature $^{13}C\{^1H\}$ NMR spectrum of $[H_2B(3,5\text{-}(CF_3)_2Pz)_2]Cu(Cyp\text{-}2)$ in $CDCl_3$ shows a peak at δ 91.1 ppm corresponding to the carbons of the copper bound olefinic moiety of cyclopropene ligand, which is an upfield shift (Δδ of 15.4 ppm; Δδ = δ free

`

ligand - δ metal complex) compared to the corresponding resonance of the free ligand Cyp-**2** (δ 106.5 ppm). The early transition metal η^2-cyclopropene complexes such as Cp*Mo(CO)$_2$(2,3-Ph$_2$-2-cyclopropene-1-carboxylate) (**86**),[276] [HB(3,5-(Me)$_2$Pz)$_3$]Nb(C$_3$H$_4$)(py)(MeCCMe) (**87**)[277] and W(3,3-Ph$_2$-cyclopropene)Cl$_2$(NPh)[P(OMe$_3$)]$_2$ (**88**) [278] with stronger metal-cyclopropene bonds display their metal bound cyclopropene carbon chemical shifts at significantly greater upfield regions: δ 71.91, 58.64 ppm; δ 74.5, 68.4 ppm; and δ 64.8 ppm, respectively. The carbonyl carbon signal of [H$_2$B(3,5-(CF$_3$)$_2$Pz)$_2$]Cu(Cyp-**2**) also shows a small but noticeable 4 ppm shift relative to that of the free ligand Cyp-**2**.

We have also synthesized two other copper(I) cyclopropene complexes using a similar route (Scheme 4.1). The [H$_2$B(3,5-(CF$_3$)$_2$Pz)$_2$]Cu(Cyp-**3**) (**75**) and [H$_2$B(3,5-(CF$_3$)$_2$Pz)$_2$]Cu(Cyp-**4**) (**76**) has been obtained in 94% and 80% yields from a reaction between **15** and the corresponding Cyp-**3** and Cyp-**4** in dichloromethane. Compounds [H$_2$B(3,5-(CF$_3$)$_2$Pz)$_2$]Cu(Cyp-**3**) and [H$_2$B(3,5-(CF$_3$)$_2$Pz)$_2$]Cu(Cyp-**4**) also show notable upfield shifts of the olefinic carbon resonances (Δδ of 21.4 and 30.2 ppm, respectively) relative to those of the free ligands Cyp-**3** and Cyp-**4**, indicating the presence of copper-olefin interactions in solution.

`

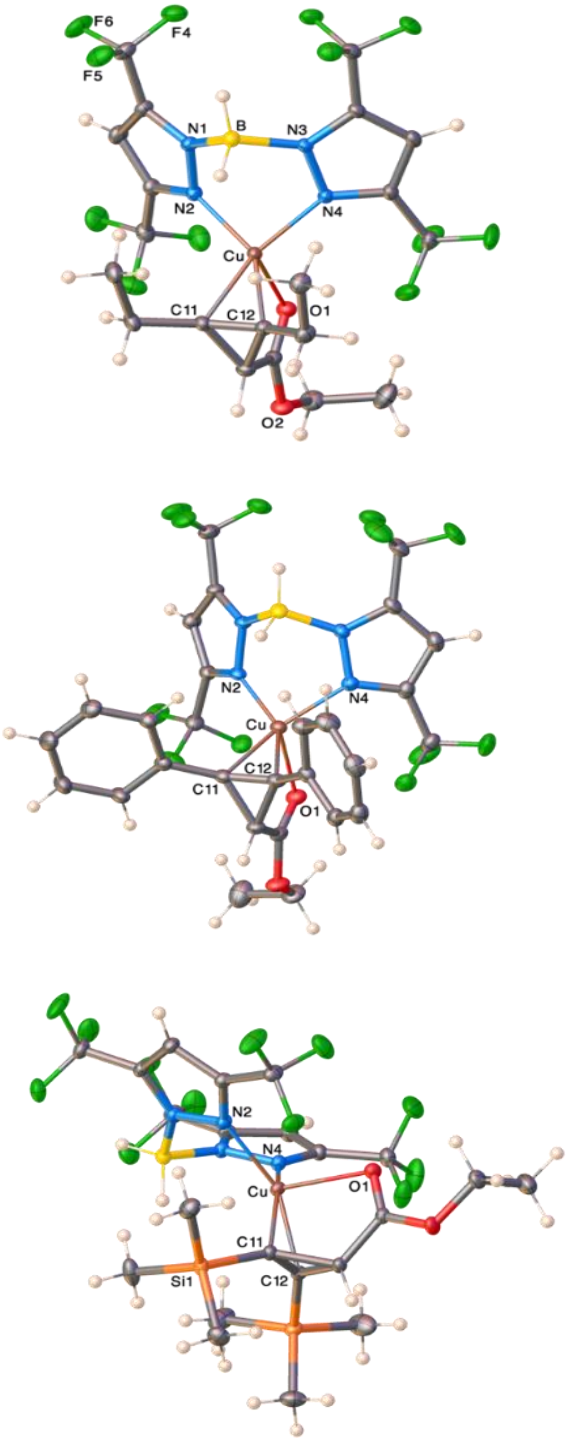

Figure 4. 2. Molecular structures of [$H_2B(3,5\text{-}(CF_3)_2Pz)_2$]Cu(Cyp-**2**) (**74**), [$H_2B(3,5\text{-}(CF_3)_2Pz)_2$]Cu(Cyp-**3**) (**75**) and [$H_2B(3,5\text{-}(CF_3)_2Pz)_2$]Cu(Cyp-**4**) (**76**), from left to right.

`

Copper(I) cyclopropene complexes $[H_2B(3,5\text{-}(CF_3)_2Pz)_2]Cu$(Cyp-**2**), $[H_2B(3,5\text{-}(CF_3)_2Pz)_2]Cu$(Cyp-**3**) and $[H_2B(3,5\text{-}(CF_3)_2Pz)_2]Cu$(Cyp-**4**) have been characterized by X-ray crystallography (Figure 4.2). Selected bond distances and angles are summarized in Table 4.1. Molecular structures show that the cyclopropene ligands are bonded to copper atoms in η^2-fashion. Interestingly, the carbonyl group of the CO_2Et moiety also coordinates to copper, albeit weakly as evident from the relatively long Cu-O bond distances (2.2625(10)-2.2983(7) Å) compared to typical Cu-O(ester) separations of ~2.00 Å (Table S2)[69] as well as 1.954 Å of $[HB(3,5\text{-}(CF_3)_2Pz)_3]Cu$(Cyp-**2**) noted below, and nearly trigonal planar copper sites with sum of angles (excluding oxygen) at copper of ~354-356º compared to 360º and 328º for ideal trigonal planar and tetrahedron arrangements, respectively. The copper bound C=C distances (1.3481(12), 1.3583(18) and 1.3659(11) Å) display a significant lengthening relative to typical C=C distances of free cyclopropenes (e.g., 1.296 Å for parent cyclopropene[279] and 1.2968(12) Å for Cyp-**3** (see supporting information for the crystal structure)). The olefinic carbon centers of copper coordinated cyclopropene ligands in $[H_2B(3,5\text{-}(CF_3)_2Pz)_2]Cu$(Cyp-**2**), $[H_2B(3,5\text{-}(CF_3)_2Pz)_2]Cu$(Cyp-**3**) and $[H_2B(3,5\text{-}(CF_3)_2Pz)_2]Cu$(Cyp-**4**) show clear pyramidalizations with sum of the angles of 340-343º at olefinic carbons (not involving copper).

`

Table 4. 1. Selected bond distances (Å) and angles (º) of copper(I) complexes $[H_2B(3,5\text{-}(CF_3)_2Pz)_2]Cu$(Cyp-**2**) (**74**), $[H_2B(3,5\text{-}(CF_3)_2Pz)_2]Cu$(Cyp-**3**) (**75**), $[H_2B(3,5\text{-}(CF_3)_2Pz)_2]Cu$(Cyp-**4**) (**76**) and $[HB(3,5\text{-}(CF_3)_2Pz)_3]Cu$(Cyp-**2**) (**77**) [a].

Parameter	$[H_2B(3,5\text{-}(CF_3)_2Pz)_2]Cu$(Cyp-**2**) (**74**)	$[H_2B(3,5\text{-}(CF_3)_2Pz)_2]Cu$(Cyp-**3**) (**75**)	$[H_2B(3,5\text{-}(CF_3)_2Pz)_2]Cu$(Cyp-**4**) (**76**)	$[HB(3,5\text{-}(CF_3)_2Pz)_3]Cu$(Cyp-**2**) (**77**)[a]
C=C	1.3481(12)	1.3583(18)	1.3659(11)	1.269(4) *1.286(4)*
Cu-C	2.0303(9) 2.0185(8)	2.0266(13) 2.0187(13)	2.0306(8) 2.0311(8)	
Cu-O	2.2983(7)	2.2625(10)	2.2818(6)	1.956(4) *1.951(2)*
Cu-N	2.0036(7) 2.0051(7)	1.9964(11) 1.9917(11)	2.0263(7) 2.0056(7)	2.074(2) 2.050(2) 2.108(2) *2.054(2)* *2.047(2)* *2.116(2)*
C-C(H)-C (interior cyclopropene)	52.66(5)	53.12(8)	52.97(5)	49.35(19) *49.92(18)*
Cu-C=C-R (dihedral)	123.63 123.20	121.07 121.73	123,22 122.63	
Σ angles at Cu omitting O	354.55	356.19	354.48	271.99 *271.81*
Σ angles at C(=C) (not involving Cu)	342.79 342.49	340.33 342.99	339.91 340.94	360.00 359.98 *359.91* *360.00*

[a] Data for second molecules in the asymmetric unit *in italics*

There are no copper cyclopropene η^2-complexes for comparison. However, search of CSD[69] revealed that structural data are available for a few

`

transition metal η^2-cyclopropenes complexes,[276-278, 280-290] and they all show much longer cyclopropene C=C bond distances (with an average of 1.448 Å for 14 molecules spanning 1.50(1) Å for a Pt(0) complex $(PPh_3)_2Pt$(1,2-Me_2-cyclopropene) (**89**)[280] to 1.407 Å for a Mo(II)[276] adduct, Cp*$Mo(CO)_2$(2,3-Ph_2-2-cyclopropene-1-carboxylate)) (**90**) relative to the corresponding bond distance in $[H_2B(3,5\text{-}(CF_3)_2Pz)_2]$Cu(Cyp-**2**), $[H_2B(3,5\text{-}(CF_3)_2Pz)_2]$Cu(Cyp-**3**) and $[H_2B(3,5\text{-}(CF_3)_2Pz)_2]$Cu(Cyp-**4**) of 1.3481(12), 1.3583(18) and 1.3659(11) Å, respectively. This indicates that compared to these early transition metal complexes, the σ/π-interaction between d^{10}-copper(I) and cyclopropenes in $[H_2B(3,5\text{-}(CF_3)_2Pz)_2]$Cu(Cyp-**2**), $[H_2B(3,5\text{-}(CF_3)_2Pz)_2]$Cu(Cyp-**3**) and $[H_2B(3,5\text{-}(CF_3)_2Pz)_2]$Cu(Cyp-**4**) are weaker. The cyclopropene interior C-C(H)-C bond angle involving the bridge-head carbon is another indicator of relatively weaker interaction (and greater ring-strain) in the copper complexes which is at ~53º while the corresponding angle is much larger in the early transition metal complexes noted above (range from 55-59º with an average of 57º), approaching typical cyclopropane ring angle of 60º from the starting 50.4º of free cyclopropene.[279] These observations are not surprising since, unlike early transition metal ions, copper(I) is not a metal known for strong π-backbonding.[113] The highly fluorinated supporting ligand on copper makes the π-backbonding even weaker in these complexes (although it can enhance the olefin→Cu electrostatic interactions and Lewis acidity at Cu). The ^{13}C NMR chemical shifts described above are also consistent with bond distance and angle changes. We have also collected Raman and IR data of the $[H_2B(3,5\text{-}(CF_3)_2Pz)_2]$Cu(Cyp-**2**), $[H_2B(3,5\text{-}(CF_3)_2Pz)_2]$Cu(Cyp-**3**) and $[H_2B(3,5\text{-}(CF_3)_2Pz)_2]$Cu(Cyp-**4**) complexes (see ESI) but, unfortunately, the assignment

`

of cyclopropene C=C stretch was obscured by the presence of aromatic C=C and C=N stretching signals in the same region.

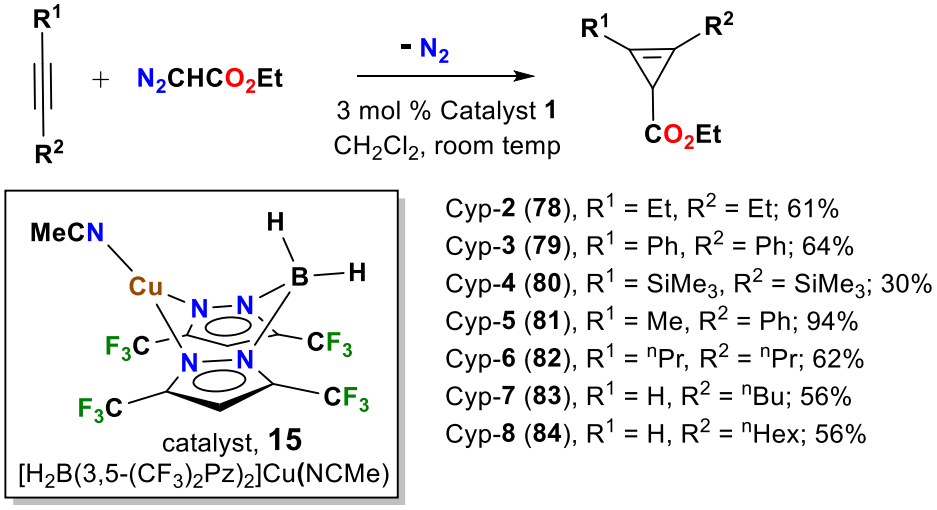

Figure 4. 3. The $[H_2B(3,5\text{-}(CF_3)_2Pz)_2]Cu(NCMe)$ (**15**) catalyzed cyclopropenation of alkynes with ethyl diazoacetate

Considering the importance of new metal mediated synthetic routes to cyclopropenes, we tested the prowess of **15** in cyclopropenation chemistry using internal alkynes and ethyl diazoacetate (EDA) as the carbene source (Scheme 2). The Cyp-**2**, Cyp-**3** and Cyp-**4** used in the copper coordinating chemistry (Scheme 1) were of particular interest. At room temperature, the reaction involving 3 mol% of catalyst **15** (based on EDA) and 1:3 molar ratio of EDA to 3-hexyne produced Cyp-**2** in 61% isolated and 71% NMR yield, while the remaining EDA ended up as diethyl fumarate and maleate. Quite interestingly, copper cyclopropene complex $[H_2B(3,5\text{-}(CF_3)_2Pz)_2]Cu$(Cyp-**2**) can also function as a catalyst remarkably well affording Cyp-**2** over 90% yield. It suggests that $[H_2B(3,5\text{-}(CF_3)_2Pz)_2]Cu$(Cyp-**2**) could play a direct role in

`

cyclopropenation catalytic cycle or as a resting state. These cyclopropene product yields are respectable compared to the yields observed with other copper catalyzed cyclopropenations. Diarylated and disilyl substituted Cyp-**3** and Cyp-**4,** as well as several other cyclopropenes with alkyl-aryl substituent combination or with longer alkyl substituents (e.g., Cyp-**6**) can also be obtained using **15** as the catalyst and the appropriate alkyne substrate. The isolated yield of cyclopropene Cyp-**4**, however, was poor but still better than 18% yield of CuBr mediated route to closely related Cyp-**4** analog.[291]

We then tested the cyclopropenation of terminal alkynes, 1-hexyne and 1-octyne using the same process utilized with internal alkynes to obtain Cyp-**7** and Cyp-**8**. Although the isolated product yields were disappointing initially, analyses of crude reaction mixtures revealed high product yields. It became clear that the issue was the copper mediated decomposition of terminal cyclopropene products during the workup of the reaction mixture rather than with the cyclopropenation step. In fact, a reaction of $[H_2B(3,5\text{-}(CF_3)_2Pz)_2]Cu(NCMe)$ with independently prepared Cyp-**7** and Cyp-**8** in CH_2Cl_2 led to the decomposition of the cyclopropene to yet unidentified products, even above -50 ºC. Copper mediated cyclopropene ring-opening as well as carbometalation chemistry is well-known and the products depend on the nature of the copper source.[268, 270-274] Thus, based on these observations, we improved the procedure by using a slightly larger ratio of alkyne:EDA followed by treatment with H_2S to deactivate the catalyst before the workup of the reaction mixture, which led to Cyp-**7** and Cyp-**8** in 56% and 37% isolated yields, respectively.

`

Challenges with cyclopropenation process of terminal alkynes using $[H_2B(3,5\text{-}(CF_3)_2Pz)_2]Cu(NCMe)$ prompted us to test the more sterically demanding tris(pyrazolyl)borate catalyst $[HB(3,5\text{-}(CF_3)_2Pz)_3]Cu(NCMe)$ (**91**).[19] Gratifyingly, it produced Cyp-**8** in excellent, 93% yield. It could be that the resulting Cyp-**8** is less prone to decomposition by $[HB(3,5\text{-}(CF_3)_2Pz)_3]Cu(NCMe)$ due to the steric crowding at the copper. Interestingly, the cyclopropenation of the internal alkyne, 3-hexyne by $[HB(3,5\text{-}(CF_3)_2Pz)_3]Cu(NCMe)$ was somewhat less effective relative $[H_2B(3,5\text{-}(CF_3)_2Pz)_2]Cu(NCMe)$ under the same conditions (NMR yields of Cyp-**2**: 61% and 71% respectively for the two catalysts), perhaps due to the steric effects. Nevertheless, the differential reactivity is a useful observation and provides opportunities for further catalyst optimizations.

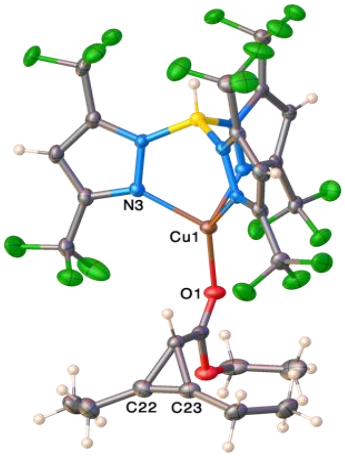

Figure 4. 4. Molecular structure of tris(pyrazolyl)borate ligand supported $[HB(3,5\text{-}(CF_3)_2Pz)_3]Cu(Cyp\text{-}\mathbf{2})$.

Next, we investigated the coordination chemistry of $[HB(3,5\text{-}(CF_3)_2Pz)_3]Cu$ with cyclopropenes. The in-situ generated [HB(3,5-

`

$(CF_3)_2Pz)_3$]Cu with Cyp-**2** afforded a 1:1 cyclopropene complex of copper(I), [HB(3,5-$(CF_3)_2Pz)_3$]Cu(Cyp-**2**) in 59% yield (Scheme 1). The $^{13}C\{^1H\}$ NMR data of [HB(3,5-$(CF_3)_2Pz)_3$]Cu(Cyp-**2**) exhibited only a small change in olefinic carbon resonance (1.6 ppm), in contrast to [H_2B(3,5-$(CF_3)_2Pz)_2$]Cu(Cyp-**2**), indicating less involvement of the olefinic moiety in the adduct formation. Indeed, the X-ray crystal structure of [HB(3,5-$(CF_3)_2Pz)_3$]Cu(Cyp-**2**) revealed it to be a solely O-bonded Cyp-**2** via the ester group rather than an η^2-cyclopropene complex (Figure 2). A comparison of metrical parameters of [HB(3,5-$(CF_3)_2Pz)_3$]Cu(Cyp-**2**) to [H_2B(3,5-$(CF_3)_2Pz)_2$]Cu(Cyp-**2**) summarized in Table 1 nicely illustrates the effect of Cu(I) on the cyclopropene C=C bond, C-C(H)-C angle, as well as the differences between weakly and strongly bound C=O•••Cu bonds of the ester moiety, in the two systems. The C=O stretch of [HB(3,5-$(CF_3)_2Pz)_3$]Cu(Cyp-**2**) in IR displays a 76 cm^{-1} reduction due to this latter interaction, while the corresponding lowering in [H_2B(3,5-$(CF_3)_2Pz)_2$]Cu(Cyp-**2**) is only 34 cm^{-1} (see ESI).

[H_2B(3,5-$(CF_3)_2Pz)_2$]Cu(3-hexyne) + Cyp-**2** ⇌ [H_2B(3,5-$(CF_3)_2Pz)_2$]Cu(Cyp-**2**) + 3-hexyne K_c = 0.12; eq. 1

[H_2B(3,5-$(CF_3)_2Pz)_2$]Cu(Cyp-**2**) + 3-hexyne ⇌ [H_2B(3,5-$(CF_3)_2Pz)_2$]Cu(3-hexyne) + Cyp-**2** K_c = 9.1; eq. 2

[H_2B(3,5-$(CF_3)_2Pz)_2$]Cu(NCMe) + Cyp-**2** ⇌ [H_2B(3,5-$(CF_3)_2Pz)_2$]Cu(Cyp-**2**) + MeCN K_c = 11.0; eq. 3

Considering that copper catalyzed cyclopropenation of alkynes producing cyclopropenes likely involves several ligand exchanges, we also assessed the

`

relative binding affinities of MeCN, Cyp-**2** and 3-hexyne with [H_2B(3,5-(CF_3)$_2$Pz)$_2$]Cu using isolable compounds. Details of [H_2B(3,5-(CF_3)$_2$Pz)$_2$]Cu(3-hexyne) are given in the supporting materials. The relative equilibrium concentrations were measured using NMR spectroscopy at various temperatures. The equilibrium constants K_c for eq. 1 and the control experiment noted in eq. 2 (to ensure equilibrium was achieved under reverse conditions) are 0.12 and 9.1, respectively at 243 K, which are consistent for a system in equilibrium for the forward and reverse directions. The data indicate that the alkyne preferentially binds to copper(I) over the cyclopropene, despite the predisposition of strained alkenes for metal ion coordination. Both the precursor alkyne and product cyclopropene also have a greater affinity to [(CF_3)$_2$Bp]Cu fragment than acetonitrile. For example, K_c for eq. 3 is 11.0 at 243 K.

4.4 Summary

In summary, we have isolated for the first time, a group of copper η^2-cyclopropene complexes using a highly fluorinated, bis(pyrazolyl)borate auxiliary ligand, and a Cu-O bonded linkage isomer using a bulkier tris(pyrazolyl)borate ligand support and characterized them using multiple methods including X-ray crystallography. The cyclopropenes used in this work as well as several others were also obtained in reasonable to excellent yields by the copper catalyzed cyclopropenation process involving the same ligand supports. We are currently probing these interesting complexes more deeply and the chemistry of cyclopropenes with other important metal ions.

`

Chapter 5

Experimental Details

`

5.1 General Methods

All manipulations were carried out under an atmosphere of purified nitrogen using standard Schlenk techniques or in a MBraun glovebox equipped with a -25 °C refrigerator unless otherwise noted. Solvents were purchased from commercial sources, purified before use. NMR spectra were recorded at 25 °C on a JEOL Eclipse 500 spectrometer (^{1}H, 500.16 MHz ^{13}C, 125.78 MHz, and ^{19}F, 470.62 MHz), JEOL Eclipse 400 spectrometer (^{1}H, 500.16 and 399.78 MHz ^{13}C, 125.78 and 100.52 MHz, and ^{19}F, 470.62 and 376.17 MHz) unless otherwise noted. ^{1}H and ^{13}C NMR spectra are referenced to the solvent peak (^{1}H; $CDCl_3$ δ 7.26, CD_2Cl_2 δ 5.32, $(CD_3)_2SO$ δ 2.5, $(CD_3)_2CO$ δ 2.05 ^{13}C; $CDCl_3$ δ 77.16, $(CD_3)_2SO$ δ 39.52, $(CD_3)_2CO$ δ 29.8). ^{1}H NMR coupling constants (J) are reported in Hertz (Hz) and multiplicities are indicated as follows: s (singlet), d (doublet), t (triplet), pent (pentet), m (multiplet), dd (doublet of doublet), pd (pentet of doublet). ^{19}F NMR values were referenced to external $CFCl_3$. Melting points were obtained on a Mel-Temp II apparatus and were not corrected. Elemental analyses were performed using a Perkin-Elmer Model 2400 CHN analyzer. IR spectra were collected at room temperature on a Shimadzu IR Prestige-21 FTIR containing an ATR attachment using pure liquid or solid materials, with instrument resolution at 2 cm^{-1}. Raman data were collected on a Horiba Jobin Yvon LabRAM Aramin Raman spectrometer with a HeNe laser source of 633 nm or on a Thermo Scientific DXR3 Raman microscope with a HeNe laser source of 633 nm by placing pure solid materials on a glass slide. TLC visualization was accompanied by UV light or $KMnO_4$ stains. All other reactants and reagents were purchased from commercial sources. The ethylene used is Chemically pure grade (99.5%) and purchased from AirGas. Heating

`

was accomplished by either a heating mantle or a silicone oil bath. The $[H_2B(3,5\text{-}(CF_3)_2Pz)_2]Cu(NCMe)$ (**1**)[66] and $\{\mu\text{-}[3,5\text{-}(CF_3)_2Pz]Cu\}_3$[166], $[HB(3,5\text{-}(CF_3)_2Pz)_3]Na(THF)$[2], $[HB(3,5\text{-}(CF_3)_2Pz)_3]Cu(C_2H_4)$,[9] $[\{H_2C(3,5\text{-}(CH_3)_2Pz)_2\}Cu(NCMe)][BF_4]$,[229] $[\{H_2C(3,5\text{-}(CH_3)_2Pz)_2\}Ag(C_2H_4)][SbF_6]$,[229], *p*-Tolyl azide, [41, 292] and 2-Diazo-1,1,1-trifluoroethane[293] was prepared according to the literature procedure. All other reactants and reagents were purchased from commercial sources. Acetylene gas was freed from acetone and purified before use.[178] All other reactants and reagents were purchased from commercial sources.

CAUTION: *Thallium compounds are toxic. Care must be taken when manipulating thallium containing materials.*

Due care must be taken when working with acetylene gas. It is known to produce explosive combinations with oxygen, and also form potentially explosive acetylides and other materials with copper salts.[179]

Although we have not experienced problems in the handling of diazo reagents described in this work, care should be taken when working with them due to their potentially explosive nature.[294]

`

5.2 Experimental Section for Chapter 2

5.2.1 Experimental Section for Chapter 2 Part 1

Synthesis of Metal Complexes

$[H_2B(3,5\text{-}(CF_3)_2Pz)_3]Cu(C_2H_4)$ (13): $[(CF_3)_2Bp]Cu(NCMe)$(**1**) (0.15 g, 0.29 mmol) was dissolved in 5 mL dichloromethane and stirred for ~3-5 min while bubbling ethylene. The reaction mixture was concentrated with continuous flow of ethylene and kept at -20 °C to obtain X-ray quality colorless crystals of $[(CF_3)_2Bp]Cu(C_2H_4)$. Yield: 92%. M.P.: 99-105 °C (decomposition). Anal. Calc. $C_{12}H_8BCuF_{12}N_4$: C, 28.23; H, 1.58%; N, 10.97%. Found: C, 27.97%; H, 1.78%; N, 11.28%. ^{1}H NMR ($CDCl_3$): δ (ppm) 6.89 (s, 2H, Pz*H*), 4.69 (s, 4H, C_2H_4), 3.80 (br, 2H, BH_2). ^{19}F NMR ($CDCl_3$): δ (ppm) -59.8 (s), -60.9 (s). $^{13}C\{^1H\}$ NMR ($CDCl_3$): δ (ppm) 142.2 (q, $^2J_{C\text{-}F}$ = 39.6 Hz, C-3/C-5), 139.7 (q, $^2J_{C\text{-}F}$ = 42.0 Hz, C-3/C-5), 120.1 (q, $^1J_{C\text{-}F}$ =268.7 Hz, CF_3), 119.2 (q, $^1J_{C\text{-}F}$ =269.9 Hz, CF_3), 106.3 (C-4), 86.6 (br, C=C). ^{13}C NMR (^{1}H coupled ^{13}C) ($CDCl_3$): δ (ppm) 142.2 (q, $^2J_{C\text{-}F}$ = 43.2 Hz, C-3/C-5), 139.7 (q, $^2J_{C\text{-}F}$ = 45.6 Hz, C-3/C-5), 120.1 (q, $^1J_{C\text{-}F}$ =268.7 Hz, CF_3), 119.2 (q, $^1J_{C\text{-}F}$ =271.1 Hz, CF_3), 106.3 (d, $^1J_{C\text{-}H}$ =187.1 Hz, C-4), 86.9 (t, $^1J_{C\text{-}H}$=160.8 Hz, C=C). IR (cm^{-1}): 2932, 2548 ($\bar{\upsilon}_{B\text{-}H}$), 2398 ($\bar{\upsilon}_{B\text{-}H}$), 1552, 1501, 1426, 1399, 1254, 1174, 1139, 1115, 1099, 1043, 1018, 1003, 960, 954, 897, 828. Raman (cm^{-1}), selected peaks: 1539 (C=C).

$\{[H_2B(3,5\text{-}(CF_3)_2Pz)_3]Cu\}_3$ (14): $[H_2B(3,5\text{-}(CF_3)_2Pz)_3]Cu(C_2H_4)$ (**13**) (0.15 g, 0.29 mmol) was dissolved in 5 mL hexanes and the solvent was distilled off using a short path distillation a apparatus by heating in an oil bath . The product was dissolved in minimum amount of hexanes and kept at -20 °C refrigerator to

`

obtain x-ray quality colorless crystals of {[$H_2B(3,5\text{-}(CF_3)_2Pz)_3$]Cu}$_3$. Yield: 87%. M.P.: 126-129 °C (decomposition in air at this temp.). Anal. Calc. $C_{30}H_{12}B_3Cu_3F_{36}N_{12}$: C, 24.89%; H, 0.84%; N, 11.61%. Found: C, 24.64%; H, 1.24%; N, 11.31%. ^{1}H NMR ($(CD_3)_2SO$): δ (ppm) 7.13 (s, 6H, Pz*H*), 3.60 (br, 6H, BH_2). ^{1}H NMR ($CDCl_3$): δ (ppm) 7.06 (s, 6H, Pz*H*), 4.32 (br, 6H, BH_2). ^{1}H NMR (CD_2Cl_2): δ (ppm) 7.11 (s, 6H, Pz*H*), 4.30 (br, 6H, BH_2). ^{19}F NMR ($(CD_3)_2SO$): δ (ppm) -58.1 (s), -60.3 (s). ^{13}C{^{1}H} NMR ($(CD_3)_2SO$): δ (ppm) 139.7 (q, $^2J_{C\text{-}F}$ = 37.2 Hz, C-3/C-5), 136.0 (q, $^2J_{C\text{-}F}$ = 39.6 Hz, C-3/C-5), 120.4 (q, $^1J_{C\text{-}F}$ =267.5 Hz, CF_3), 119.5 (q, $^1J_{C\text{-}F}$ =268.7 Hz, CF_3), 104.9 (C-4). IR (cm^{-1}): 2969, 2543 ($\bar{\upsilon}_{B\text{-}H}$), 2383 ($\bar{\upsilon}_{B\text{-}H}$), 1556, 1502, 1471, 1387, 1259, 1152, 1148, 1139, 1110, 1096, 1072, 1049, 1037, 1021, 1017, 878, 833. Raman (cm^{-1}) : 2705, 2540, 1760, 1699, 1660, 1553, 1476, 1386, 1258, 1191, 997.

X-ray Data Collection and Structure Determinations

A suitable crystal covered with a layer of hydrocarbon/Paratone-N oil was selected and mounted on a Cryo-loop, and immediately placed in the low-temperature nitrogen stream. The X-ray intensity data were measured at 100(2) K on a Bruker D8 Quest with a Photon 100 CMOS detector equipped with an Oxford Cryosystems 700 series cooler, a graphite monochromator, and a Mo Kα fine-focus sealed tube (λ = 0.71073 Å). Intensity data were processed using the Bruker Apex program suite. Absorption corrections were applied by using SADABS.[295] Initial atomic positions were located by SHELXT,[296] and the structures of the compounds were refined by the least-squares method using SHELXL[297] within Olex2 GUI.[298] All the non-hydrogen atoms were refined anisotropically. The hydrogen atoms of ethylene and BH_2 moieties of [$H_2B(3,5\text{-}$

`

$(CF_3)_2Pz)_3]Cu(C_2H_4)$ and $\{[H_2B(3,5\text{-}(CF_3)_2Pz)_3]Cu\}_3$ were located in difference Fourier maps, included and refined freely with isotropic displacement parameters. The remaining hydrogen atoms were included in their calculated positions and refined as riding on the atoms to which they are joined. X-ray structural figures were generated using Olex2.[298] The CCDC 2088726-2088727 files contain the supplementary crystallographic data. These data can be obtained free of charge via http://www.ccdc.cam.ac.uk/conts/retrieving.html or from the Cambridge Crystallographic Data Centre (CCDC), 12 Union Road, Cambridge, CB2 1EZ, UK).

The $\{[H_2B(3,5\text{-}(CF_3)_2Pz)_3]Cu\}_3$ crystallizes with disordered lattice solvent molecules, n-hexane. The presence of a solvent molecule could easily be seen by the residual peaks, consistent with a carbon chain, located in the open channels. Unfortunately, it was disordered over multiple positions, and also lies on a symmetry element, and therefore could not be modeled satisfactorily even with restraints. Consequently, it was removed from the electron density map using Olex2 Solvent Mask command. Based on this solvent mask calculation, and 188 electrons were found in a volume of 800 A^3 in 2 voids per unit cell. This is consistent with the presence of $0.5[C_6H_{14}]$ per Asymmetric Unit which accounts for 200 electrons per unit cell.

`

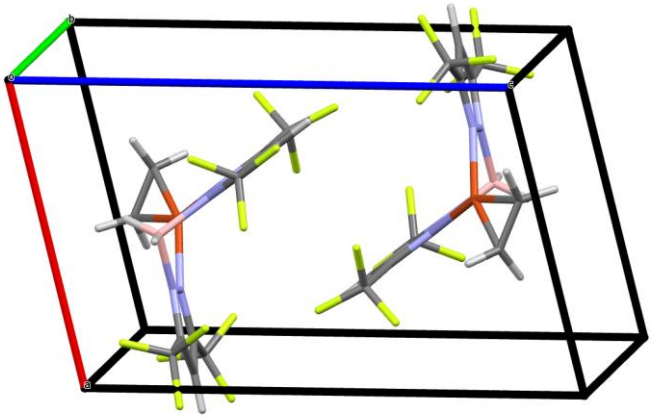

Figure 5.2.1. 1. Crystal packing diagram of $[H_2B(3,5\text{-}(CF_3)_2Pz)_3]Cu(C_2H_4)$ (**13**). There are no empty spaces (voids), based on the calculations using CCDC Mercury 2020.3.0 using a probe radius of 1.2 Å and approximate grid spacing of 0.7 Å.

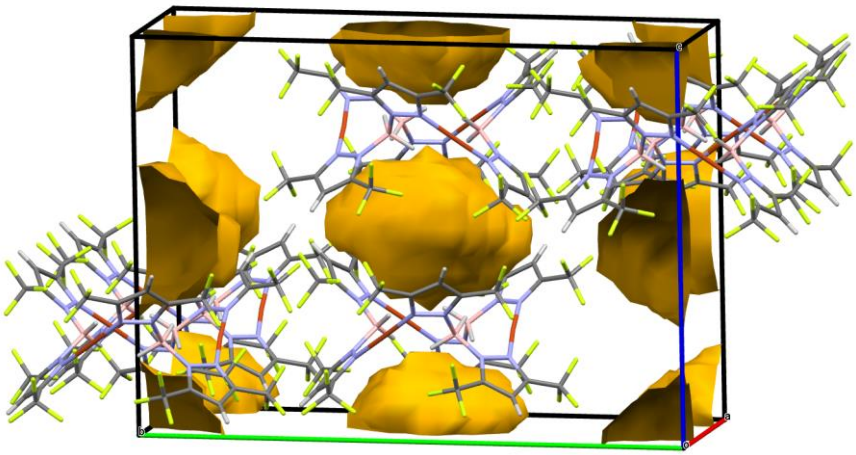

Figure 5.2.1. 2. Crystal packing diagram of $\{[H_2B(3,5\text{-}(CF_3)_2Pz)_3]Cu\}_3$ (**14**) showing empty spaces (voids).

This was calculated using CCDC Mercury 2020.3.0 using a probe radius of 1.2 Å and approximate grid spacing of 0.7 Å, came to 699 $Å^3$ (13.1% unit cell volume). Calculation of voids using 1.65 Å probe radius (considering smallest

`

dimension of ethylene based on estimated size of ethylene 3.28 x 4.18 x 4.84 $Å^3$) gave a void volume of 621 $Å^3$ (11.7% unit cell volume). As noted in the experimental section, these voids are occupied by disordered hexane in the crystal, which could not be modeled and was treated and removed with Olex2 solvent mask command.

Adsorption Isotherm and Breakthrough Experiments

Single-component gas sorption measurement. The gas sorption isotherms were collected on an automatic volumetric adsorption apparatus (Micromeritics ASAP 2020 surface area analyzer). Before the sorption measurements, the as-synthesized sample was dried under high vacuum for 12 h at 313 K, giving the activated $\{[H_2B(3,5\text{-}(CF_3)_2Pz)_3]Cu\}_3$ (14 The pure-component isotherm data for C_2H_4 and C_2H_6 in $\{[H_2B(3,5\text{-}(CF_3)_2Pz)_3]Cu\}_3$ (**14**) was fitted with the single-site Langmuir-Freundlich model.

$$N = N_{\max} \times \frac{bp^{1/n}}{1 + b\ p^{1/n}}$$

where p (unit: kPa) is the pressure of the bulk gas at equilibrium with the adsorbed phase, N (unit: mmol g^{-1}) is the adsorbed amount per mass of adsorbent, $N_{\max}$ (unit: mmol g^{-1}) is the saturation capacities, b (unit: 1/kPa) is the affinity coefficient and n represents the deviation from an ideal homogeneous surface. The fitted parameter values are presented in Supplementary Table S8.

IAST calculations of adsorption selectivities. The adsorption selectivity for C_2H_4/C_2H_6 separation is defined by

`

$$S_{ads} = \frac{q_1 / q_2}{p_1 / p_2}$$

q_1 and q_2 are the molar loadings in the adsorbed phase in equilibrium with the bulk gas phase with partial pressures p_1 and p_2.

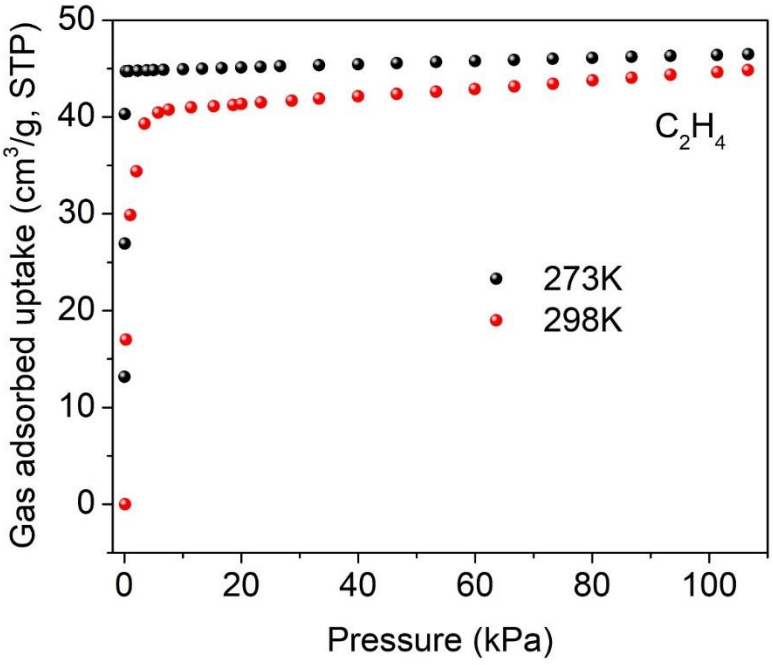

Figure 5.2.1. 3. Single-component sorption isotherms of C_2H_4 for {[H_2B(3,5-(CF_3)$_2$Pz)$_3$]Cu}$_3$ at 298K (red) and 273K (black).

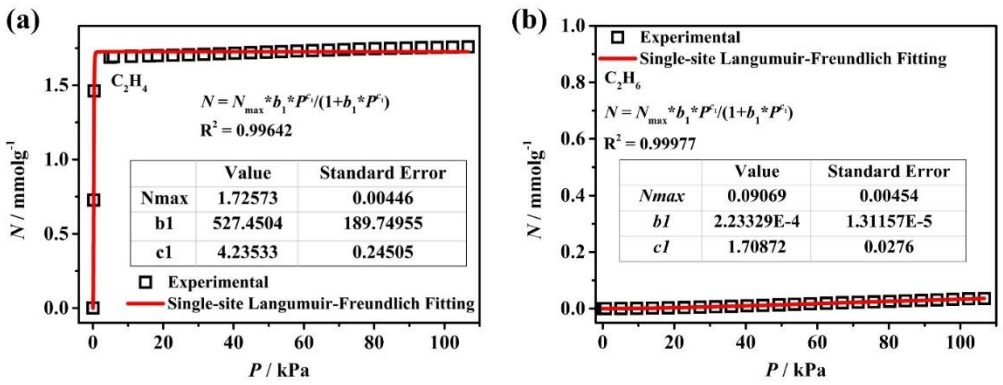

Figure 5.2.1. 4. Langmuir-Freundlich fitting of the C_2H_4 (a) and C_2H_6 (b) sorption data at 298 K for {[H_2B(3,5-(CF_3)$_2$Pz)$_3$]Cu}$_3$ (**14**).

`

Table 5.2.1. 1. Langmuir-Freundlich parameter fits for C_2H_4 and C_2H_6 at 298 K in $\{[H_2B(3,5\text{-}(CF_3)_2Pz)_3]Cu\}_3$ (**14**).

Adsorbates	N^{max} (mmol g^{-1})	b (kPa^{-1})	1/n
C_2H_4	1.72573	527.4504	4.23533
C_2H_6	0.09069	2.23329E-4	1.70872

Breakthrough separation experiments. The breakthrough experiments were carried out in dynamic gas breakthrough set-up. A stainless-steel column with inner dimensions of 4 × 81 mm was used for sample packing. Microcrystalline sample (1.1597 g) was then packed into the column. The column was placed in a temperature-controlled environment (maintained at 298 K). The mixed gas flow and pressure were controlled by using a pressure control valve and a mass flow controller (Figure S16). Outlet effluent from the column was continuously monitored using gas chromatography (GC-2014, SHIMADZU) with a thermal conductivity detector (TCD). The column packed with sample was firstly purged with He flow (40 mL min^{-1}) for 2 h at room temperature 298 K. The mixed gas flow rate during breakthrough process is 2 mL min^{-1} using 50/50 (v/v) C_2H_4/C_2H_6. After the breakthrough experiment, the sample was regenerated under vacuum at 40 ℃ for 24 h.

`

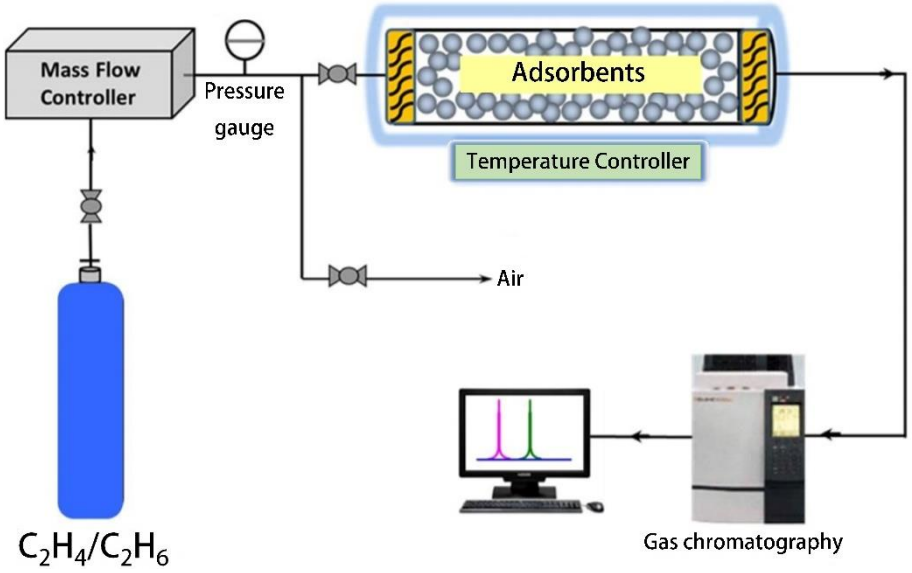

Figure 5.2.1. 5. Schematic illustration of the apparatus for the breakthrough experiments.

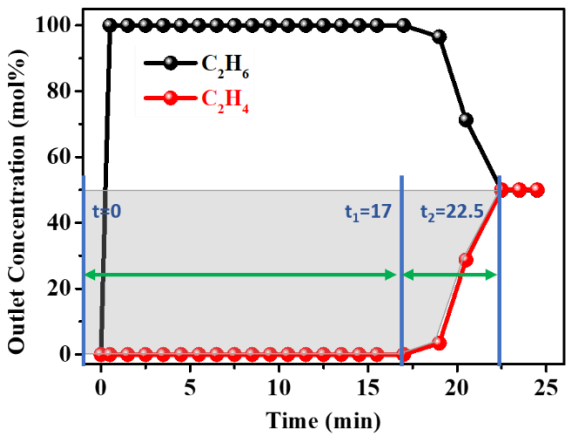

Sample weight: 1.1597g
Flow rate of C_2H_4 (50%):
q = 1 mL/min = 0.0408 mmol/min

During the duration before breakthrough point 0-t_1:
The captured amount of C_2H_4 : Q = qt_1 = 0.0408 mmol/min × 17 min = 0.70 mmol, corresponding to 0.60 mmol/g.
The maximum loading for C_2H_4 during the time interval 0-t_2:
$Q_{max} = q\int_0^{\infty}[C_i^o - Ci(t)]dt$ = 0.83 mmol corresponding to 0.72 mmol/g.

Figure 5.2.1. 6. The calculation for captured amount of C_2H_4 during the breakthrough process in $\{[H_2B(3,5\text{-}(CF_3)_2Pz)_3]Cu\}_3$ (**14**). During the duration before the breakthrough point (0–t_1), the captured C_2H_4 is 0.7 mmol, corresponding to 0.60 mmol/g. Considering the continuous C_2H_4 adsorption during the mass transfer zone (t_1–t_2), the integration of the grey area above the

`

entire breakthrough curve gave the maximum loading of the sample to be 0.83 mmol, corresponding to 0.72 mmol/g (1.30 mol/L).

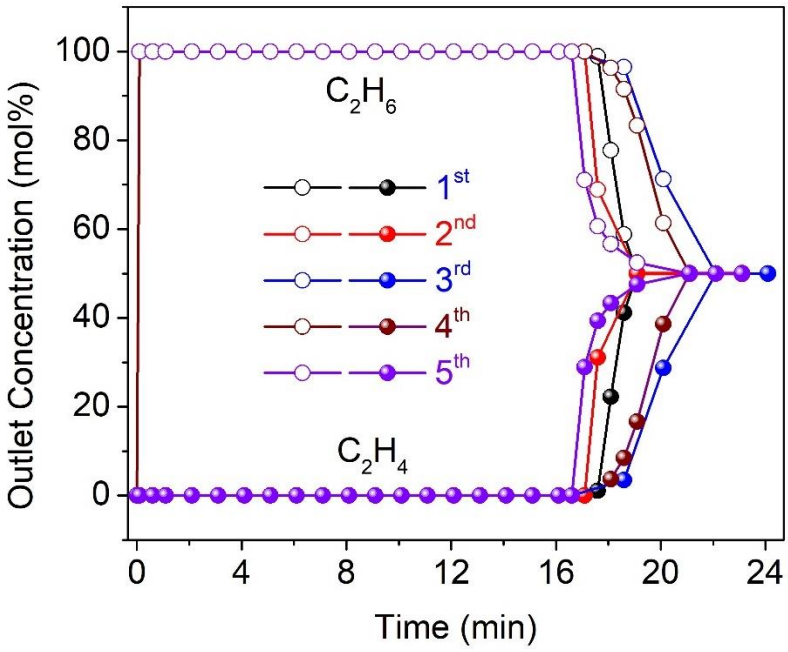

Figure 5.2.1. 7. Multiple cycles of breakthrough curves for equimolar binary mixture of C_2H_4/C_2H_6 at 298 K and 1 bar. The breakthrough experiments were carried out in a packed column at a flow rate of 2.0 mL min^{-1}. Points are experimental data, and lines are drawn to guide the eye.

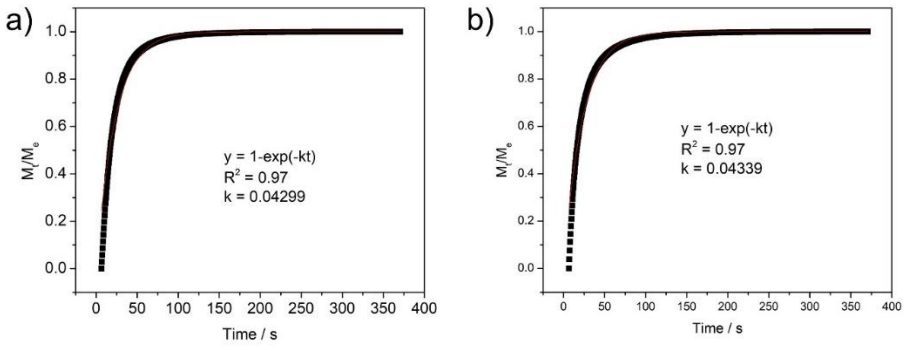

`

Figure 5.2.1. 8. Kinetic profile of {[$H_2B(3,5\text{-}(CF_3)_2Pz)_3$]Cu}$_3$ with different crystal sizes (0.3 mm < a (left) <0.45 mm, b (right) > 0.45 mm) for C_2H_4 adsorptions at 298K and 0.49 bar.

***In- situ* Synchrotron Powder Diffraction Data Collection (XRD)**

In-situ powder diffraction data of copper complexes in ethylene and He atmosphere were collected using the monochromatic X-rays available at the 17-BM. We used a beam (300 μm diameter beam size) with 0.45303 Å wavelength at the Advanced Photon Source, Argonne National Laboratory in combination with a VAREX 4343 amorphous-Si flat panel detector. A sample of analytically pure [$H_2B(3,5\text{-}(CF_3)_2Pz)_3$]Cu($C_2H_4$) was loaded into 1.0 mm quartz capillaries with glass wool on either side. The capillary with sample was then loaded into the gas flow-cell,[299] to perform in situ PXRD experiments. At one end the gas cell was connected to a two-way valve which allowed changing between a 1 atm helium flow and a high-pressure syringe pump (Teledyne ISCO 500D) which was filled with ethene gas.

Data Processing

The raw images were processed within GSAS-II,[300] refining the sample-to-detector distance and tilt of the detector relative to the beam based on data obtained for a LaB_6 standard.[301] Collected and integrated *in situ* powder diffraction data sets were trimmed, normalized and plotted using 2DFLT software.

`

Ethylene desorption experiment: The ethylene desorption experiment started with the pure $[H_2B(3,5\text{-}(CF_3)_2Pz)_3]Cu(C_2H_4)$ sample in the capillary. It was heated under helium flow as we allow ethylene desorption to proceed, while monitoring composition of the system by PXRD. At around 320K, significant ethylene loss (peak position and intensity change) was started and completed at around 343K. This observation is consistent with data from NMR experiments and the synthesis of ethylene free $[H_2B(3,5\text{-}(CF_3)_2Pz)_3]Cu$ noted in the manuscript via separate routes.

Ethylene loading experiment: After several PXRD scans of in-situ generated sorbent, the gas flow cell was connected to the syringe pump and helium gas in the capillary was exchanged with an ethylene flow of 1 bar (100 kPa). There was peak position and intensity change immediately after application of ethylene pressure to the ethylene free sorbent, indicating formation of new crystallographic phase which was same as the $[H_2B(3,5\text{-}(CF_3)_2Pz)_3]Cu(C_2H_4)$.

`

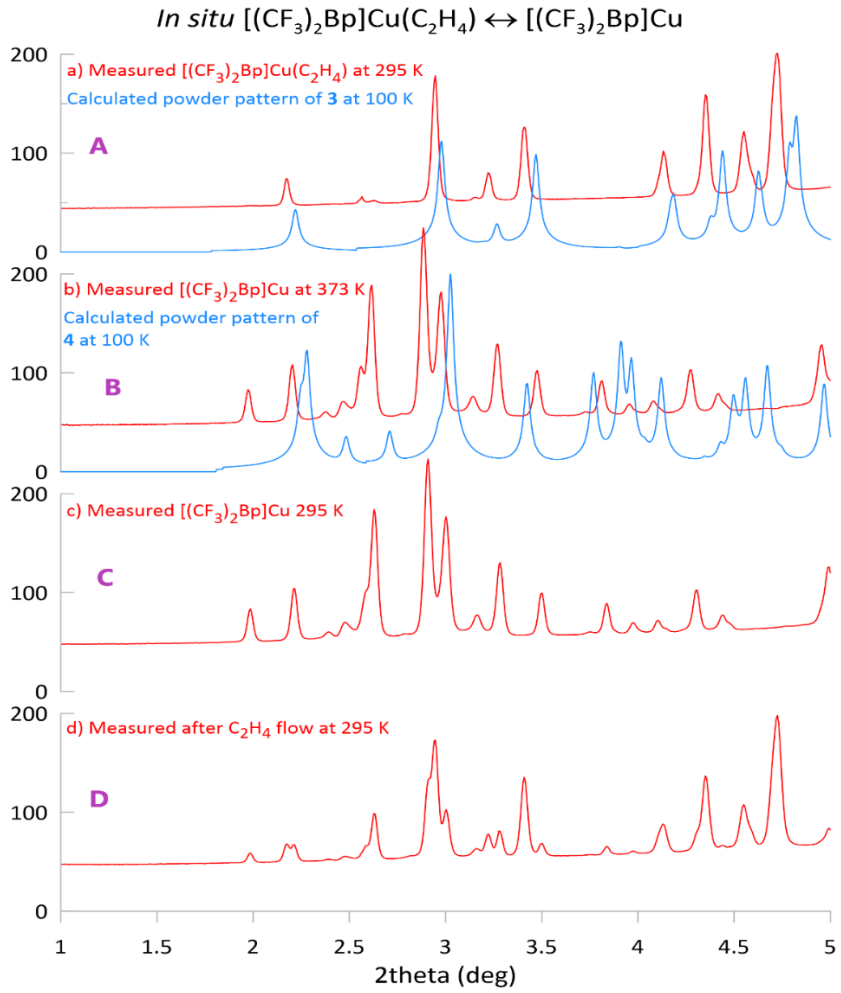

Figure 5.2.1. 9. Analysis of PXRD data

Figure 5.2.1.9 (A). A comparison of calculated (based on 100K single crystal X-ray data (SCXD)) and experimental PXRD patterns of $[H_2B(3,5\text{-}(CF_3)_2Pz)_3]Cu(C_2H_4)$ (**13**) at 295K; this shows that the monomer phase at the start is essentially the same as **13**, accounting for thermal expansion. (B) A comparison of calculated PXRD pattern of $\{[H_2B(3,5\text{-}(CF_3)_2Pz)_3]Cu\}_3$ (**14,** which was a solvated product obtained via a solution route) from SCXD collected at 100K and PXRD of the $[H_2B(3,5\text{-}(CF_3)_2Pz)_3]Cu$ phase at 373 K resulted from ethylene removal from solid **13** in a capillary gas flow cell (page

`

S30). This suggests a possible presence of a different $[H_2B(3,5\text{-}(CF_3)_2Pz)_3]Cu$ phase. (C) PXRD pattern of ethylene free $[H_2B(3,5\text{-}(CF_3)_2Pz)_3]Cu$ phase at 295K; it was synthesized by a solid state reaction in a larger scale by removing ethylene from solid **13** at ~60°C under reduced pressure. This material crystallizes as trinuclear **14** from hexane. (D) Formation of $[H_2B(3,5\text{-}(CF_3)_2Pz)_3]Cu(C_2H_4)$ (**13**) upon introduction of ethylene (1 atm at 295K) to $[H_2B(3,5\text{-}(CF_3)_2Pz)_3]Cu$ phase in the solid state.

`

5.2.2 Experimental Section for Chapter 2 Part 2.2

Synthesis of Compounds

(2-Chloroethyl)pentafluoro-λ^6-sulfane: A 3-necked 2 L reactor was charged with 500 mL of CH_2Cl_2 and cooled to -90 °C. Then ethylene (~ 20 g, 0.714 mol, 1.2 equiv) and SF_5Cl (95 g, 0.585 mol, 1.0 equiv; obtained according to the previous report[302]) were condensed to the reactor. Et_3B (20 mL, 1.0 M in hexanes) was added at -90 °C, and the mixture was allowed to slowly warm up by passing a weak current of ethylene through the solution. When the temperature reached -50 °C, an additional portion of Et_3B (10 mL, 1.0 M in hexanes) was added, and the current of ethylene was stopped. The mixture was allowed to warm to room temperature. The solution was washed with cold water (with ice), dried, and distilled at atmospheric pressure using a rectification column. The product was obtained with impurities of methylene chloride and 1,2-dichloroethane. Yield: 130 g of crude, ~ 50% purity, 58%, colorless oil. ^{1}H NMR (500 MHz, $CDCl_3$): δ (ppm) 5.37 – 5.24 (m, 2H), 4.01 – 3.98 (m, 2H). ^{19}F{^{1}H} NMR (470 MHz, $CDCl_3$): δ (ppm) 81.8 (pent, $^2J_{FF}$ = 147 Hz, 1F), 65.3 (d, $^2J_{FF}$ = 146, 4F).

Pentafluoro(vinyl)-λ^6-sulfane (19): A 500 mL round bottom flask was charged with a solution of 40% KOH (100 mL) and a solution of crude (2-chloroethyl)pentafluoro-λ^6-sulfane (40 g) in 60 mL of isopropanol. A distillation column was attached to the flask, and the mixture was heated up to boiling (~ 60 °C oil bath temperature). As the product was distilled off, the temperature was increased to 100 °C. The distillate can be used for the next step, despite the possible impurity of methylene. If water gets into the product during

`

distillation, additional washing with water and drying will be needed. Yield: 25 g of crude, ~ 70% purity, 99%, colorless oil. ^{1}H NMR (400 MHz, $CDCl_3$): δ (ppm) 6.77 – 6.59 (m, 1H), 6.02 (d, *J* = 16.0 Hz, 1H), 5.84 – 5.68 (m, 1H). ^{19}F{^{1}H} NMR (376 MHz, $CDCl_3$): δ (ppm) 81.2 (pent, $^{2}J_{FF}$ = 151 Hz, 1F), 59.6 (d, $^{2}J_{FF}$ = 150 Hz, 4F).

5-(Pentafluoro-λ^{6}-sulfanyl)-4,5-dihydro-3*H*-pyrazole (20): Crude pentafluoro(vinyl)-λ^{6}-sulfane (30 g, 0.136 mol, 1.0 equiv) was dissolved in MTBE (150 mL) and a solution of diazomethane (freshly prepared, 6.3 g, 0.15 mol, 1.1 equiv) in MTBE (50 mL) was added at -10 °C. The color of diazomethane disappeared after 30 min, and the mixture was warmed up to a room temperature. The mixture was concentrated under reduced pressure. Yield: 22.7 g, 85%, yellow oil (ca. 80% purity). ^{1}H NMR (500 MHz, $CDCl_3$): δ 7.34 (br, SC*H*N is overlapped with $CHCl_3$ signal), 4.63 (d, *J* = 11.8 Hz, 1H), 4.54 (d, *J* = 11.8 Hz, 1H), 4.39 – 4.29 (m, 1H), 3.70 – 3.55 (m, 1H).^{19}F{^{1}H} NMR (376 MHz, $CDCl_3$): δ (ppm) 79.2 (pent, $^{2}J_{FF}$ = 148 Hz, 1F), 57.6 (d, $^{2}J_{FF}$ = 147 Hz, 4F).

5-(Pentafluoro-λ^{6}-sulfanyl)-1*H*-pyrazole (17): To a solution of 5-(pentafluoro-λ^{6}-sulfanyl)-4,5-dihydro-3*H*-pyrazole (30 g, 0.15 mol, 1.0 equiv) in CH_3CN (500 mL) was added MnO_2 (60 g, 0.69 mol, 4.6 equiv). The mixture was heated to 80 °C in oil bath with a thermocouple and stirred at this temperature for 16 h. The mixture was filtered through a thick layer of silica gel. The filtrate was concentrated under reduced pressure and dissolved in a 1M NaOH solution (150 mL), then the mixture was acidified with 3M HCl. The product was extracted with $CHCl_3$ (3 × 100 mL), concentrated, recrystallized

`

from hexane and dried. Yield: 11.5 g, 38%, white solid, m.p. = 115-116 °C. ^{1}H NMR (400 MHz, $CDCl_3$): δ (ppm) 12.04 (br s, 1H, N*H*), 7.70 (d, $^{3}J_{HH}$ = 1.0 Hz, 1H, C*H*N), 6.68 (d, $^{3}J_{HH}$ = 2.5 Hz, 1H, C*H*C). ^{13}C{^{1}H} NMR (100 MHz, $CDCl_3$): δ (ppm) 159.8 (pent, $^{2}J_{FC}$ = 25 Hz, *C*SF_5), 130.4 (*C*HN), 104.1 (br m, *C*HC). ^{19}F{^{1}H} NMR (376 MHz, $CDCl_3$): δ (ppm) 79.9 (pent, $^{2}J_{FF}$ = 152 Hz, 1F), 63.5 (d, $^{2}J_{FF}$ = 152 Hz, 4F). LCMS $(M+H)^+$: 195. HRMS (ESI-TOF) *m/z*: $[M + H]^+$ calcd for $C_3H_4F_5N_2S$ 195.0015; found 195.0002.

[$Ph_2B(3\text{-}(SF_5)Pz)_2$]Na (21): 5-(Pentafluoro-λ^{6}--sulfanyl)-1*H*-pyrazole (**1**) (0.20 g, 1.03 mmol) and $NaBPh_4$ (0.12 g, 0.34 mmol) were mixed in a high pressure tube and heated at 180 ºC for 4 h. The reaction mixture was cooled to room temperature and washed with hexanes (3 X 5 mL). The solid was dried under vacuum to get pale orange solid. Yield: 50%. M.P.: 195-198 °C (decomposition). ^{1}H NMR ($(CD_3)_2CO$): δ (ppm) 7.93 (br, 2H, Pz*H*), 7.79-7.30 (m, 6H, Ph*H*), 7.17-7.05 (m, 4H, Ph*H*), 6.70 (d, *J* = 2.3 Hz, 2H, Pz*H*). ^{19}F NMR ($(CD_3)_2CO$): δ (ppm) 81.4 (pent, $^{2}J_{F\text{-}F}$ = 154.8 Hz, 2F), 63.0 (d, $^{2}J_{F\text{-}F}$ = 154.8 Hz, 8F). ^{13}C{^{1}H} NMR ($(CD_3)_2CO$): δ (ppm) 160.5 (br, C-3), 135.6, 134.9, 133.1, 131.8, 131.1, 128.0, 127.3, 103.9 (C-4).

[$Ph_2B(3\text{-}(SF_5)Pz)_2$]Cu($C_2H_4$) (23): [$Ph_2B(3\text{-}(SF_5)Pz)_2$]Na (0.10 g, 0.17 mmol) and Tl(OAc) (0.05 g, 0.19 mmol) were dissolved 5 mL of $CHCl_3$ in a Schlenk flask and refluxed for 1 h. The reaction mixture was cooled to room temperature and filtered through a pad of celite in a frit funnel. The solvent was evaporated to get the crude product. This crude product is suitable for the synthesis of copper complex. It is possible to remove the impurity, presumably the

`

unreacted sodium salt, by passing the dichloromethane solution of crude material through an alumina column. Dichloromethane from the eluent was evaporated to obtain cleaner the thallium adduct, $[Ph_2B(3\text{-}(SF_5)Pz)_2]Tl$ (**22**)as white powder. Yield: 72%, ^1H NMR ($CDCl_3$): δ (ppm) 7.72 (br, 2H, Pz*H*), 7.41-7.35 (m, 6H, Ph*H*), 7.06 (br, 4H, Ph*H*), 6.48 (d, J = 2.3 Hz, 2H, Pz*H*). ^{19}F NMR ($CDCl_3$): δ (ppm) 82.8 (pd, $^2J_{F\text{-}F}$ = 154 Hz, $^4J_{Tl\text{-}F}$ = 75.6 Hz, 2F), 65.5 (dd, $^4J_{Tl\text{-}F}$ = 777.3 Hz, $^2J_{F\text{-}F}$ = 154 Hz, 8F). $^{13}C\{^1H\}$ NMR ($CDCl_3$): δ (ppm) 159.2 (br, C-3), 148.3 (br), 138.2, 135.1, 128.7, 128.2, 102.2 (C-4). $[Ph_2B(3\text{-}(SF_5)Pz)_2]Tl$ and $[Cu(OTf)]_2{\bullet}C_7H_8$ (0.05 g, 0.09 mmol) were taken in a 50 mL Schlenk flask and 10 mL ethylene-saturated CH_2Cl_2 was added into it. The reaction mixture was stirred for 3 h at room temperature. Ethylene gas was bubbled for three times during the reaction (30 seconds each time). The reaction mixture was filtered through a pad celite in a frit funnel. The filtrate was concentrated with continuous flow of ethylene and kept at -20 °C to obtain X-ray quality colorless crystals of $[Ph_2B(3\text{-}(SF_5)Pz)_2]Cu(C_2H_4)$. Yield: 89%. M.P.: 110-113 °C (decomposition). Anal. Calc. $C_{20}H_{18}BCuF_{10}N_4S_2$: C, 37.37; H, 2.82%; N, 8.72%. Found: C, 36.99%; H, 2.68%; N, 8.34%. ^1H NMR ($CDCl_3$): δ (ppm) 7.63 (br, 2H, Pz*H*), 7.35-7.28 (m, 5H, Ph*H*), 7.24-7.23 (m, 3H, Ph*H*), 6.64-6.62 (m, 2H, Ph*H*), 6.54 (d, J = 2.9 Hz, 2H, Pz*H*), 3.72 (s, 4H, C_2H_4). ^{19}F NMR ($CDCl_3$): δ (ppm) 80.8 (pent, $^2J_{F\text{-}F}$ = 153 Hz, 2F), 65.4 (d, $^2J_{F\text{-}F}$ = 153 Hz, 8F). $^{13}C\{^1H\}$ NMR ($CDCl_3$): δ (ppm) 159.4(br, C-3), 137.7 (C-2), 136.1, 133.9, 128.1, 127.9, 127.7, 103.5 (C-4), 86.4 (C=C). IR (cm^{-1}): 3010, 2933, 2862, 2360, 2337, 1539, 1497, 1432, 1389, 1305, 1273, 1195, 1149, 1077, 984, 977, 892, 849, 815. Raman (cm^{-1}): 3161, 3152, 3137, 3055, 3044, 2996, 1593, 1568,

`

1538, 1371, 1315, 1278, 1273, 1232, 1188, 1156, 1142, 1078, 1072, 1031, 1017, 1000, 981, 959, 833, 827.

[$Ph_2B(3\text{-}(SF_5)Pz)_2$]Cu(CO) (24): [$Ph_2B(3\text{-}(SF_5)Pz)_2$]Cu($C_2H_4$) (0.03 g, 0.05 mmol) was dissolved in 3 mL CH_2Cl_2 and stirred for ~1-2 min while bubbling carbon monoxide. The reaction mixture was concentrated with continuous flow of carbon monoxide and kept at -20 °C to obtain X-ray quality colorless crystals of [$Ph_2B(3\text{-}(SF_5)Pz)_2$]Cu(CO). Yield: 98%. M.P.: 105-107 °C (decomposition). ^{1}H NMR ($CDCl_3$): δ (ppm) 7.64 (br, 2H, Pz*H*), 7.37-7.34 (m, 7H, Ph*H*), 6.96 (br, 3H, Ph*H*), 6.53 (d, *J* = 1.7 Hz, 2H, Pz*H*). ^{19}F NMR ($CDCl_3$): δ (ppm) 80.2 (pent, $^2J_{F\text{-}F}$ = 154.8 Hz, 2F), 65.1 (d, $^2J_{F\text{-}F}$ = 154.8 Hz, 8F). ^{13}C{^{1}H} NMR ($CDCl_3$): δ (ppm) 170.6 (br, CO), 159.0(br, C-3), 143.1 (br), 137.2, 135.0, 128.3, 128.1, 103.5 (C-4). IR (cm^{-1}): 3024, 2967, 2121 ($\bar{\upsilon}_{C\equiv O}$), 1498, 1445, 1431, 1393, 1322, 1306, 1264, 1198, 1157, 1143, 1077, 987, 979, 849, 814.

[$Ph_2B(3\text{-}(CF_3)Pz)_2$]Na (25): The 3-($CF_3$)PzH (2.00 g, 14.70 mmol) and $NaBPh_4$ (1.70 g, 4.90 mmol) were mixed in a 25 mL long Schlenk flask and heated at 150 ºC for 4 h during which the benzene was removed using a short path distillation apparatus. The reaction mixture was cooled to room temperature and washed with hexanes (3 X 15 mL). The remaining solid was dried under vacuum to get pure product as white solid. Yield: 52%. M.P.: 215-218 °C (decomposition). Anal. Calc. $C_{20}H_{14}BF_6N_4Na$: C, 52.43; H, 3.08%; N, 12.23%. Found: C, 52.80%; H, 3.46%; N, 11.90%. ^{1}H NMR (($CD_3)_2SO$): δ (ppm) 7.10-7.03 (m, 12H, Pz*H* & Ph*H*), 6.42 (d, *J* = 1.72 Hz, 2H, Pz*H*). ^{19}F NMR (($CD_3)_2SO$): δ (ppm) -59.0 (s). ^{13}C{^{1}H} NMR (($CD_3)_2SO$): δ (ppm) 151.6,

`

140.4 (q, $^{2}J_{C\text{-}F}$ = 36.0 Hz, C-3/C-5), 135.6, 133.7, 126.1, 124.8, 122.9 (q, $^{1}J_{C\text{-}F}$ =267.5 Hz, CF_3), 101.4 (C-4). IR (cm^{-1}): 3117, 3060, 1515, 1496, 1434, 1369, 1259, 1165, 1125, 1113, 1060, 1007, 970, 883, 845, 814.

[$Ph_2B(3\text{-}(CF_3)Pz)_2$]Tl (26): [$Ph_2B(3\text{-}(CF_3)Pz)_2$]Na (1.00 g, 2.18 mmol) and Tl(OAc) (0.58 g, 2.28 mM) were dissolved 30 mL of $CHCl_3$ in a Schlenk flask and refluxed for 1 h. The reaction mixture was cooled to room temperature and filtered through a pad of celite in a frit funnel. The solvent was evaporated to get the product as white powder. Yield: 88%. M.P.: 194-197 °C (decomposition). Anal. Calc. $C_{20}H_{14}BF_6N_4Tl$: C, 37.56; H, 2.21%; N, 8.76%. Found: C, 37.21%; H, 2.18%; N, 8.48%. ^{1}H NMR ($CDCl_3$): δ (ppm) 7.74 (d, *J* = 1.2 Hz, 2H, Pz*H*), 7.38-7.32 (m, 6H, Ph*H*), 7.01 (br, 4H, Ph*H*), 6.49 (s, 1H, Pz*H*). ^{19}F NMR ($CDCl_3$): δ (ppm) -60.2 (d, $^{4}J_{Tl\text{-}F}$ = 575.8 Hz). $^{13}C\{^{1}H\}$ NMR ($CDCl_3$): δ (ppm) 148.9, 143.0 (q, $^{2}J_{C\text{-}F}$ = 43.2 Hz, C-3/C-5), 138.9, 135.0, 128.5, 127.9, 122.2 (q, $^{1}J_{C\text{-}F}$ =268.7 Hz, CF_3), 102.7 (C-4). IR (cm^{-1}): 2945, 1558, 1431, 1364, 1274, 1260, 1236, 1150, 1126, 1115, 1052, 1037, 999, 974.

[$Ph_2B(3\text{-}(CF_3)Pz)_2$]Cu($C_2H_4$) (27): [$Ph_2B(3\text{-}(CF_3)Pz)_2$]Tl (0.10 g, 0.16 mmol) and $[Cu(OTf)]_2.C_7H_8$ (0.05 g, 0.09 mmol) were taken in a 50 mL Schlenk flask and 10 mL ethylene-saturated CH_2Cl_2 was added into it. The reaction mixture was stirred for 3 h at room temperature. Ethylene gas was bubbled for three times during the reaction (30 seconds each time). The reaction mixture was filtered through a pad celite in a frit funnel. The filtrate was concentrated with continuous flow of ethylene and kept at -20 °C to obtain X-ray quality colorless crystals of [$Ph_2B(3\text{-}(CF_3)Pz)_2$]Cu($C_2H_4$). Yield: 91%. M.P.: 115-117 °C

`

(decomposition). Anal. Calc. $C_{22}H_{18}BCuF_8N_4$: C, 50.16; H, 3.44%; N, 10.64%. Found: C, 49.81%; H, 3.25%; N, 10.29%. ^{1}H NMR ($CDCl_3$): δ (ppm) 7.65 (s, 2H, Pz*H*), 7.29 (br, 6H, Ph*H*), 6.95 (br, 4H, Ph*H*), 6.54 (s, 2H, Pz*H*), 3.69 (s, 4H, C_2H_4). ^{19}F NMR ($CDCl_3$): δ (ppm) -60.6 (s). ^{13}C{^{1}H} NMR ($CDCl_3$): δ (ppm) 142.7 (q, $^2J_{C\text{-}F}$ = 37.2 Hz, C-3/C-5), 138.0, 134.9 (br), 127.6, 120.9 (q, $^1J_{C\text{-}F}$ =268.7 Hz, CF_3), 103.7 (C-4), 82.7 (C=C). IR (cm^{-1}): 3009, 2928, 2851, 1531, 1524, 1495, 1433, 1424, 1371, 1274, 1268, 1258, 1194, 1184, 1166, 1159, 1128, 1077, 1012, 976, 956, 944, 891. Raman (cm^{-1}): 3173, 3157, 3152, 3138, 3067, 3052, 2983, 1593, 1569, 1531, 1521, 1388, 1381, 1371, 1269, 1185, 1168, 1159, 1144, 1083, 1032, 1011, 1000, 974, 944, 836.

$[Ph_2B(3\text{-}(CF_3)Pz)_2]Cu(CO)$ (28): $[Ph_2B(3\text{-}(CF_3)Pz)_2]Cu(C_2H_4)$ (0.10 g, 0.05 mmol) was dissolved in 8 mL CH_2Cl_2 and stirred for ~3-5 min while bubbling carbon monoxide. The reaction mixture was concentrated with continuous flow of carbon monoxide and kept at -20 °C to obtain X-ray quality colorless crystals of $[Ph_2B(3\text{-}(CF_3)Pz)_2]Cu(CO)$ Yield: 99%. M.P.: 115-117 °C (decomposition). Anal. Calc. $C_{21}H_{14}BCuF_6N_4O$: C, 47.89; H, 2.68%; N, 10.64%. Found: C, 47.58%; H, 2.55%; N, 10.48%. ^{1}H NMR ($CDCl_3$): δ (ppm) 7.63 (d, *J* = 1.2 Hz, 2H, Pz*H*), 7.34-7.29 (m, 6H, Ph*H*), 6.90-6.89 (m, 4H, Ph*H*), 6.54 (d, *J* = 2.3 Hz, 2H, Pz*H*). ^{19}F NMR ($CDCl_3$): δ (ppm) -61.2 (s). ^{13}C{^{1}H} NMR ($CDCl_3$): δ (ppm) 171.3 (C≡O), 145.1, 142.7 (q, $^2J_{C\text{-}F}$ = 37.2 Hz, C-3/C-5), 138.1, 134.5, 127.9, 120.9 (q, $^1J_{C\text{-}F}$ =269.9 Hz, CF_3), 103.6 (C-4). IR (cm^{-1}): 3011, 2932, 2854, 2117 ($\bar{\upsilon}_{C\equiv O}$), 1524, 1491, 1433, 1370, 1275, 1259, 1199, 1166, 1160, 1135, 1083, 1076, 1012, 893, 835.

`

[$Ph_2B(3\text{-}(SF_5)Pz)_2$]Ag($C_2H_4$) (29): [[$Ph_2B(3\text{-}(SF_5)Pz)_2$]Tl (0.10 g, 0.13 mmol) and Ag(OTf) (0.03 g, 0.13 mmol) were taken in a 50 mL Schlenk flask and 10 mL ethylene-saturated CH_2Cl_2 was added into it. The reaction mixture was stirred for 3 h at room temperature. Ethylene gas was bubbled for three times during the reaction (30 second each time). The reaction mixture was filtered through a pad celite in a frit funnel. The filtrate was concentrated with continuous flow of ethylene and kept at -20 °C to obtain X-ray quality colorless crystals of [$Ph_2B(3\text{-}(SF_5)Pz)_2$]Ag($C_2H_4$).. Yield: 86%. ^{1}H NMR ($CDCl_3$): δ (ppm) 7.69 (brs, 2H, Pz*H*), 7.31-7.30 (m, 6H, Ph*H*), 6.95 (br, 4H, Ph*H*), 6.49 (d, *J* = 2.3 Hz, 2H, Pz*H*), 4.73 (s, 4H, C_2H_4). ^{19}F NMR ($CDCl_3$): δ (ppm) 81.7 (pent, $^2J_{F\text{-}F}$ = 154.8 Hz, 2F), 64.5 (d, $^2J_{F\text{-}F}$ = 154.8 Hz, 8F). ^{13}C{^{1}H} NMR ($CDCl_3$): δ (ppm) 160.1 (br, C-3), 137.7 (C-2), 134.7 (br), 132.8, 127.7, 127.5, 103.8 (br, C=C), 103.5 (C-4).

[$Ph_2B(3\text{-}(CF_3)Pz)_2$]Ag($C_2H_4$) (30): [$Ph_2B(3\text{-}(CF_3)Pz)_2$]Tl (0.10 g, 0.16 mmol) and Ag(OTf) (0.04 g, 0.16 mmol) were taken in a 50 mL Schlenk flask and 10 mL ethylene-saturated CH_2Cl_2 was added into it. The reaction mixture was stirred for 3 h at room temperature. Ethylene gas was bubbled for three times during the reaction (30 second each time). The reaction mixture was filtered through a pad celite in a frit funnel. The filtrate was concentrated with continuous flow of ethylene and kept at -20 °C to obtain X-ray quality colorless crystals of [$Ph_2B(3\text{-}(CF_3)Pz)_2$]Ag($C_2H_4$). Yield: 83%. ^{1}H NMR ($CDCl_3$): δ (ppm) 7.72 (s, 2H, Pz*H*), 7.28-7.27 (m, 6H, Ph*H*), 6.91 (br, 4H, Ph*H*), 6.50 (br, 2H, Pz*H*), 4.67 (s, 4H, C_2H_4). ^{19}F NMR ($CDCl_3$): δ (ppm) -61.3 (s). ^{13}C{^{1}H}

`

NMR ($CDCl_3$): δ (ppm) 146.9, (br), 142.8 (q, $^2J_{C\text{-}F}$ = 37.2 Hz, C-3/C-5), 138.5, 134.7 (br), 127.5, 127.1, 121.4 (q, $^1J_{C\text{-}F}$ =268.7 Hz, CF_3), 102.8 (C-4), 101.8 (C=C).

Cyclopropanations Reactions

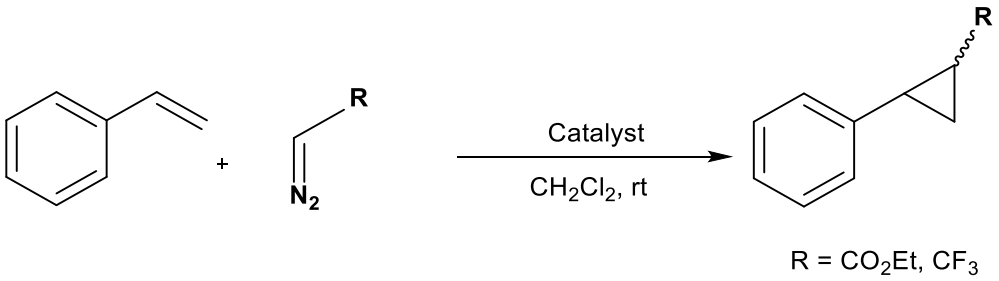

General method for the cyclopropanation: A Schlenk flask was charged with the styrene (2.8 mmol, 10.0 equiv.), catalyst (5 mol%) and dichloromethane (5.0 mL) under a nitrogen atmosphere. A dichloromethane solution of diazocompound (0.28 mmol) was added to the reaction via a syringe pump over 5 h. Following the complete addition of the diazocompound, the reaction mixture was stirred for 5 h. NMR yield was calculated using 1,3,5-tris(trifluoromethyl)benzene (^{1}H NMR was used to calculate the yield of ethyldiazoacetate reactions (ester CH_2 peak) and ^{19}F NMR was used to calculate the yield of 2-diazo-l,l,l-trifluoroethane reactions (CF_3 peak)).

X-ray Data Collection and Structure Determinations

A suitable crystal covered with a layer of hydrocarbon/Paratone-N oil was selected and mounted on a Cryo-loop, and immediately placed in the low-temperature nitrogen stream. The X-ray intensity data of $[Ph_2B(3\text{-}(SF_5)Pz)_2]Cu(C_2H_4)$ and $[Ph_2B(3\text{-}(CF_3)Pz)_2]Cu(C_2H_4)$ were measured at 100 K,

`

on a Bruker system with a SMART APEX II CCD area detector system, while data of $[Ph_2B(3\text{-}(SF_5)Pz)_2]Cu(CO)$ and $[Ph_2B(3\text{-}(CF_3)Pz)_2]Cu(CO)$ were measured at 100(2) K on a Bruker D8 Quest with a PHOTON II 7 CPAD detector. Both instruments were equipped with an Oxford Cryosystems 700 series cooler, a graphite monochromator, and a Mo Kα fine-focus sealed tube (λ = 0.71073 Å). Intensity data were processed using the Bruker Apex program suite. Absorption corrections were applied by using SADABS.[295] Initial atomic positions were located by SHELXT,[296] and the structures of the compounds were refined by the least-squares method using SHELXL[297] within Olex2 GUI.[298] All the non-hydrogen atoms were refined anisotropically. The hydrogen atoms of ethylene moieties of $[Ph_2B(3\text{-}(SF_5)Pz)_2]Cu(C_2H_4)$ and $[Ph_2B(3\text{-}(CF_3)Pz)_2]Cu(C_2H_4)$ were located in difference Fourier maps, included and refined freely with isotropic displacement parameters. The remaining hydrogen atoms were included in their calculated positions and refined as riding on the atoms to which they are joined. The $[Ph_2B(3\text{-}(SF_5)Pz)_2]Cu(C_2H_4)$ and $[Ph_2B(3\text{-}(SF_5)Pz)_2]Cu(CO)$ complexes crystallize in $P\bar{1}$ space group with two chemically identical molecules in the asymmetric unit. X-ray structural figures were generated using Olex2.[298] The **CCDC** 2104704-2104707 files contain the supplementary crystallographic data. These data can be obtained free of charge via http://www.ccdc.cam.ac.uk/conts/retrieving.html or from the Cambridge Crystallographic Data Centre (CCDC), 12 Union Road, Cambridge, CB2 1EZ, UK).

Computational Studies

All calculations were carried out by using relativistic DFT methods employing the ADF code[255] with the all-electron triple-ζ Slater basis set plus the double-

`

polarization (STO-TZ2P) basis set in conjunction with the Becke-Perdew (BP86) functional[298] within the generalized gradient approximation (GGA). London dispersion corrections were taken into account via the pairwise Grimme (BP86-D3) approach.[303] Geometry optimizations were performed without any symmetry restrain via the analytical energy gradient method implemented by Versluis and Ziegler,[304] with energy convergence criteria set at 10^{-4} Hartree, gradient convergence criteria at 10^{-4} Hartree/Å, and radial convergence of 10^{-3} Å. Scalar relativistic effects were considered through the ZORA Hamiltonian.[305]

The interaction energy is further dissected into several chemically meaningful terms according to the Energy Decomposition Analysis (EDA) of Ziegler and Rauk.[306, 307]

$$\Delta E_{int} = \Delta E_{Pauli} + \Delta E_{elstat} + \Delta E_{orb} + \Delta E_{disp}$$

where ΔE_{Pauli} term involves the electron repulsion between occupied orbitals from the different fragments. ΔE_{elstat} and ΔE_{orb} are related to the stabilizing electrostatic and covalent character of the interaction, respectively. The contribution from dispersion interaction (ΔE_{disp}) is evaluated using the pairwise correction of Grimme (D3). Bonding analysis is given in terms of bonding contributions to ΔE_{orb} by using the Natural Orbitals for Chemical Valence extension of the EDA method (EDA-NOCV),[308] resulting in deformation densities accounting for the individual in- and out-flow of charges related to the bonding pattern.

`

Table 5.2.2. 1. Calculated IR ῡ(C=C) stretching frequencies (cm^{-1}) and selected bond distances from optimized structures (Å)

Parameter	[$Ph_2B(3\text{-}(SF_5)Pz)_2$]Cu($C_2H_4$)	[$Ph_2B(3\text{-}(CF_3)Pz)_2$]Cu($C_2H_4$)	[$Ph_2B(3\text{-}(CH_3)Pz)_2$]Cu($C_2H_4$)
ῡ(C=C)	1516.3	1513.5	1509.3
C=C	1.383	1.386	1.389
Cu-C	2.047	2.045	2.029
Cu-C	2.050	2.051	2.034

Table 5.2.2. 2. Calculated proton affinities of $[Ph_2B(3\text{-}(R)Pz)_2]^-$ ligands with R= $-SF_5$, $-CF_3$, and $-CH_3$. Values in $kJ{\cdot}mol^{-1}$.

Parameter	$[Ph_2B(3\text{-}(SF_5)Pz)_2]^-$	$[Ph_2B(3\text{-}(CF_3)Pz)_2]^-$	$[Ph_2B(3\text{-}(CH_3)Pz)_2]^-$
proton affinity	936.5	944.1	1016.5

For comparison with experimental data, calculated and experimentally determined proton affinities for 3,5-$(CH_3)_2$PzH are 967.2 and 933.5 $kJ{\cdot}mol^{-1}$ respectively.

`

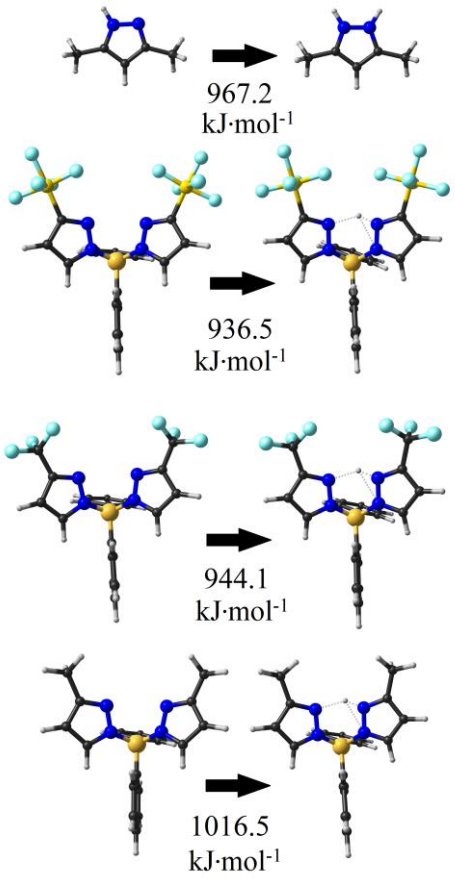

From top to bottom, the figures represent:

$3,5\text{-}(CH_3)_2PzH + H^+ \rightarrow [3,5\text{-}(CH_3)_2PzH_2]^+$

$[Ph_2B(3\text{-}(SF_5)Pz)_2]^- + H^+ \rightarrow [Ph_2B(3\text{-}(SF_5)Pz)_2]H$

$[Ph_2B(3\text{-}(CF_3)Pz)_2]^- + H^+ \rightarrow [Ph_2B(3\text{-}(CF_3)Pz)_2]H$

$[Ph_2B(3\text{-}(CH_3)Pz)_2]^- + H^+ \rightarrow [Ph_2B(3\text{-}(CH_3)Pz)_2]H$

Figure 5.2.2. 1. Proton affinities (PA) were calculated for equations given above, in which proton affinity is defined as the negative of the molar enthalpy change (DH) for the hypothetical gas-phase protonation reactions.

`

Table 5.2.2. 3. Energy decomposition analyses for the C_2H_4-Cu interaction, for different $[Ph_2B(3\text{-}(R)Pz)_2]Cu(C_2H_4)$ complexes, in which R= -SF_5, -CF_3, and -CH_3. Values in kcal·mol^{-1}. In addition, the contribution from both π_2^*-backbonding and σ-donation is given accounting for π_2*-C_2H_4 ← Cu and π_1-C_2H_4 → Cu bonding schemes, respectively. In addition, charge distribution analysis (*q*) obtained from Hirshfeld charge analysis is given.

Parameter	$[Ph_2B(3\text{-}(SF_5)Pz)_2]Cu(C_2H_4)$		$[Ph_2B(3\text{-}(CF_3)Pz)_2]Cu(C_2H_4)$		$[Ph_2B(3\text{-}(CH_3)Pz)_2]Cu(C_2H_4)$	
ΔE_{int}	-44.9		-45.9		-45.2	
ΔE_{Pauli}	114.0		112.5		125.4	
ΔE_{disp}	-6.5	4.1%[a]	-5.6	3.5%[a]	-5.3	3.1%[a]
ΔE_{elstat}	-95.2	59.9%[a]	-95.0	59.9%[a]	-102.1	59.9%[a]
ΔE_{orb}	-57.2	36.0%[a]	-57.9	36.6%[a]	-63.2	37.1%[a]
π_1-C_2H_4 → Cu	-17.1	29.9%[b]	-16.5	28.5%[b]	-15.5	24.5%[b]
π_2*-C_2H_4 ← Cu	-31.4	54.9%[b]	-33.5	57.9%[b]	-40.2	63.7%[b]
ΔE_{orb}^{rest}	-8.7		-7.8		-7.5	
[c]Popul. π_1	1.82		1.83		1.85	
[c]Popul. π_2*	0.22		0.27		0.30	
*q*L	-0.28		-0.28		-0.24	
*q*Cu	0.33		0.34		0.34	
q(C_2H_4)	-0.05		-0.06		-0.10	

[a]Percentage contribution to the total attractive interactions ΔE_{elstat}+ ΔE_{orb} + ΔE_{disp}.

[b]Percentage contribution to the total orbital interactions ΔE_{orb}.

[c]Polulation in a.u. for theylene π_1 and π_2* orbitals in the resulting complex.

`

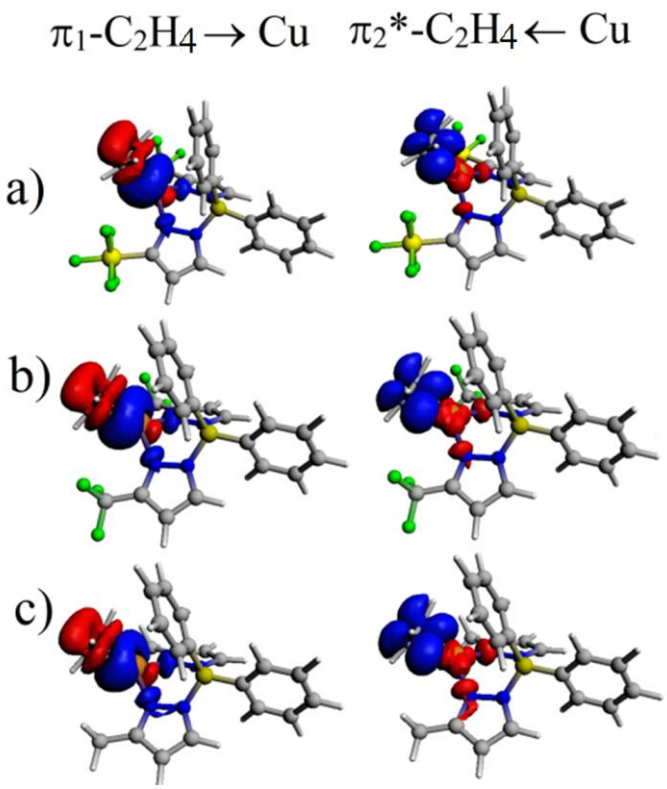

Figure 5.2.2. 2. Selected deformation densities from the NOCV-EDA analysis, for $[Ph_2B(3\text{-}(CF_3)Pz)_2]Cu(C_2H_4)$ (a), $[Ph_2B(3\text{-}(SF_5)Pz)_2]Cu(C_2H_4)$ (b), and $[Ph_2B(3\text{-}(CH_3)Pz)_2]Cu(C_2H_4)$ (c), accounting for σ-donation (left) and π-backbonding (right) in the formation of ethylene-copper complexes. Charge flow from red to blue.

Table 5.2.2. 4. Energy decomposition analyses for the C_2H_4-Cu and C_2H_4-Ni interaction for isoelectronic $[H_2B(3\text{-}(CH_3)Pz)_2]Cu(C_2H_4)$ (**Cu-BH_2**) and $[H_2C(3\text{-}(CH_3)Pz)_2]Ni(C_2H_4)$ (**Ni-CH_2**) complexes. Values in kcal·mol^{-1}. In addition, the contribution from both π_2^*-backbonding and σ-donation is given accounting for π_2*-C_2H_4 ← Cu/Ni and π_1-C_2H_4 → Cu/Ni bonding schemes, respectively. In addition, charge distribution analysis (*q*) obtained from

`

Hirshfeld charge analysis (where L = $[H_2B(3\text{-}(CH_3)Pz)_2]$ or $[H_2C(3\text{-}(CH_3)Pz)_2]$ fragment) and calculated $\bar{\upsilon}$(C=C) (in cm^{-1}) are also given.

This calculation was performed to compare the π-backbonding and σ-donation components of closely related, Cu(I) and Ni(0) systems in their ethylene complexes.

Parameter	$[H_2B(3\text{-}(CH_3)Pz)_2]Cu(C_2H_4)$		$[H_2C(3\text{-}(CH_3)Pz)_2]Ni(C_2H_4)$	
ΔE_{int}	-44.1		-78.6	
ΔE_{Pauli}	123.1		173.4	
ΔE_{disp}	-7.2	4.3%[a]	-7.4	2.9% [a]
ΔE_{elstat}	-98.7	59.1% [a]	-137.2	54.4% [a]
ΔE_{orb}	-61.2	36.6% [a]	-107.5	42.7% [a]
π_1-$C_2H_4 \rightarrow$ Cu/Ni	-15.6	25.5% [b]	-13.6	12.7% [b]
π_2*-$C_2H_4 \leftarrow$ Cu/Ni	-39.0	63.6% [b]	-86.8	80.7% [b]
ΔE_{orb}^{rest}	-6.7	10.9% [b]	-7.1	6.6% [b]
*q*L	-0.28		0.12	
*q*Cu/*q*Ni	0.36		0.17	
q(C_2H_4)	-0.08		-0.29	
$\bar{\upsilon}$(C=C) Calc.	1513.9		1458.3	

[a]Percentage contribution to the total attractive interactions $\Delta E_{elstat} + \Delta E_{orb} + \Delta E_{disp}$.

[b]Percentage contribution to the total orbital interactions ΔE_{orb}.

`

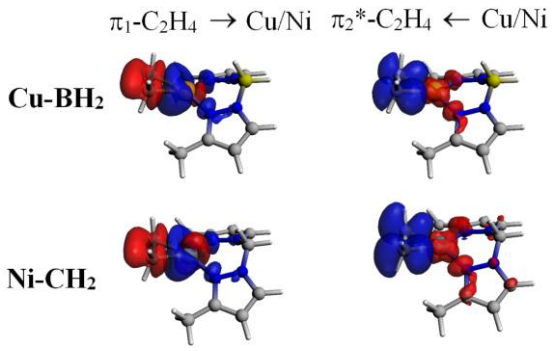

Figure 5.2.2. 3. Selected deformation densities from the NOCV-EDA analysis for C_2H_4-Cu and C_2H_4-Ni interaction for the isoelectronic $[H_2B(3\text{-}(CH_3)Pz)_2]Cu(C_2H_4)$ (**Cu-BH_2**) and $[H_2C(3\text{-}(CH_3)Pz)_2]Ni(C_2H_4)$ (**Ni-CH_2**) complexes. Charge flow from red to blue.

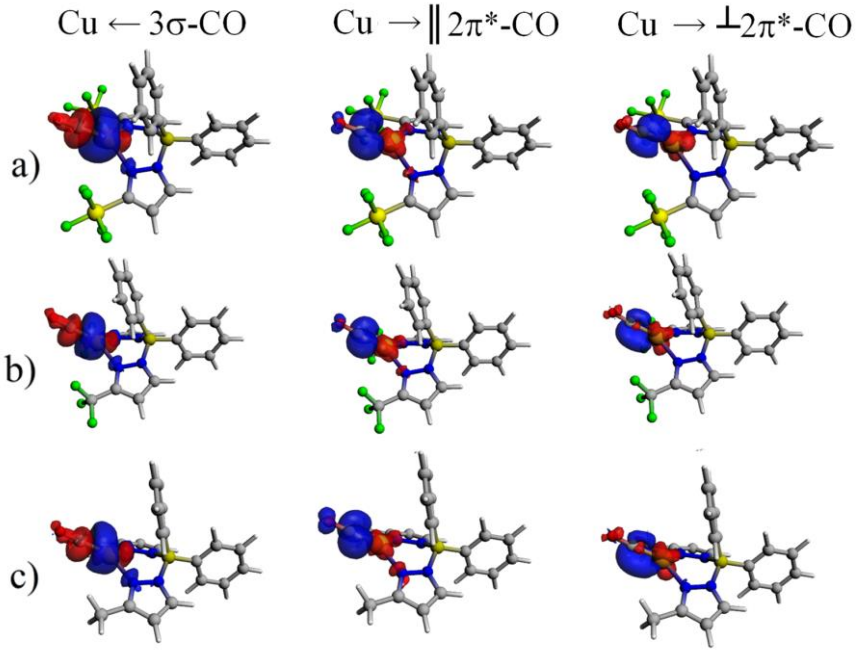

Figure 5.2.2. 4. Selected deformation densities from the NOCV-EDA analysis, for $[Ph_2B(3\text{-}(SF_5)Pz)_2]Cu(CO)$ (**a**), $[Ph_2B(3\text{-}(CF_3)Pz)_2]Cu(CO)$ (**b**), and $[Ph_2B(3\text{-}(CH_3)Pz)_2]Cu(CO)$ (**c**) accounting for σ-donation, and perpendicular and parallel in relation to the Cu-N_2 plane π-backbonding in the formation of copper-CO complexes. Charge flow from red to blue.

`

Table 5.2.2. 5. Energy decomposition analyses for the Cu-CO interaction, for different $[Ph_2B(3\text{-}(R)Pz)_2]Cu(CO)$ complexes, with R= $-SF_5$, $-CF_3$, and $-CH_3$. Values in kcal·mol^{-1}. In addition the contribution from both $\parallel 2\pi^*$- and $\perp 2\pi^*$-backbonding, and $3\sigma \rightarrow Cu$ donation are given. In addition, charge distribution analysis (*q*) obtained from Hirshfeld charge analysis (where L = $[Ph_2B(3\text{-}(R)Pz)_2]$ fragment) and calculated $\bar{\upsilon}$(CO) (in cm^{-1}) are also given.

Parameter	$[Ph_2B(3\text{-}(SF_5)Pz)_2]Cu(CO)$		$[Ph_2B(3\text{-}(CF_3)Pz)_2]Cu(CO)$		$[Ph_2B(3\text{-}(CH_3)Pz)_2]Cu(CO)$	
ΔE_{int}	-39.9		-39.8		-40.9	
ΔE_{Pauli}	116.1		118.6		125.2	
ΔE_{disp}	-3.9	2.5%[a]	-3.2	2.0%[a]	-2.7	1.6%[a]
ΔE_{elstat}	-95.6	61.2%[a]	-97.2	61.3%[a]	-100.4	60.5%[a]
ΔE_{orb}	-56.6	36.3%[a]	-58.1	36.7%[a]	-62.9	37.9%[a]
3σ-CO → Cu	-14.6	25.8%[b]	-14.1	24.3%[b]	-14.2	22.6%[b]
$\parallel 2\pi^*$-CO ← Cu	-18.3	32.4%[b]	-19.7	33.9%[b]	-23.6	37.5%[b]
$\perp 2\pi^*$-CO ← Cu	-13.1	23.2%[b]	-13.8	23.7%[b]	-15.1	24.0%[b]
ΔE_{orb}^{rest}	-10.6	18.6%[b]	-10.5	18.1%[b]	-10.0	15.9%[b]
*q*L	-0.21		-0.21		-0.20	
*q*Cu	0.31		0.32		0.34	
q(CO)	-0.10		-0.11		-0.14	
$\bar{\upsilon}$(CO) Calc.	2110.0		2099.0		2080.3	
$\bar{\upsilon}$(CO) Exp.	2121		2117			

[a]Percentage contribution to the total attractive interactions $\Delta E_{elstat} + \Delta E_{orb} + \Delta E_{disp}$.

[b]Percentage contribution to the total orbital interactions ΔE_{orb}.

`

Thermochemical parameters for C_2H_4 replacement by CO at 298 K. values in kcal·mol^{-1}.

$[Ph_2B(3\text{-}(SF_5)Pz)_2]Cu(C_2H_4) + CO \rightarrow [Ph_2B(3\text{-}(SF_5)Pz)_2]Cu(CO) + C_2H_4$

ΔG^{298K}	1.30
ΔH	1.59
$T\Delta S$	0.29

$[Ph_2B(3\text{-}(CF_3)Pz)_2]Cu(C_2H_4) + CO \rightarrow [Ph_2B(3\text{-}(CF_3)Pz)_2]Cu(CO) + C_2H_4$

ΔG^{298K}	0.59
ΔH	3.47
$T\Delta S$	2.87

`

5.3 Experimental Section for Chapter 3

5.3.1 Experimental Section for Chapter 3 Part 3.1

Synthesis of Metal Complexes

$[H_2B(3,5\text{-}(CF_3)_2Pz)_2]Cu(C_2H_2)$ (37): $[H_2B(3,5\text{-}(CF_3)_2Pz)_2]Cu(NCMe)$ (0.15 g, 0.29 mmol) was dissolved in 7 mL dichloromethane and stirred for ~10 min while bubbling acetylene. The reaction mixture was concentrated with continuous flow of acetylene and kept at -20 °C to obtain X-ray quality colorless crystals of $[H_2B(3,5\text{-}(CF_3)_2Pz)_2]Cu(C_2H_2)$. Yield: >90%. M.P.: 78-79 °C. Anal. Calc. $C_{12}H_6BCuF_{12}N_4$: C, 28.34%; H, 1.19%; N, 11.02%. Found: C, 28.18%; H, 1.17%; N, 11.04%. ^{1}H NMR ($CDCl_3$): δ (ppm) 6.93 (s, 2H, Pz*H*), 4.70 (s, 2H, ≡C*H*), 4.00 (br, 2H, B*H*). ^{19}F NMR ($CDCl_3$): δ (ppm) -59.8 (s), -60.7 (s). $^{13}C\{^1H\}$ NMR ($CDCl_3$): δ (ppm) 142.2 (q, $^2J_{C\text{-}F}$ = 39.6 Hz, C-3/C-5), 139.9 (q, $^2J_{C\text{-}F}$ = 41.2 Hz, C-3/C-5), 120.1 (q, $^1J_{C\text{-}F}$ =268.7 Hz, CF_3), 119.2 (q, $^1J_{C\text{-}F}$ =271.1 Hz, CF_3), 106.4 (C-4), 80.2 (C≡C). ^{13}C (^{1}H coupled) NMR ($CDCl_3$): δ (ppm) 142.2 (q, $^2J_{C\text{-}F}$ = 38.4 Hz, C-3/C-5), 139.9 (q, $^2J_{C\text{-}F}$ = 40.8 Hz, C-3/C-5), 120.1 (q, $^1J_{C\text{-}F}$ =268.7 Hz, CF_3), 119.2 (q, $^1J_{C\text{-}F}$ =271.1 Hz, CF_3), 106.4 (d, $^1J_{C\text{-}H}$ = 187.1 Hz, C-4), 80.3 (dd, $^1J_{C\text{-}H}$ = 251.9 Hz, $^2J_{C\text{-}H}$ = 43.2 Hz, C≡C). Raman (cm^{-1}), selected peak: 1819 (C≡C).

$[H_2B(3,5\text{-}(CF_3)_2Pz)_2]Cu(HC{\equiv}CSiMe_3)$ (38): $[H_2B(3,5\text{-}(CF_3)_2Pz)_2]Cu(NCMe)$ (0.15 g, 0.29 mmol) was dissolved in 7 mL dichloromethane. Trimethylsilylacetylene (48 μL, 0.35 mmol) was added to the reaction mixture and stirred overnight. The solvent was evaporated to get white powder product. The product was dissolved in dichloromethane and kept at -20 °C to obtain X-

`

ray quality colorless crystals of $[H_2B(3,5\text{-}(CF_3)_2Pz)_2]Cu(HC{\equiv}CSiMe_3)$. Yield: 91%. M.P.: 59-61 °C. Anal. Calc. $C_{15}H_{14}BCuF_{12}N_4Si$: C, 31.02%; H, 2.43%; N, 9.65%. Found: C, 30.64%; H, 2.07%; N, 9.98%. ^{1}H NMR ($CDCl_3$): δ (ppm) 6.88 (s, 2H, Pz*H*), 4.81 (s, 1H, ≡C*H*), 3.92 (br, 2H, B*H*), 0.24 (s, 9H, Si(CH_3)$_3$). ^{19}F NMR ($CDCl_3$): δ (ppm) -59.9 (s), -61.0 (s). ^{13}C{^{1}H} NMR ($CDCl_3$): δ (ppm) 141.8 (q, $^2J_{C\text{-}F}$ = 38.4 Hz, C-3/C-5), 139.8 (q, $^2J_{C\text{-}F}$ = 43.2 Hz, C-3/C-5), 120.2 (q, $^1J_{C\text{-}F}$ =269.9 Hz, CF_3), 119.3 (q, $^1J_{C\text{-}F}$ =269.9 Hz, CF_3), 106.2 (C-4), 97.8 (C≡C), 97.2 (C≡C), -0.2 (Si*C*H$_3$). Raman (cm^{-1}), selected peak: 1870 (C≡C).

[H$_2$B(3,5-(CF$_3$)$_2$Pz)$_2$]Cu(EtC≡CEt) (**47**): This was synthesized as reported earlier[109] and crystallized using dichloromethane at -20 °C to obtain crystals suitable for X-ray analysis.

1-(*p*-tolyl)-1*H*-1,2,3-triazole (**53**)[167]: From acetylene and *p*-tolyl azide as described in the general method (see above). ^{1}H NMR (500 MHz, $CDCl_3$): δ 8.01 (s, 1H, =CH), 7.86 (s, 1H, =CH), 7.60 (d, *J* = 8.0 Hz, 2H, Ar*H*), 7.30 (d, *J* = 8.0 Hz, 2H, Ar*H*), 2.40 (s, 3H, ArCH_3). ^{13}C{^{1}H} NMR (125 MHz, $CDCl_3$): δ 139.1, 134.8 (2C), 130.4, 122.3, 120.7, 21.2.

4-propyl-1-(*p*-tolyl)-1*H*-1,2,3-triazole (54)[309]: From 1-Pentyne and *p*-tolyl azide as described in the general method (see above). ^{1}H NMR (500 MHz, $CDCl_3$): δ 7.68 (s, 1H, =CH), 7.59 (d, *J* = 8.0 Hz, 2H, Ar*H*), 7.29 (d, *J* = 8.0 Hz, 2H, Ar*H*), 2.76 (t, *J* = 7.5 Hz, 2H, =CCH_2), 2.41 (s, 3H, ArCH_3), 1.78-1.73 (m, 2H, =CCH$_2$CH_2), 1.01 (t, *J* = 7.5 Hz, 3H, =CCH$_2$CH$_2$CH_3). ^{13}C{^{1}H} NMR (125 MHz, $CDCl_3$): δ 149.0, 138.5, 135.1, 130.2, 120.4, 119.0, 27.8, 22.8, 21.2, 13.9.

`

4-butyl-1-(*p*-tolyl)-1*H*-1,2,3-triazole (**55**)[309]: From 1-Hexyne and *p*-tolyl azide as described in the general method (see above). ^{1}H NMR (500 MHz, $CDCl_3$): δ 7.67 (s, 1H, =CH), 7.50 (d, *J* = 6.9 Hz, 2H, Ar*H*), 7.17 (d, *J* = 6.9 Hz, 2H, Ar*H*), 2.70 (t, *J* = 6.9 Hz, 2H, =CCH_2), 2.29 (s, 3H, ArCH_3), 1.64-1.61 (m, 2H, =CCH$_2$CH_2), 1.36-1.32 (m, 2H, =CCH$_2$CH$_2$CH_2), 0.87 (t, *J* = 6.9 Hz, 3H, =CCH$_2$CH$_2$CH$_2$CH_3). ^{13}C{^{1}H} NMR (125 MHz, $CDCl_3$): δ 148.9, 138.2, 134.8, 129.9, 120.0, 118.8, 31.4, 25.2, 22.2, 20.8, 13.7.

4-octyl-1-(*p*-tolyl)-1*H*-1,2,3-triazole (**56**)[310]: From 1-Decyne and *p*-tolyl azide as described in the general method (see above). ^{1}H NMR (500 MHz, $CDCl_3$): δ 7.68 (s, 1H, =CH), 7.59 (d, *J* = 8.0 Hz, 2H, Ar*H*), 7.29 (d, *J* = 8.0 Hz, 2H, Ar*H*), 2.78 (t, *J* = 7.5 Hz, 2H, =CCH_2), 2.41 (s, 3H, ArCH_3), 1.75-1.69 (m, 2H, =CCH$_2$CH_2), 1.41-1.27 (m, 10H, =CCH$_2$CH$_2$CH_2CH_2CH_2CH_2CH_2), 0.88 (t, *J* = 7.5 Hz, 3H, =CCH$_2$CH$_2$CH$_2$CH$_2$CH$_2$CH$_2$CH$_2$CH_3). ^{13}C NMR{^{1}H} (125 MHz, $CDCl_3$): δ 149.2, 138.6, 135.2, 130.3, 120.5, 118.9, 32.0, 29.6, 29.5, 29.4, 29.3, 25.9, 22.8, 21.2, 14.3.

4-phenyl-1-(*p*-tolyl)-1*H*-1,2,3-triazole (**57**)[309]: From Phenylacetylene and *p*-tolyl azide as described in the general method (see above). ^{1}H NMR (500 MHz, $CDCl_3$): δ 8.16 (s, 1H, =CH), 7.92-7.90 (m, 2H, Ar*H*), 7.67-7.65 (m, 2H, Ar*H*), 7.47-7.44 (m, 2H, Ar*H*), 7.38-7.32 (m, 3H, Ar*H*), 2.43 (s, 3H, ArCH_3). ^{13}C{^{1}H} NMR (125 MHz, $CDCl_3$): δ 148.4, 139.0, 134.9, 130.5, 130.4, 129.0, 128.5, 125.9, 120.5, 117.7, 21.2.

`

1-(*p*-tolyl)-4-(trimethylsilyl)-1*H*-1,2,3-triazole (**58**)[311]: From Trimethylsilylacetylene and *p*-tolyl azide as described in the general method (see above). ^{1}H NMR (500 MHz, $CDCl_3$): δ 7.93 (s, 1H, =CH), 7.53 (d, *J* = 8.6 Hz, 2H, Ar*H*), 7.19 (d, *J* = 8.6 Hz, 2H, Ar*H*), 2.31 (s, 3H, ArCH_3), 0.31 (s, 9H, Si(CH_3)$_3$). ^{13}C{^{1}H} NMR (125 MHz, $CDCl_3$): δ 147.0, 138.3, 134.6, 130.0, 127.2, 120.5, 20.9, -1.2.

Details of CuAAC chemistry involving several alkynes and p-tolyl azide

General method I for the synthesis of triazoles: A 50 mL Schlenk flask was charged with the selected alkyne (1.0. mmol), [H_2B(3,5-(CF_3)$_2$Pz)$_2$]Cu(NCMe) (1 mol%) and toluene (5.0 mL) under a nitrogen atmosphere. *p*-tolyl azide (1.0 mmol) was added to the reaction and stirred at 110 °C for 12 h. The solvent was removed under reduced pressure. The residue was dissolved in dichloromethane and filtered through a celite. The dichloromethane was evaporated to get pure product.

General method II for the synthesis of triazoles: A round bottom flask was charged with the selected alkyne (1.0. mmol), *p*-tolyl azide (1.0 mmol), and EtOH (5.0 mL). [H_2B(3,5-(CF_3)$_2$Pz)$_2$]Cu(NCMe) (10 mol%) was added to the reaction and stirred at 40 °C for 12 h. The solvent was evaporated. The product was isolated using column chromatography (Ethyl acetate/hexanes).

General method III for the synthesis of triazoles: A 5 mL vias was charged with selected alkyne (1.0. mmol), *p*-tolyl azide (1.0 mmol), and dichloromethane (3.0 mL). {μ-[3,5-(CF_3)$_2$Pz]Cu}$_3$ (1 mol%) was added to the reaction and stirred at room temperature for 12 h. The yield was calculated using 1,3,5-(trimethoxy)benzene as internal standard.

`

X-ray data Collection and Structure Determinations

A suitable crystal covered with a layer of hydrocarbon/Paratone-N oil was selected and mounted on a Cryo-loop and immediately placed in the low temperature nitrogen stream. The X-ray intensity data were measured at 100(2) K on a Bruker D8 Quest with a Photon 100 CMOS detector equipped with an Oxford Cryosystems 700 series cooler, a graphite monochromator, and a Mo Kα fine-focus sealed tube (λ = 0.71073 Å). Intensity data were processed using the Bruker Apex program suite. Absorption corrections were applied by using SADABS.[295] Initial atomic positions were located by SHELXT,[296] and the structures of the compounds were refined by the least-squares method using SHELXL[297] within Olex2 GUI.[298] All the non-hydrogen atoms were refined anisotropically. The hydrogen atoms of $B\underline{H}_2$ moieties as well as acetylenic C≡C<u>H</u> were located in difference Fourier maps, included and refined freely with isotropic displacement parameters. The remaining hydrogen atoms were included in their calculated positions and refined as riding on the atoms to which they are joined. X-ray structural figures were generated using Olex2.[298] The CCDC 2065196-2065198 files contain the supplementary crystallographic data of $[H_2B(3,5\text{-}(CF_3)_2Pz)_2]Cu(C_2H_2)$ (**37**), $[H_2B(3,5\text{-}(CF_3)_2Pz)_2]Cu(HC{\equiv}CSiMe_3)$ (**38**) and $[H_2B(3,5\text{-}(CF_3)_2Pz)_2]Cu(EtC{\equiv}CEt)$ (**47**).[109] These data can be obtained free of charge via http://www.ccdc.cam.ac.uk/conts/retrieving.html or from the Cambridge Crystallographic Data Centre (CCDC), 12 Union Road, Cambridge, CB2 1EZ, UK). Additional details are provided in the supporting information section.

`

Table 5.3.1. 1. Selected bond distances (Å) and angles (º) and C≡C stretching frequency for mononuclear $[H_2B(3,5\text{-}(CF_3)_2Pz)_2]Cu(C_2H_2)$ (**37**), $[H_2B(3,5\text{-}(CF_3)_2Pz)_2]Cu(EtC{\equiv}CEt)$ (**47**), and $[H_2B(3,5\text{-}(CF_3)_2Pz)_2]Cu(PhC{\equiv}CH)$ (**49**) (top-row of figures below from L to R), and dinuclear $Cu_2(\mu\text{-}[4\text{-Br-}3,5\text{-}(CF_3)_2Pz])_2(HC{\equiv}CH)_2$ (**35**), $Cu_2(\mu\text{-}[3,5\text{-}(CF_3)_2Pz])_2(EtC{\equiv}CEt)_2$ (**48**), and $Cu_2(\mu\text{-}[3,5\text{-}(CF_3)_2Pz])_2(HC{\equiv}CPh)_2$ (**50**) (bottom-row of figures below from L to R).

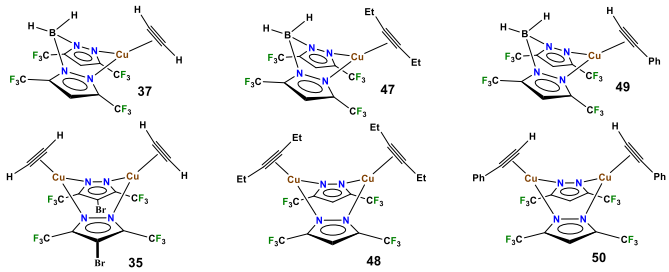

Parameter \ Complex	$[H_2B(3,5\text{-}(CF_3)_2Pz)_2]Cu(C_2H_2)$ (**37**)	$Cu_2(\mu\text{-}[4\text{-Br-}3,5\text{-}(CF_3)_2Pz])_2(HC{\equiv}CH)_2$ (**35**)*	$[H_2B(3,5\text{-}(CF_3)_2Pz)_2]Cu(EtC{\equiv}CEt)$ (**47**)	$Cu_2(\mu\text{-}[3,5\text{-}(CF_3)_2Pz])_2(EtC{\equiv}CEt)_2$ (**48**)	$[H_2B(3,5\text{-}(CF_3)_2Pz)_2]Cu(HC{\equiv}CPh)$ **(49)**	$Cu_2(\mu\text{-}[3,5\text{-}CF_3)_2Pz])_2(HC{\equiv}CPh)_2$ **(50)****
Cu-C	1.972(3) 1.973(3)	1.966(3) 1.974(3)	1.9818(16) 1.9862(16)	1.9844(13) 1.9766(17) 1.9741(18) 1.9758(16)	1.936(4) 2.003(4)	1.944(3) 1.987(3) 1.944(3) 2.014(3)
C≡C	1.225(5)	1.227(4)	1.235(2)	1.225(3) 1.228(3)	1.205(6)	1.228(4) 1.225(4)
Cu-N	1.981(3) 1.981(3)	1.9697(18) 1.9742(18)	1.9992(14) 2.0022(14)	1.9750(14) 1.9921(14) 1.9873(14) 1.9850(14)	1.989(3) 1.991(3)	1.976(2) 1.962(2) 1.986(2) 1.967(2) 1.969(2) 1.984(2) 1.958(2) 1.968(2)
C-Cu-C	36.17(14)	36.29(11)	36.26(7)	36.03(8) 36.22(7)	35.56(18)	36.38(12) 36.01(13) 35.91(12) 36.66(12)
N-Cu-N	96.63(10)	98.94(8)	91.94(6)	96.62(6) 98.35(6)	94.16(11)	99.77(9) 100.57(9) 100.98(9) 98.88(9)
C≡C-C	-	-	160.33(17) 162.90(17)	161.72(18) 161.5(2) 160.30(18) 161.19(19)	163.5(4)	160.7(3) 162.2(3) 162.4(3) 160.0(3)
ῡ(C≡C)	1819	1811	2064	2033, 2066	1927	1918, 1928, 1950
ref	*This work*	167	This work and 109	*168*	*66*	*167*

*$Cu_2(\mu\text{-}[4\text{-Br-}3,5\text{-}(CF_3)_2Pz])_2(HC{\equiv}CH)_2$ sites on a plane of symmetry

**There are two molecules of $Cu_2(\mu\text{-}[3,5\text{-}(CF_3)_2Pz])_2(HC{\equiv}CPh)_2$ in the asymmetric unit

`

Computational Studies

Geometry optimizations and subsequent calculations were done using the ADF2019 code. Triple-ξ and two polarization functions (STO-TZ2P) basis sets were employed within the generalized gradient approximation (GGA) according to the BP86 exchange-correlation functional and the empirical dispersion correction to DFT (DFT-D) given by the pair-wise Grimme correction (D3)[303, 312-314] and Becke-Johnson damping functions.[315, 316] Energy convergence criterion was set to 10^{-5} Hartree, gradient convergence criteria to 10^{-4} Hartree/Å, and radial convergence criteria to 10^{-3} Å, to achieve final relaxed structures. The energy decomposition analysis (EDA)[304, 306, 307] describes ΔE_{int} in terms of different meaningful quantities accounting for the electrostatic interaction (ΔE_{elstat}) between the defined fragments, the repulsive exchange (ΔE_{Pauli}) interaction owing to the four-electron/two-orbital repulsion between occupied orbitals from the different fragments. The orbital (covalent) interaction (ΔE_{orb}), which comes from the orbital relaxation and the orbital mixing between the fragments. Moreover, the dispersion interaction (ΔE_{disp}) was evaluated via the pairwise correction of Grimme (DFT-D3), denoting a stabilizing character. The counterpoise method was employed to overcome basis set superposition error (BSSE), denoting values lower than 2.0 kcal mol^{-1}. According to:

$$\Delta E_{int} = \Delta E_{Pauli} + \Delta E_{elstat} + \Delta E_{orb} + \Delta E_{disp}$$

`

Table 5.3.1. 2. Energy decomposition analysis of the interaction energy for $(Ph_3P)_2Ni(C_2H_2)$ species accounting for the acetylene coordination. Values in kcal.mol^{-1}. Vibrational frequencies in cm^{-1}. Experimental value from [184].

ΔE_{Pauli}	172.1	
ΔE_{Elstat}	-132.1	53.2%
ΔE_{orb}	-107.8	43.4%
ΔE_{Disp}	-8.3	3.4%
ΔE_{int}	-75.9	
π→Ni	-77.6	72.0%
σ←Ni	-15.3	14.2%
$\nu_{C\equiv C}$		
Calc.	1641	
Exp.	1630	

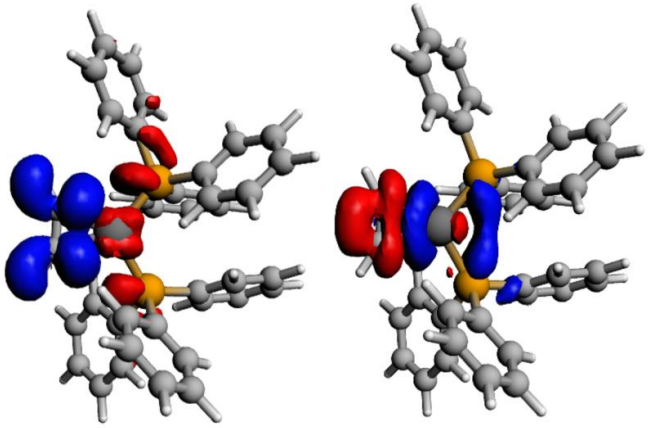

Figure 5.3.1. 1. Deformation densities account for the π-backbonding (left) and σ-donation (right) contribution to the bonding scheme in the formation of $(Ph_3P)_2Ni(C_2H_2)$. Charge flow from red to blue.

`

5.3.2 Experimental Section for Chapter 3 Part 3.2

Synthesis of Metal Complexes

[$Ph_2B(3\text{-}(CF_3)Pz)_2$]Cu($C_2H_2$) (62): [$Ph_2B(3\text{-}(CF_3)_2Pz)_2$]Cu($C_2H_4$) (0.15 g, 0.28 mmol) was dissolved in 5 mL dichloromethane and stirred for ~3-5 min while bubbling acetylene. The reaction mixture was concentrated with continuous flow of acetylene and kept at -20 °C to obtain X-ray quality colorless crystals of [$Ph_2B(3\text{-}(CF_3)_2Pz)_2$]Cu($C_2H_2$). Yield: 98%. M.P.: 118-120 °C (decomposition). Anal. Calc. $C_{22}H_{16}BCuF_6N_4$: C, 50.36; H, 3.07%; N, 10.68%. Found: C, 50.10%; H, 3.25%; N, 10.28%. ^{1}H NMR ($CDCl_3$, 500.16 MHz, 298 K): δ (ppm) 7.64 (s, br, 2H, Pz*H*), 7.25-7.23 (m, 6H, Ph*H*), 6.90 (br, 4H, Ph*H*), 6.56 (d, *J* = 2.0 Hz, 2H, Pz*H*), 4.22 (s, 2H, C_2H_2). ^{19}F NMR ($CDCl_3$, 470.62 MHz, 298 K): δ (ppm) -60.3 (s). ^{13}C{^{1}H} NMR ($CDCl_3$, 125.77 MHz, 298 K): δ (ppm) 146.3 (br), 142.8 (q, $^2J_{C\text{-}F}$ = 37.2 Hz, C-3), 138.3, 134.5 (br), 127.6, 127.4, 121.1 (q, $^1J_{C\text{-}F}$ =269.9 Hz, CF_3), 103.9 (C-4), 78.7 (C≡C). IR (cm^{-1}): 3202, 2932, 2212, 1807 (C≡C), 1523, 1496, 1433, 1369, 1275, 1259, 1211, 1084, 1078, 1012, 1003, 976. Raman (cm^{-1}): 3149, 3050, 1807(C≡C), 1593, 1522, 1372, 1176, 1143, 1032, 1000, 978.

[$Ph_2B(3\text{-}(CF_3)Pz)_2$]Ag($C_2H_2$) (63): [$Ph_2B(3\text{-}(CF_3)_2Pz)_2$]Tl (0.10 g, 0.16 mmol) and Ag(OTf) (0.044 g, 0.17 mmol) were placed in a Schlenk flask under nitrogen atmosphere. CH_2Cl_2 (10 mL) and benzene (1.0 mL) were combined in a separate Schlenk flask and slowly added via syringe. The resulting solution was stirred for 4 h at room temperature and filtered through a bed of celite to remove a white precipitate. The resulting solution was concentrated to ~25%

`

volume under reduced pressure and purified acetylene was gently bubbled through the solution for 2 minutes. The resulting mixture was placed in a freezer maintained at -20 °C to obtain colorless X-ray quality crystals of [$Ph_2B(3\text{-}(CF_3)_2Pz)_2$]Ag($C_2H_2$).Yield: 52%. M.P.: 109-112 °C (decomposition). ^{1}H NMR ($CDCl_3$, 500.16 MHz, 298 K): δ (ppm) 7.71 (s, br, 2H, Pz*H*), 7.25 (m, br, 6H, Ph*H*), 6.91 (br, 4H, Ph*H*), 6.50 (d, *J* = 2.3 Hz, 2H, Pz*H*), 2.13 (s, 2H, C_2H_2). ^{19}F NMR ($CDCl_3$, 470.62 MHz, 298 K): δ (ppm) -61.3 (s). ^{13}C{^{1}H} NMR ($CDCl_3$, 125.77 MHz, 298 K): δ (ppm) 147.3 (br), 142.7 (q, $^2J_{C\text{-}F}$ = 35.6 Hz, C-3), 138.7, 134.6 (br), 127.6, 127.0, 121.5 (q, $^1J_{C\text{-}F}$ =268.7 Hz, CF_3), 102.8 (C-4), 70.9 (C≡C). IR (cm^{-1}): 3009, 2928, 1531, 1524, 1495, 1433, 1424, 1370, 1274, 1268, 1258, 1194, 1184, 1166, 1159, 1077, 1013, 976, 955. Note: This compound loses acetylene in solution. The NMR data were collected in excess acetylene (acetylene was filled in the headspace of NMR tube). The NMR spectrum shows two different species, desired product and acetylene dissociated molecule.

[{$H_2C(3,5\text{-}(CH_3)_2Pz)_2$}Cu($C_2H_2$)][$BF_4$] (64): [{$H_2C(3,5\text{-}(CH_3)_2Pz)_2$}Cu(NCMe)][$BF_4$] (0.15 g, 0.38 mmol) was dissolved in 10 mL dichloromethane and stirred for ~3-5 min while bubbling acetylene. The reaction mixture was concentrated with continuous flow of acetylene and kept at -20 °C to obtain X-ray quality colorless crystals of [{$H_2C(3,5\text{-}(CH_3)_2Pz)_2$}Cu($C_2H_2$)][$BF_4$].Yield: 97%. M.P.: 113.-115 °C (decomposition). Anal. Calc. $C_{13}H_{18}BCuF_4N_4$: C, 41.02; H, 4.77%; N, 14.72%. Found: C, 40.61%; H, 4.45%; N, 14.12%. ^{1}H NMR (($CD_3)_2CO$, 500.16 MHz, 298 K): δ (ppm) 6.56 (s, 2H, CH_2), 6.20 (s, 2H, Pz*H*), 5.14 (s, br, 2H, C_2H_2), 2.56 (s, 6H,

`

C*H*$_3$), 2.33 (s, 6H, C*H*$_3$). ^{13}C{^{1}H} NMR ((CD$_3$)$_2$CO, 125.77 MHz, 298 K): δ (ppm) 153.0 (C-3/C-5), 143.9 (C-3/C-5), 108.0 (C-4), 79.5 (C≡C), 57.2 (*C*H$_2$), 13.8 (*C*H$_3$), 10.9 (*C*H$_3$). IR (cm^{-1}): 3233, 3257, 2927, 2854, 1812 (C≡C), 1557, 1468, 1441, 1437, 1420, 1393, 1385, 1284, 1275, 1148, 1051, 1038, 1003, 976, 961. Raman (cm^{-1}): 2976, 2957, 2933, 1812 (C≡C), 1762, 1699, 1658, 1461, 1389, 1275, 1254, 1052.

[{H$_2$C(3,5-(CH$_3$)$_2$Pz)$_2$}Ag(C$_2$H$_2$)][SbF$_6$] (65): [{H$_2$C(3,5-(CH$_3$)$_2$Pz)$_2$}Ag(C$_2$H$_4$)][SbF$_6$] (0.15 g, 0.26 mmol) was dissolved in 10 mL dichloromethane and stirred for ~2-3 min while bubbling acetylene. The reaction mixture was concentrated with continuous flow of acetylene and kept at -20 °C to obtain X-ray quality colorless crystals of [{H$_2$C(3,5-(CH$_3$)$_2$Pz)$_2$}Ag(C$_2$H$_2$)][SbF$_6$]. Yield: 93%. M.P.:119-122 °C (decomposition). Anal. Calc. C$_{13}$H$_{18}$AgF$_6$N$_4$Sb: C, 27.21; H, 3.16%; N, 9.76%. Found: C, 26.91%; H, 2.90%; N, 9.71%. ^{1}H NMR (CD$_2$Cl$_2$, 500.16 MHz, 298 K): δ (ppm) 6.35 (s, 2H, C*H*$_2$), 6.22 (s, 2H, Pz*H*), 2.39 (s, 6H, C*H*$_3$), 2.31 (s, 6H, C*H*$_3$), 2.25 (s, 2H, C$_2$*H*$_2$). ^{13}C{^{1}H} NMR (CD$_2$Cl$_2$, 125.77 MHz, 298 K): δ (ppm) 153.2 (C-3/C-5), 145.3 (C-3/C-5), 109.1 (C-4), 71.7 (C≡C), 61.2 (*C*H$_2$), 15.1 (*C*H$_3$), 11.8 (*C*H$_3$). IR (cm^{-1}): 3198, 2933, 2860, 2366, 1557, 1466, 1422, 1392, 1384, 1285, 1232, 1155, 1043, 981.

[HB(3,5-(CF$_3$)$_2$Pz)$_3$]Cu(C$_2$H$_2$) (66): [HB(3,5-(CF$_3$)$_2$Pz)$_3$]Cu(C$_2$H$_4$) (0.15 g, 0.21 mmol) was dissolved in 5 mL dichloromethane and stirred for ~3-5 min while bubbling acetylene. The remaining solvent was evaporated to obtain [HB(3,5-(CF$_3$)$_2$Pz)$_2$]Cu(C$_2$H$_2$) as white powder. X-ray quality colorless crystals

`

of [HB(3,5-$(CF_3)_2$Pz)$_3$]Cu(C_2H_2) was obtained in acetylene saturated toluene at -20 °C. Yield: 98%. M.P.: 135-138 °C (decomposition). Anal. Calc. $C_{17}H_6BCuF_{18}N_6$: C, 28.73; H, 0.85%; N, 11.83%. Found: C, 29.15%; H, 1.10%; N, 12.20%. ^{1}H NMR ($CDCl_3$, 500.16 MHz, 298 K): δ (ppm) 6.94 (s, 3H, Pz*H*), 4.50 (s, 2H, C_2H_2). ^{19}F NMR ($CDCl_3$, 470.62 MHz, 298 K): δ (ppm) -59.2(s), -60.7(s). ^{13}C{^{1}H} NMR ($CDCl_3$, 125.77 MHz, 298 K): δ (ppm) 143.5 (q, $^2J_{C\text{-}F}$ = 39.6 Hz, C-3/C-5), 140.0 (q, $^2J_{C\text{-}F}$ = 38.4 Hz, C-3/C-5), 120.0 (q, $^1J_{C\text{-}F}$ =269.9 Hz, CF_3), 119.1 (q, $^1J_{C\text{-}F}$ =271.1 Hz, CF_3), 107.1 (C-4), 75.8 (C≡C). IR (cm^{-1}): 3235, 2932, 2623 (B-H), 1849 (C≡C), 1558, 1497, 1396, 1368, 1265, 1247, 1178, 1134, 1098, 1080, 1042, 999, 989. Raman (cm^{-1}):3321, 3224, 3169, 2704, 1845 (C≡C), 1762, 1699, 1658, 1500, 1472, 1386, 1259, 993.

[HB(3-(CF_3),5-(Ph)Pz)$_3$]Cu(C_2H_2) (67): [HB(3-(CF_3),5-(Ph)Pz)$_3$]Na(THF) (0.200 g, 0.270 mmol) and [CuOTf]$_2$·C_6H_6 (0.076 g, 0.151 mmol) were placed in a Schlenk flask under nitrogen atmosphere. CH_2Cl_2 (20 mL) and benzene (2.0 mL) were combined in a separate Schlenk flask and slowly added via syringe. The resulting solution was stirred overnight at room temperature and filtered through a bed of Celite to remove a white precipitate. The resulting solution was concentrated to ~25% volume under reduced pressure and purified acetylene was gently bubbled through the solution for 2 minutes. The resulting mixture was placed in a freezer maintained at -20 °C to obtain colorless x-ray quality crystals. Yield: 0.136 g, 69%. M.P.: 103-154 °C (slowly decomposes over this wide temperature range with a final melting point of the residue at 225 °C). Analysis Calcd. for $C_{32}H_{21}CuBF_9N_6$: C, 52.30; H, 2.88; N, 11.44%. Found. C,

`

52.43; H, 2.76; N, 11.59%. ^{1}H NMR ($CDCl_3$, 500.16 MHz, 298 K): δ (ppm) 7.27 (t, 3H, Ph-*H*, *J* = 7.5 Hz), 6.94 (t, 6H, Ph-*H*, *J* =7.7 Hz), 6.87 (d, 6H, Ph-*H*, *J* = 7.2 Hz), 6.56 (s, 3H, Pz*H*), 4.66 (s, 2H, C_2H_2). ^{19}F NMR (CD_2Cl_2, 470.62 MHz, 298 K): δ (ppm) -60.0 (s). ^{13}C{^{1}H} NMR ($CDCl_3$, 125.77 MHz, 298 K) δ (ppm): 150.4 (s, *C*(C_6H_5)), 142.7 (q, $^{2}J_{C-F}$ = 38.4 Hz, *C*CF_3), 130.6 (Ph), 129.8 (Ph), 128.5 (Ph), 128.0 (Ph), 121.2 (q, $^{1}J_{C-F}$ = 272.3 Hz, *C*F_3), 105.3 (C-4), 76.5 (C_2H_2). ^{1}H NMR (CD_2Cl_2, 500.16 MHZ, 298 K): δ (ppm) 7.28 (t, 3H, Ph*H*, *J* = 7.5 Hz), 6.96 (t, 6H, Ph*H*, *J* = 7.7 Hz), 6.89 (d, 6H, Ph*H*, *J* = 7.5 Hz), 6.60 (s, 3H, C*H*), 4.72 (s, 2H, C_2H_2). ^{19}F NMR (CD_2Cl_2, 470.62 MHz, 298 K): δ (ppm) -60.3 (s). ^{13}C{^{1}H} NMR (CD_2Cl_2, 125.77 MHz, 298 K): δ (ppm) 151.0 (*C*(C_6H_5)), 142.7 (q, $^{2}J_{C-F}$ = 38.4 Hz, *C*CF_3), 130.7 (Ph), 130.0 (Ph), 128.9 (Ph), 128.3 (Ph), 121.6 (q, $^{1}J_{C-F}$ = 272.3 Hz, *C*F_3), 105.5 (C-4), 76.8 (C_2H_2). IR (Selected peaks, cm^{-1}): 2644 (B-H). Raman (Selected peaks, cm^{-1}): 1829 (C≡C).

[HB(3-(CF_3),5-(Ph)Pz)$_3$]Ag(C_2H_2) (68): [HB(3-(CF_3),5-(Ph)Pz)$_3$]Na(THF) (0.25 g, 0.34 mmol) and AgOTf (0.095 g, 0.37 mmol) were placed in a Schlenk flask under nitrogen atmosphere. CH_2Cl_2 (20 mL) and benzene (2.0 mL) were combined in a separate Schlenk flask and slowly added via syringe. The resulting solution was stirred overnight at room temperature and filtered through a bed of Celite to remove an orange precipitate. The resulting solution was concentrated to ~25% volume under reduced pressure and purified acetylene was gently bubbled through the solution for 2 minutes. The resulting mixture was placed in a freezer maintained at -20 °C to obtain colorless x-ray quality crystals. Yield: 0.186 g, 71%. M.P.: 103-148 °C (slowly decomposes over this

`

wide temperature range with a final melting point of the residue at 225 °C). Analysis Calcd. for $C_{32}H_{21}AgBF_9N_6$: C, 49.32; H, 2.72; N, 10.79%. Found. C, 49.70; H, 2.64; N, 10.53%. ^{1}H NMR (CD_2Cl_2, 500.16 MHz, 298 K): δ (ppm) 7.23 (t, 3H, Ph*H*, *J* = 7.5 Hz), 6.94 (t, 6H, Ph*H*, *J* = 7.5 Hz), 6.89 (d, 6H, Ph*H*, *J* = 6.9 Hz), 6.56 (s, 3H, C*H*), 4.72 (br, 1H, B*H*), 3.59 (s, 2H, C_2H_2). ^{13}C{^{1}H} NMR (CD_2Cl_2, 125.77 MHz, 298 K): δ (ppm) 151.9 (s, *C*(C_6H_5)), 142.9 (q, $^{2}J_{C\text{-}F}$ = 37.2 Hz, *C*CF_3), 131.3 (Ph), 130.0 (Ph), 128.5 (Ph), 128.2 (Ph), 122.0 (q, $^{1}J_{C\text{-}F}$ = 268.7 Hz, *C*F_3), 104.9 (*C*H), 66.7 (s, C_2H_2). ^{19}F NMR (CD_2Cl_2, 470.62 MHz, 298 K): δ (ppm) -61.3 (s). IR (Selected peaks, cm^{-1}): 2629 (B-H). Raman (Selected peaks, cm^{-1}): 1895 (C≡C).

X-ray data Collection and Structure Determinations

A suitable crystal covered with a layer of hydrocarbon/Paratone-N oil was selected and mounted on a Cryo-loop, and immediately placed in the low temperature nitrogen stream. The X-ray intensity data were measured at 100(2) K on a Bruker D8 Quest with a Photon 100 ($[Ph_2B(3\text{-}(CF_3)Pz)_2]Ag(C_2H_2)$, $[\{H_2C(3,5\text{-}(Me)_2Pz)_2\}Cu(C_2H_2)][BF_4]$, $[\{H_2C(3,5\text{-}(Me)_2Pz)_2\}Ag(C_2H_2)][SbF_6]$) or Photon II ($[Ph_2B(3\text{-}(CF_3)Pz)_2]Cu(C_2H_2)$, $[HB(3,5\text{-}(CF_3)_2Pz)_3]Cu(C_2H_2)$) detector equipped with an Oxford Cryosystems 700 series cooler, a Triumph monochromator, and a Mo Kα fine-focus sealed tube (λ = 0.71073 Å). Intensity data were processed using the Bruker Apex3 or Apex4 program suite. Absorption corrections were applied by using SADABS.[295] Initial atomic positions were located by direct methods using SHELXT,[296] and the structures of the compounds were refined by the least-

`

squares method using SHELXL[297] within Olex2 GUI.[298] The [HB(3,5-$(CF_3)_2Pz)_3$]Cu(C_2H_2) crystallized with two molecules of toluene, and sits on a crystallographic mirror plane containing B, Cu, a pyrazolyl ring, and centroid of the acetylene ligand. All the non-hydrogen atoms were refined anisotropically. Hydrogen atoms were included at calculated positions and refined riding on corresponding carbons, except hydrogen atoms on acetylene carbons of [$Ph_2B(3\text{-}(CF_3)Pz)_2$]Cu($C_2H_2$), [$Ph_2B(3\text{-}(CF_3)Pz)_2$]Ag($C_2H_2$), and [{$H_2C(3,5\text{-}(Me)_2Pz)_2$}Cu($C_2H_2$)][$BF_4$], which were located from difference map and refined freely. X-ray structural figures were generated using Olex2.[298] CCDC **2152321-2152325** files contain the supplementary crystallographic data. These data can be obtained free of charge via http://www.ccdc.cam.ac.uk/conts/retrieving.html or from the Cambridge Crystallographic Data Centre (CCDC), 12 Union Road, Cambridge, CB2 1EZ, UK). Further details are given in the CIF.

Computational Studies

Geometry optimizations of the complexes were performed without symmetry constraints using the Gaussian09 optimizer together with Turbomole 7.1[317] energies and gradients at the BP86[317, 318]/def2-TZVPP[319] level of theory using the D3 dispersion correction suggested by Grimme et al.[314] and the resolution-of-identity (RI) approximation.[320] This level is denoted RI-BP86-D3/def2-TZVPP. Vibrational analysis was performed to ensure that the optimized geometry corresponds to an energy minimum. Natural Bond Orbital (NBO) calculations were carried out using the NBO6.0 program[242] at the BP86-D3/def2-TZVPP level using the optimized the RI-BP86-D3/def2-TZVPP geometries.

`

The interaction ΔE_{int} between the selected fragments is analyzed with the help of the Energy Decomposition Analysis (EDA) method.[306] Within this approach, ΔE_{int} can be decomposed into the following physically meaningful terms:

$$\Delta E_{int} = \Delta E_{elstat} + \Delta E_{Pauli} + \Delta E_{orb} + \Delta E_{disp}$$

The term ΔE_{elstat} corresponds to the classical electrostatic interaction between the unperturbed charge distributions of the deformed reactants and is usually attractive. The Pauli repulsion ΔE_{Pauli} comprises the destabilizing interactions between occupied orbitals and is responsible for any steric repulsion. The orbital interaction ΔE_{orb} accounts for electron-pair bonding, charge transfer (interaction between occupied orbitals on one moiety with unoccupied orbitals on the other, including HOMO–LUMO interactions), and polarization (empty-occupied orbital mixing on one fragment due to the presence of another fragment). Finally, the ΔE_{disp} term takes into account the interactions which are due to dispersion forces. Moreover, the NOCV (Natural Orbital for Chemical Valence)[117] extension of the EDA method has been also used to further partition the ΔE_{orb} term. The EDA-NOCV approach provides pairwise energy contributions for each pair of interacting orbitals to the total bond energy.

The program package AMS 2020.101[321] was used for the EDA-NOCV calculations at the same BP86-D3 level, in conjunction with a triple- ζ -quality basis set using uncontracted Slater-type orbitals (STOs) augmented by two sets of polarization functions with a frozen-core approximation for the core electrons.[322] Auxiliary sets of s, p, d, f, and g STOs were used to fit the molecular densities and to represent the Coulomb and exchange potentials accurately in each SCF cycle. Scalar relativistic effects were incorporated by

`

applying the zeroth-order regular approximation (ZORA).[305, 323, 324] This level of theory is denoted ZORA-BP86-D3/TZ2P//RI-BP86-D3/def2-TZVPP.

`

5.4 Experimental for Chapter 4

Synthesis of Compounds

[H_2B(3,5-(CF_3)$_2$Pz)$_2$]Cu(Cyp-**2) (74)**: [H_2B(3,5-(CF_3)$_2$Pz)$_2$]Cu(NCMe) (100 mg, 0.19 mmol) and ethyl 2,3-diethylcycloprop-2-enecarboxylate (Cyp-**2**, 33 mg, 0.19 mmol) were dissolved in 10 mL dichloromethane and stirred overnight under nitrogen atmosphere. The solvent was evaporated to get white solid product. The product was dissolved in minimum amount of hexanes and kept at -20 °C refrigerator to obtain x-ray quality crystals of [H_2B(3,5-(CF_3)$_2$Pz)$_2$]Cu(Cyp-2). Yield: 82%. M.P.: 76-79 °C (decomposition). Anal. Calc. $C_{20}H_{20}BCuF_{12}N_4O_2$: C, 36.91%; H, 3.10%; N, 8.61%. Found: C, 36.95%; H, 3.40%; N, 8.67%. ^{1}H NMR ($CDCl_3$): δ (ppm) 6.86 (s, 2H, Pz*H*), 4.35 (q, *J* = 6.9 Hz, 2H, OC*H*$_2$), 3.89 (br, 2H, B*H*$_2$), 2.58-2.52 (m, 2H, =CC*H*$_2$), 2.28 (s, 1H, C*H*), 2.23-2.17 (m, 2H, =CC*H*$_2$), 1.38 (t, *J* = 6.9 Hz, 3H, OCH_2CH_3), 1.03 (t, J = 7.5 Hz , 6H, $=CCH_2CH_3$). ^{19}F NMR ($CDCl_3$): δ (ppm) -59.7 (s), -61.6 (s). ^{13}C{^{1}H} NMR ($CDCl_3$): δ (ppm) 181.1 (br, C=O), 142.3 (q, $^2J_{C\text{-}F}$ = 39.6 Hz, C-3/C-5), 139.3 (q, $^2J_{C\text{-}F}$ = 42.0 Hz, C-3/C-5), 120.0 (q, $^1J_{C\text{-}F}$ =268.7 Hz, CF_3), 119.4 (q, $^1J_{C\text{-}F}$ =269.9 Hz, CF_3), 106.6 (C-4), 91.1 (br, C=C), 62.7 (s, O*C*H$_2$), 33.2 (br, *C*H), 22.3 (s, =C*C*H$_2$), 14.3 (OCH_2CH_3), 11.4 (s, $=CCH_2CH_3$). IR (cm^{-1}): 2549, 2441, 1689 (C=O), 1552, 1497, 1469, 1399, 1380, 1348, 1267, 1250, 1213, 1166, 1153, 1100, 1045, 1005, 990, 893, 861. Raman (cm^{-1}), selected peaks: 1552, 1701.

[H_2B(3,5-(CF_3)$_2$Pz)$_2$]Cu(Cyp-**3) (75)**: [H_2B(3,5-(CF_3)$_2$Pz)$_2$]Cu(NCMe) (100 mg, 0.19 mmol) and ethyl 2,3-diphenylcycloprop-2-enecarboxylate (Cyp-**3**, 76

`

mg, 0.19 mmol) were dissolved in 10 mL dichloromethane and stirred overnight under nitrogen atmosphere. The solvent was evaporated to get white solid product. The product was dissolved in minimum amount of hexanes and kept at -20 °C refrigerator to obtain x-ray quality crystals of [$H_2B(3,5\text{-}(CF_3)_2Pz)_2$]Cu(Cyp-3). Yield: 94%. M.P.: 115-118 °C (decomposition). Anal. Calc. $C_{28}H_{20}BCuF_{12}N_4O_2$: C, 45.03%; H, 2.70%; N, 7.50%. Found: C, 45.38%; H, 2.60%; N, 7.88%. ^{1}H NMR ($CDCl_3$): δ (ppm) 7.65-7.64 (m, 4H, Ar*H*), 7.32 (br, 6H, Ar*H*), 6.67 (s, 2H, Pz*H*), 4.49 (br, 2H, OCH_2), 4.20 (br, 2H, BH_2), 2.96 (s, 1H, C*H*), 1.48 (br, 3H, OCH_2CH_3). ^{19}F NMR ($CDCl_3$): δ (ppm) -59.7 (s), -61.6 (s). ^{13}C{^{1}H} NMR ($CDCl_3$): δ (ppm) 179.9 (br, C=O), 142.2 (q, $^2J_{C\text{-}F}$ = 39.6 Hz, C-3/C-5), 139.2 (q, $^2J_{C\text{-}F}$ = 41.2 Hz, C-3/C-5), 131.0 (Ar), 129.3 (Ar), 128.8 (Ar), 128.2 (Ar), 119.7 (q, $^1J_{C\text{-}F}$ =269.9 Hz, CF_3), 119.4 (q, $^1J_{C\text{-}F}$ =269.9 Hz, CF_3), 106.4 (C-4), 86.2 (br, C=C), 63.4 (br, OCH_2), 32.6 (br, *C*H), 14.4 (OCH_2CH_3). IR (cm^{-1}): 2928, 2551, 2415, 1692 (C=O), 1559, 1498, 1448, 1398, 1378, 1339, 1266, 1254, 1219, 1157, 1105, 1098, 1045, 1014, 1000, 890, 865, 823. Raman (cm^{-1}), selected peak: 1595, 1644.

[$H_2B(3,5\text{-}(CF_3)_2Pz)_2$]Cu(Cyp-**4) (76)**: [$H_2B(3,5\text{-}(CF_3)_2Pz)_2$]Cu(NCMe) (100 mg, 0.19 mmol) and ethyl 2,3-bis(trimethylsilyl)cycloprop-2-enecarboxylate (Cyp-**4**,19 mg, 0.19 mmol) were dissolved in 10 mL dichloromethane and stirred overnight under nitrogen atmosphere. The solvent was evaporated to get white solid product. The product was dissolved in minimum amount of hexanes and kept at -20 °C refrigerator to obtain x-ray quality crystals of [$H_2B(3,5\text{-}(CF_3)_2Pz)_2$]Cu(Cyp-4). Yield: 80%. M.P.: 119-122 °C (decomposition). Anal. Calc. $C_{22}H_{28}BCuF_{12}N_4O_2Si_2$: C, 35.76%; H, 3.82%; N, 7.58%. Found: C,

`

36.10%; H, 4.12%; N, 7.24%. ^{1}H NMR ($CDCl_3$): δ (ppm) 6.83 (s, 2H, Pz*H*), 4.37 (q, *J* = 6.9 Hz, 2H, OCH_2), 4.07 (br, 2H, BH_2), 1.81 (s, 1H, C*H*), 1.39 (t, *J* = 6.9 Hz, 3H, OCH_2CH_3), 0.01 (s, 18H, $Si(CH_3)_3$). ^{19}F NMR ($CDCl_3$): δ (ppm) -59.7 (s), -61.1 (s). $^{13}C\{^{1}H\}$ NMR ($CDCl_3$): δ (ppm) 182.5 (s, C=O), 142.6 (q, $^{2}J_{C\text{-}F}$ = 39.6 Hz, C-3/C-5), 139.5 (q, $^{2}J_{C\text{-}F}$ = 43.2 Hz, C-3/C-5), 119.8 (q, $^{1}J_{C\text{-}F}$ =269.9 Hz, CF_3), 119.4 (q, $^{1}J_{C\text{-}F}$ =269.9 Hz, CF_3), 106.6 (C-4), 95.0 (s, C=C), 62.8 (s, OCH_2), 26.2 (s, *C*H), 14.4 (OCH_2CH_3), -1.2 (s, $Si(CH_3)_3$). IR (cm^{-1}): 2552, 2447, 1683 (C=O), 1547, 1494, 1469, 1398, 1375, 1330, 1267, 1249, 1216, 1192, 1150, 1147, 1099, 1045, 996, 899, 890, 843. Raman (cm^{-1}), selected peak: 1550, 1683.

[HB(3,5-(CF_3)$_2$Pz)$_3$]Cu(Cyp-**2) (77)**: [HB(3,5-(CF_3)$_2$Pz)$_3$]Na(THF) (0.05 g, 0.07 mmol) and $(CuOTf)_2$•C_6H_6 (18 mg, 0.03 mmol)were dissolved in 5 mL toluene and stirred at 100 °C for 3 h. The reaction mixture was filtered through celite and the solvent was evaporated under vacuum. The residue was dissolved in 3 mL dichloromethane. A dichloromethane (2 mL) solution of ethyl 2,3-diethylcycloprop-2-enecarboxylate (Cyp-**2**, 12 mg, 0.07 mmol) was added to the resulting copper complex and stirred for 5 h. The solvent was evaporated to get white powder product. The product was dissolved in dichloromethane and kept at -20 °C to obtain X-ray quality colorless crystals of [HB(3,5-(CF_3)$_2$Pz)$_3$]Cu(Cyp-**2**). Yield: 59%. M.P.: 142-144 °C (decomposition). Anal. Calc. $C_{25}H_{20}BCuF_{18}N_6O_2$: C, 35.21%; H, 2.36%; N, 9.85%. Found: C, 35.05%; H, 2.27%; N, 9.89%. ^{1}H NMR ($CDCl_3$): δ (ppm) 6.89 (s, 3H, Pz*H*), 5.06 (br, 1H, B*H*), 4.24 (q, *J* = 7.2 Hz, 2H, OCH_2), 2.49-2.40 (m, 4H, =CCH_2), 2.27 (s, 1H, C*H*), 1.27 (t, *J* = 7.16 Hz, 3H, OCH_2CH_3), 1.15 (t, J = 7.5 Hz , 6H,

`

=CCH$_2$C*H$_3$). ^{19}F NMR ($CDCl_3$): δ (ppm) -58.8 (s), -61.7 (s). ^{13}C{^{1}H} NMR ($CDCl_3$): δ (ppm) 180.9 (br, C=O), 142.6 (q, $^2J_{C\text{-}F}$ = 38.4 Hz, C-3/C-5), 139.6 (q, $^2J_{C\text{-}F}$ = 43.2 Hz, C-3/C-5), 120.3 (q, $^1J_{C\text{-}F}$ =268.7 Hz, CF_3), 119.3 (q, $^1J_{C\text{-}F}$ =271.1 Hz, CF_3), 106.5 (C-4), 104.9 (s, C=C), 61.6 (s, O*C*H$_2$), 24.8 (s, *C*H), 18.5 (s, =C*C*H$_2$), 14.3 (OCH$_2$*C*H$_3$), 11.5 (s, =CCH$_2$*C*H$_3$). IR (cm^{-1}): 3167, 2990, 2948, 2633, 1647 (C=O), 1559, 1498, 1467, 1374, 1270, 1248, 1182, 1158, 1146, 1078, 1041, 994, 831. Raman (cm^{-1}), selected peak: 1555, 1652, 1914. In contrast to the bis(pyrazolyl)borate analog, our initial attempt to [HB(3,5-(CF$_3$)$_2$Pz)$_3$]Cu(Cyp-**2**) via [HB(3,5-(CF$_3$)$_2$Pz)$_3$]Cu(NCMe) and Cyp-**2** at room temperature was unsuccessful.

[H$_2$B(3,5-(CF$_3$)$_2$Pz)$_2$]Cu(EtC≡CEt) (47): [H$_2$B(3,5-(CF$_3$)$_2$Pz)$_2$]Cu(NCMe) (0.15 g, 0.29 mmol) was dissolved in 7 mL dichloromethane. 3-hexyne (39 μL, 0.35 mmol) was added to the reaction mixture and stirred overnight. The solvent was evaporated to get white powder product. The product was dissolved in dichloromethane and kept at -20 °C to obtain colorless crystals of [H$_2$B(3,5-(CF$_3$)$_2$Pz)$_2$]Cu(EtC≡CEt). Yield: 80%. M.P.: 81-83 °C (decomposition). Anal. Calc. $C_{16}H_{14}BCuF_{12}N_4$: C, 34.03%; H, 2.50%; N, 9.92%. Found: C, 34.31%; H, 2.19%; N, 9.56%. ^{1}H NMR ($CDCl_3$): δ (ppm) 6.86 (s, 2H, Pz*H*), 3.94 (br, 2H, B*H*$_2$), 2.48 (q, *J* = 7.5 Hz, 4H, ≡CC*H*$_2$ ×2), 1.21 (t, *J* = 7.5 Hz, 6H, ≡CCH$_2$C*H*$_3$ ×2). ^{19}F NMR ($CDCl_3$): δ (ppm) -59.8 (s), -61.6 (s). ^{13}C{^{1}H} NMR ($CDCl_3$): δ (ppm) 141.6 (q, $^2J_{C\text{-}F}$ = 38.4 Hz, C-3/C-5), 139.7 (q, $^2J_{C\text{-}F}$ = 40.8 Hz, C-3/C-5), 120.2 (q, $^1J_{C\text{-}F}$ =269.9 Hz, CF_3), 119.3 (q, $^1J_{C\text{-}F}$ =271.1 Hz, CF_3), 106.1 (C-4), 91.0 (C≡C), 16.7 (*C*H$_2$), 14.8 (*C*H$_3$). Raman (cm^{-1}), selected peak: 2064 (C≡C).

`

Ethyl 2,3-diethylcycloprop-2-enecarboxylate (Cyp-**2, 78**)[325]: From 3-Hexyne and ethyl diazoacetate as described in the general method (see above). Colorless oil (61%). ^{1}H NMR (500 MHz, $CDCl_3$): δ 4.04 (q, *J* = 6.9 Hz, 2H, OC*H*$_2$), 2.35 (q, *J* = 7.5 Hz, 4H, =CC*H*$_2$), 1.98 (s, 1H, C*H*), 1.17 (t, *J* = 6.9 Hz, 3H, OCH_2CH_3), 1.08 (t, *J* = 7.5 Hz, 6H, $=CCH_2CH_3$). ^{13}C{^{1}H} NMR (125 MHz, $CDCl_3$): δ 177.1, 106.5, 59.7, 22.2, 18.1, 14.4, 11.7.

Ethyl 2,3-diphenylcycloprop-2-enecarboxylate (Cyp-**3, 79**)[326]: From Diphenylacetylene and ethyl diazoacetate as described in the general method (see above). White solid (64%). ^{1}H NMR (500 MHz, $CDCl_3$): δ 7.73-7.71 (m, 4H, Ar*H*), 7.51-7.48 (m, 4H, Ar*H*), 7.42-7.39 (m, 2H, Ar*H*), 4.23 (q, *J* = 6.9 Hz, 2H, OC*H*$_2$), 2.87 (s, 1H, C*H*), 1.28 (t, *J* = 6.9 Hz, 3H, OCH_2CH_3). ^{13}C{^{1}H} NMR (125 MHz, $CDCl_3$): δ 174.9, 129.9, 129.3, 128.9, 127.1, 107.6, 60.4, 21.7, 14.4.

Ethyl 2,3-bis(trimethylsilyl)cycloprop-2-enecarboxylate (Cyp-**4, 80**)[327]: From Diphenylacetylene and ethyl diazoacetate as described in the general method (see above). Colorless oil (30%). ^{1}H NMR (500 MHz, $CDCl_3$): δ 4.06 (q, *J* = 6.9 Hz, 2H, OC*H*$_2$), 1.88 (s, 1H, C*H*), 1.20 (t, *J* = 6.9 Hz, 3H, OCH_2CH_3), 0.20 (s, 18H, $Si(CH_3)_3$. ^{13}C{^{1}H} NMR (125 MHz, $CDCl_3$): δ 177.6, 125.2, 59.8, 18.6, 14.6, -1.5.

Ethyl 2-methyl-3-phenylcycloprop-2-enecarboxylate (Cyp-**5, 81**)[328]: From 1-Phenyl-1-propyne and ethyl diazoacetate as described in the general method (see above). Colorless oil (94%). ^{1}H NMR (500 MHz, $CDCl_3$): δ 7.47-7.45 (m,

`

2H, Ar*H*), 7.40-7.37 (m, 2H, Ar*H*), 7.32-7.29 (m, 1H, Ar*H*), 4.19-4.12 (m, 2H, OCH_2), 2.43 (s, 1H, C*H*), 2.33 (s, 3H, , =CCH_3), 1.25 (t, *J* = 6.9 Hz, 3H, OCH_2CH_3). $^{13}C\{^1H\}$ NMR (125 MHz, $CDCl_3$): δ 175.8, 129.3, 128.7, 128.6, 127.2, 106.4, 105.3, 60.2, 22.6, 14.5, 10.8.

Ethyl 2,3-dipropylcycloprop-2-enecarboxylate (Cyp-**6, 82**)[326]: From 4-Octyne and ethyl diazoacetate as described in the general method (see above). Colorless oil oil (62%). ^1H NMR (500 MHz, $CDCl_3$): δ 4.09 (q, *J* = 6.9 MHz, 2H, OCH_2), 2.37 (t, *J* = 7.5 Hz, 4H, =CCH_2), 2.02 (s, 1H, C*H*), 1..60-1.53 (m, 4H, $=CCH_2CH_2$), 1.22 (t, *J* = 6.9 Hz, 3H, OCH_2CH_3), 0.94 (t, *J* = 7.5 Hz, 6H, $=CCH_2CH_2CH_3$). $^{13}C\{^1H\}$ NMR (125 MHz, $CDCl_3$): δ 177.2, 105.8, 59.9, 26.7, 22.4, 20.5, 14.5, 14.0.

Ethyl 2-butylcycloprop-2-enecarboxylate (Cyp-**7, 83**)[328]: From 1-Hexyne and ethyl diazoacetate as described in the general method (see above). Colorless oil (56%). ^1H NMR (500 MHz, $CDCl_3$): δ 6.32 (m, 1H, ,=C*H*), 4.16-4.08 (m, 2H, OCH_2), 2.50-2.47 (m, 2H, =CCH_2), 2.12-2.11 (m, 1H, C*H*), 1.59-1.53 (m, 2H, $=CCH_2CH_2$), 1.42-1.34 (m, 2H, CH_2), 1.27-1.23 (m, 3H, OCH_2CH_3), 0.92-0.89 (m, 3H, CH_3). $^{13}C\{^1H\}$ NMR (125 MHz, $CDCl_3$): δ 176.7, 115.7, 94.0, 60.2, 28.8, 24.8, 22.3, 19.8, 14.5, 13.8.

Ethyl 2-hexylcycloprop-2-enecarboxylate (Cyp-**8, 84**)[327]: From 1-Octyne and ethyl diazoacetate as described in the general method (see above). Colorless oil (37%). ^1H NMR (500 MHz, $CDCl_3$): δ 6.29 (m, 1H, =C*H*), 4.12-4.08 (m, 2H, OCH_2), 2.48-2.45 (m, 2H, =CCH_2), 2.09 (m, 1H, C*H*), 1.58-1.52 (m, 2H,

`

=CCH$_2$C*H$_2$*), 1.33-1.21 (m, 9H, CH$_2$CH$_2$CH$_2$ & OCH$_2$C*H$_3$*), 0.86-0.84 (m, 3H, C*H$_3$*). ^{13}C{^{1}H} NMR (125 MHz, $CDCl_3$): δ 176.7, 115.7, 94.0, 60.2, 31.6, 28.9, 26.7, 25.0, 22.6, 19.8, 14.4, 14.1.

Low Temperature Proton NMR Spectroscopy Study for Equilibrium Constant Determinations

[(CF$_3$)$_2$Bp]Cu(3-hexyne) + Cyp-**2** ⇌ [(CF$_3$)$_2$Bp]Cu(Cyp-**2**) + 3-hexyne

Ethyl 2,3-diethylcycloprop-2-enecarboxylate (Cyp-**2**; 5.96 mg, 0.035 mmol) was added to an NMR tube containing a CD_2Cl_2 solution of [(CF$_3$)$_2$Bp]Cu(3-hexyne) (20 mg, 0.035 mmol). The tube was shaken and placed in the probe of an NMR spectrometer. The temperature was gradually cooled from room temperature to -40 °C. The data were collected at room temperature, 10 °C, 0 °C, -20 °C, -30 °C, and - 40 °C. The relative concentration of [(CF$_3$)$_2$Bp]Cu(Cyp-**2**), [(CF$_3$)$_2$Bp]Cu(3-hexyne), Cyp-**2**, and 3-hexyne were determined by integrating the resonance corresponding to the protons of bound [4.35 ppm, 2H] and free [4.04 ppm, 2H] Ethyl 2,3-diethylcycloprop-2-enecarboxylate (Cyp-**2**) and the resonances corresponding to the proton of bound [1.21 ppm, 6H] and free [2.48 ppm, 4H] 3-hexyne.

The equilibrium constant Keq = [[(CF$_3$)$_2$Bp]Cu(Cyp-**2**)][3-hexyne]/[[(CF$_3$)$_2$Bp]Cu(3-hexyne)][Cyp-**2**] = 0.12 at -30 °C was determined. (The peaks at room temperature, 10 °C, 0 °C, and -20 °C were broad and overlapping. It was difficult to integrate the peaks individually).

`

$[(CF_3)_2Bp]Cu(Cyp\text{-}\mathbf{2})$ + 3-hexyne ⇌ $[(CF_3)_2Bp]Cu$(3-hexyne) + Cyp-**2**

To ensure that the equilibrium was achieved under these conditions, the following control experiment was performed. 3-hexyne (1.26 mg, 0.015 mmol) was added to an NMR tube contained CD_2Cl_2 solution of $[(CF_3)_2Bp]Cu(Cyp\text{-}\mathbf{2})$ (10 mg, 0.015 mmol). The tube was shaken and placed in the probe of an NMR spectrometer. The temperature was gradually cooled from room temperature to -40 °C. The data were collected at room temperature, 10 °C, 0 °C, -20 °C, -30 °C, and - 40 °C. The relative concentrations of $[(CF_3)_2Bp]Cu(Cyp\text{-}\mathbf{2})$, $[(CF_3)_2Bp]Cu$(3-hexyne), Cyp-**2**, and 3-hexyne were determined as described in the above paragraph.

The equilibrium constant determined from this experiment Keq = $[[(CF_3)_2Bp]Cu(cyp\text{-}\mathbf{2})]$[3-hexyne]/$[[(CF_3)_2Bp]Cu$(3-hexyne)][Cyp-**2**] = 0.11 at -30 °C was not significantly different from that obtained from treatment of $[H_2B(3,5\text{-}(CF_3)_2Pz)_2]Cu$(3-hexyne) with Cyp-**2**.

$[(CF_3)_2Bp]Cu(NCMe)$ + Cyp-**2** ⇌ $[(CF_3)_2Bp]Cu(Cyp\text{-}\mathbf{2})$ + MeCN

Ethyl 2,3-diethylcycloprop-2-enecarboxylate (Cyp-**2 ;** 6.44 mg, 0.038 mmol) was added to an NMR tube containing a CD_2Cl_2 solution of $[(CF_3)_2Bp]Cu(NCMe)$ (**1**; 20 mg, 0.038 mmol). The tube was shaken and placed in the probe of an NMR spectrometer. The temperature was gradually cooled from room temperature to -50 °C. The data were collected at room temperature,

`

10 °C, 0 °C, -20 °C, -30 °C, and -40 °C. The reaction was attained equilibrium at -30 °C. The relative concentration of $[(CF_3)_2Bp]Cu(Cyp\text{-}\mathbf{2})$, **1**, Cyp-**2**, and MeCN were determined by integrating the resonance corresponding to the protons of bound [4.35 ppm, 2H] and free [4.04 ppm, 2H] Ethyl 2,3-diethylcycloprop-2-enecarboxylate (Cyp-**2**) and the resonances corresponding to the proton of bound [2.3 ppm, 3H] and free [2.03 ppm, 3H] MeCN.

The equilibrium constant Keq = $[[(CF_3)_2Bp]Cu(Cyp\text{-}\mathbf{2})][MeCN]/[[(CF_3)_2Bp]Cu(NCMe)][Cyp\text{-}\mathbf{2}]$ = 10.98 at -30 °C was determined.

$[(CF_3)_2Bp]Cu(NCMe) + 3\text{-hexyne} \rightleftharpoons [(CF_3)_2Bp]Cu(3\text{-hexyne}) + MeCN$

3-Hexyne (3.14 mg, 0.038 mmol) was added to an NMR tube containing a CD_2Cl_2 solution of $[(CF_3)_2Bp]Cu(NCMe)$ (**1**; 20 mg, 0.038 mmol). The tube was shaken and placed in the probe of an NMR spectrometer. The temperature was gradually cooled from room temperature to -50 °C. The data were collected at room temperature, 10 °C, 0 °C, -20 °C, -30 °C, - 40 °C and -50 °C. The reaction shifted towards the products as soon as the reagents were mixed. It stayed as the product at all temperatures.

Then excess acetonitrile was added to this reaction mixture (NMR tube) and ^1H NMR data was collected at room temperature. The spectrum showed only starting materials and excess free acetonitrile in the reaction mixture (from ^1H NMR) indicating that the mixture is in equilibrium and it is possible to drive the reaction back with a large excess of acetonitrile.

`

Cyclopropenation for Alkynes

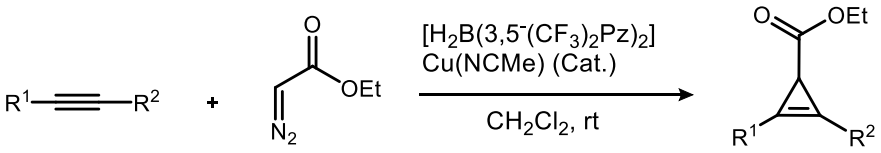

General Method for the Synthesis of Cyclopropenes (from Internal Alkynes): A 50 mL Schlenk flask was charged with the selected internal alkyne (4.5 mmol, 3.0 equiv.), $[(CF_3)_2Bp]Cu(NCMe)$ (3 mol%) and dichloromethane (20 mL) under a nitrogen atmosphere. Ethyl diazoacetate (1.5 mmol) was added to the reaction via a syringe pump over 10 h. Following the complete addition of the ethyl diazoacetate, the reaction mixture was stirred for 2 h and the solvent was removed under reduced pressure. The residue was purified by flash column chromatography (Ethylacetate:Hexanes).

General Method for the Synthesis of Cyclopropenes (from Terminal Alkynes): A 50 mL Schlenk flask was charged with the selected terminal alkyne (7.5 mmol, 5.0 equiv.), $[(CF_3)_2Bp]Cu(NCMe)$ (3 mol%) and dichloromethane (20 mL) under a nitrogen atmosphere. Ethyl diazoacetate (1.5 mmol) was added to the reaction via a syringe pump over 10 h. Following the complete addition of the ethyl diazoacetate, H_2S gas (generated by slowly adding hydrochloric acid to Na_2S) was bubbled to quench the reaction. The solvent was filtered through filter paper. The filtrate was concentrated, and the residue was purified using column chromatography (Ethylacetate:Hexanes).

`

X-ray Data Collection and Structure Determinations

A suitable crystal covered with a layer of hydrocarbon/Paratone-N oil was selected and mounted on a Cryo-loop and immediately placed in the low temperature nitrogen stream. The X-ray intensity data were measured at 100(2) K on a Bruker D8 Quest with a Photon 100 CMOS detector equipped with an Oxford Cryosystems 700 series cooler, a Triumph monochromator, and a Mo Kα fine-focus sealed tube (λ = 0.71073 Å). Intensity data were processed using the Bruker ApexIII program suite. Absorption corrections were applied by using SADABS.[296] Initial atomic positions were located by direct methods using SHELXT,[297] and the structures of the compounds were refined by the least-squares method using SHELXL.[298] All the non-hydrogen atoms were refined anisotropically. The hydrogen atoms of [$(CF_3)_2$Bp]Cu(Cyp-**2**), [$(CF_3)_2$Bp]Cu(Cyp-**3**) and [$(CF_3)_2$Bp]Cu(Cyp-**4**) attached to the boron atoms were located in difference Fourier maps, included and refined freely with isotropic displacement parameters. All the other hydrogen atoms of [$(CF_3)_2$Bp]Cu(Cyp-**2**), [$(CF_3)_2$Bp]Cu(Cyp-**3**), [$(CF_3)_2$Bp]Cu(Cyp-**4**), [$(CF_3)_2$Tp]Cu(Cyp-**4**), and Cyp-**3** were placed at calculated positions and refined using a riding model. X-ray structural figures were generated using Olex2.[298] The CCDC **2032777**-**2032781** contains the supplementary crystallographic data. These data can be obtained free of charge *via* http://www.ccdc.cam.ac.uk/conts/retrieving.html or from the Cambridge Crystallographic Data Centre (CCDC), 12 Union Road, Cambridge, CB2 1EZ, UK).

`

Appendix A

Spectroscopic Data of Chapter 2 Part 2.1

`

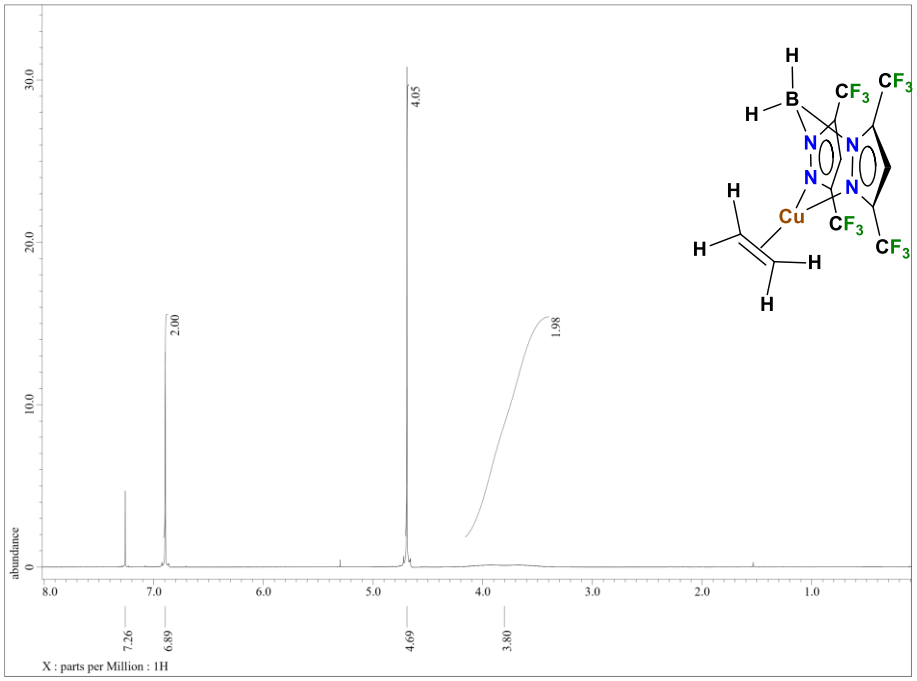

^{1}H NMR Spectrum of $[H_2B(3,5\text{-}(CF_3)_2Pz)_3]Cu(C_2H_4)$ **(13)** in $CDCl_3$.

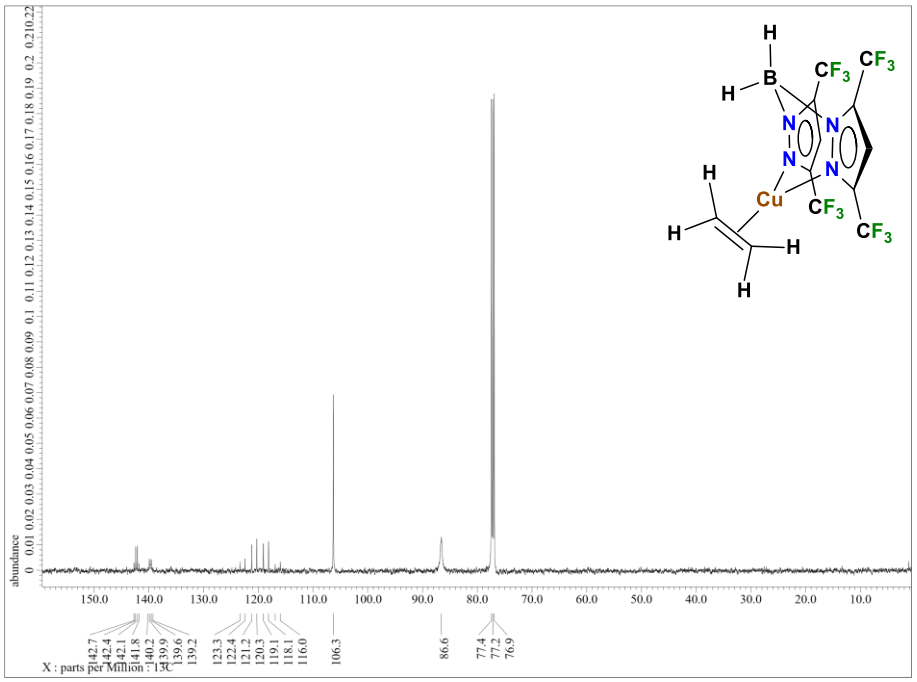

^{13}C NMR Spectrum of $[H_2B(3,5\text{-}(CF_3)_2Pz)_3]Cu(C_2H_4)$ **(13)** in $CDCl_3$.

`

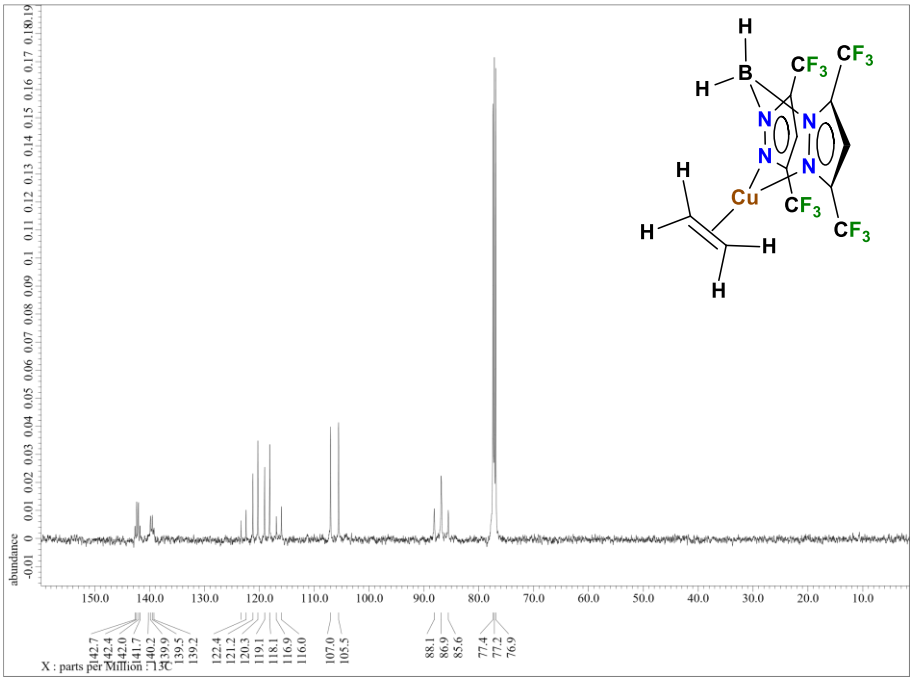

^{1}H coupled ^{13}C NMR Spectrum of $[H_2B(3,5\text{-}(CF_3)_2Pz)_3]Cu(C_2H_4)$ **(13)** in $CDCl_3$.

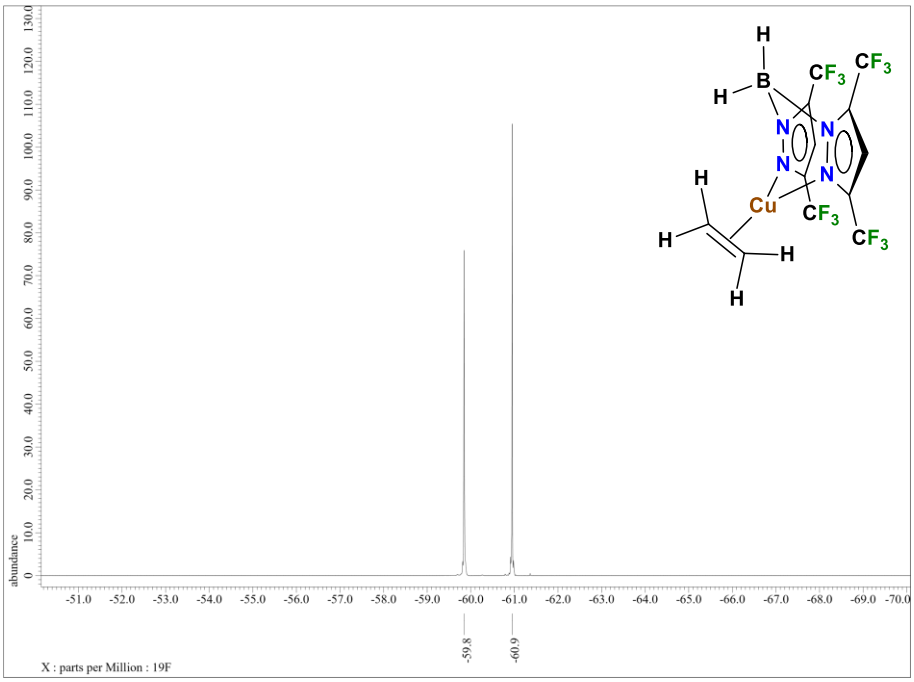

^{19}F NMR Spectrum of $[H_2B(3,5\text{-}(CF_3)_2Pz)_3]Cu(C_2H_4)$ **(13)** in $CDCl_3$.

`

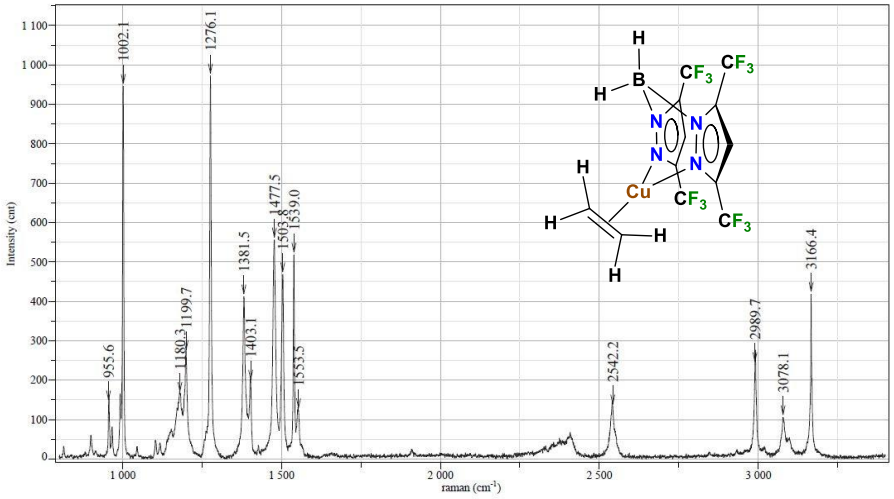

Exposition	5	Slit	100
Accumulation	1 x 21	Operator	Anurag
Laser	632.817	Sample	
Spectro	Auto	Remark	
Hole	200	Power	

Raman Spectrum of $[H_2B(3,5\text{-}(CF_3)_2Pz)_3]Cu(C_2H_4)$ **(13)**.

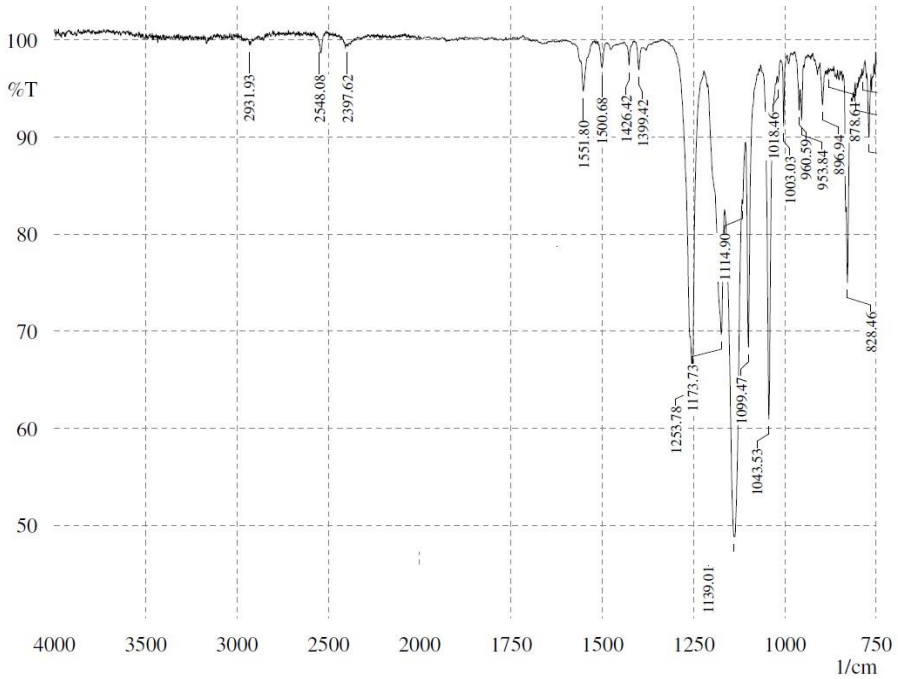

IR Spectrum of $[H_2B(3,5\text{-}(CF_3)_2Pz)_3]Cu(C_2H_4)$ **(13)** (Powder sample was used to collect the IR spectrum).

`

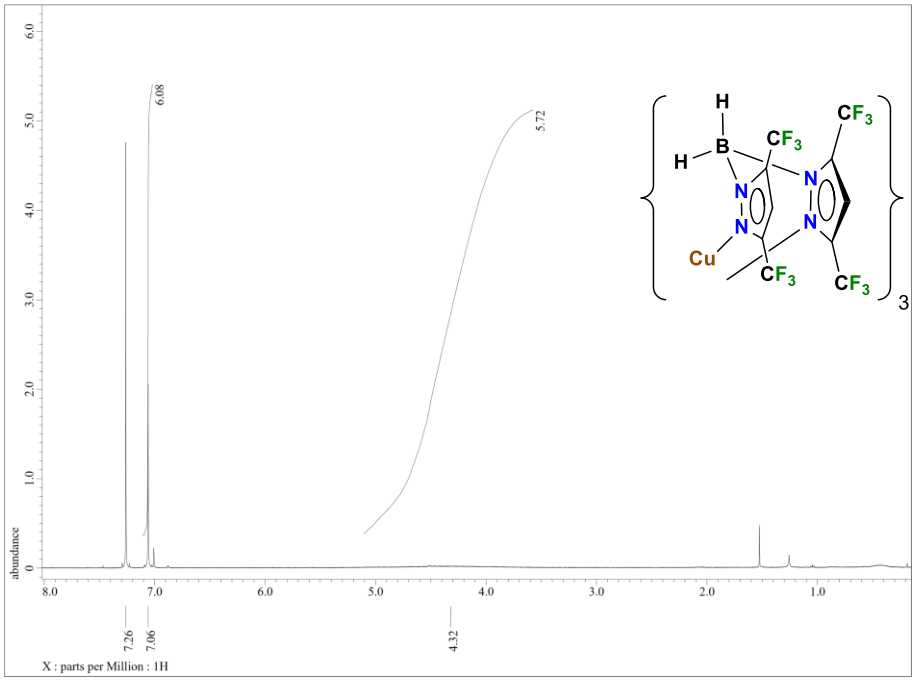

^{1}H NMR Spectrum of {[$H_2B(3,5\text{-}(CF_3)_2Pz)_3$]Cu}$_3$ **(14)** in $CDCl_3$.

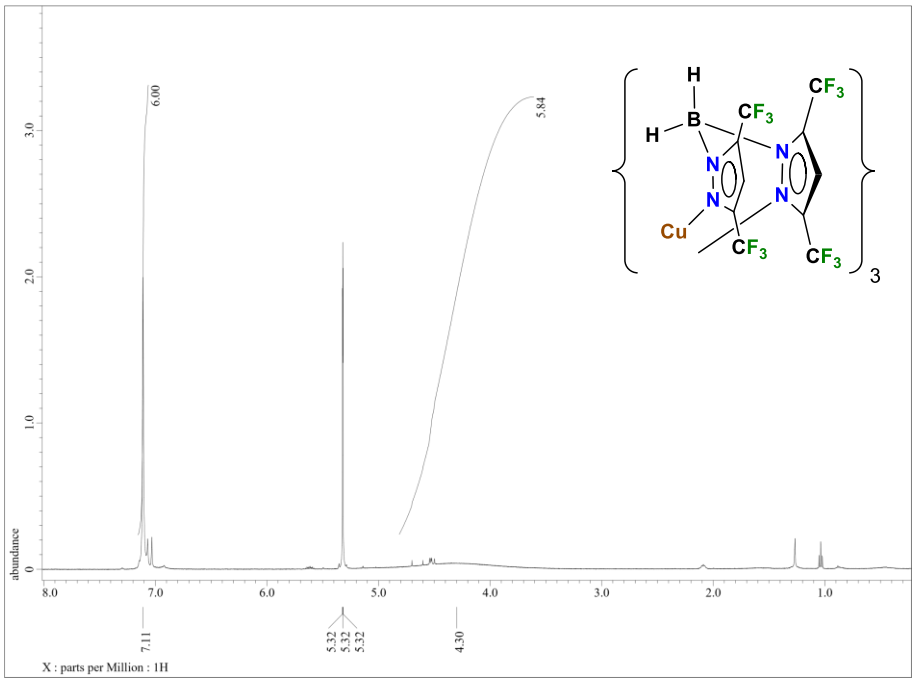

^{1}H NMR Spectrum of {[$H_2B(3,5\text{-}(CF_3)_2Pz)_3$]Cu}$_3$ **(14)** in CD_2Cl_2.

`

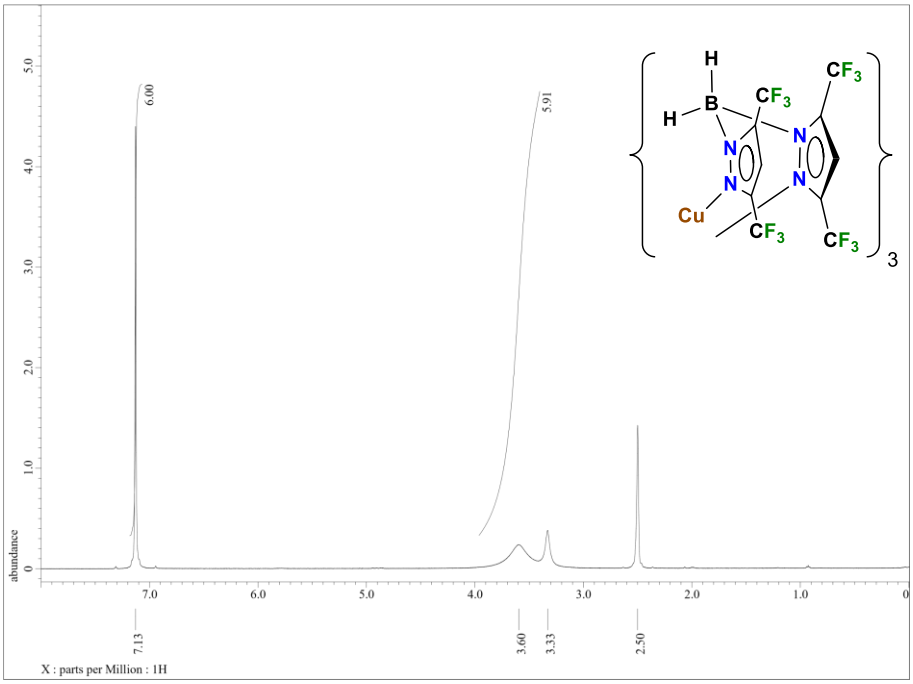

^{1}H NMR Spectrum of {[$H_2B(3,5\text{-}(CF_3)_2Pz)_3$]Cu}$_3$ **(14)** in $(CD_3)_2SO$.

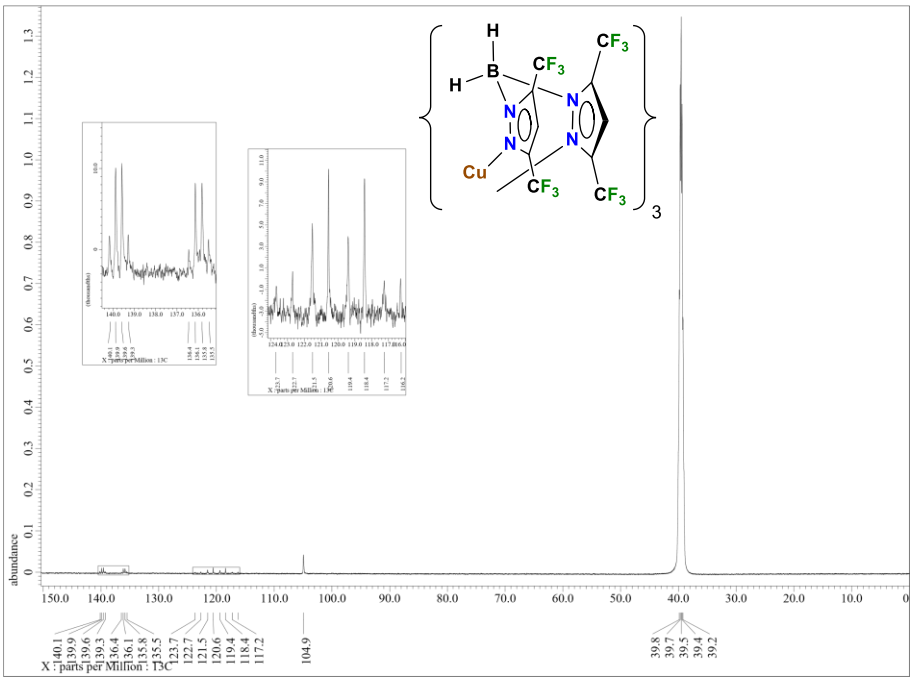

^{13}C NMR Spectrum of {[$H_2B(3,5\text{-}(CF_3)_2Pz)_3$]Cu}$_3$ **(14)** in $(CD_3)_2SO$ (DMSO was used just for ^{13}C and ^{19}F NMR due to poor solubility in $CDCl_3$ and CD_2Cl_2).

`

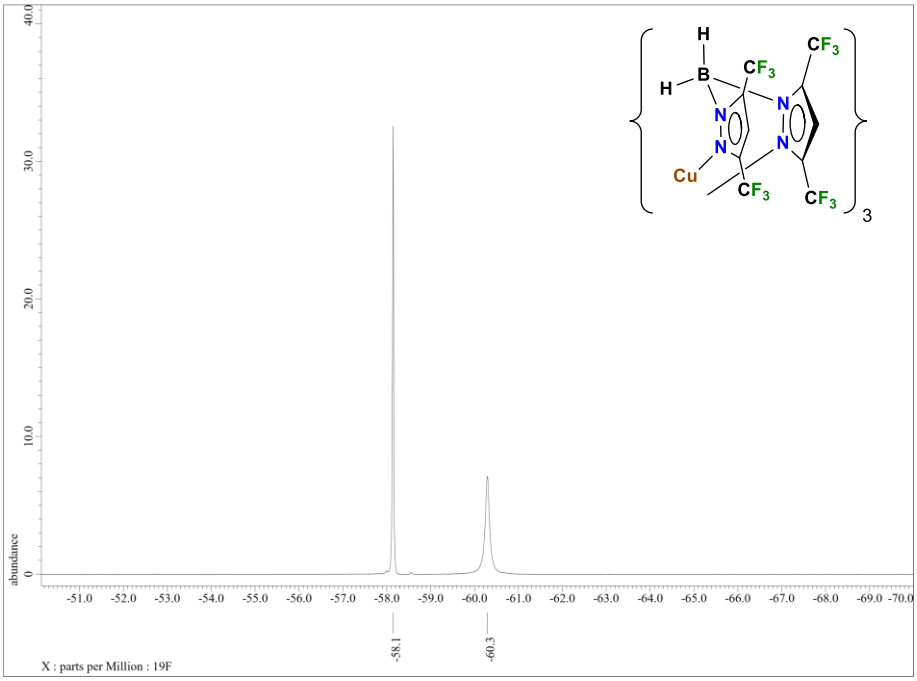

^{19}F NMR Spectrum of $\{[H_2B(3,5\text{-}(CF_3)_2Pz)_3]Cu\}_3$ **(14)** in $(CD_3)_2SO$ (DMSO was used just for ^{13}C and ^{19}F NMR due to poor solubility in $CDCl_3$ and CD_2Cl_2).

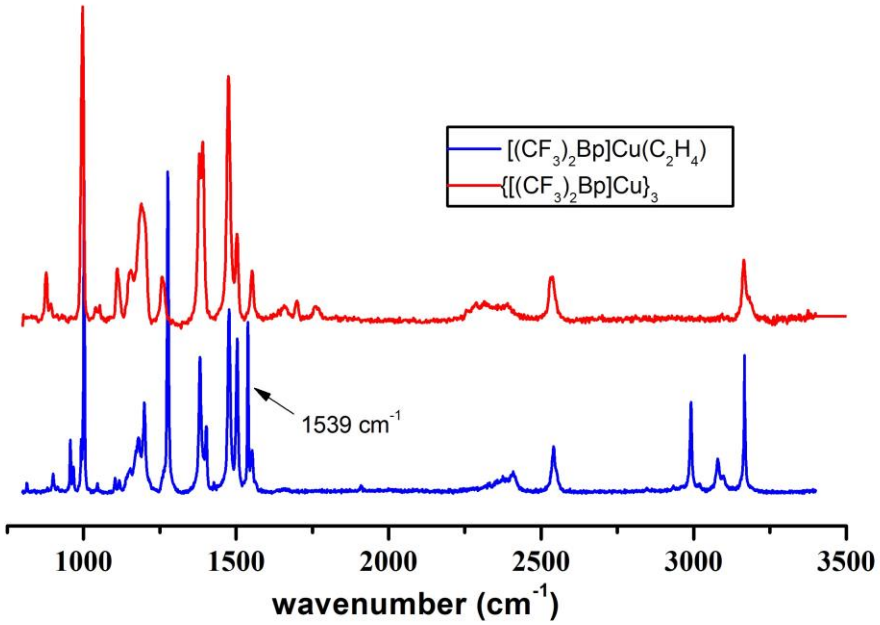

Comparison of Raman Spectra of $\{[H_2B(3,5\text{-}(CF_3)_2Pz)_3]Cu\}_3$ **(14)** and $[H_2B(3,5\text{-}(CF_3)_2Pz)_3]Cu(C_2H_4)$ **(13)**.

`

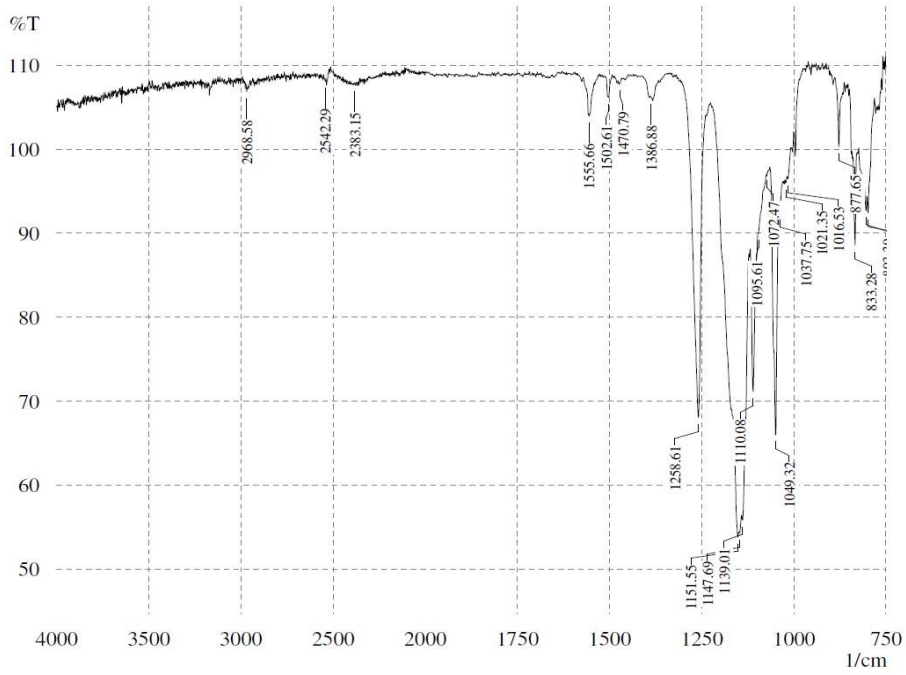

IR Spectrum of $\{[H_2B(3,5\text{-}(CF_3)_2Pz)_3]Cu\}_3$ **(14)** (Powder sample was used to collect the IR spectrum)**.**

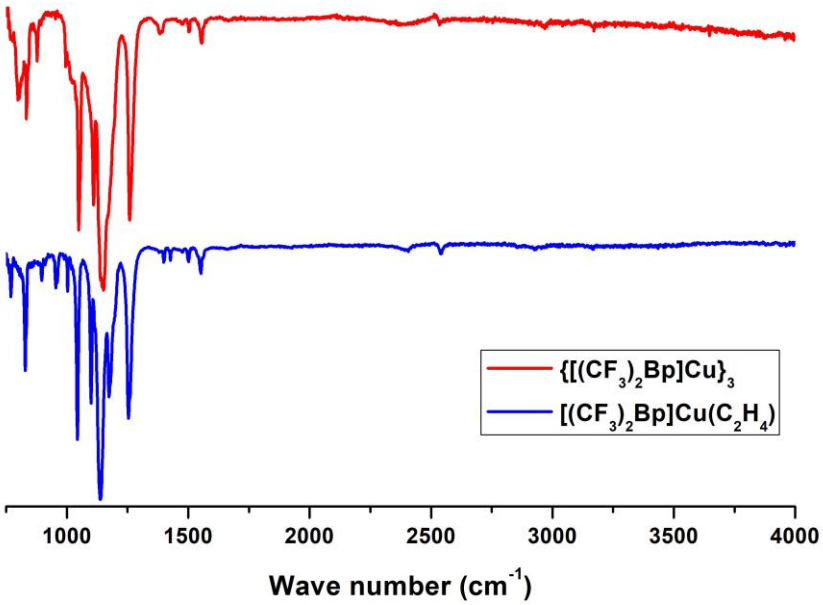

Comparison of IR Spectra of $\{[H_2B(3,5\text{-}(CF_3)_2Pz)_3]Cu\}_3$ **(14)** and $[H_2B(3,5\text{-}(CF_3)_2Pz)_3]Cu(C_2H_4)$ **(13)**.

`

Spectroscopic Data of Chapter 2 Part 2.2

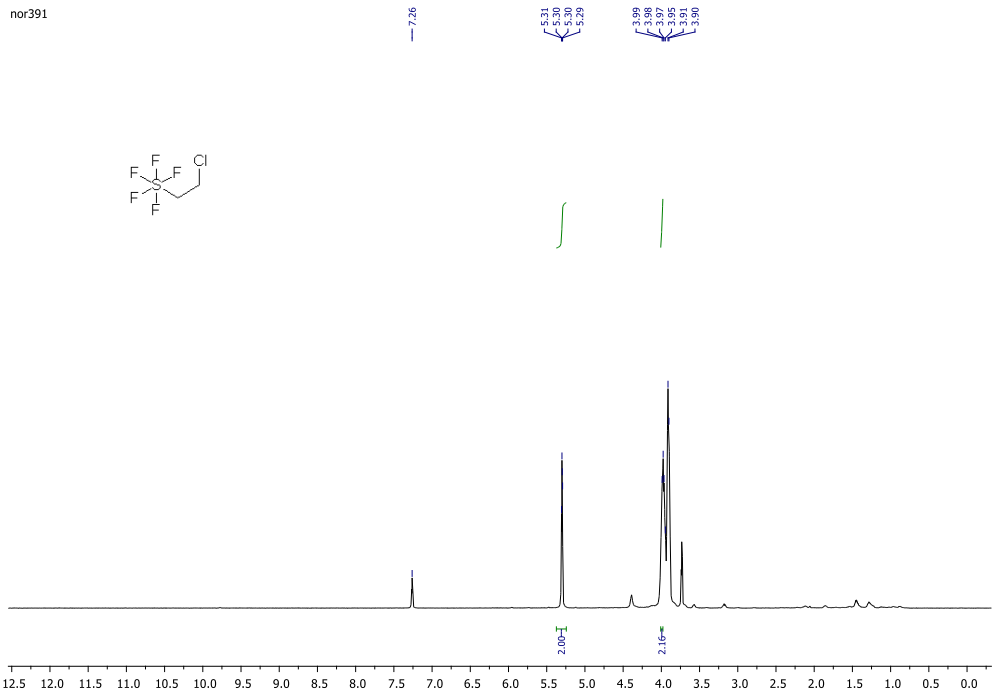

^{1}H NMR Spectrum of (2-Chloroethyl)pentafluoro-λ^{6}-sulfane in $CDCl_3$.

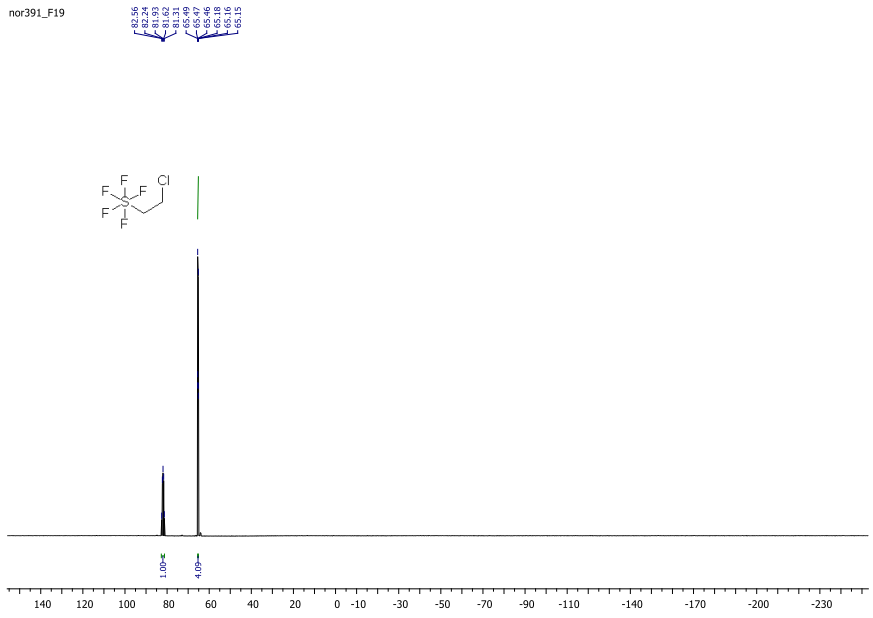

^{19}F NMR Spectrum of (2-Chloroethyl)pentafluoro-λ^{6}-sulfane in $CDCl_3$.

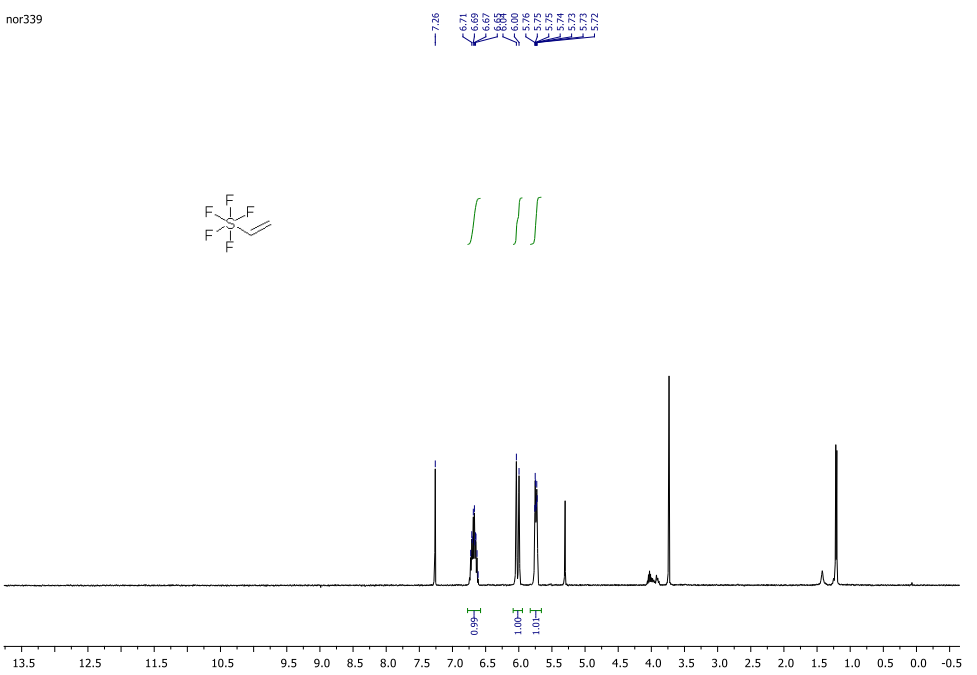

^{1}H NMR Spectrum of Pentafluoro(vinyl)-λ^{6}-sulfane (**19**) in $CDCl_3$.

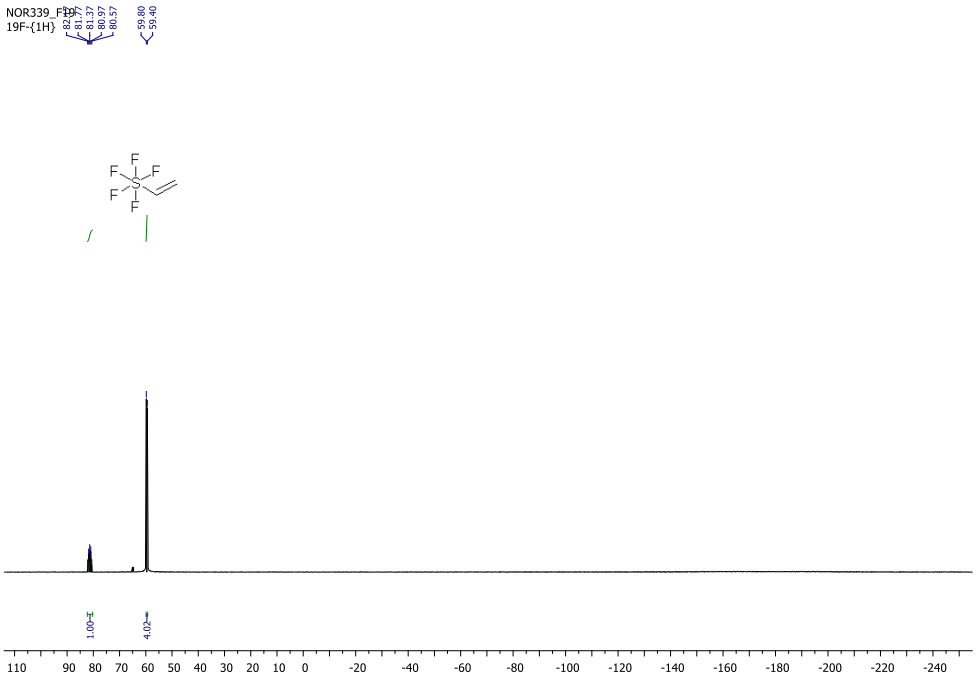

^{19}F NMR Spectrum of Pentafluoro(vinyl)-λ^{6}-sulfane (**19**) in $CDCl_3$.

`

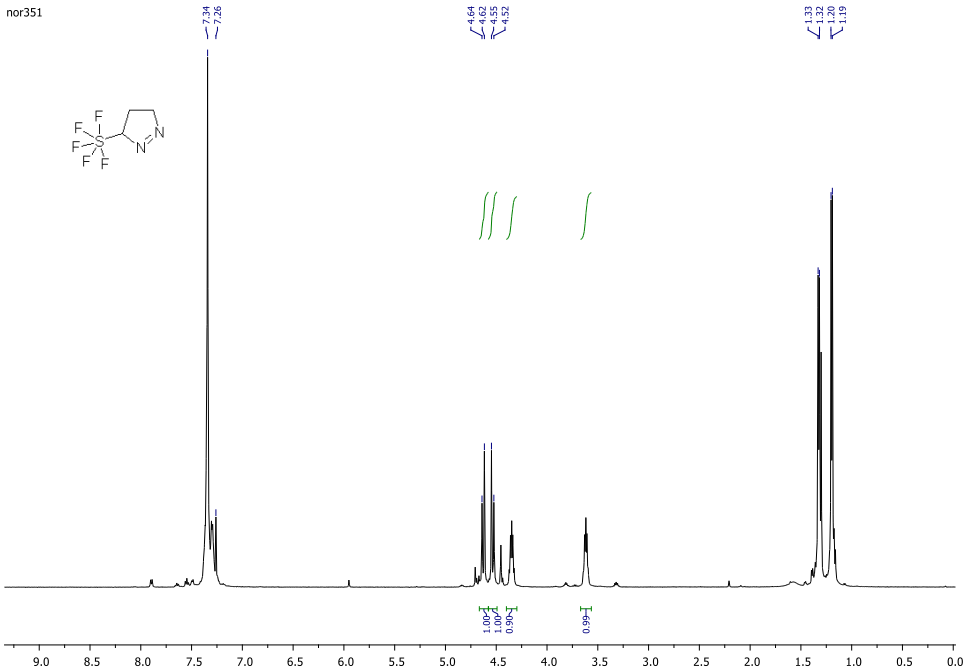

^{1}H NMR Spectrum of 5-(Pentafluoro-λ^{6}-sulfanyl)-4,5-dihydro-3*H*-pyrazole (**20**) in $CDCl_3$.

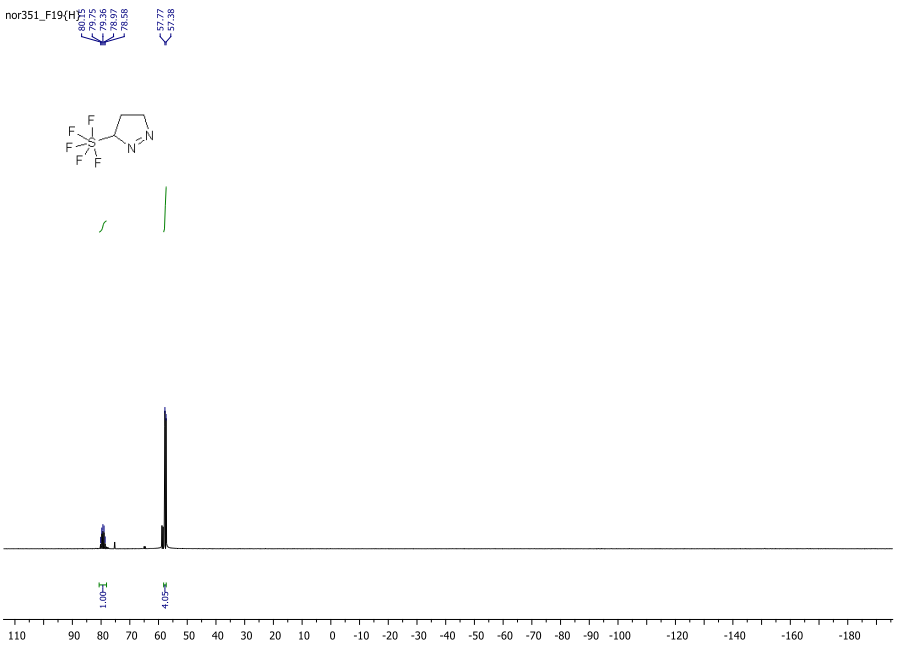

^{19}F NMR Spectrum of 5-(Pentafluoro-λ^{6}-sulfanyl)-4,5-dihydro-3*H*-pyrazole (**20**) in $CDCl_3$.

`

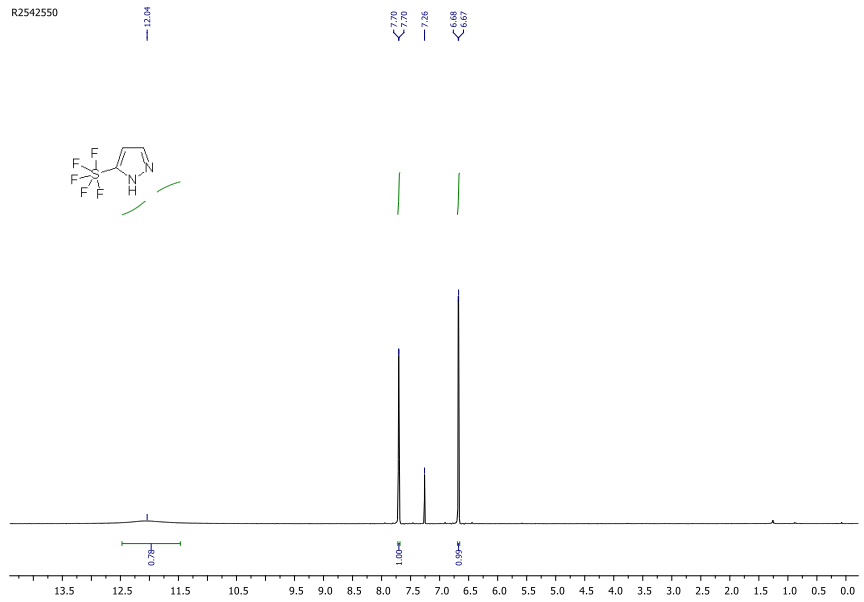

^{1}H NMR Spectrum of 5-(Pentafluoro-λ^{6}-sulfanyl)-1*H*-pyrazole (**17**) in $CDCl_3$.

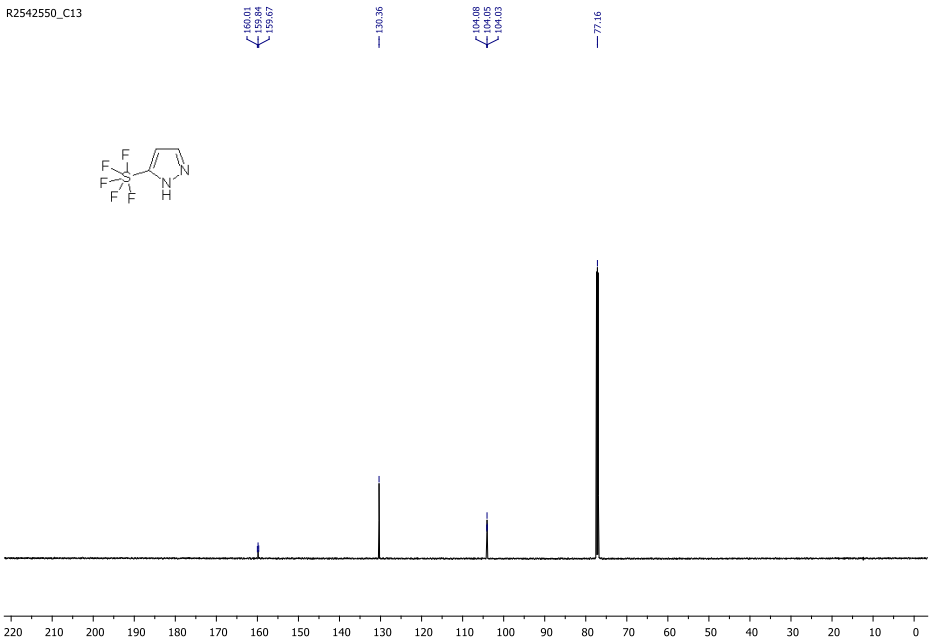

^{13}C NMR Spectrum of 5-(Pentafluoro-λ^{6}-sulfanyl)-1*H*-pyrazole (**17**) in $CDCl_3$.

`

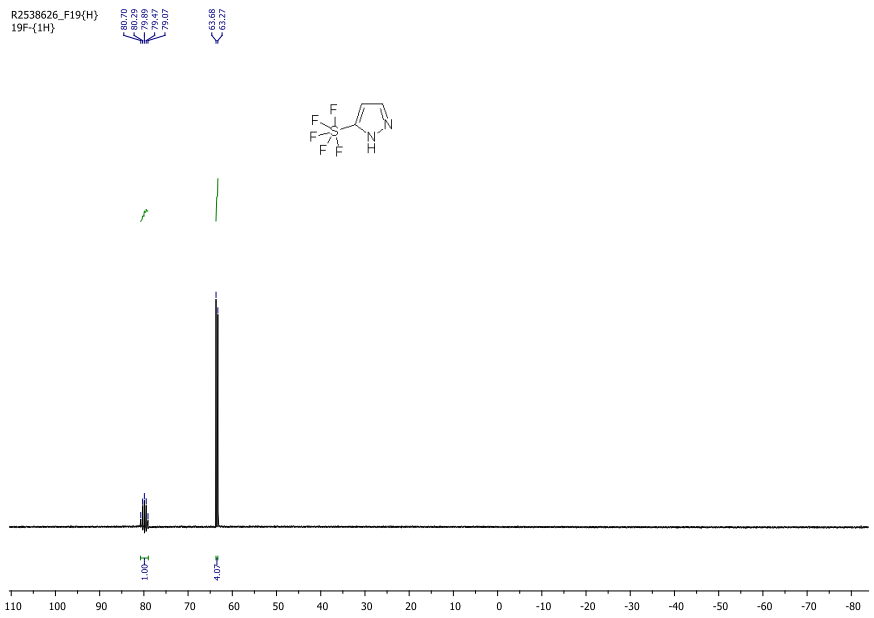

^{19}F NMR Spectrum of 5-(Pentafluoro-λ^6-sulfanyl)-1*H*-pyrazole (**17**) in $CDCl_3$.

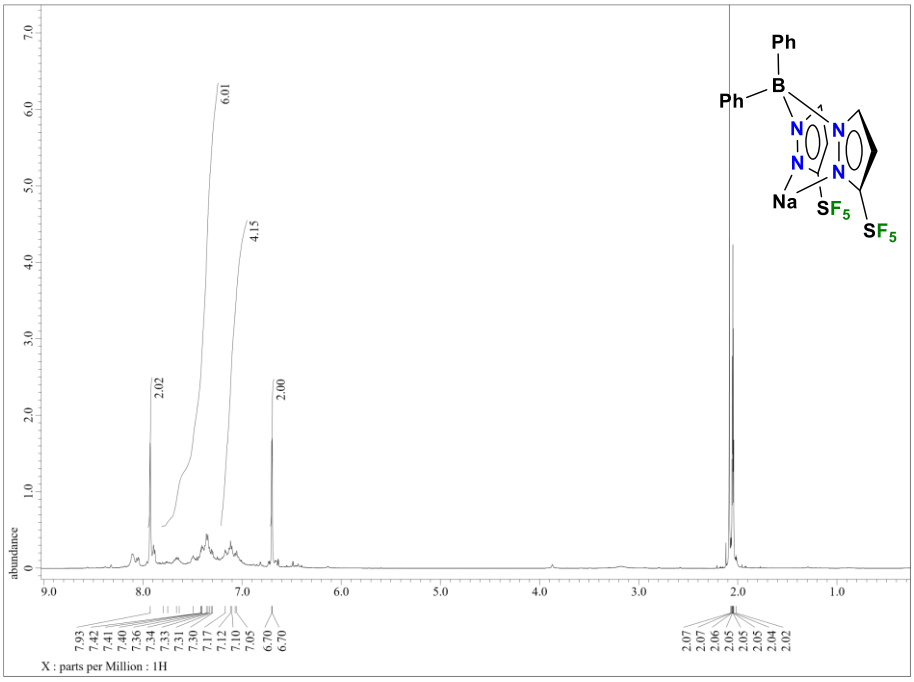

^{1}H NMR Spectrum of $[Ph_2B(3\text{-}(SF_5)Pz)_2]Na$ (**21**) in $(CD_3)_2CO$.

`

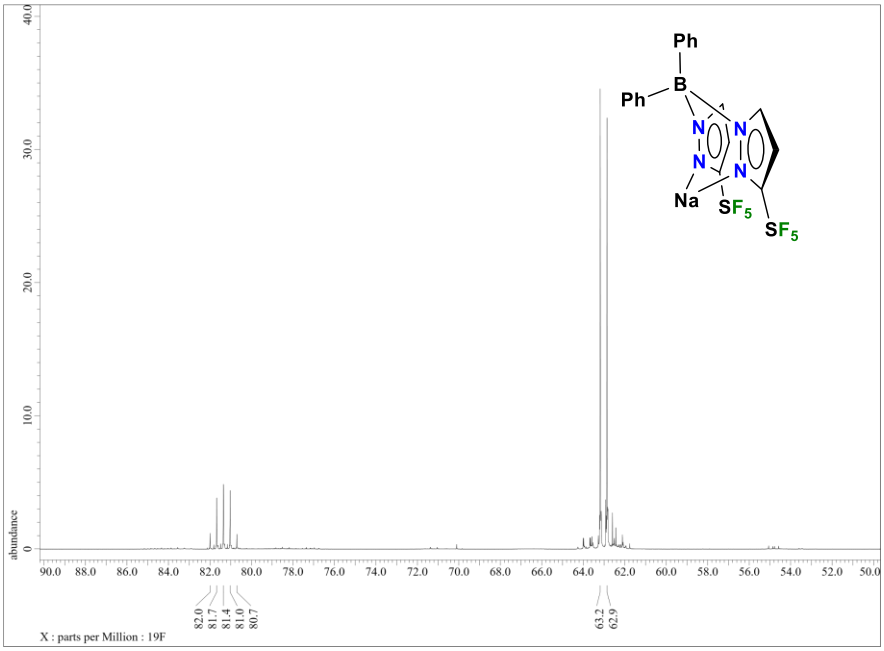

^{19}F NMR Spectrum of [$Ph_2B(3\text{-}(SF_5)Pz)_2$]Na (**21**) in $(CD_3)_2CO$.

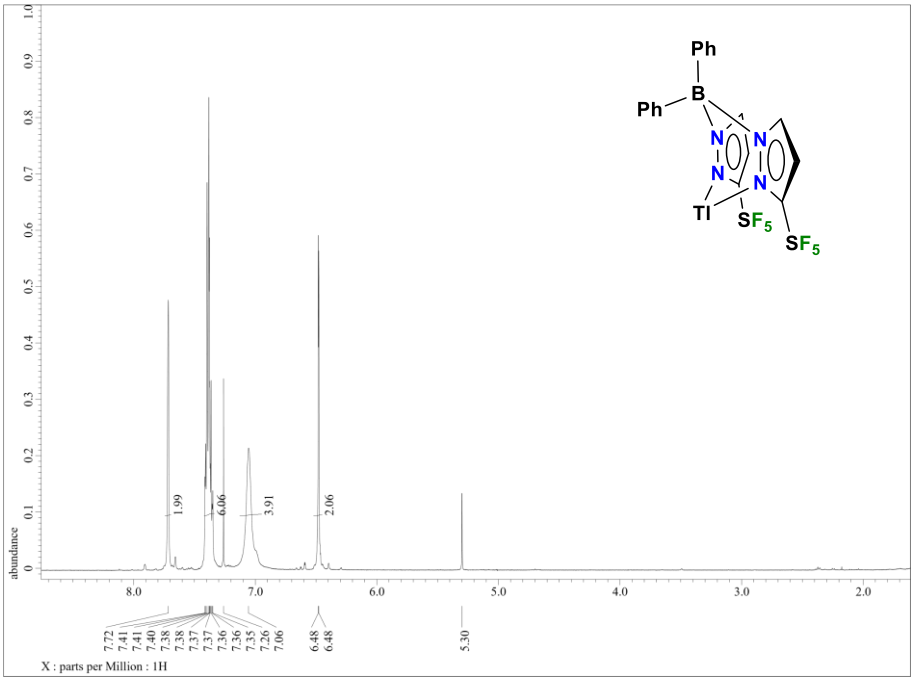

^{1}H NMR Spectrum of [$Ph_2B(3\text{-}(SF_5)Pz)_2$]Tl (**22**) in $CDCl_3$.

`

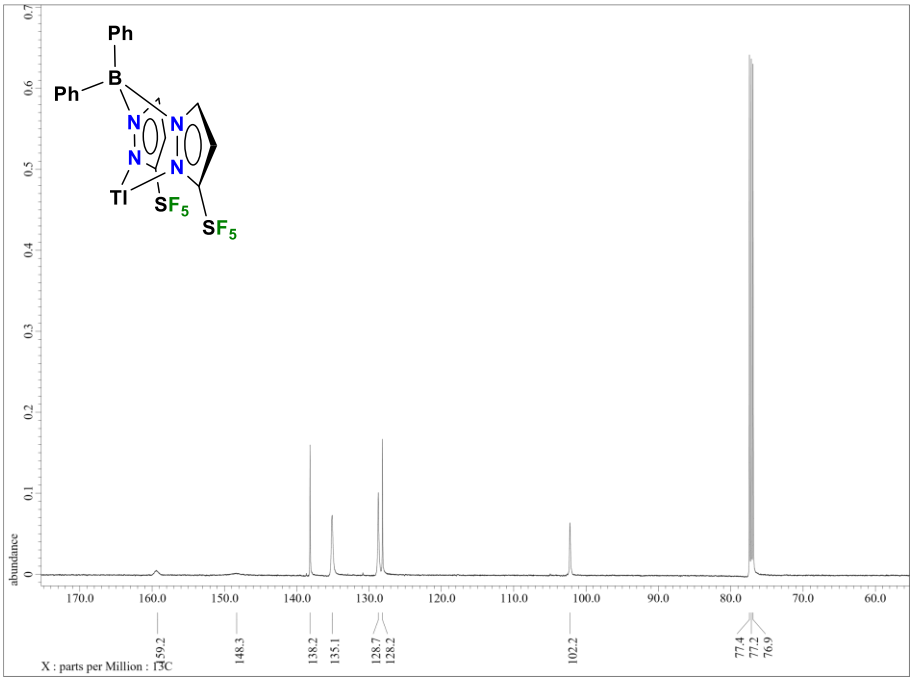

^{13}C NMR Spectrum of $Ph_2B(3\text{-}(SF_5)Pz)_2]Tl$ (**22**) in $CDCl_3$.

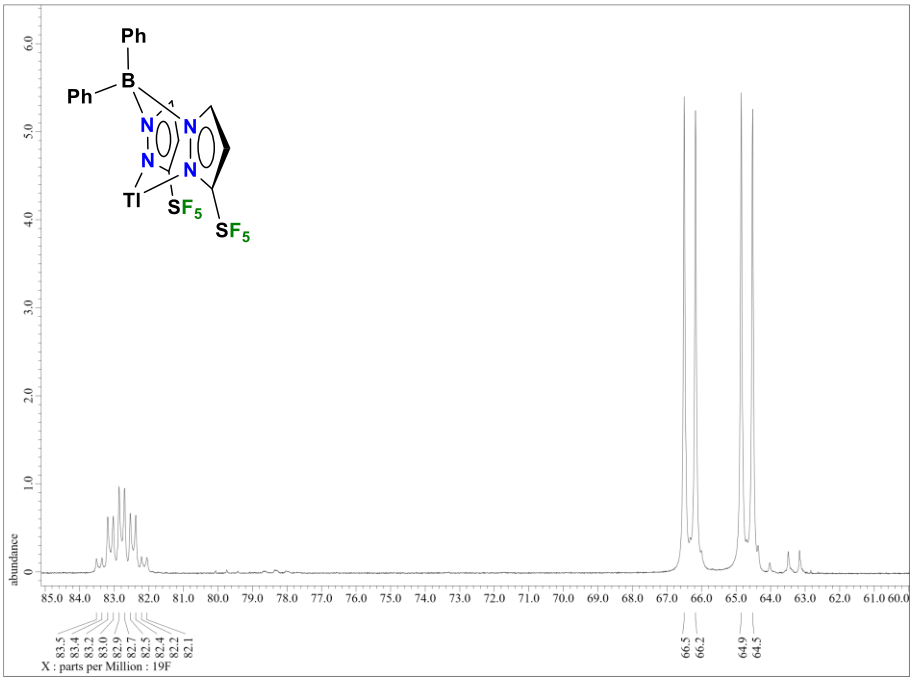

^{19}F NMR Spectrum of $[Ph_2B(3\text{-}(SF_5)Pz)_2]Tl$ (**22**) in $CDCl_3$.

`

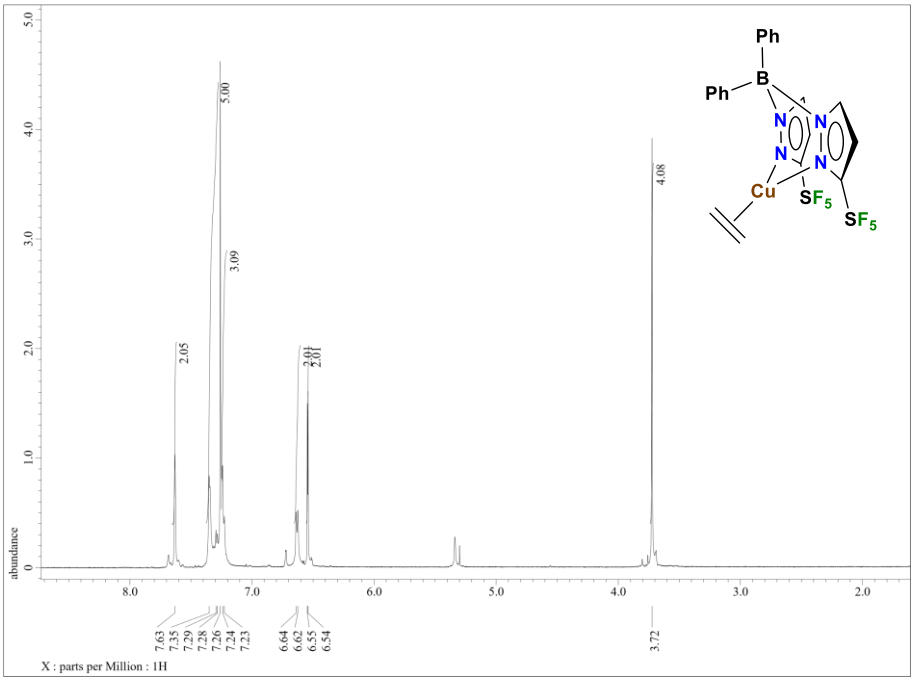

^{1}H NMR Spectrum of [$Ph_2B(3\text{-}(SF_5)Pz)_2$]Cu($C_2H_4$) (**23**) in $CDCl_3$

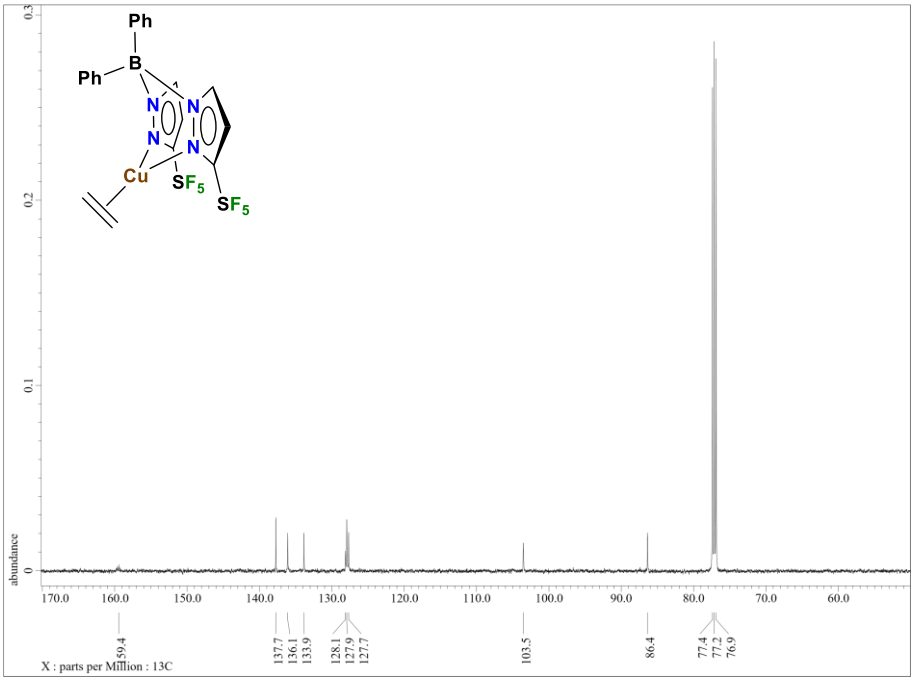

^{13}C NMR Spectrum of [$Ph_2B(3\text{-}(SF_5)Pz)_2$]Cu($C_2H_4$) (**23**) in $CDCl_3$.

`

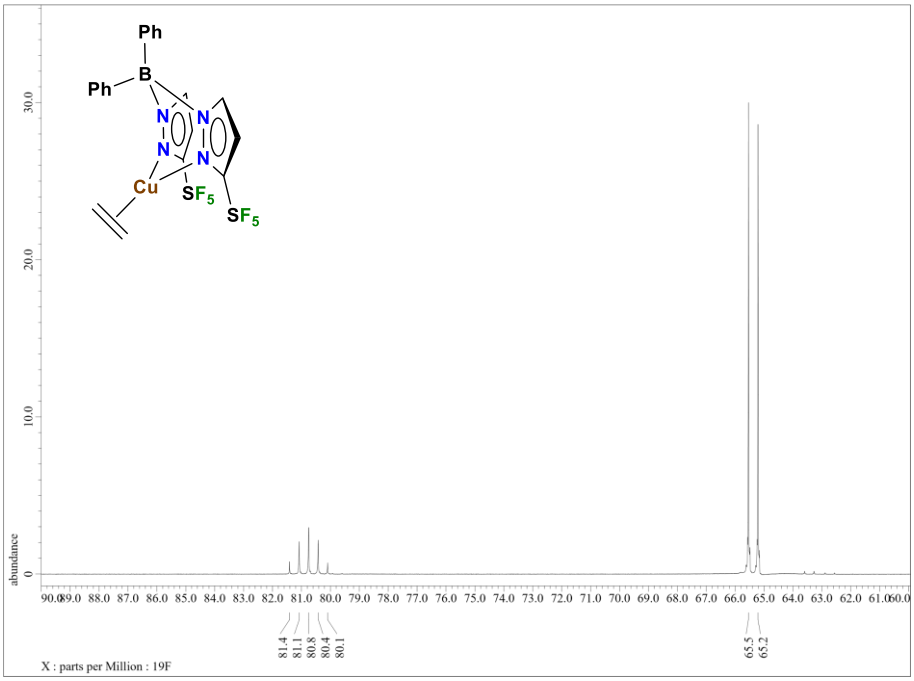

^{19}F NMR Spectrum of $[Ph_2B(3\text{-}(SF_5)Pz)_2]Cu(C_2H_4)$ (**23**) in $CDCl_3$.

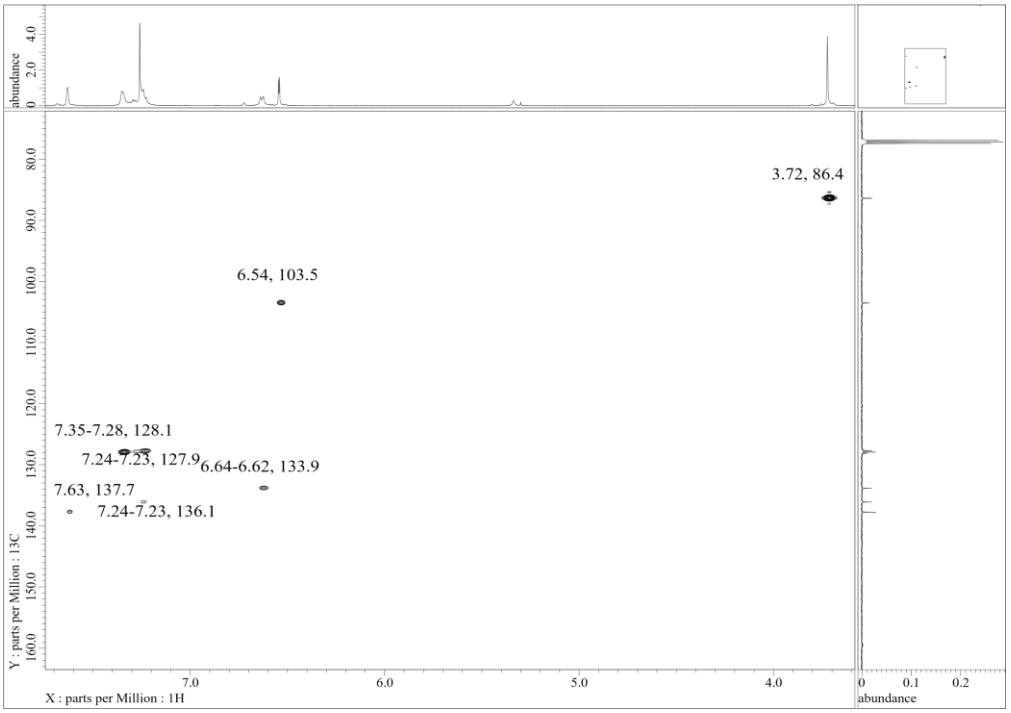

HSQC NMR Spectrum of $[Ph_2B(3\text{-}(SF_5)Pz)_2]Cu(C_2H_4)$ (**23**) in $CDCl_3$.

`

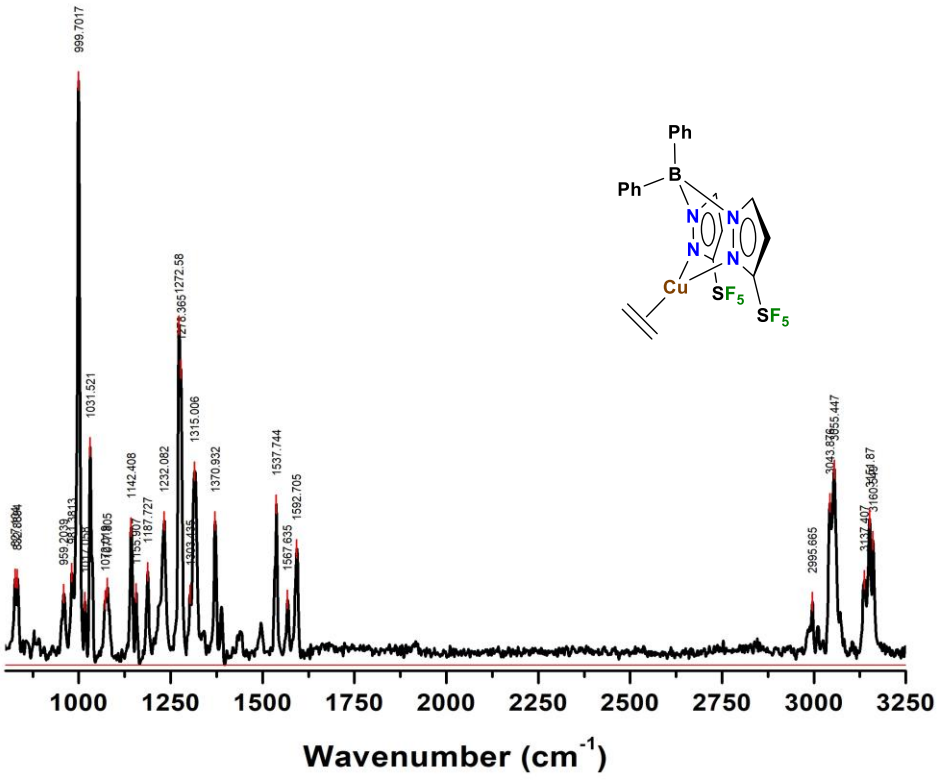

Raman Spectrum of $[Ph_2B(3\text{-}SF_5)Pz)_2]Cu(C_2H_4)$ (**23**).

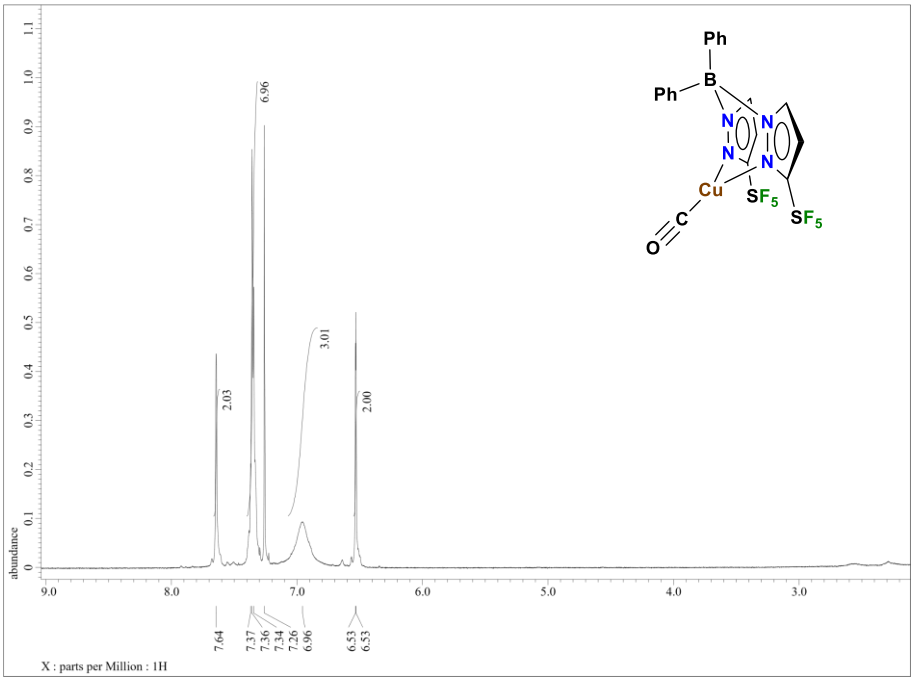

^1H NMR Spectrum of $[Ph_2B(3\text{-}(SF_5)Pz)_2]Cu(CO)$ (**24**) in $CDCl_3$

`

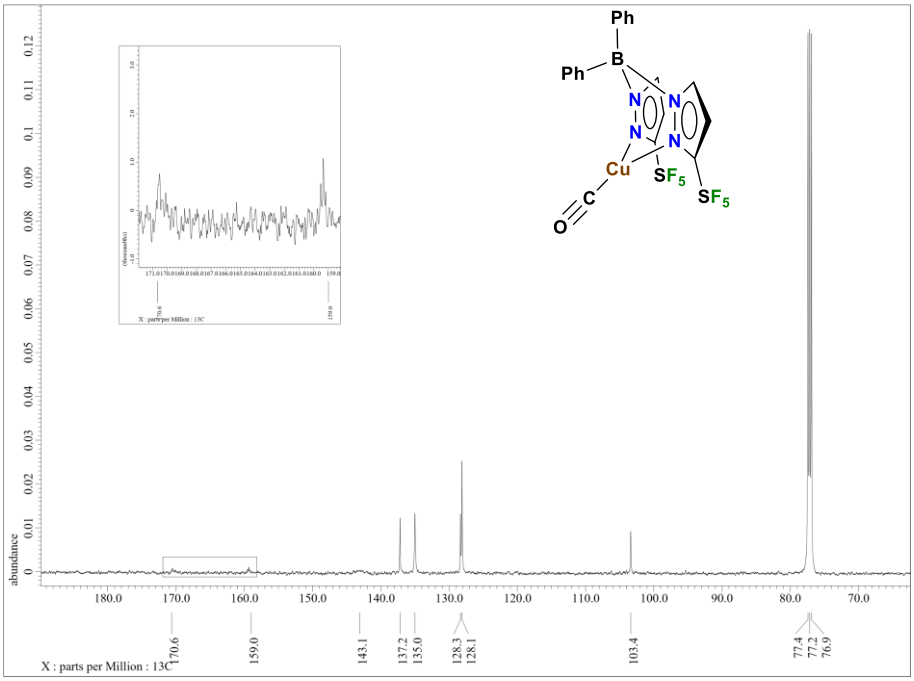

^{13}C NMR Spectrum of [$Ph_2B(3\text{-}(SF_5)Pz)_2$]Cu(CO) (**24**) in $CDCl_3$

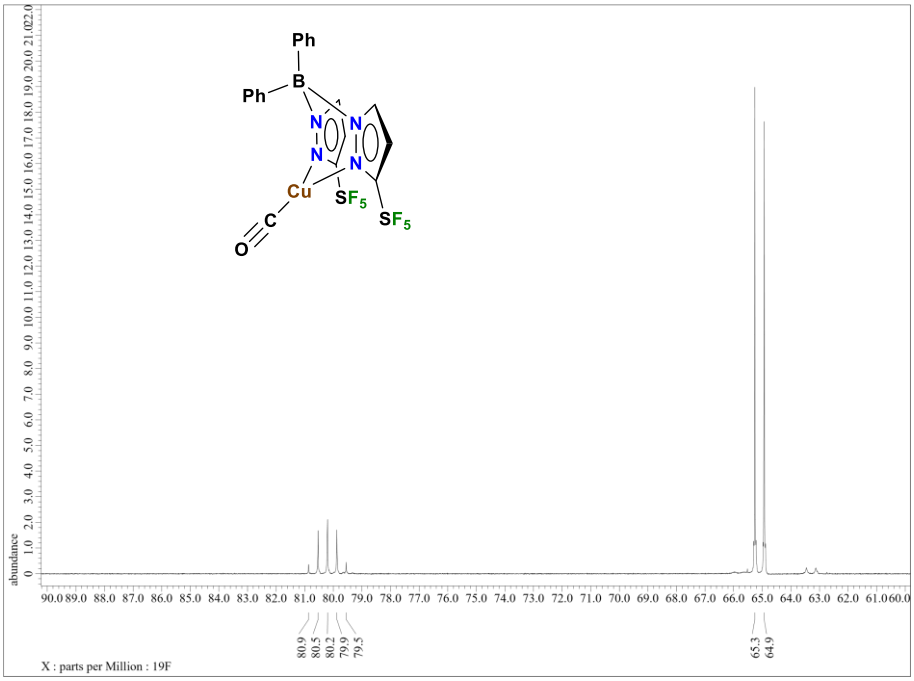

^{19}F NMR Spectrum of [$Ph_2B(3\text{-}(SF_5)Pz)_2$]Cu(CO) (**24**) in $CDCl_3$

`

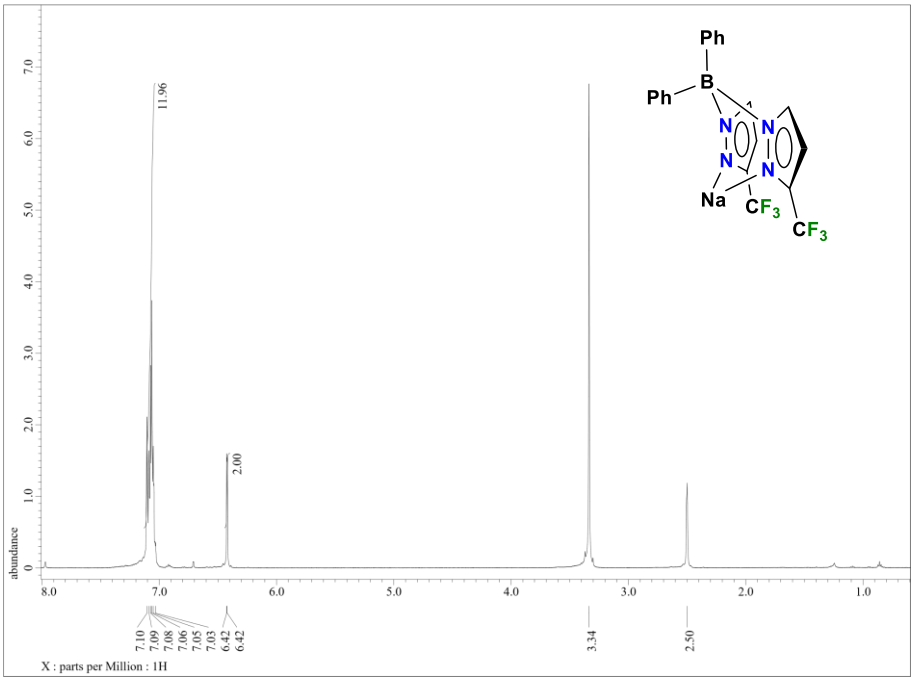

^{1}H NMR Spectrum of [$Ph_2B(3\text{-}CF_3)Pz)_2$]Na (**25**) in $(CD_3)_2SO$.

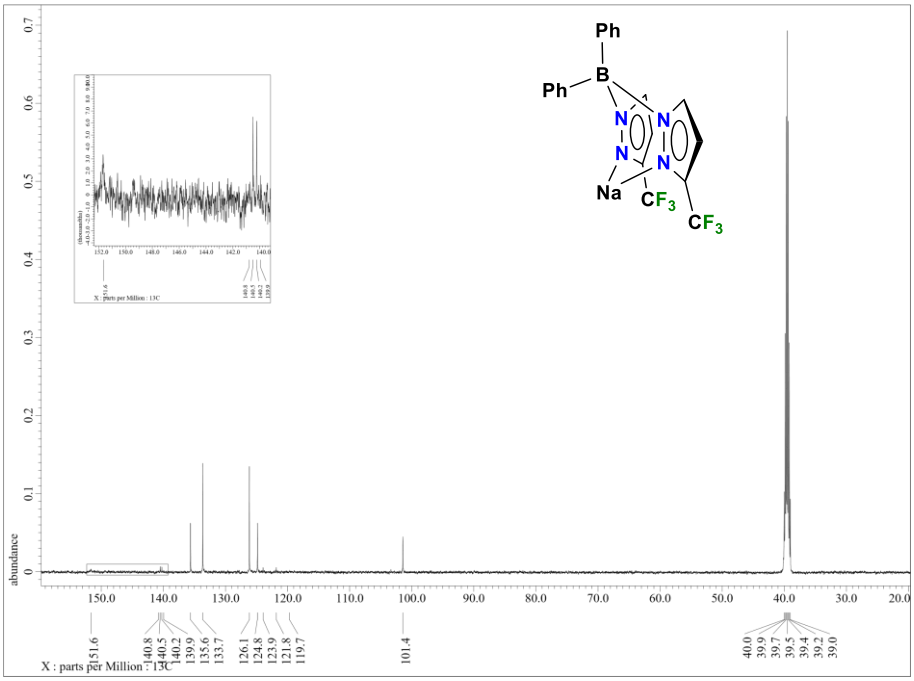

^{13}C NMR Spectrum of [$Ph_2B(3\text{-}CF_3)Pz)_2$]Na (**25**) in $(CD_3)_2SO$.

`

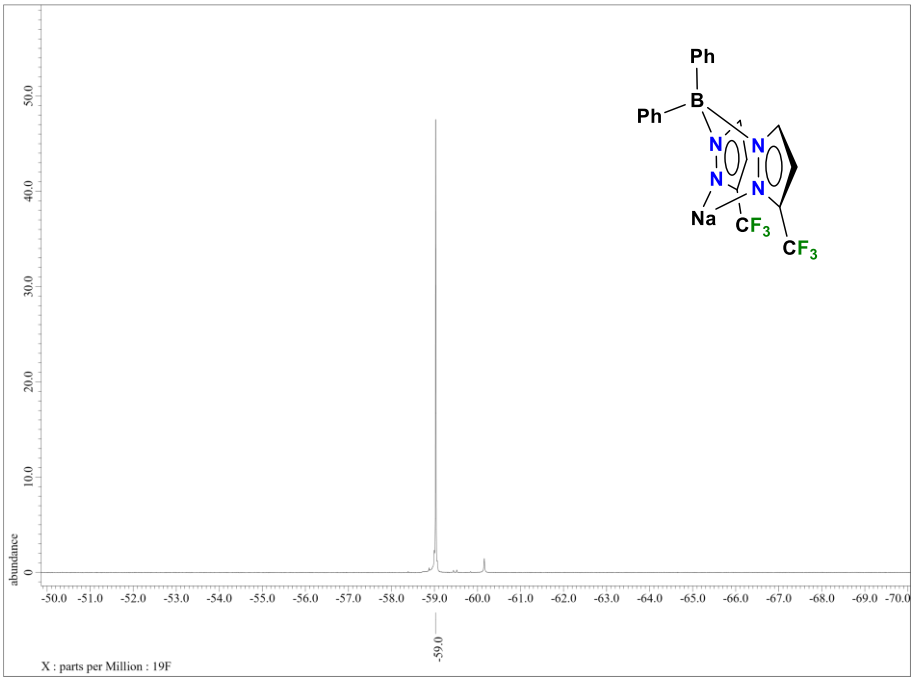

^{19}F NMR Spectrum of [$Ph_2B(3\text{-}CF_3)Pz)_2$]Na (**25**) in $(CD_3)_2SO$.

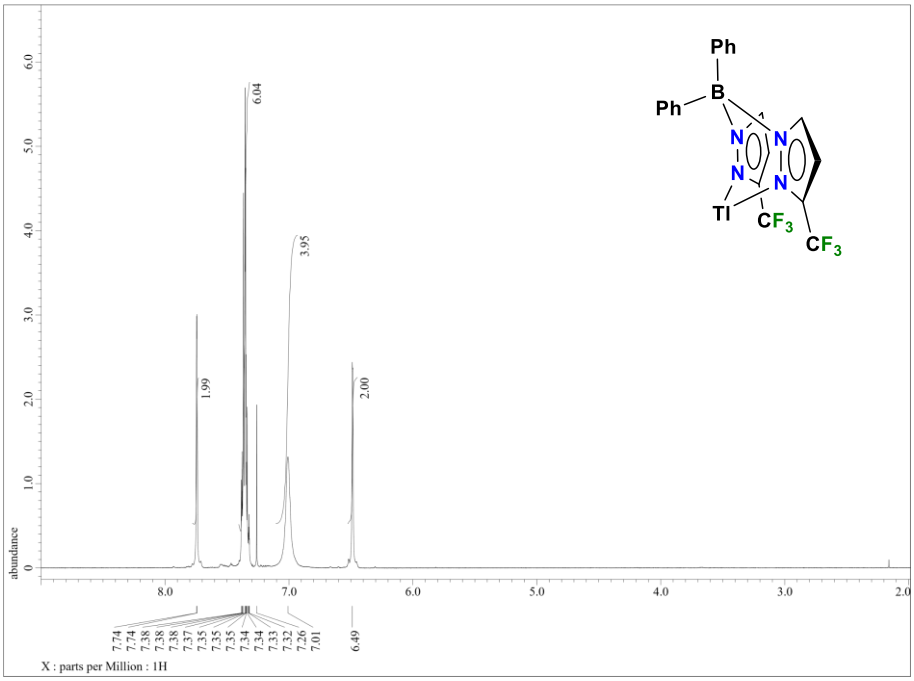

^{1}H NMR Spectrum of [$Ph_2B(3\text{-}CF_3)Pz)_2$]Tl (**26**) in $CDCl_3$

`

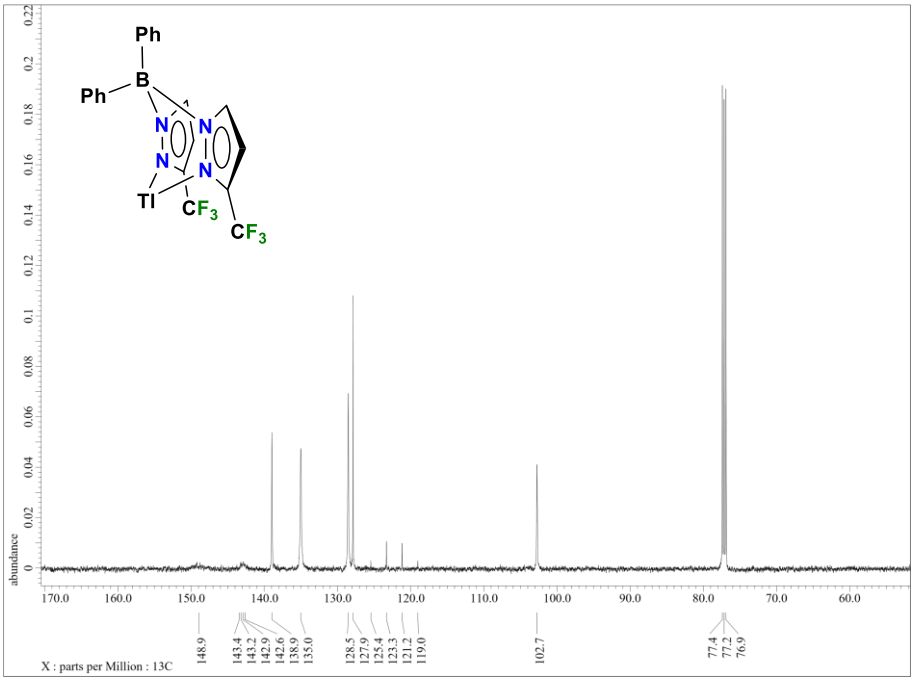

^{13}C NMR Spectrum of [$Ph_2B(3\text{-}CF_3)Pz)_2$]Tl (**26**) in $CDCl_3$.

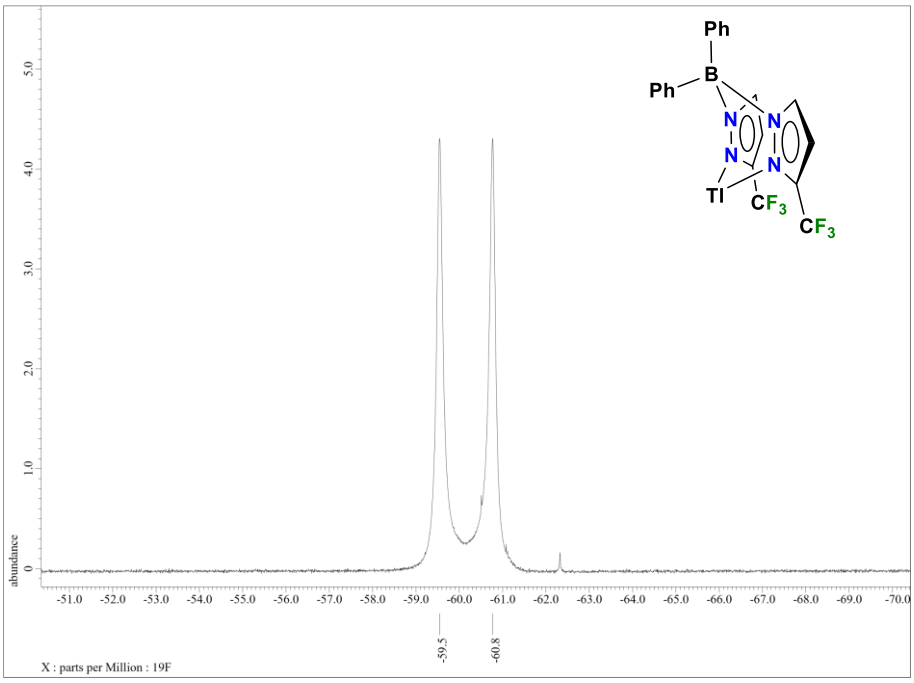

^{19}F NMR Spectrum of [$Ph_2B(3\text{-}CF_3)Pz)_2$]Tl (**26**) in $CDCl_3$.

`

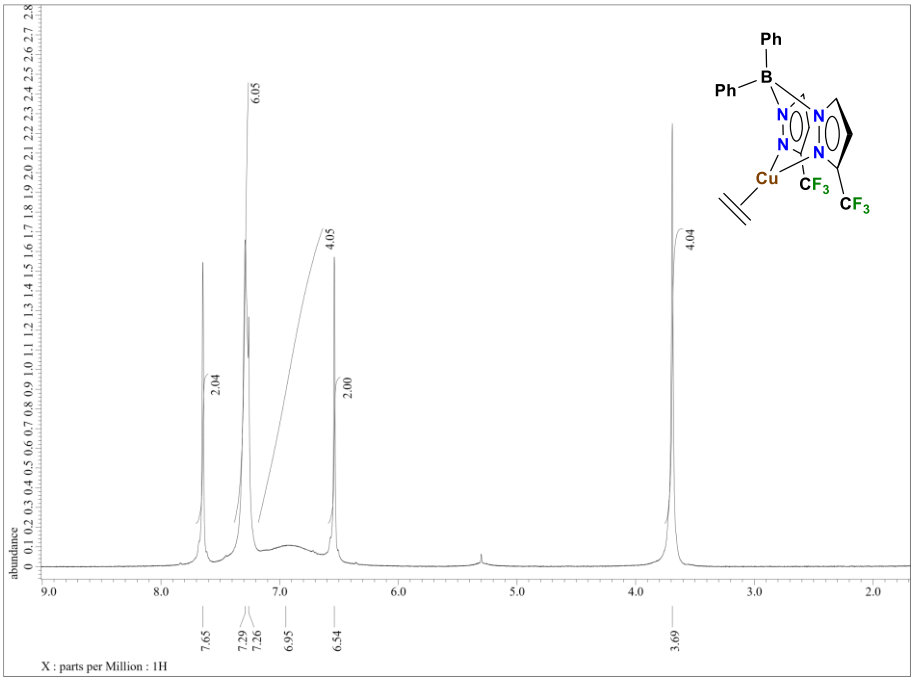

^{1}H NMR Spectrum of [$Ph_2B(3\text{-}CF_3)Pz)_2$]Cu($C_2H_4$) (**27**)in $CDCl_3$

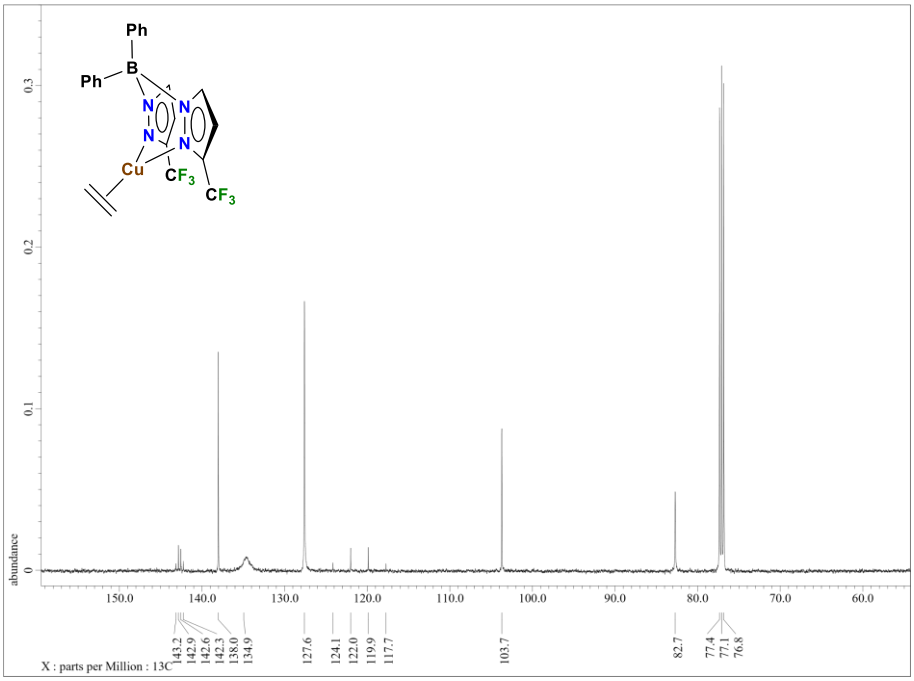

^{13}C NMR Spectrum of [$Ph_2B(3\text{-}CF_3)Pz)_2$]Cu($C_2H_4$) (**27**) in $CDCl_3$.

`

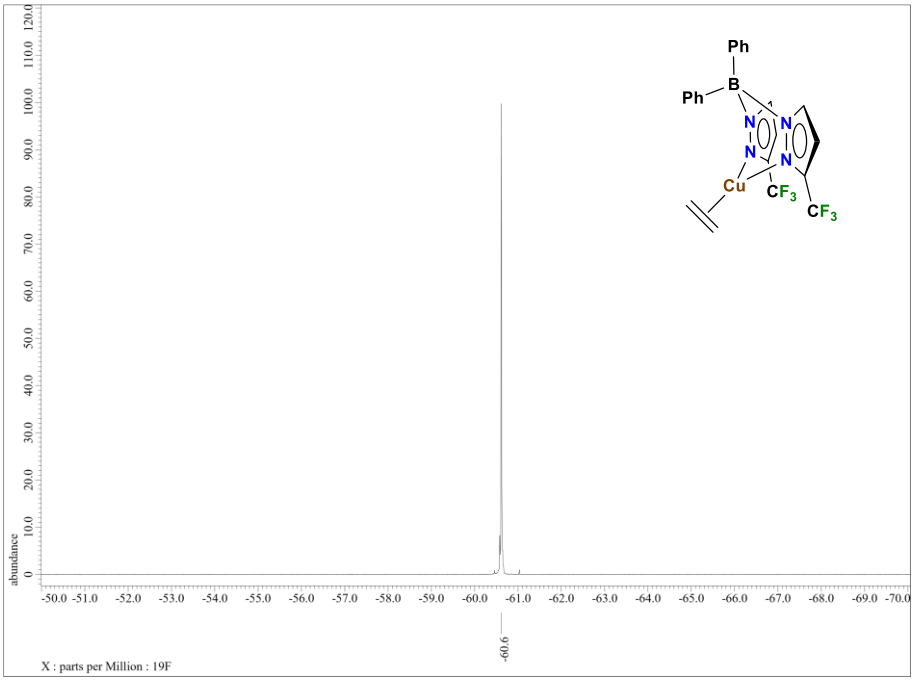

^{19}F NMR Spectrum of $[Ph_2B(3\text{-}CF_3)Pz)_2]Cu(C_2H_4)$ (**27**) in $CDCl_3$.

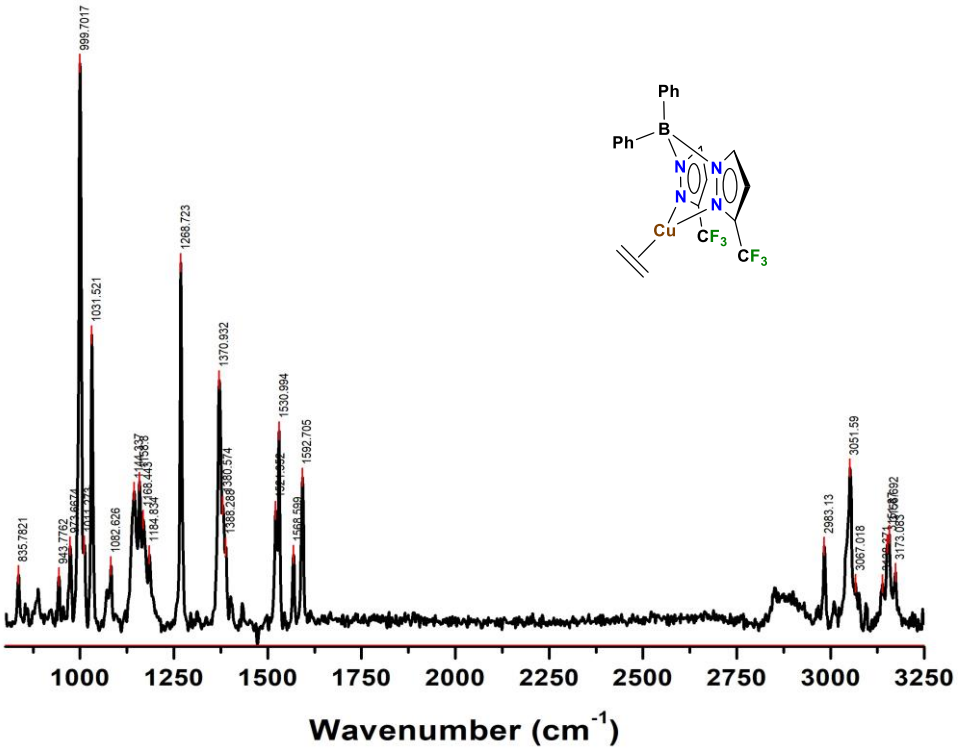

Raman Spectrum of $[Ph_2B(3\text{-}CF_3)Pz)_2]Cu(C_2H_4)$ (**27**).

`

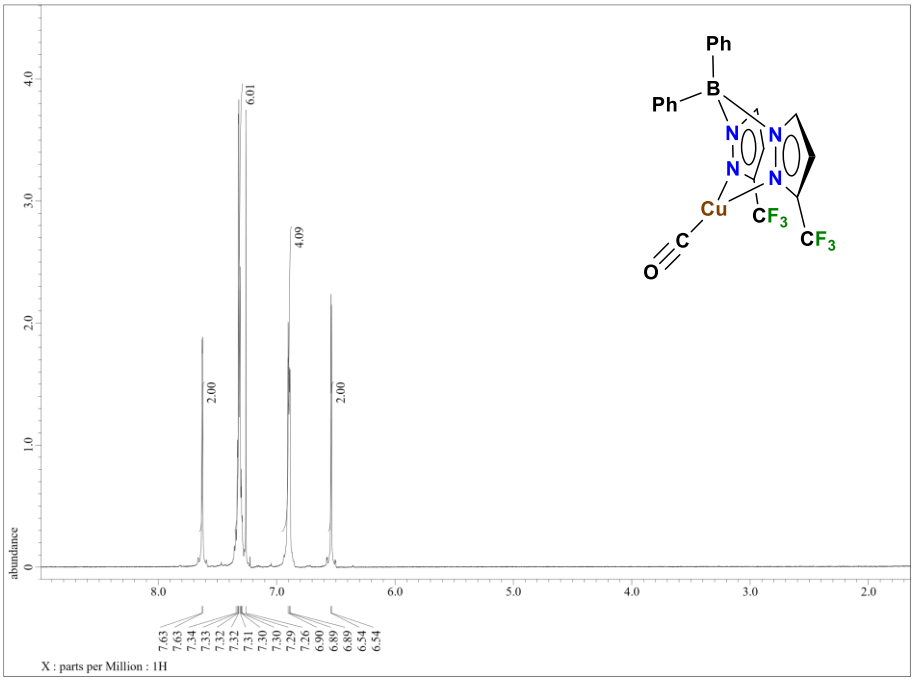

^{1}H NMR Spectrum of [$Ph_2B(3\text{-}CF_3)Pz)_2$]Cu(CO) (**28**) in $CDCl_3$

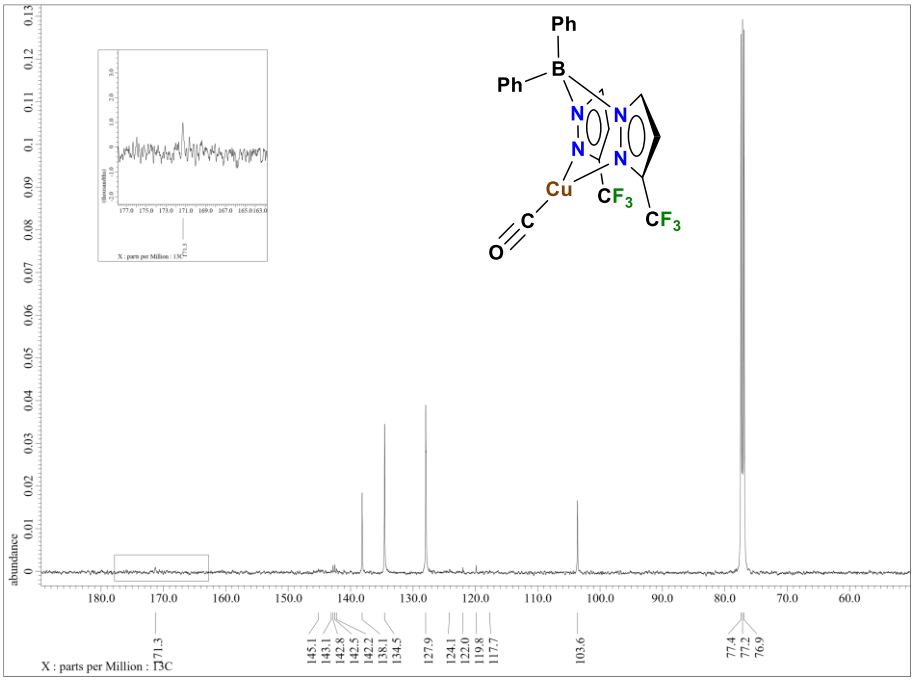

^{13}C NMR Spectrum of [$Ph_2B(3\text{-}CF_3)Pz)_2$]Cu(CO) (**28**) in $CDCl_3$.

`

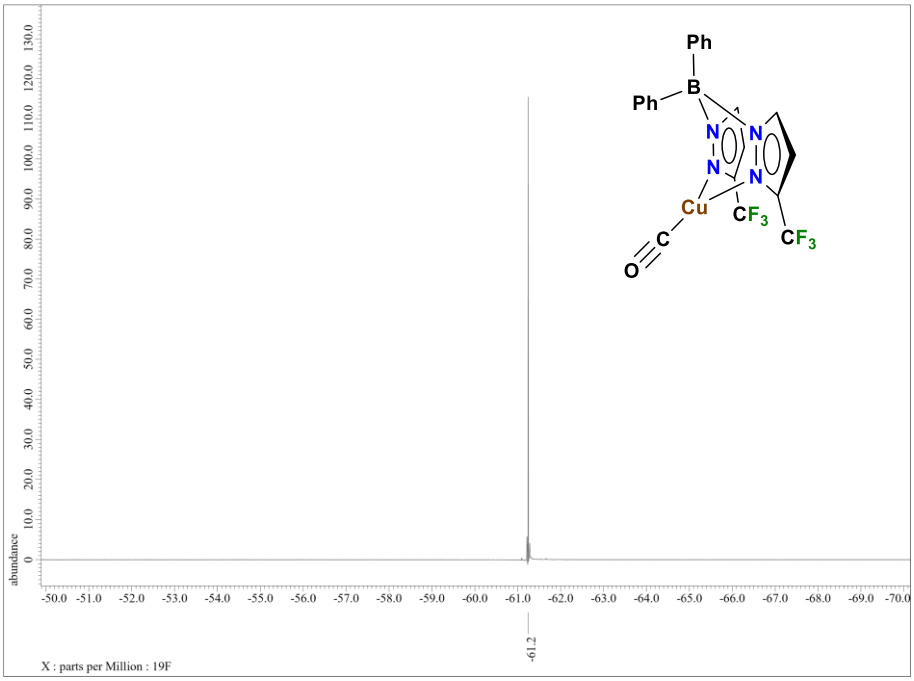

^{19}F NMR Spectrum of [$Ph_2B(3\text{-}CF_3)Pz)_2$]Cu(CO) (**28**) in $CDCl_3$.

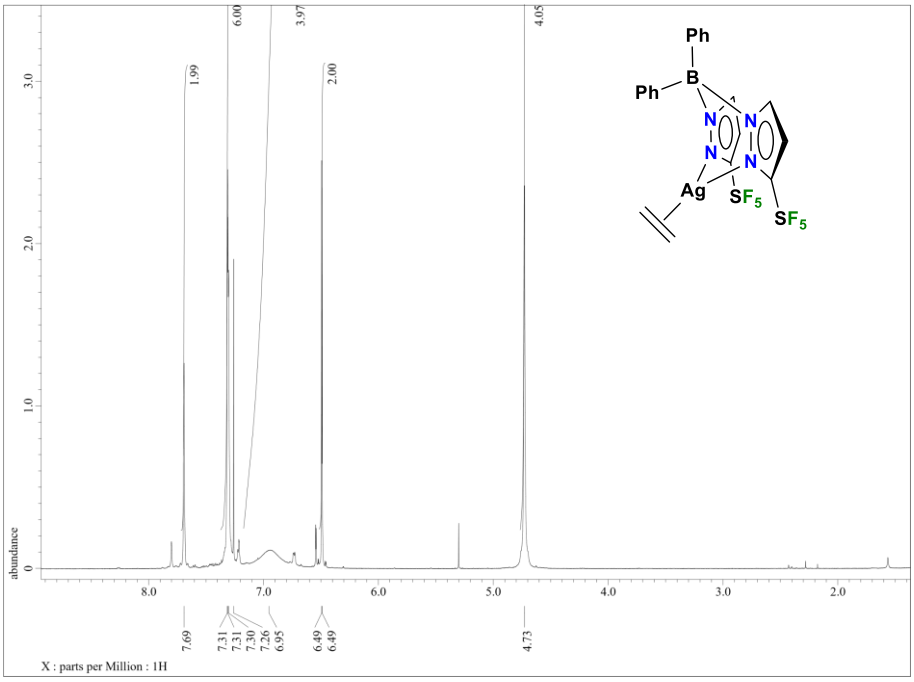

^{1}H NMR Spectrum of [$Ph_2B(3\text{-}(SF_5)Pz)_2$]Ag($C_2H_4$) (**29**) in $CDCl_3$

`

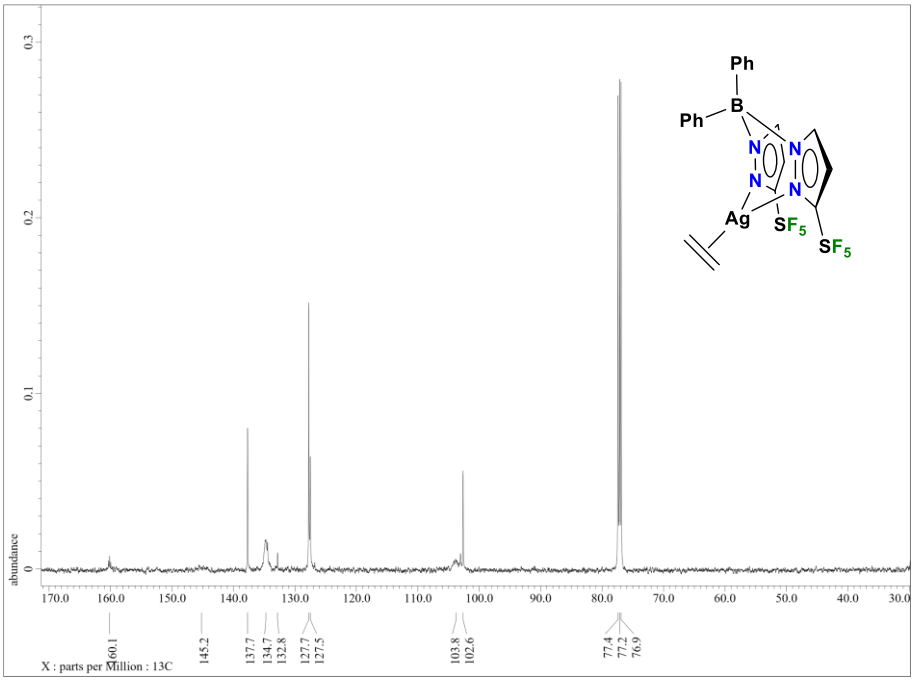

^{13}C NMR Spectrum of [$Ph_2B(3\text{-}(SF_5)Pz)_2$]Ag($C_2H_4$) (**29**) in $CDCl_3$.

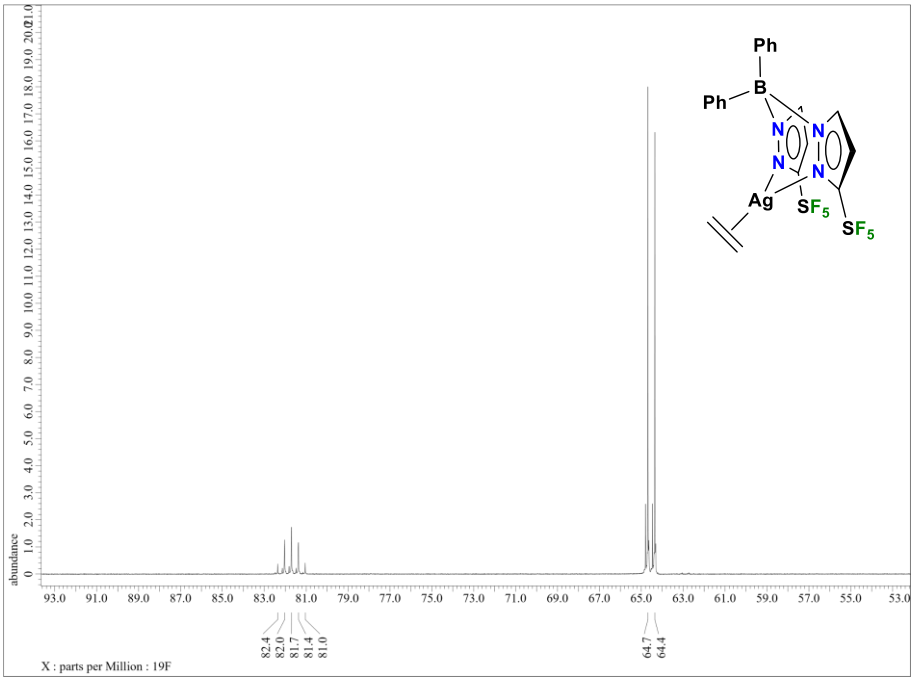

^{19}F NMR Spectrum of [$Ph_2B(3\text{-}(SF_5)Pz)_2$]Ag($C_2H_4$) (**29**) in $CDCl_3$.

`

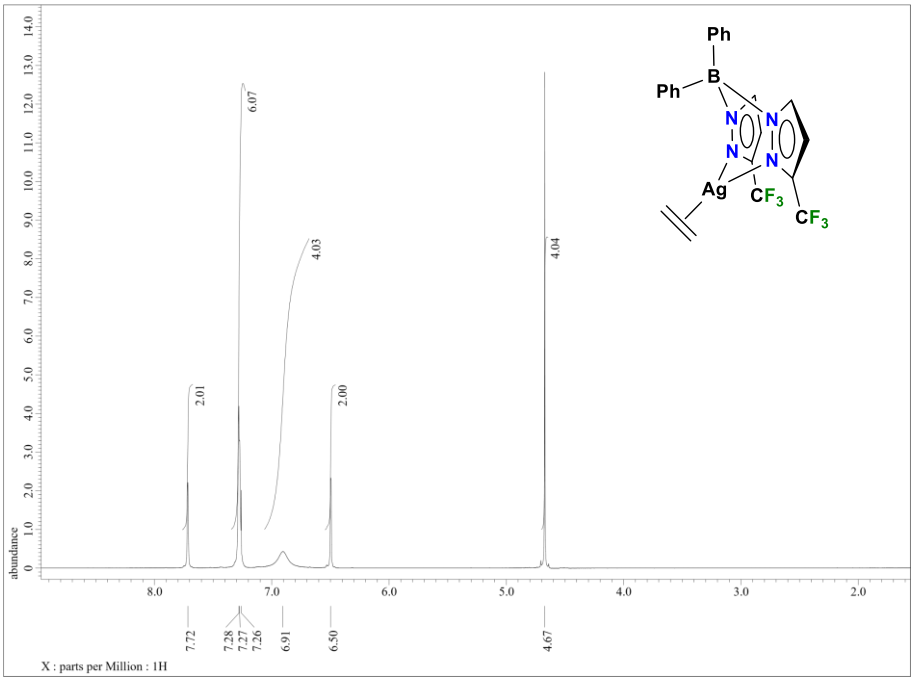

^{1}H NMR Spectrum of [$Ph_2B(3\text{-}(CF_3)Pz)_2$]Ag($C_2H_4$) (**30**) in $CDCl_3$

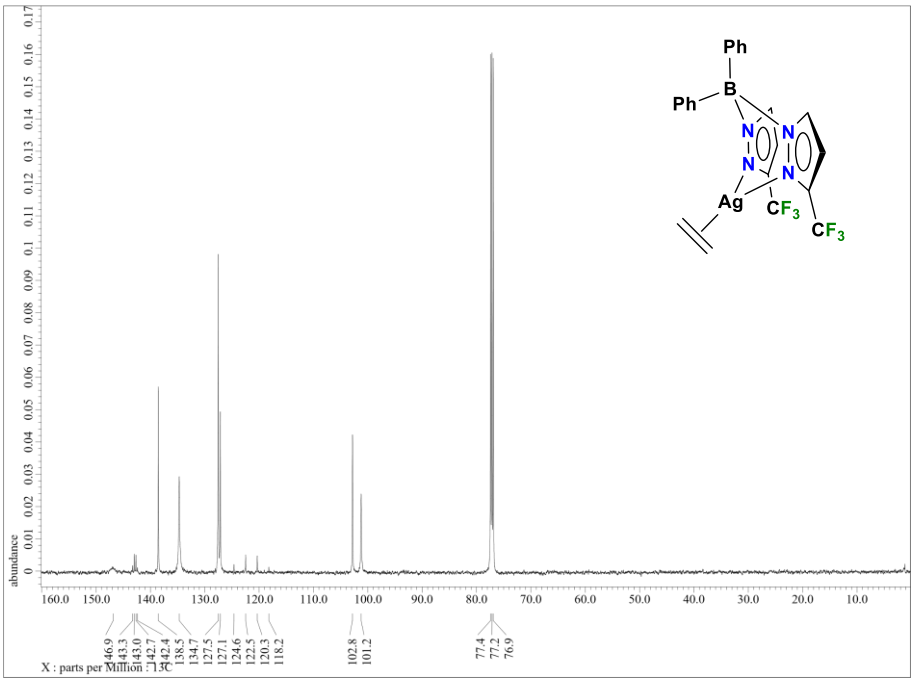

^{13}C NMR Spectrum of [$Ph_2B(3\text{-}(CF_3)Pz)_2$]Ag($C_2H_4$) (**30**) in $CDCl_3$.

`

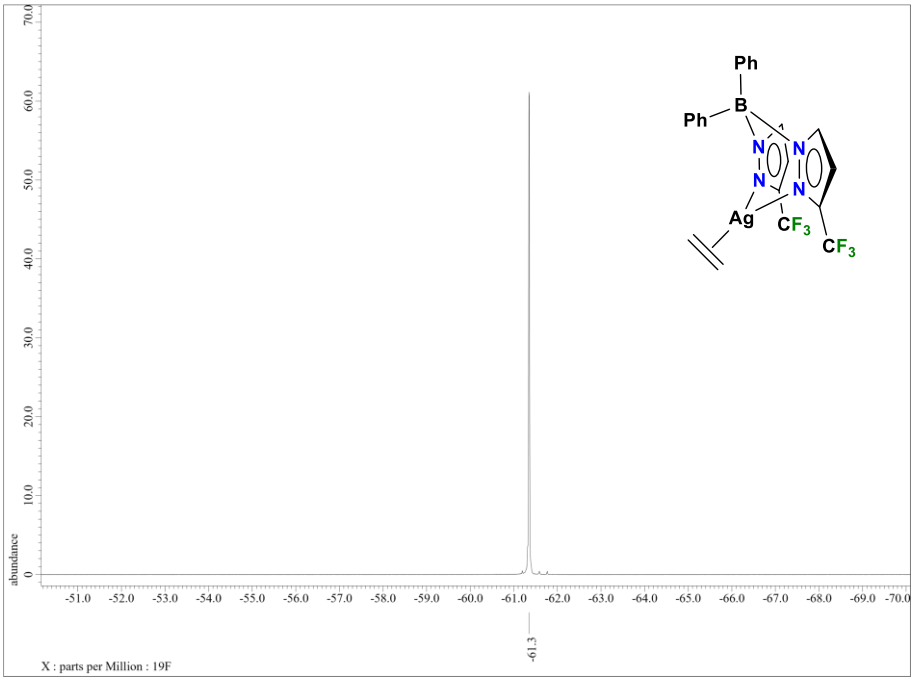

^{19}F NMR Spectrum of $[Ph_2B(3\text{-}(CF_3)Pz)_2]Ag(C_2H_4)$ (**30**) in $CDCl_3$.

`

Appendix B

Spectroscopic Data of Chapter 3 Part 3.1

`

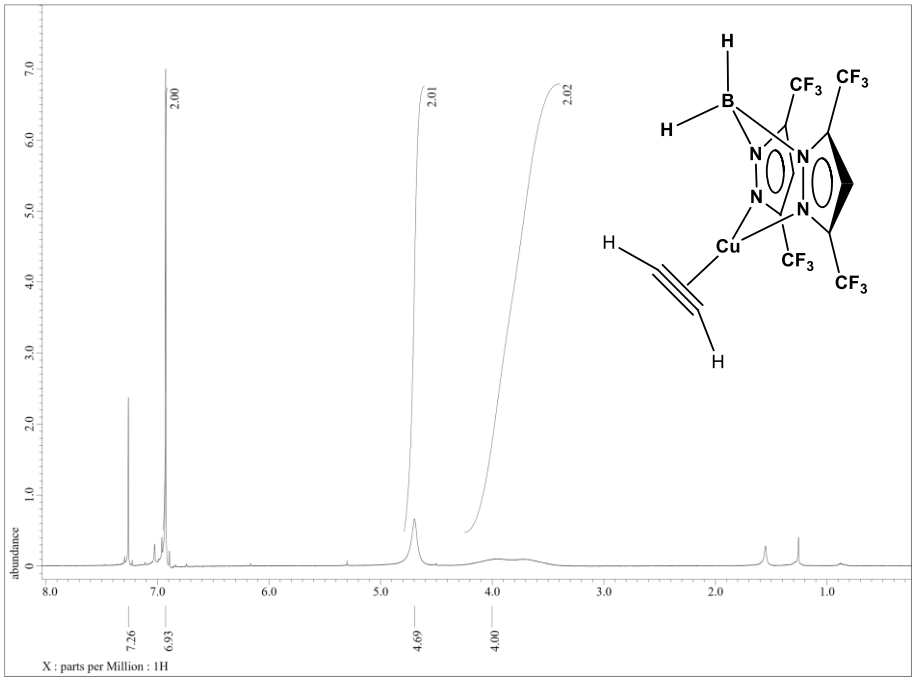

^{1}H NMR spectrum of [$H_2B(3,5\text{-}(CF_3)_2Pz)_2$]Cu($C_2H_2$) (**37**) in $CDCl_3$.

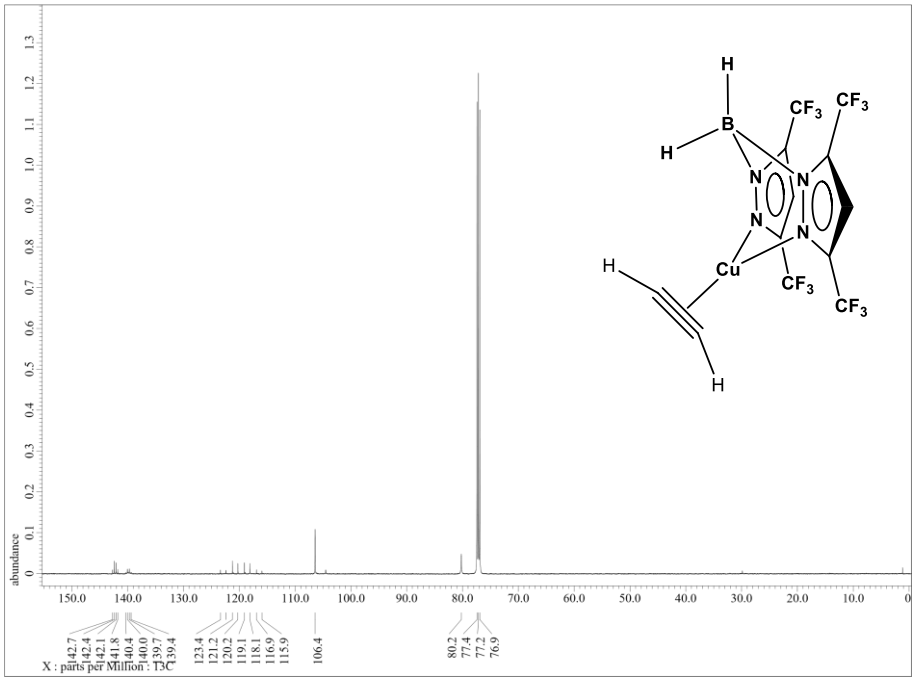

^{13}C{^{1}H} NMR spectrum of [$H_2B(3,5\text{-}(CF_3)_2Pz)_2$]Cu($C_2H_2$) (**37**) in $CDCl_3$.

`

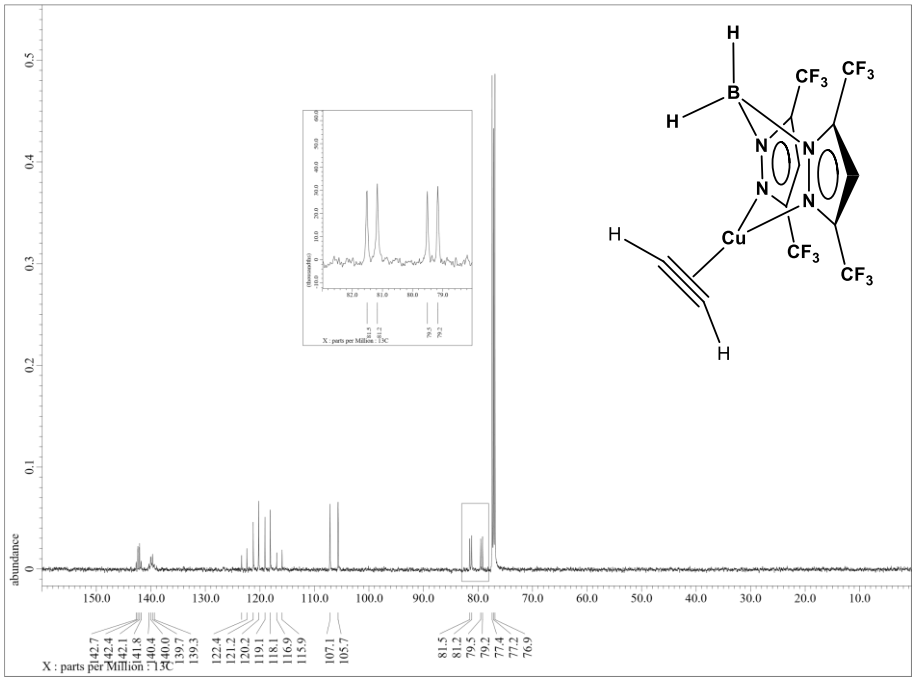

^{13}C (^{1}H coupled) NMR spectrum of $[H_2B(3,5\text{-}(CF_3)_2Pz)_2]Cu(C_2H_2)$ (**37**) in $CDCl_3$.

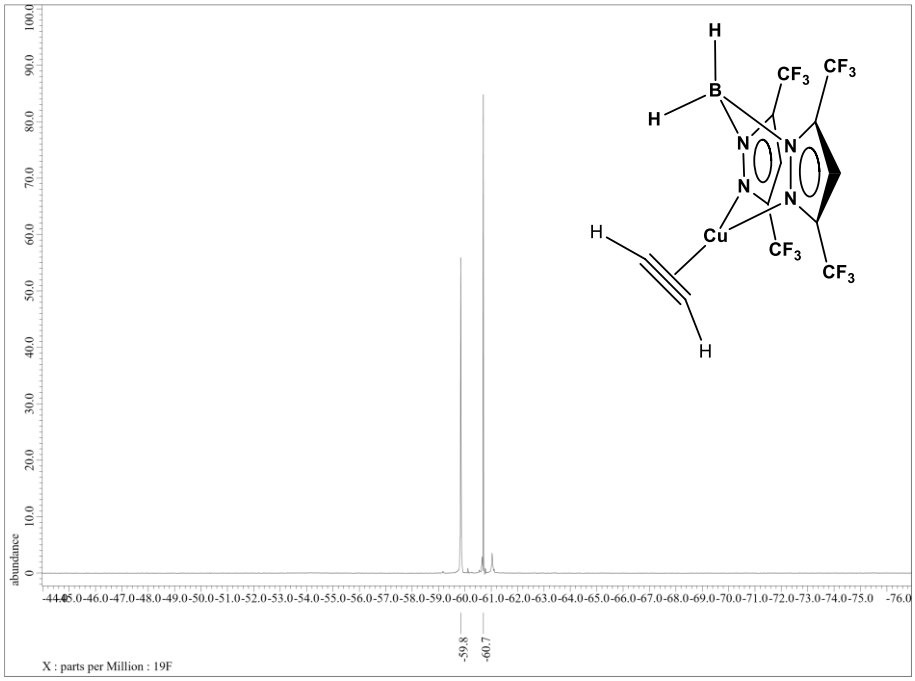

^{19}F NMR spectrum of $[H_2B(3,5\text{-}(CF_3)_2Pz)_2]Cu(C_2H_2)$ (**37**) in $CDCl_3$.

`

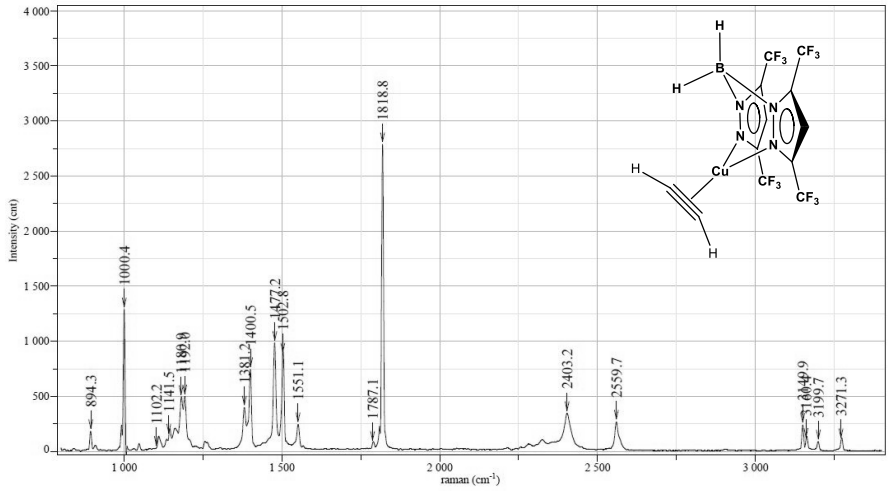

Exposition	5	Slit	100
Accumulation	5 x 4	Operator	
Laser	632.817	Sample	
Spectro	Multi	Remark	
Hole	200	Power	

Raman spectrum of $[H_2B(3,5\text{-}(CF_3)_2Pz)_2]Cu(C_2H_2)$ (**37**).

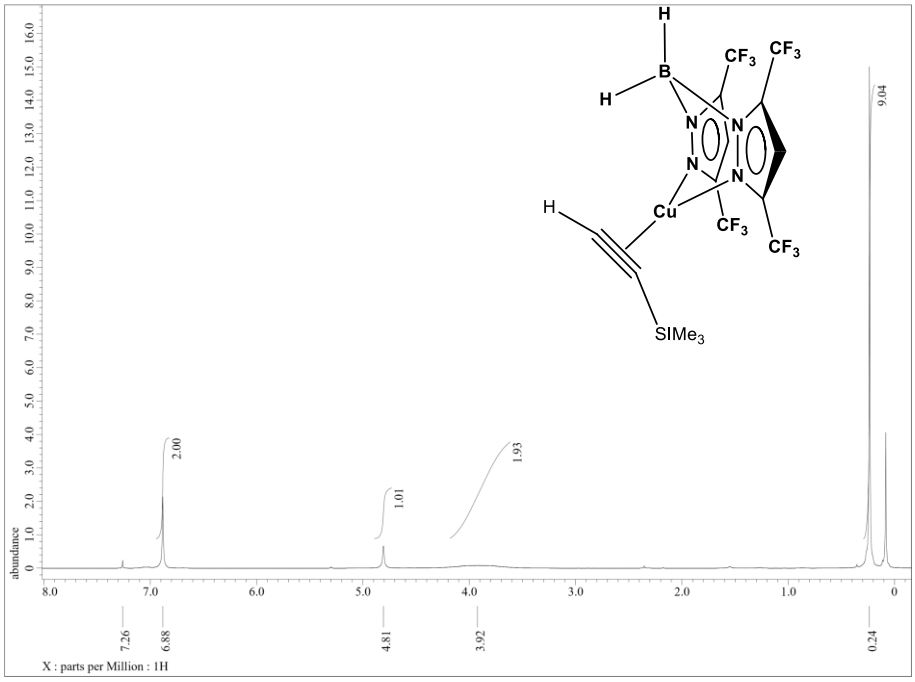

^{1}H NMR spectrum of $[H_2B(3,5\text{-}(CF_3)_2Pz)_2]Cu(HC{\equiv}CSiMe_3)$ (**38**) in $CDCl_3$.

`

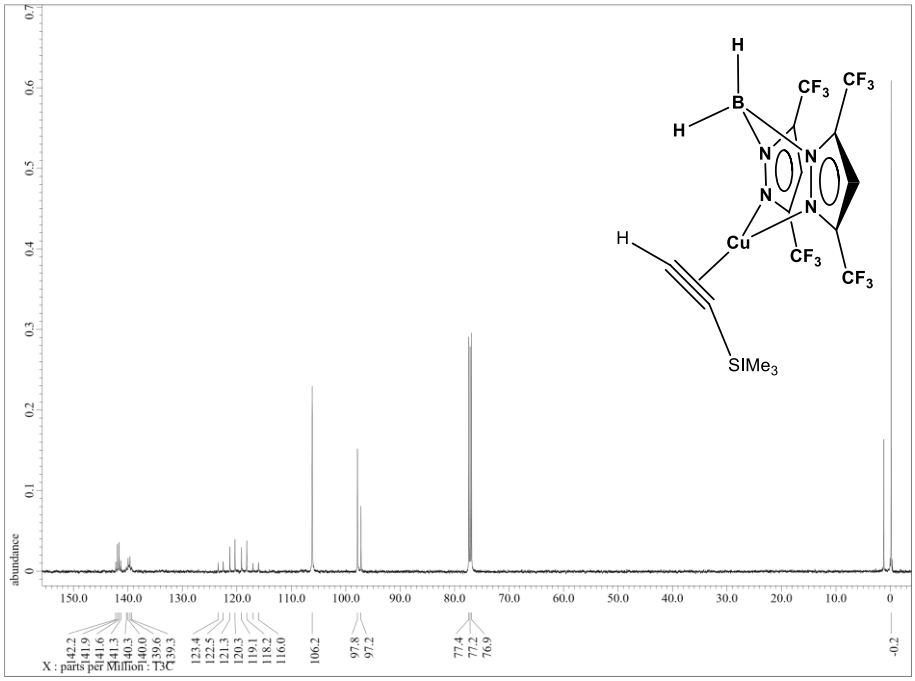

$^{13}C\{^{1}H\}$ NMR spectrum of $[H_2B(3,5\text{-}(CF_3)_2Pz)_2]Cu(HC{\equiv}CSiMe_3)$ (**38**) in $CDCl_3$.

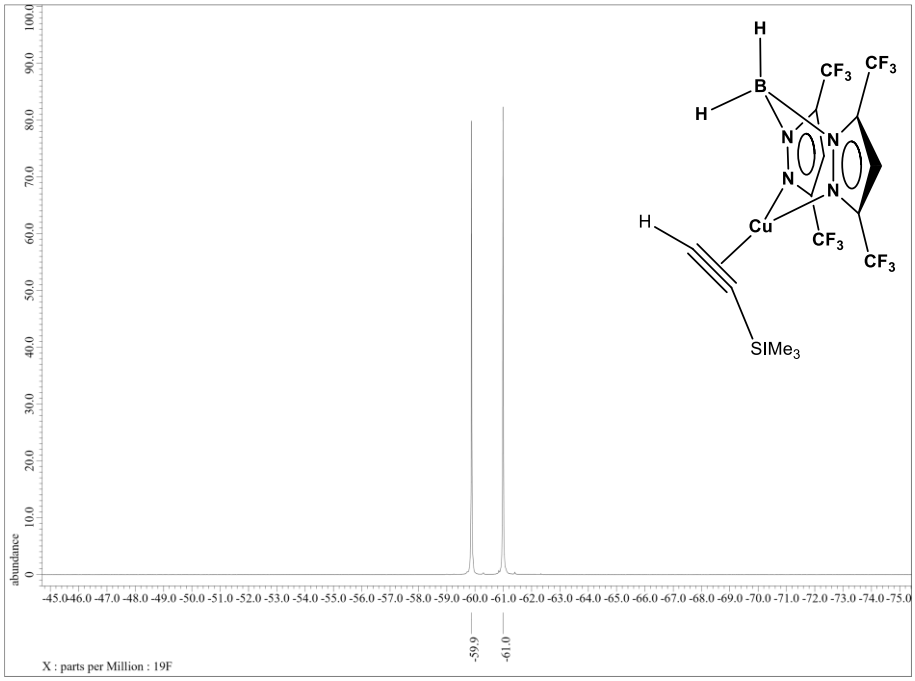

^{19}F NMR spectrum of $[H_2B(3,5\text{-}(CF_3)_2Pz)_2]Cu(HC{\equiv}CSiMe_3)$ (**38**) in $CDCl_3$.

`

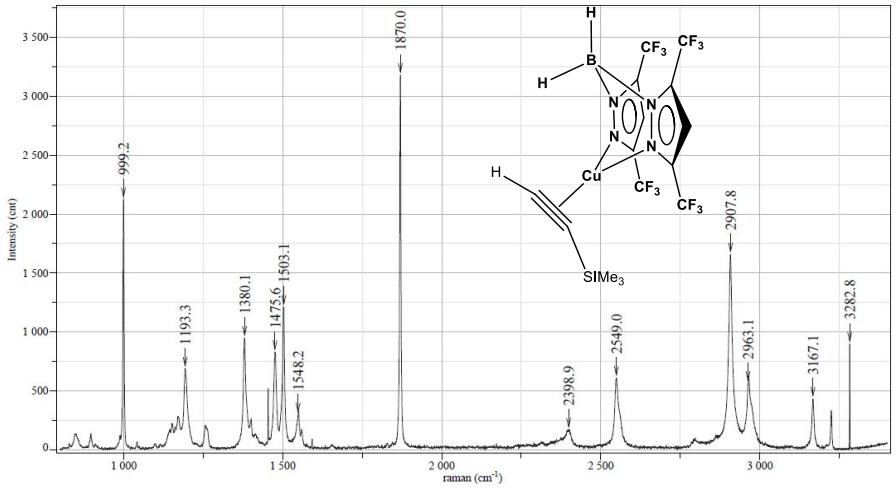

Exposition	5	Slit	100
Accumulation	1 x 21	Operator	Anurag
Laser	632.817	Sample	3,5-CF3BpCu_TMSacetylen
Spectro	Auto	Remark	
Hole	200	Power	

Raman spectrum of $[H_2B(3,5\text{-}(CF_3)_2Pz)_2]Cu(HC{\equiv}CSiMe_3)$ (**38**).

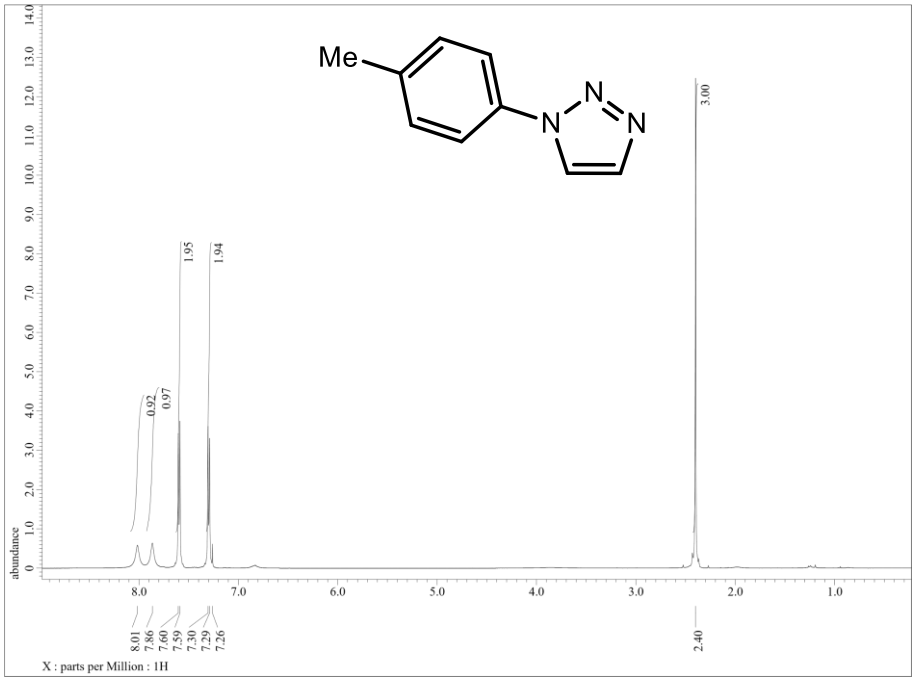

^{1}H NMR spectrum of 1-(*p*-tolyl)-1*H*-1,2,3-triazole (**53**) in $CDCl_3$.

`

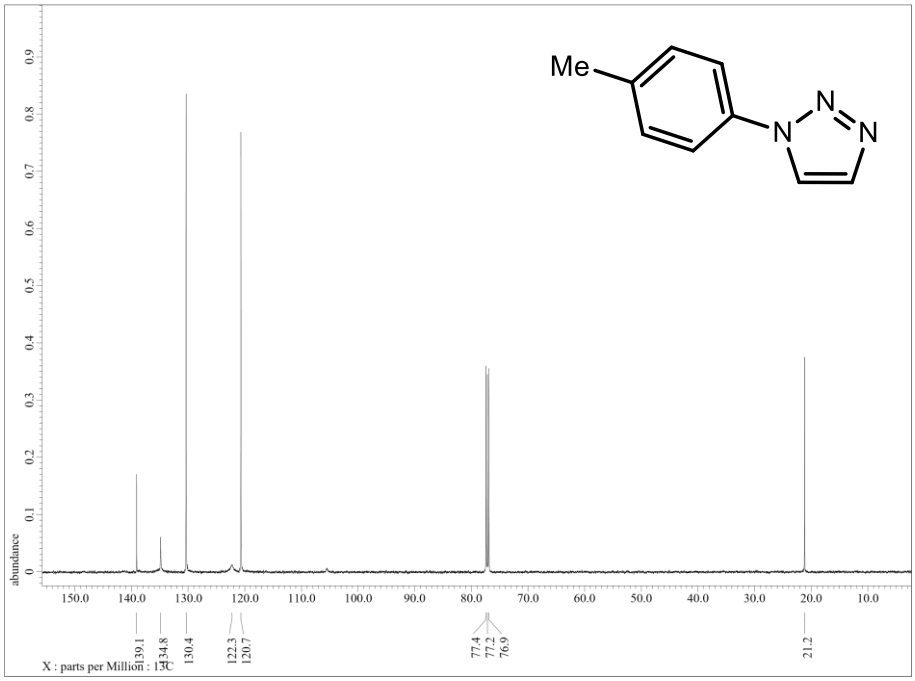

$^{13}C\{^{1}H\}$ NMR spectrum of 1-(*p*-tolyl)-1*H*-1,2,3-triazole (**53**) in $CDCl_3$.

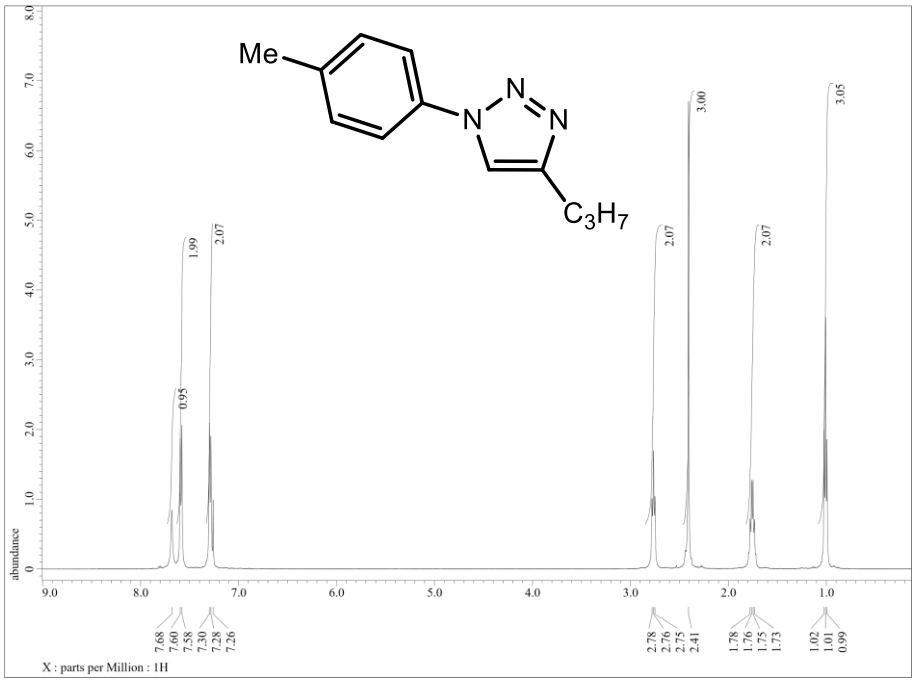

^{1}H NMR spectrum of 4-propyl-1-(*p*-tolyl)-1*H*-1,2,3-triazole (**54**) in $CDCl_3$.

`

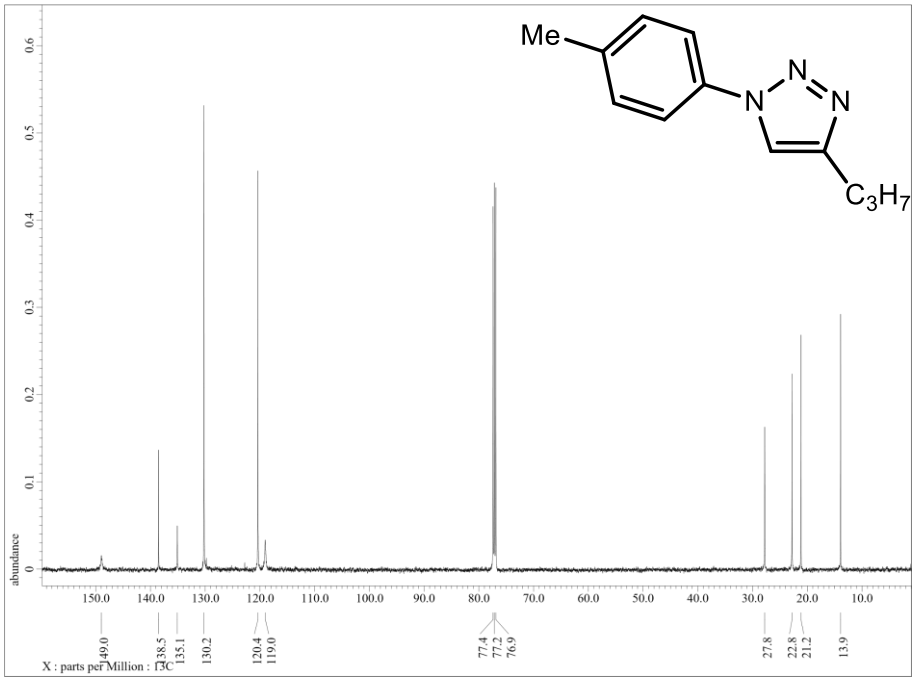

$^{13}C\{^{1}H\}$ NMR spectrum of 4-propyl-1-(*p*-tolyl)-1*H*-1,2,3-triazole (**54**) in $CDCl_3$.

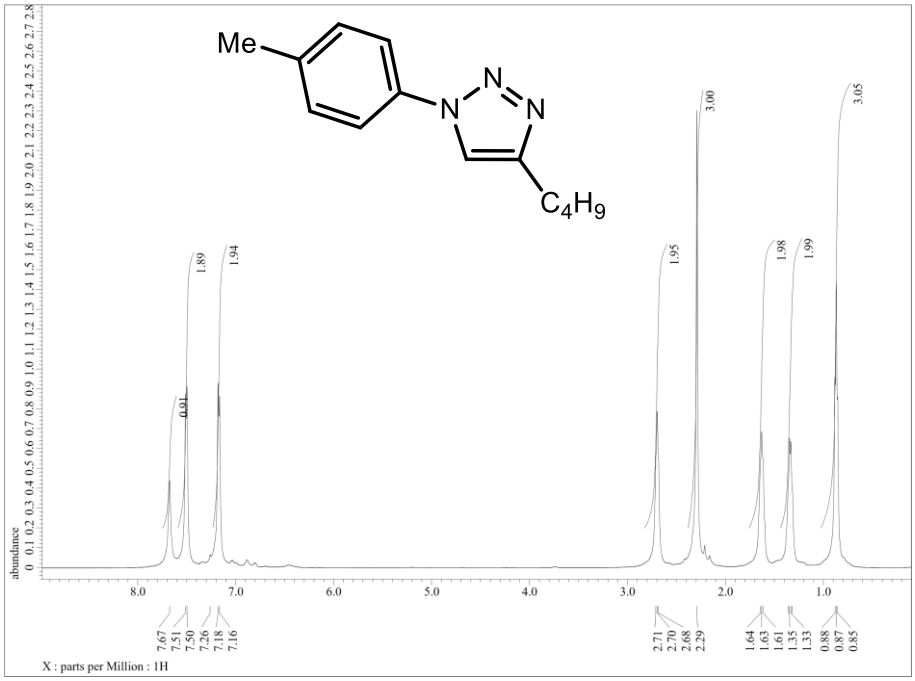

^{1}H NMR spectrum of 4-butyl-1-(*p*-tolyl)-1*H*-1,2,3-triazole (**55**) in $CDCl_3$.

`

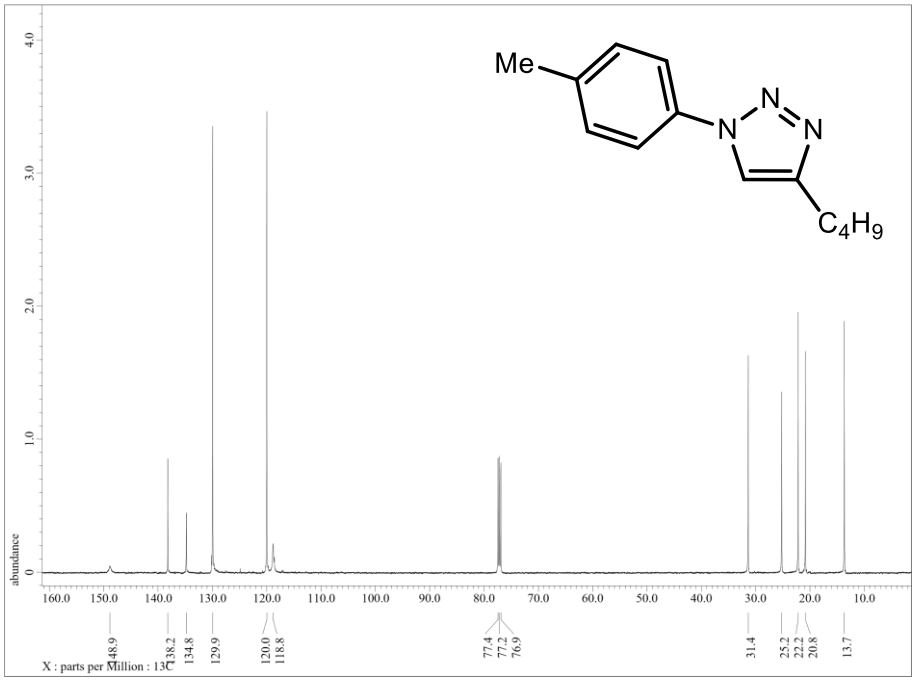

$^{13}C\{^{1}H\}$ NMR spectrum of 4-butyl-1-(*p*-tolyl)-1*H*-1,2,3-triazole (**55**) in $CDCl_3$.

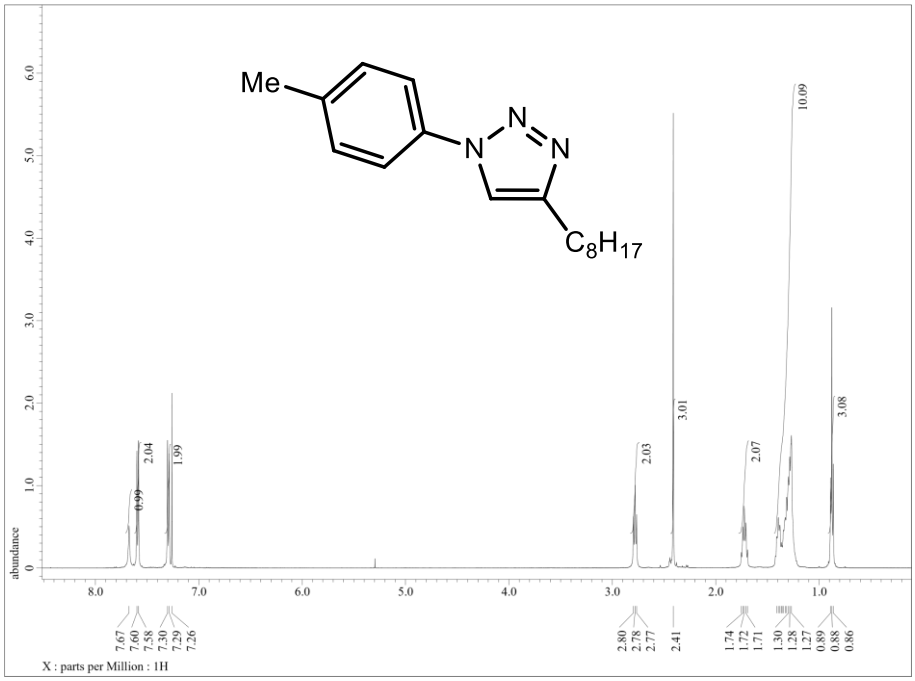

^{1}H NMR spectrum of 4-octyl-1-(*p*-tolyl)-1*H*-1,2,3-triazole (**56)** in $CDCl_3$.

`

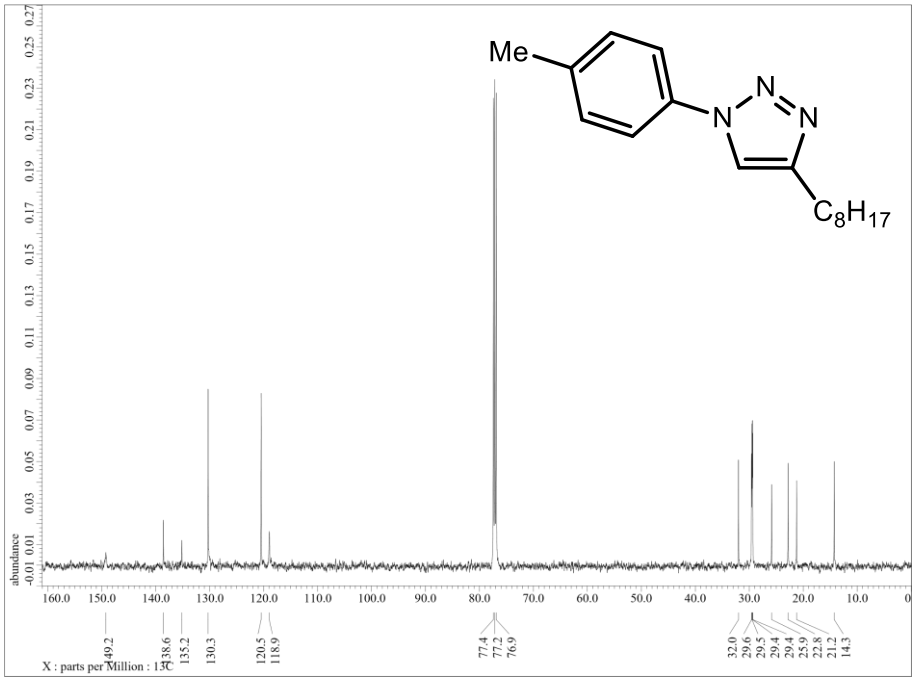

$^{13}C\{^{1}H\}$ NMR spectrum of 4-octyl-1-(*p*-tolyl)-1*H*-1,2,3-triazole (**56**) in $CDCl_3$.

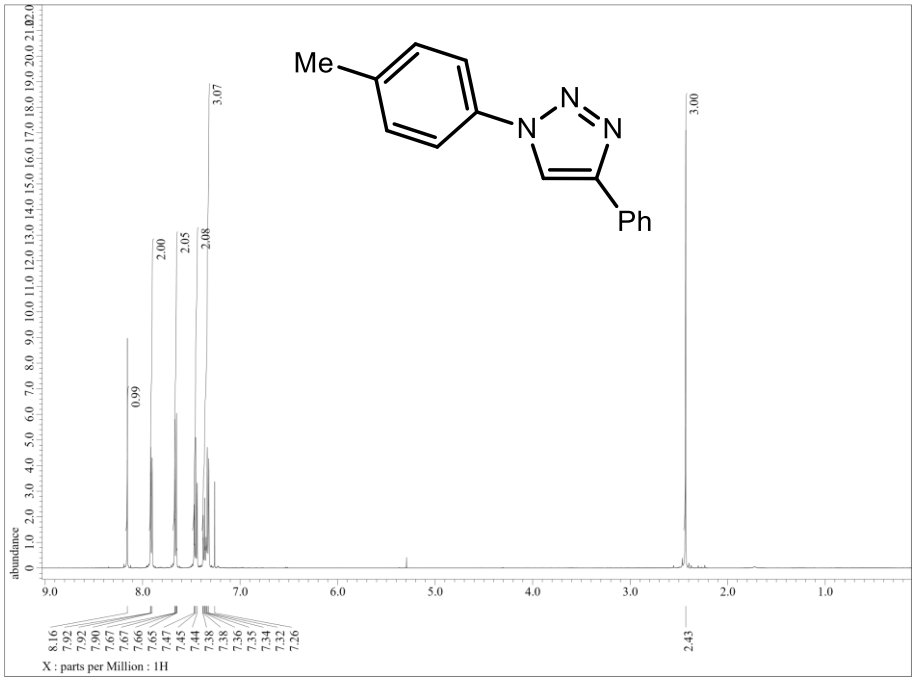

^{1}H NMR spectrum of 4-phenyl-1-(*p*-tolyl)-1*H*-1,2,3-triazole (**57**) in $CDCl_3$.

`

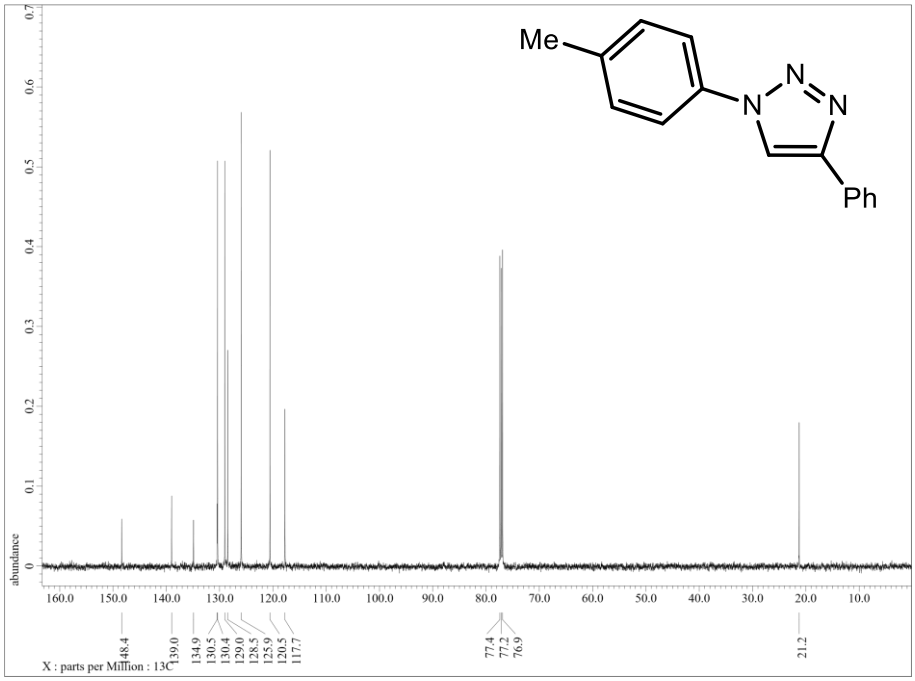

$^{13}C\{^{1}H\}$NMR spectrum of 4-phenyl-1-(*p*-tolyl)-1*H*-1,2,3-triazole (**57**) in $CDCl_3$.

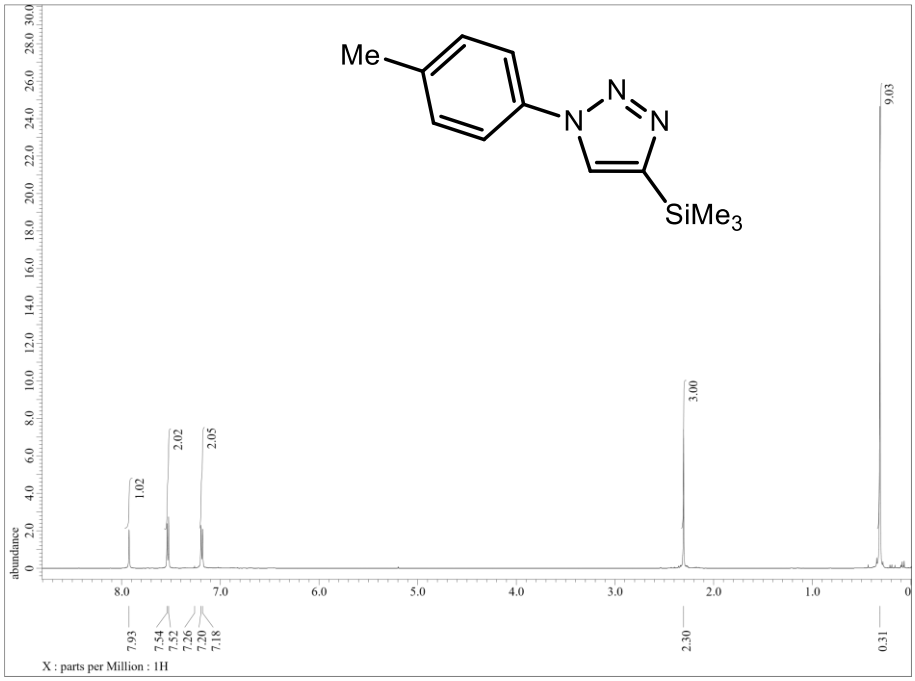

^{1}H NMR spectrum of 1-(*p*-tolyl)-4-(trimethylsilyl)-1*H*-1,2,3-triazole (**58**) in $CDCl_3$.

`

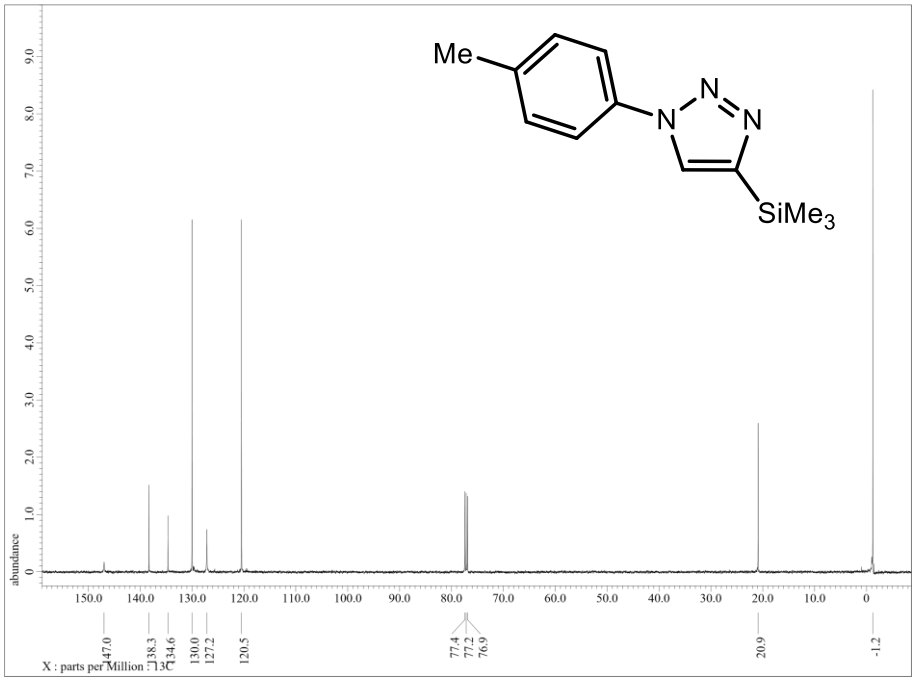

$^{13}C\{^{1}H\}$ NMR spectrum of 1-(*p*-tolyl)-4-(trimethylsilyl)-1*H*-1,2,3-triazole (**58**) in $CDCl_3$.

`

Spectroscopic Data of Chapter 3 Part 3.2

`

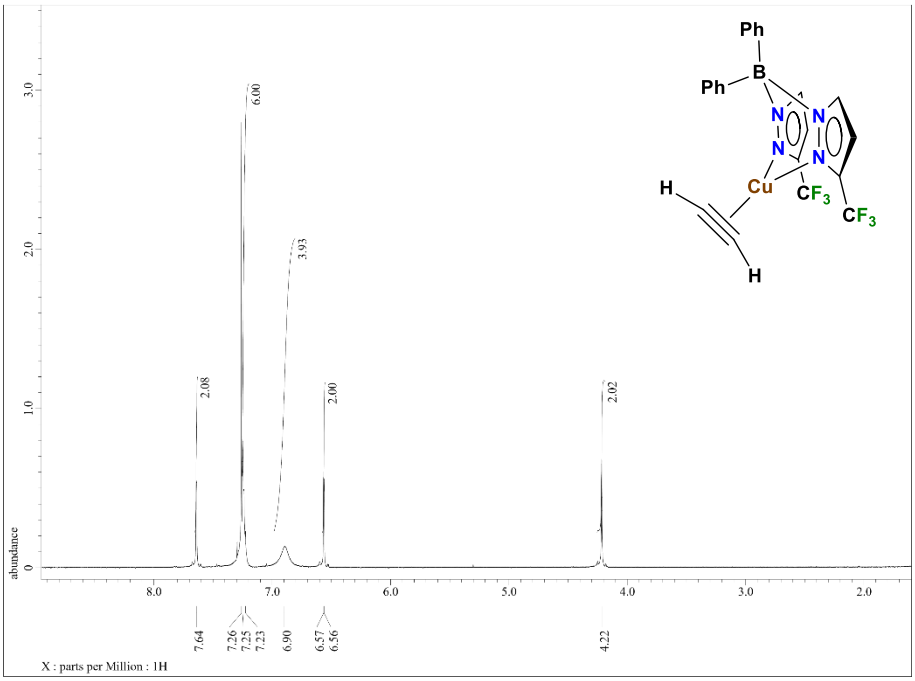

^{1}H NMR Spectrum of [$Ph_2B(3\text{-}(CF_3)Pz)_2$]Cu($C_2H_2$) (**62**) in $CDCl_3$.

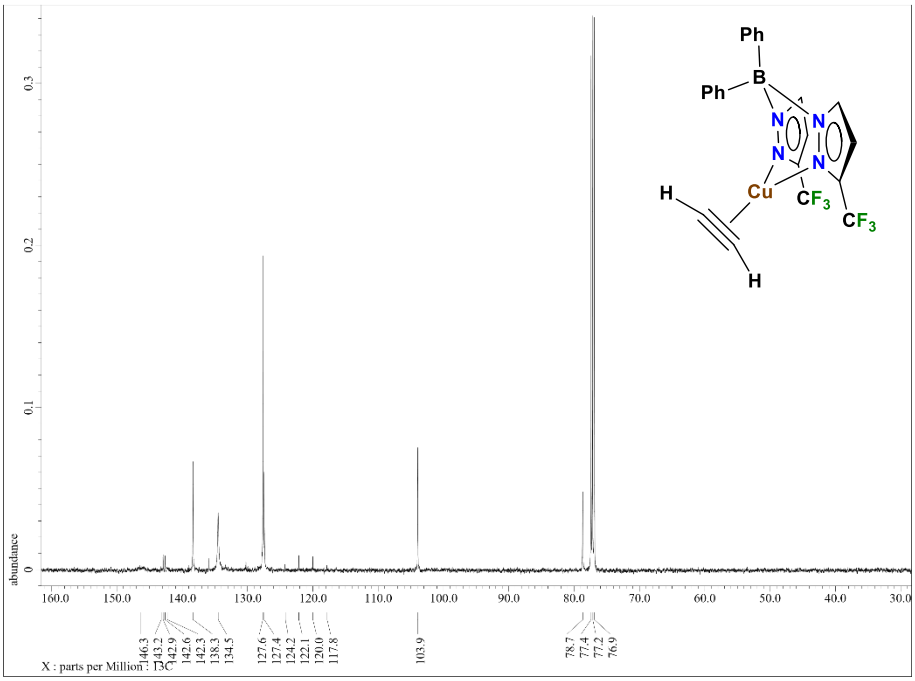

^{13}C NMR Spectrum of [$Ph_2B(3\text{-}(CF_3)Pz)_2$]Cu($C_2H_2$) (**62**) in $CDCl_3$.

`

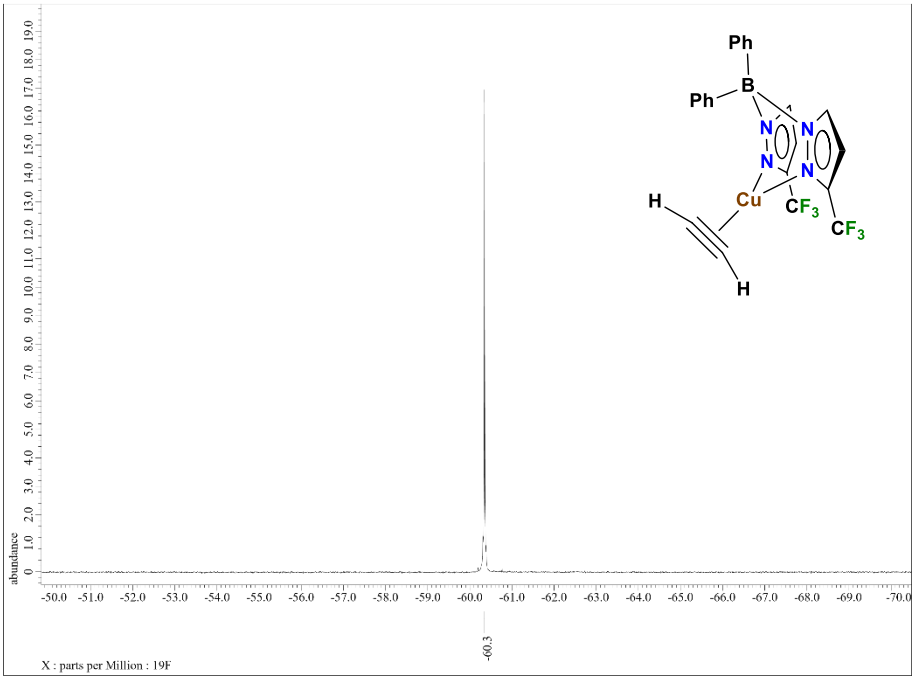

^{19}F NMR Spectrum of [$Ph_2B(3\text{-}(CF_3)Pz)_2$]Cu($C_2H_2$) (**62**) in $CDCl_3$.

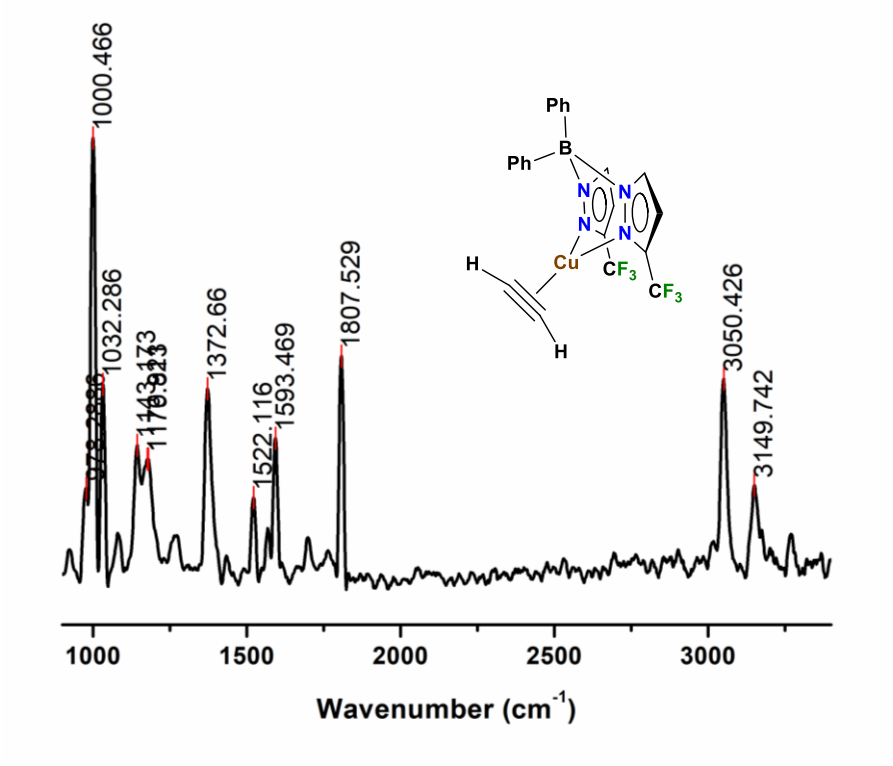

Raman Spectrum of [$Ph_2B(3\text{-}(CF_3)Pz)_2$]Cu($C_2H_2$) (**62**).

`

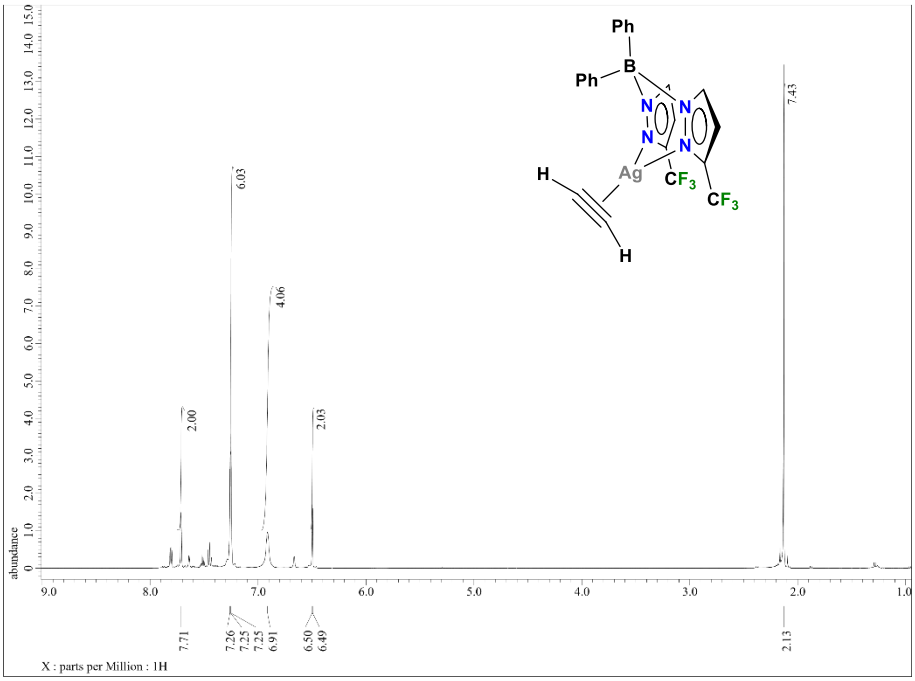

^{1}H NMR Spectrum of [$Ph_2B(3\text{-}(CF_3)Pz)_2$]Ag($C_2H_2$) (**63**) in $CDCl_3$.

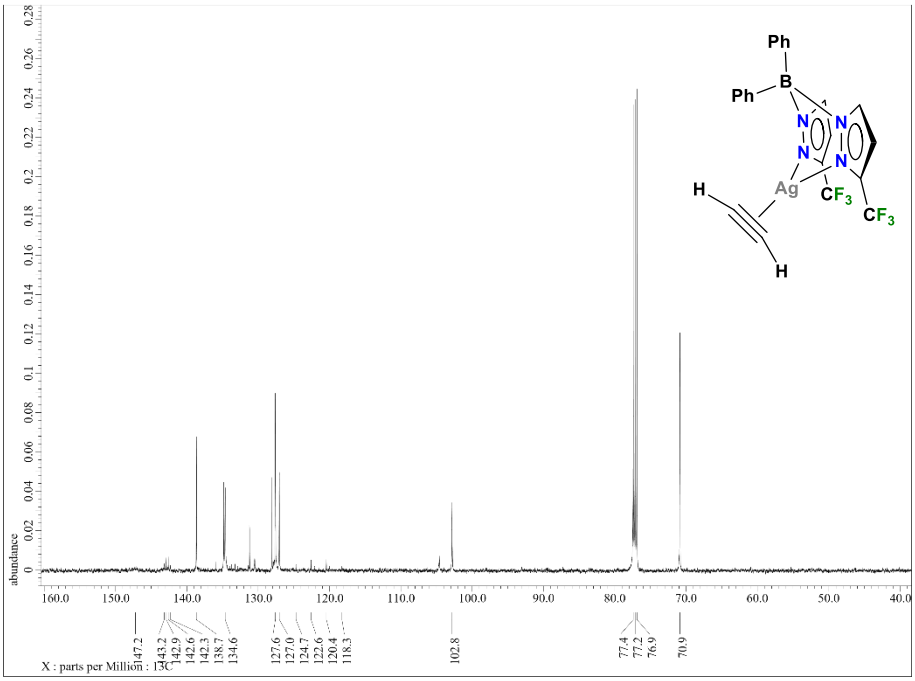

^{13}C NMR Spectrum of [$Ph_2B(3\text{-}(CF_3)Pz)_2$]Ag($C_2H_2$) (**63**) in $CDCl_3$.

`

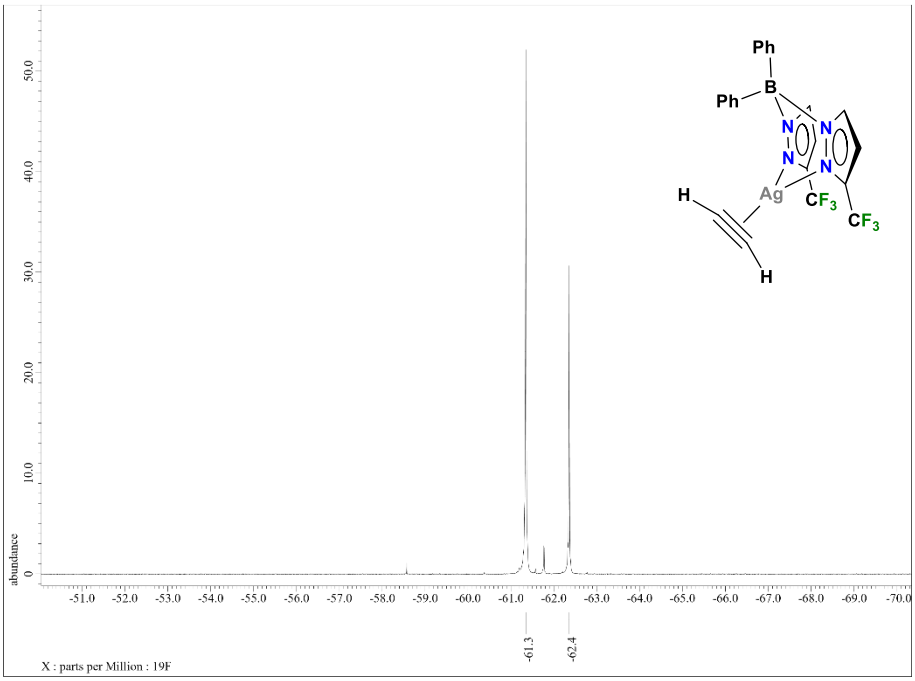

^{19}F NMR Spectrum of $[Ph_2B(3\text{-}(CF_3)Pz)_2]Ag(C_2H_2)$ (**63**) in $CDCl_3$. The peak at -62.4 ppm belongs to the acetylene dissociated product.

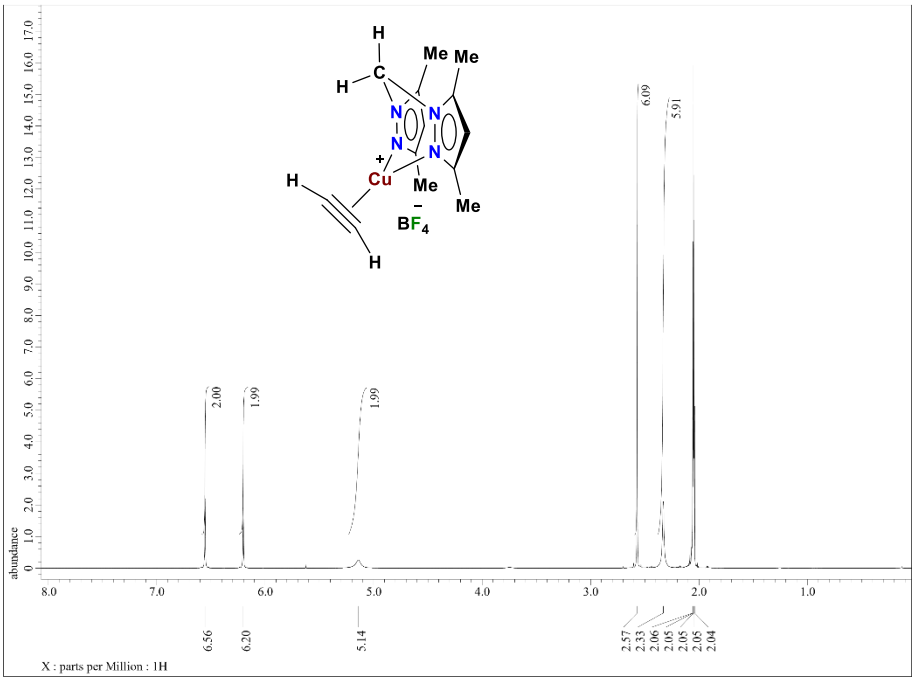

^{1}H NMR Spectrum of $[\{H_2C(3,5\text{-}(CH_3)_2Pz)_2\}Cu(C_2H_2)][BF_4]$ (**64**) in $(CD_3)_2CO$.

`

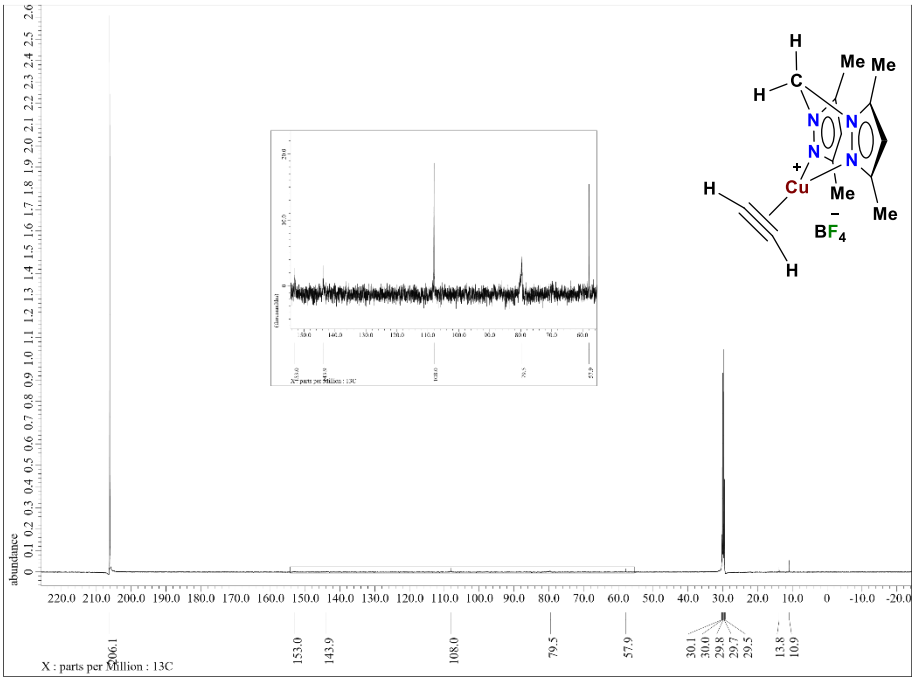

^{13}C NMR Spectrum of [{$H_2C(3,5\text{-}(CH_3)_2Pz)_2$}Cu($C_2H_2$)][$BF_4$] (**64**) in $(CD_3)_2CO$.

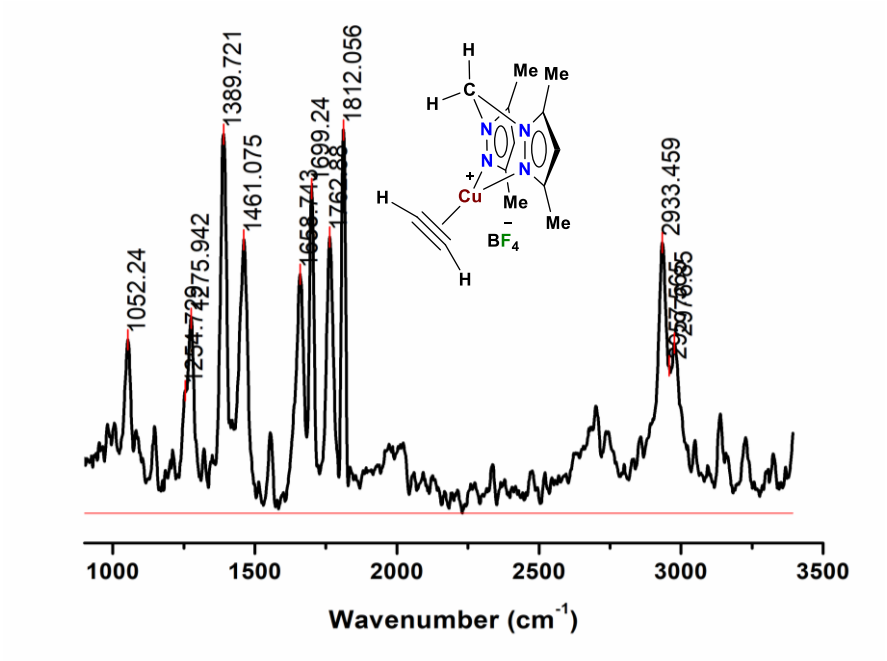

Raman Spectrum of [{$H_2C(3,5\text{-}(CH_3)_2Pz)_2$}Cu($C_2H_2$)][$BF_4$] (**64**).

`

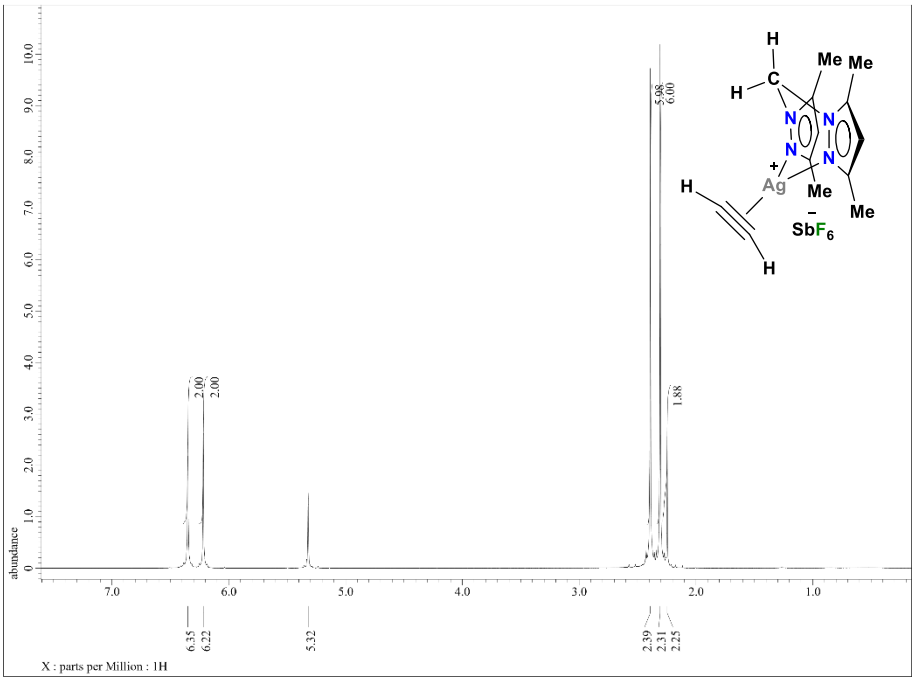

^{1}H NMR Spectrum of [{$H_2C(3,5\text{-}(CH_3)_2Pz)_2$}Ag($C_2H_2$)][$SbF_6$] (**65**) in CD_2Cl_2.

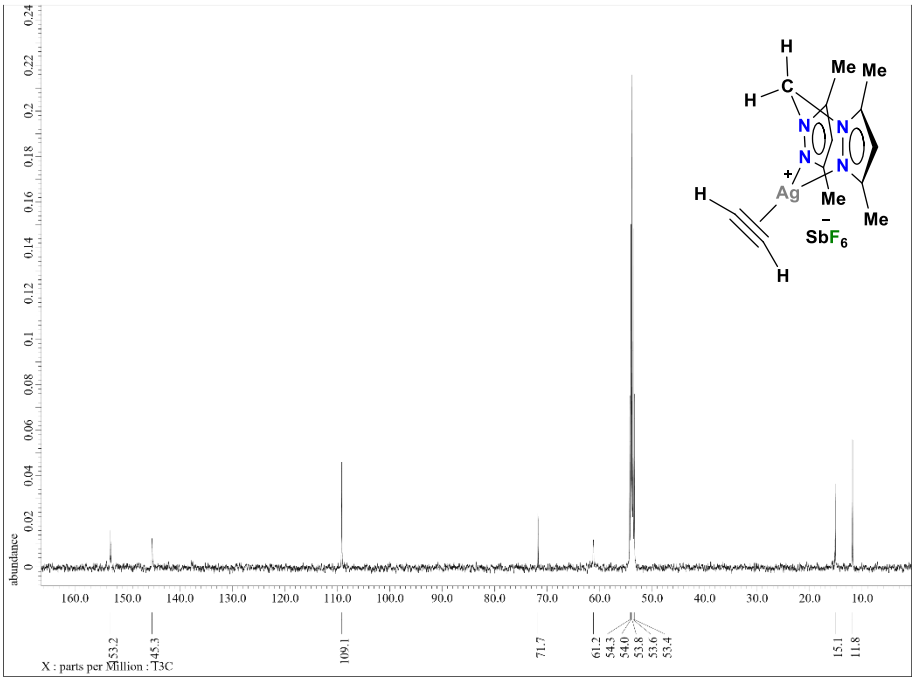

^{13}C NMR Spectrum of [{$H_2C(3,5\text{-}(CH_3)_2Pz)_2$}Ag($C_2H_2$)][$SbF_6$] (**65**) in CD_2Cl_2.

`

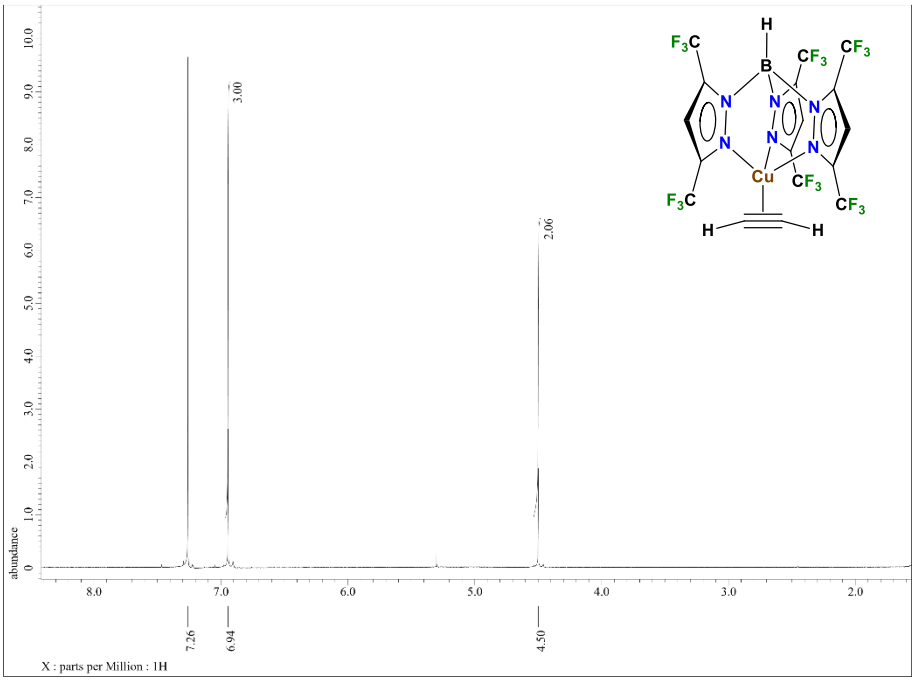

^{1}H NMR Spectrum of [HB(3,5-(CF$_3$)$_2$Pz)$_3$]Cu(C$_2$H$_2$) (**66**) in CDCl$_3$.

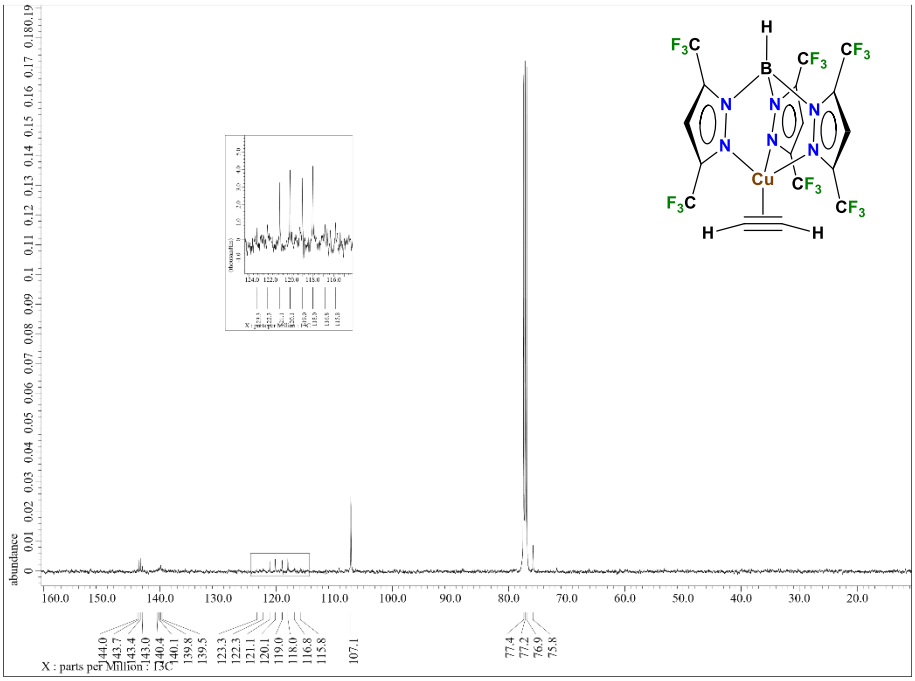

^{13}C NMR Spectrum of [HB(3,5-(CF$_3$)$_2$Pz)$_3$]Cu(C$_2$H$_2$) (**66**) in CDCl$_3$.

`

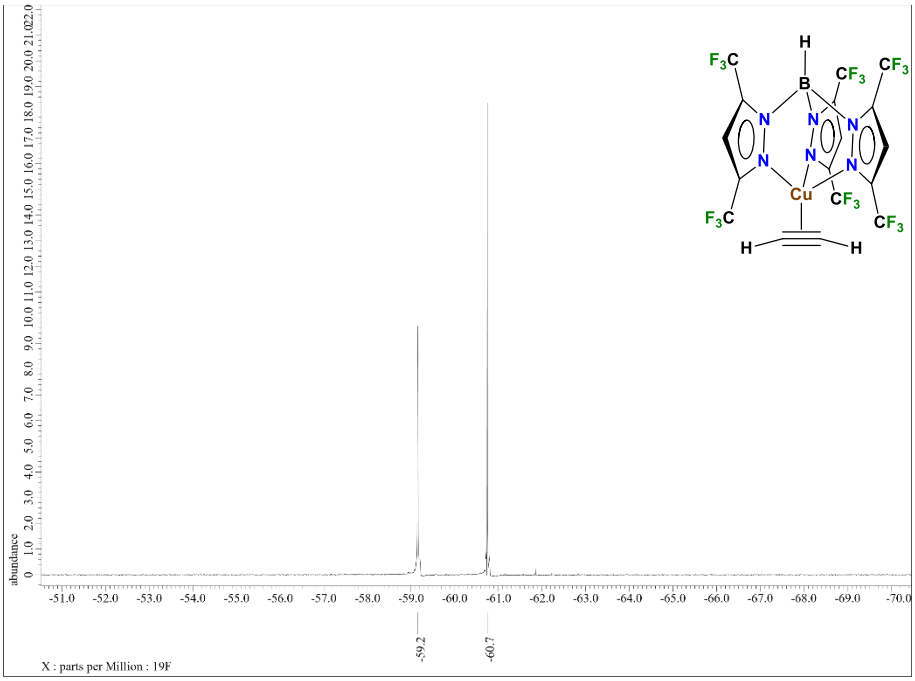

^{19}F NMR Spectrum of $[HB(3,5\text{-}(CF_3)_2Pz)_3]Cu(C_2H_2)$ (**66**) in $CDCl_3$.

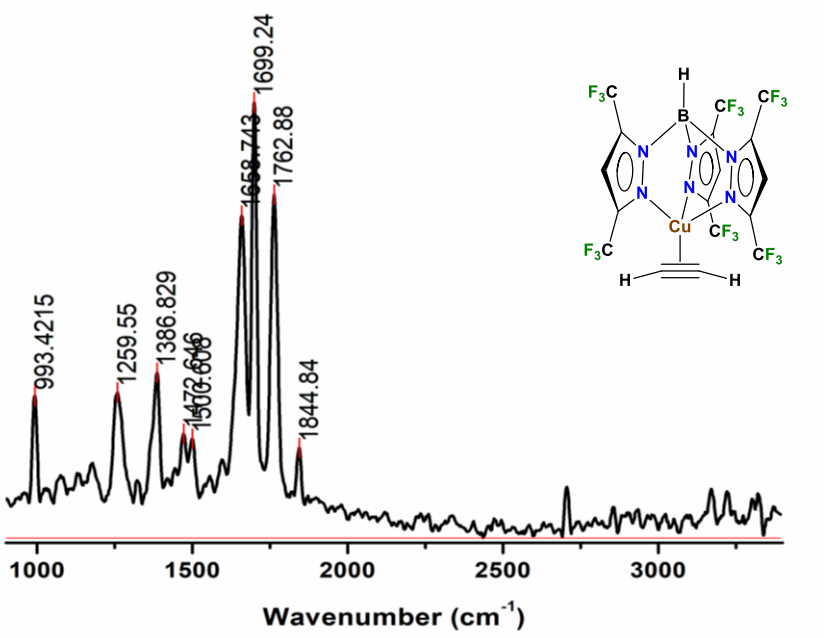

Raman Spectrum of $[HB(3,5\text{-}(CF_3)_2Pz)_3]Cu(C_2H_2)$ (**66**).

`

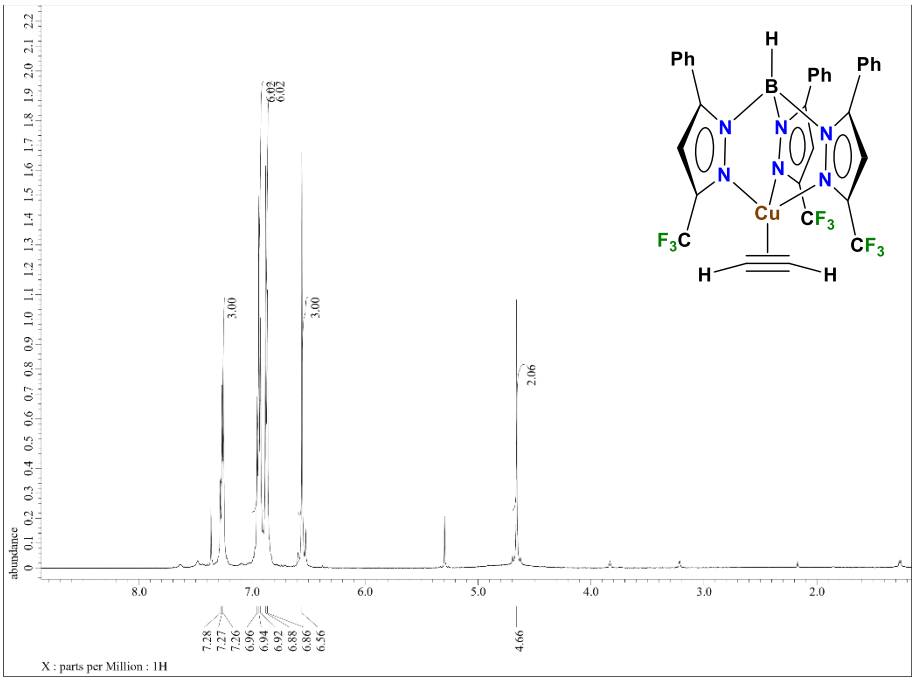

^{1}H NMR Spectrum of [HB(3-(CF_3),5-(Ph)Pz)$_3$]Cu(C_2H_2) (**67**) in $CDCl_3$.

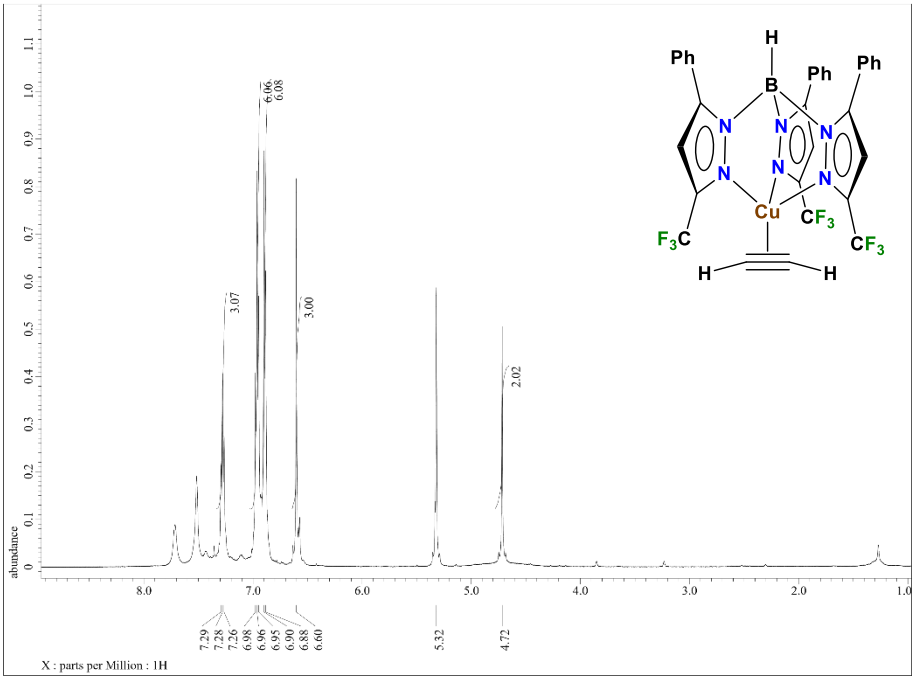

^{1}H NMR Spectrum of [HB(3-(CF_3),5-(Ph)Pz)$_3$]Cu(C_2H_2) (**67**) in CD_2Cl_2.

`

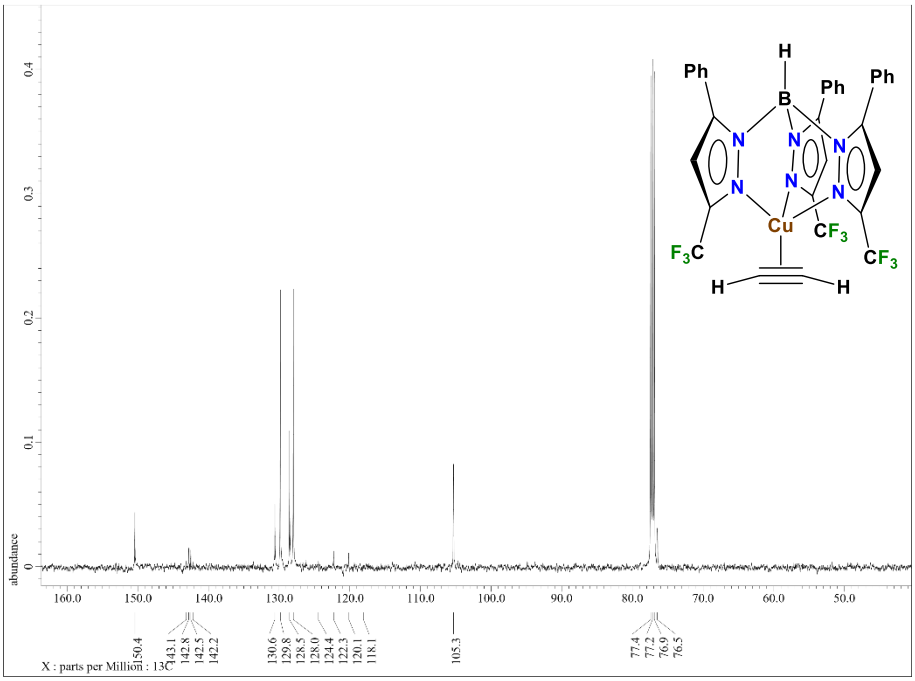

^{13}C NMR Spectrum of [HB(3-(CF_3),5-(Ph)Pz)$_3$]Cu(C_2H_2) (**67**) in $CDCl_3$.

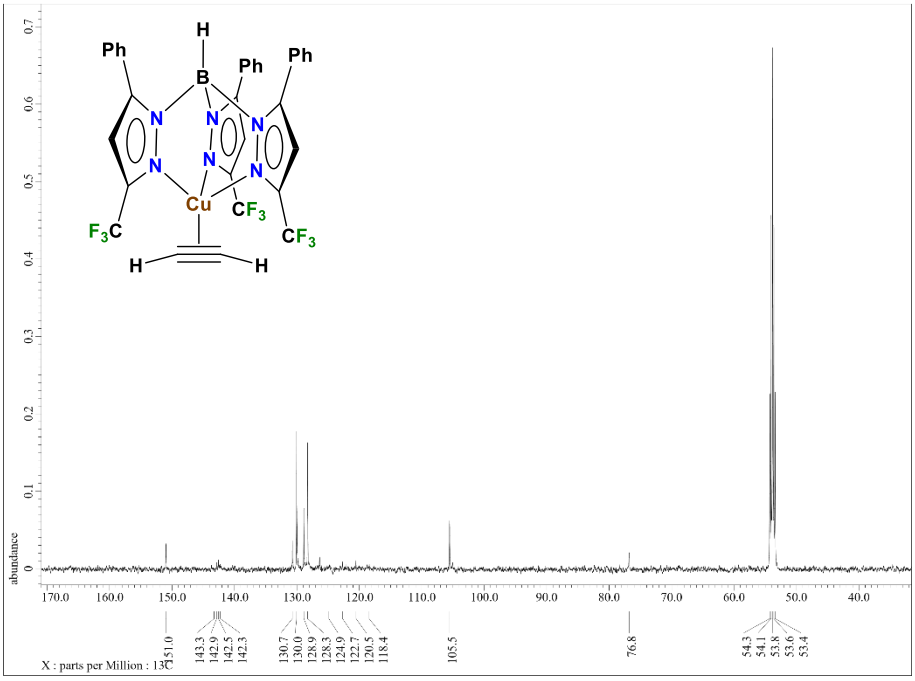

^{13}C NMR Spectrum of [HB(3-(CF_3),5-(Ph)Pz)$_3$]Cu(C_2H_2) (**67**) in CD_2Cl_2.

`

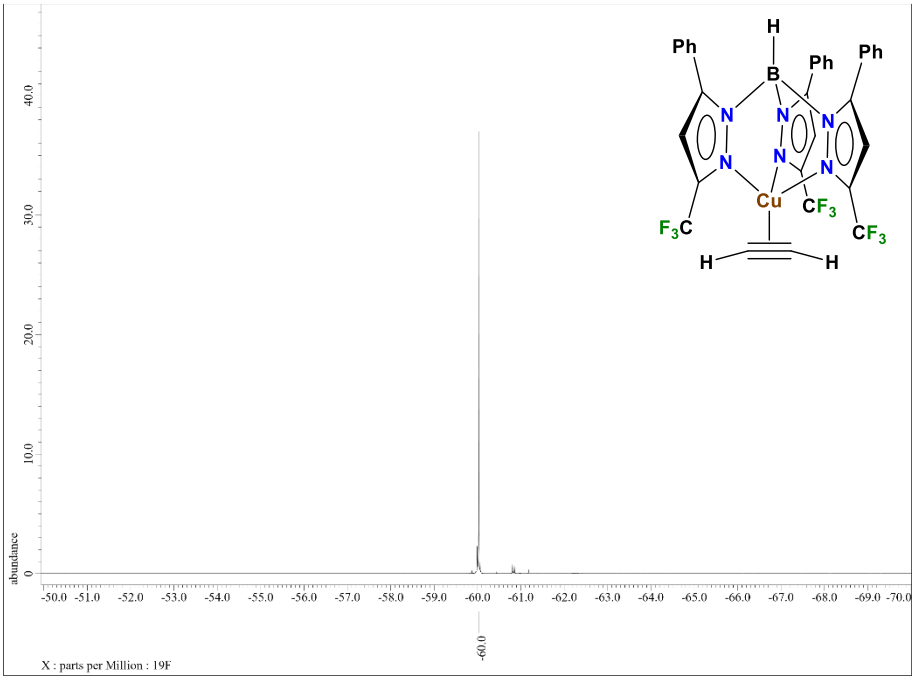

^{19}F NMR Spectrum of [HB(3-(CF_3),5-(Ph)Pz)$_3$]Cu(C_2H_2) (**67**) in $CDCl_3$

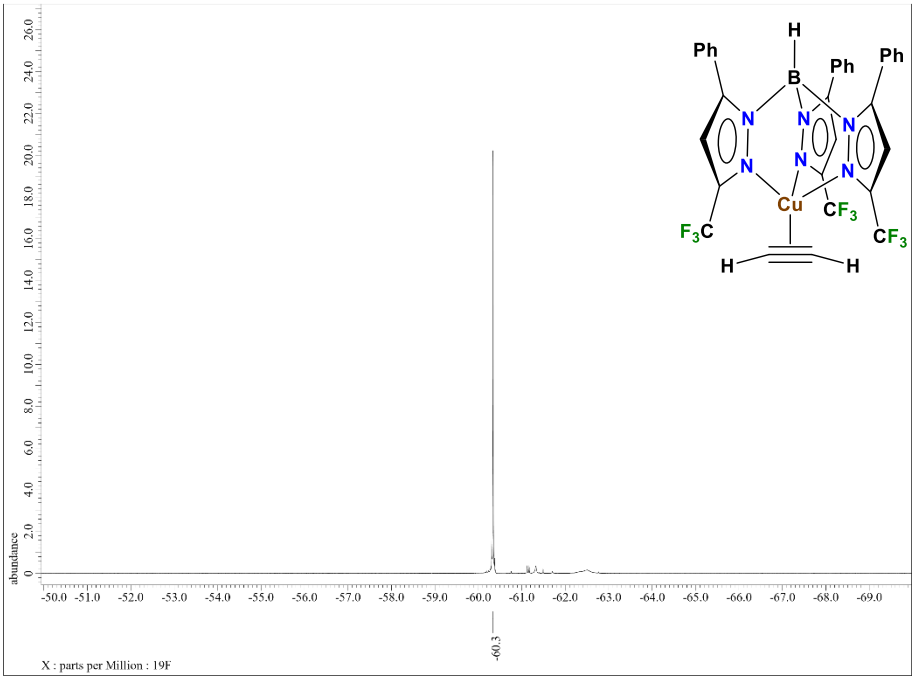

^{19}F NMR Spectrum of [HB(3-(CF_3),5-(Ph)Pz)$_3$]Cu(C_2H_2) (**67**) in CD_2Cl_2.

`

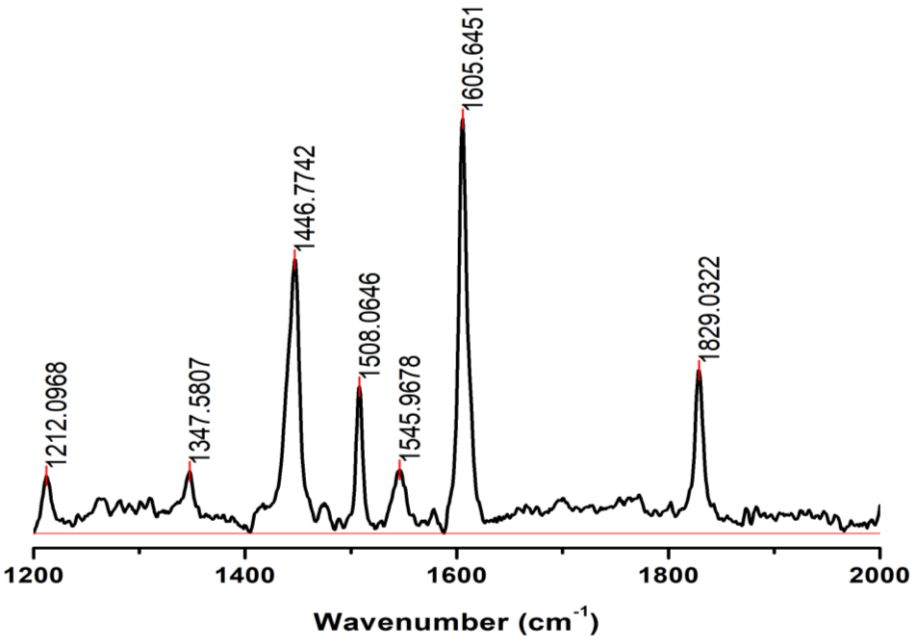

Raman Spectrum of [HB(3-(CF_3),5-(Ph)Pz)$_3$]Cu(C_2H_2) (**67**).

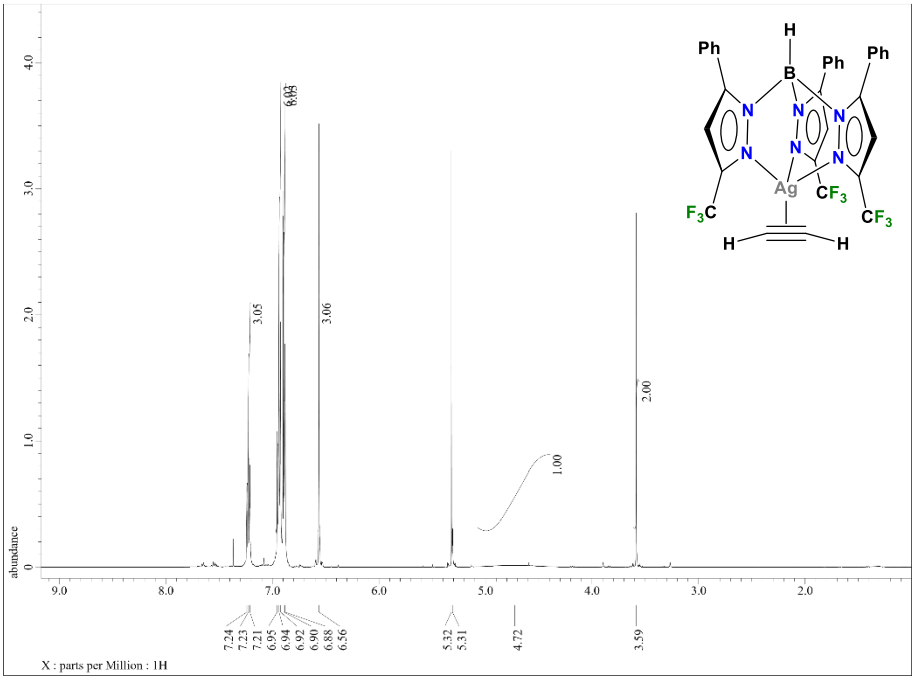

^{1}H NMR Spectrum of [HB(3-(CF_3),5-(Ph)Pz)$_3$]Ag(C_2H_2) (**68**) in CD_2Cl_2.

`

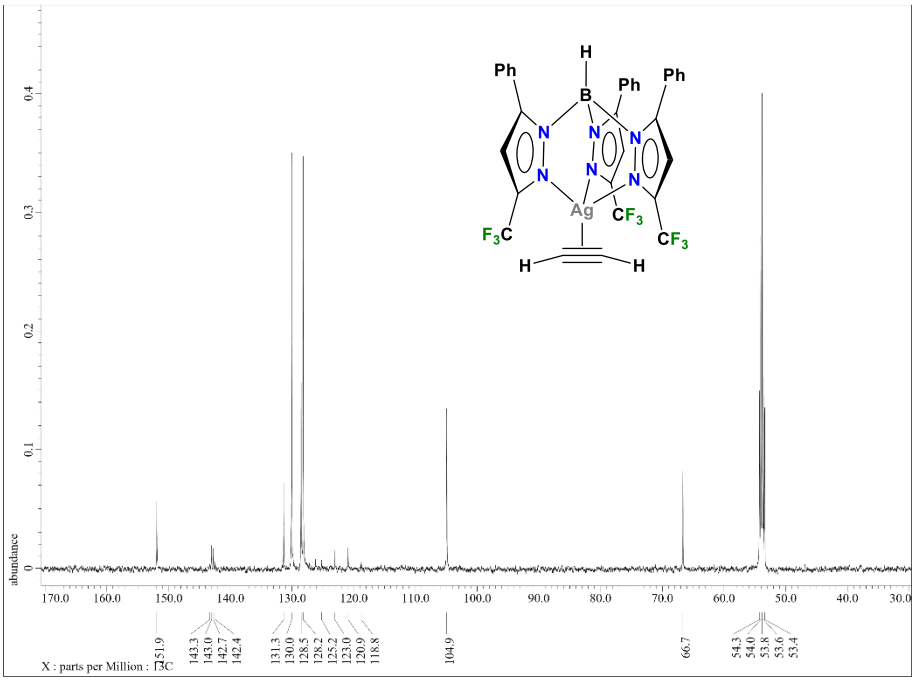

^{13}C NMR Spectrum of [HB(3-(CF_3),5-(Ph)Pz)$_3$]Ag(C_2H_2) (**68**) in CD_2Cl_2.

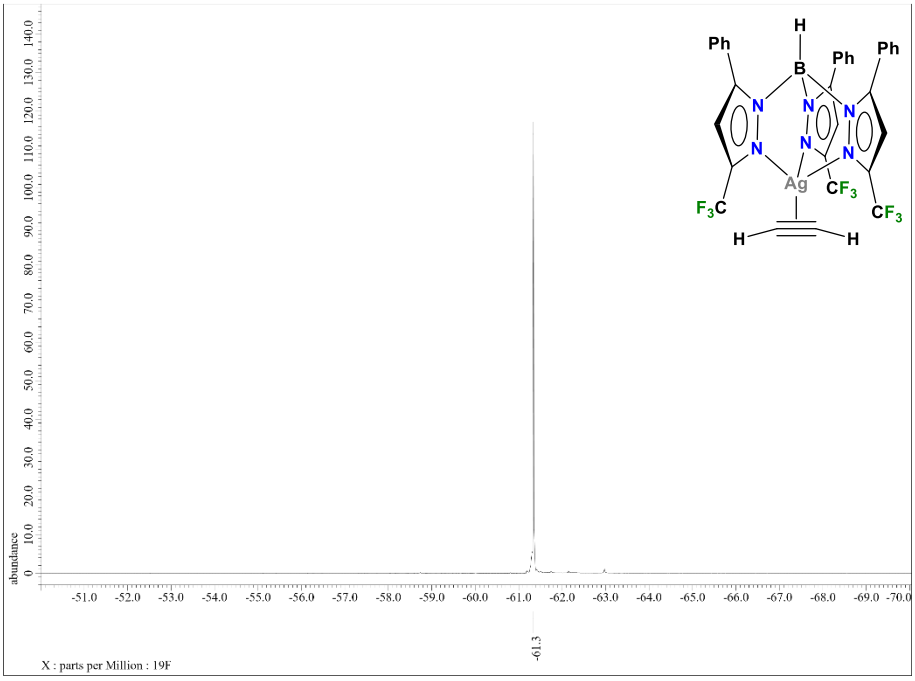

^{19}F NMR Spectrum of [HB(3-(CF_3),5-(Ph)Pz)$_3$]Ag(C_2H_2) (**68**) in CD_2Cl_2

`

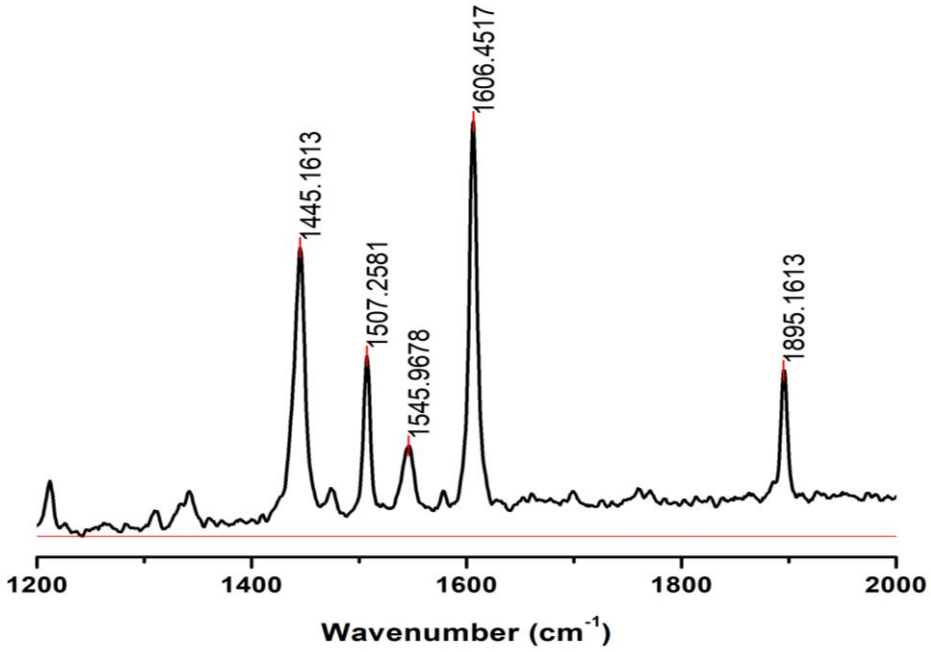

Raman Spectrum of [HB(3-(CF_3),5-(Ph)Pz)$_3$]Ag(C_2H_2) (**68**).

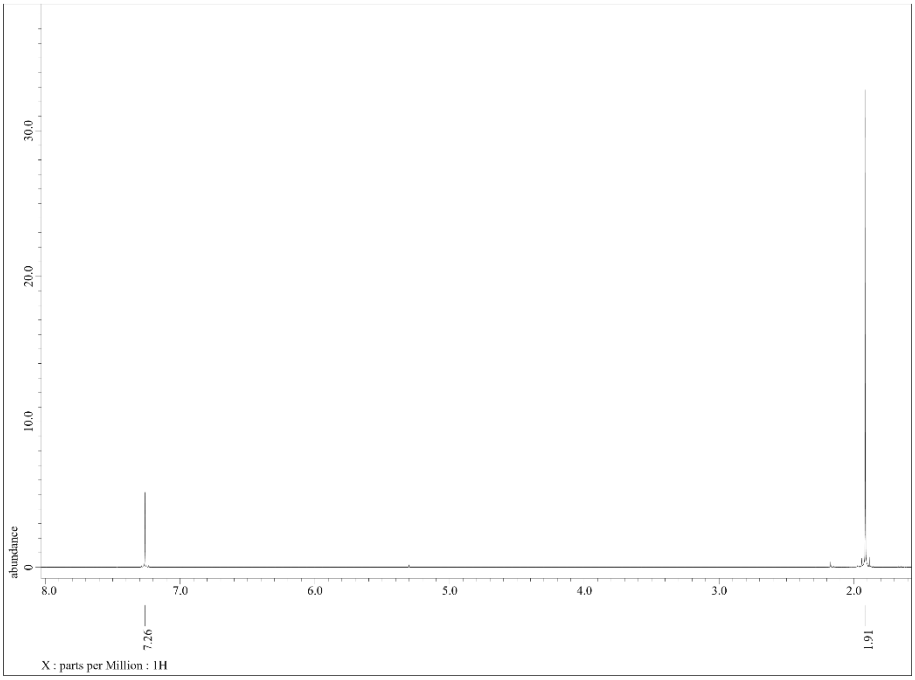

^{1}H NMR Spectrum of free acetylene in $CDCl_3$.

`

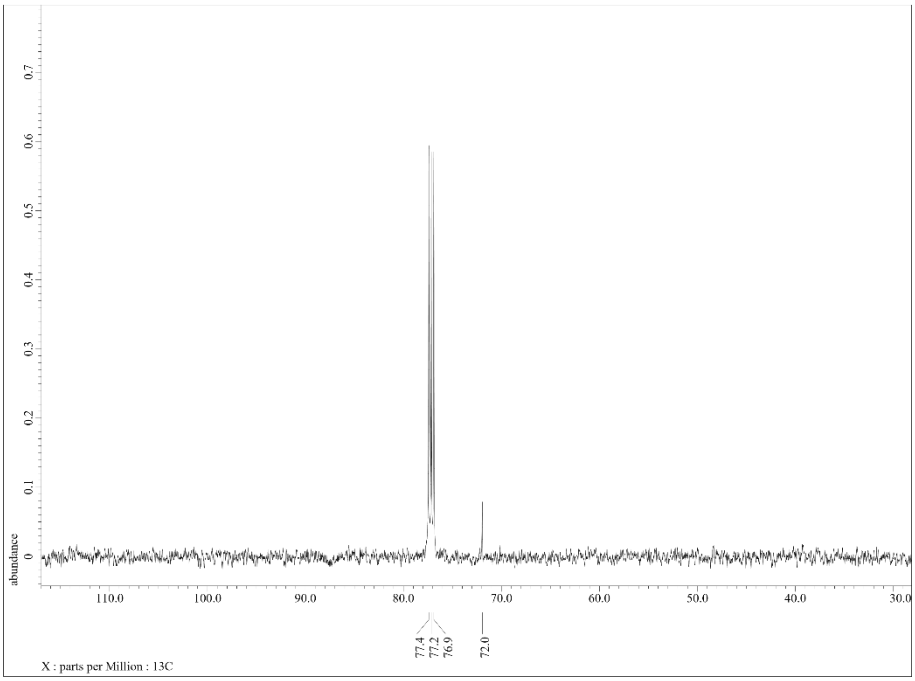

^{13}C NMR Spectrum of free acetylene in $CDCl_3$.

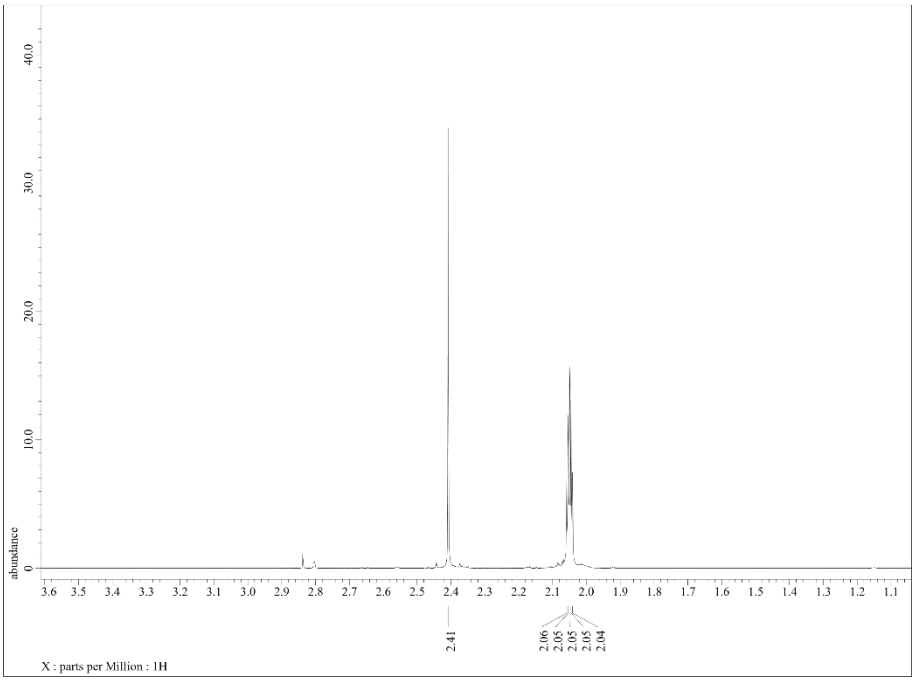

^{1}H NMR Spectrum of free acetylene in $(CD_3)_2CO$.

`

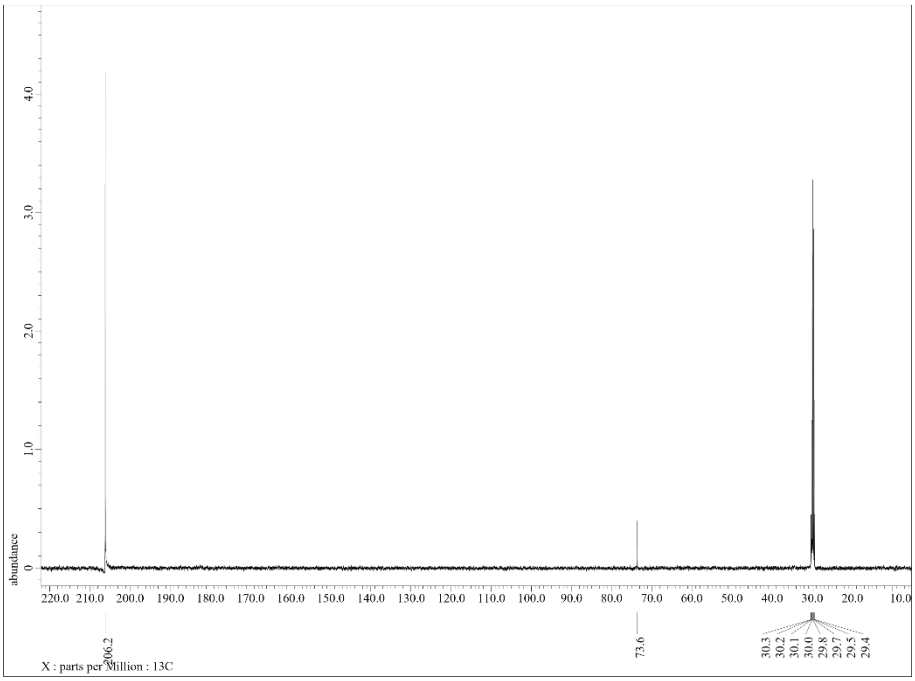

^{13}C NMR Spectrum of free acetylene in $(CD_3)_2CO$.

`

Appendix C

Spectroscopic Data of Chapter 4

`

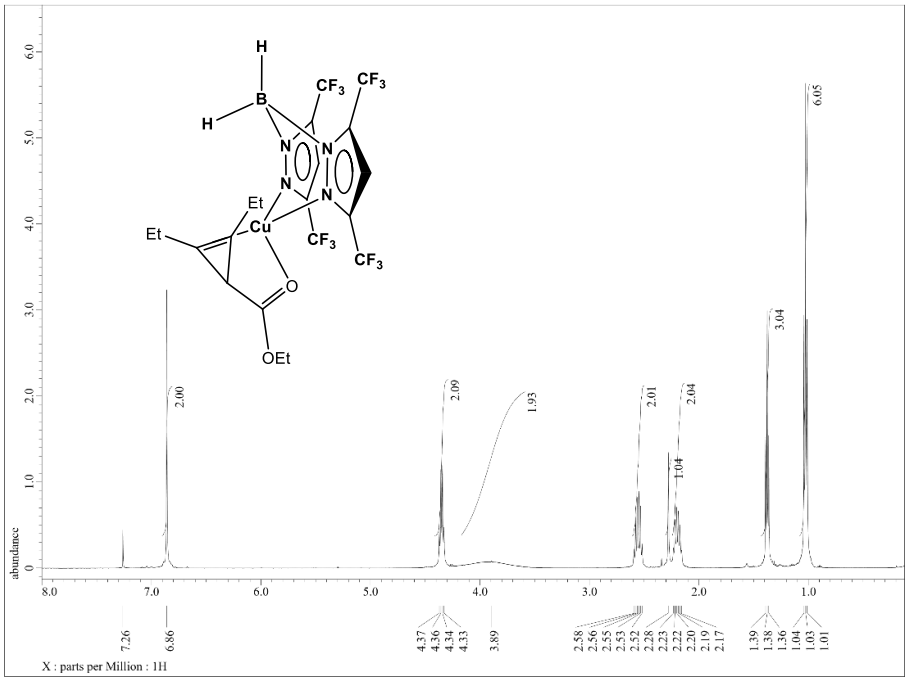

^{1}H NMR Spectrum of [$H_2B(3,5\text{-}(CF_3)_2Pz)_2$]Cu(Cyp-**2**) (**74**).

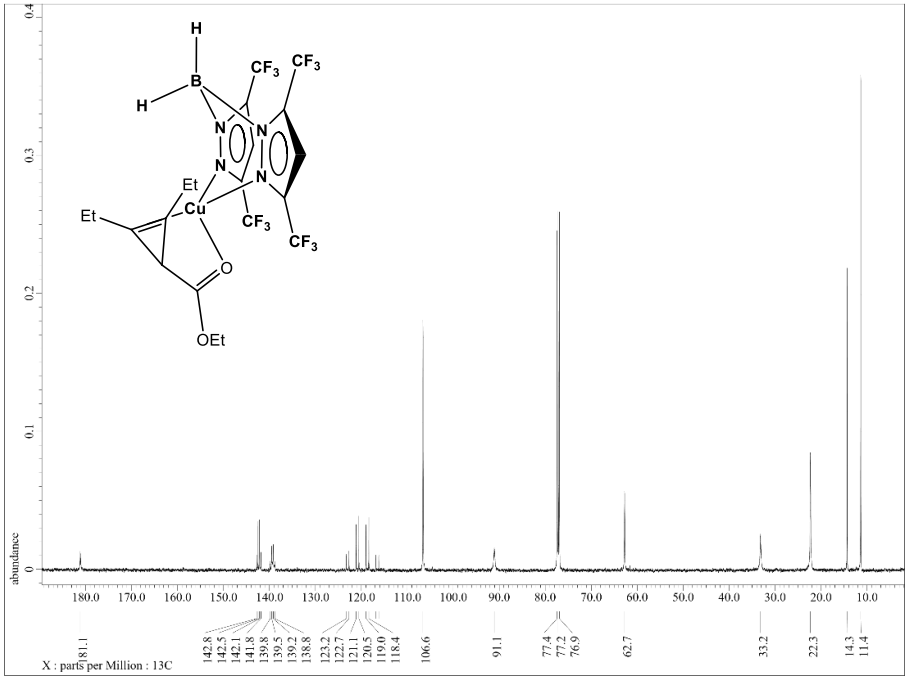

^{13}C NMR Spectrum of [$H_2B(3,5\text{-}(CF_3)_2Pz)_2$]Cu(Cyp-**2**) (**74**).

`

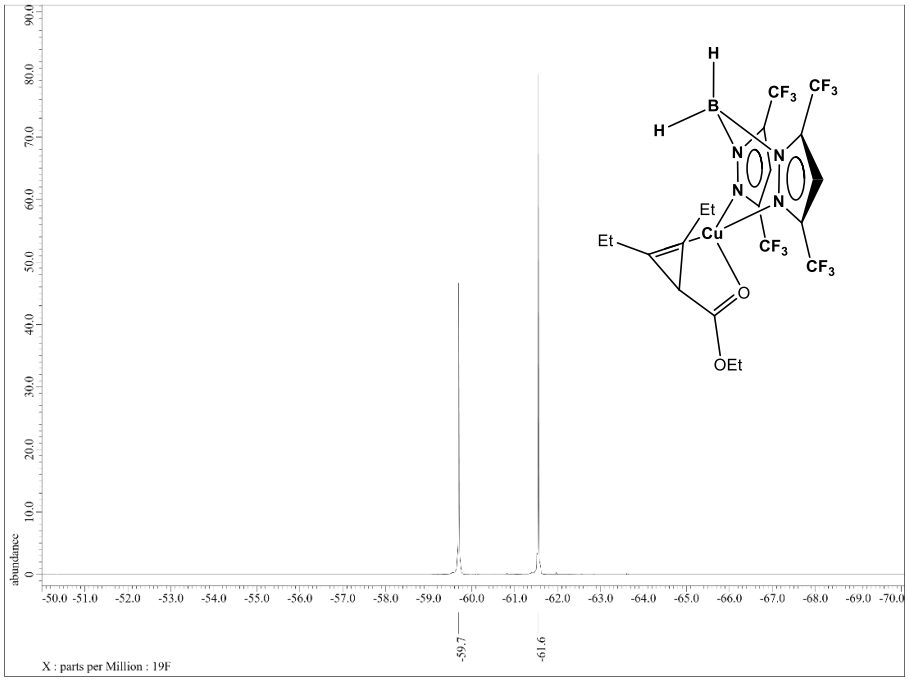

^{19}F NMR Spectrum of $[H_2B(3,5\text{-}(CF_3)_2Pz)_2]Cu(Cyp\text{-}\mathbf{2})$ (**74**).

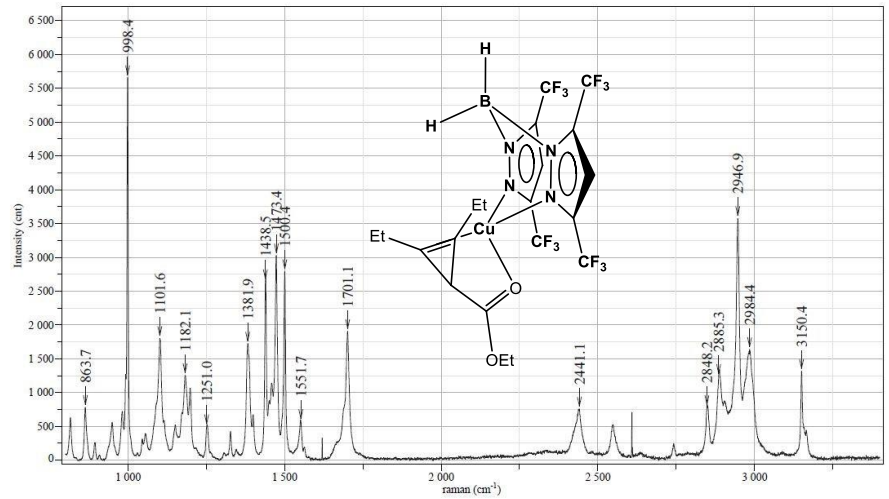

Exposition	5	Slit	100
Accumulation	1 x 44	Operator	Anurag
Laser	632.817	Sample	3-5CF3BpCu_1,2-Ditheyl-3-(
Spectro	Auto	Remark	
Hole	200	Power	

Raman Spectrum of $[H_2B(3,5\text{-}(CF_3)_2Pz)_2]Cu(Cyp\text{-}\mathbf{2})$ (**74**).

`

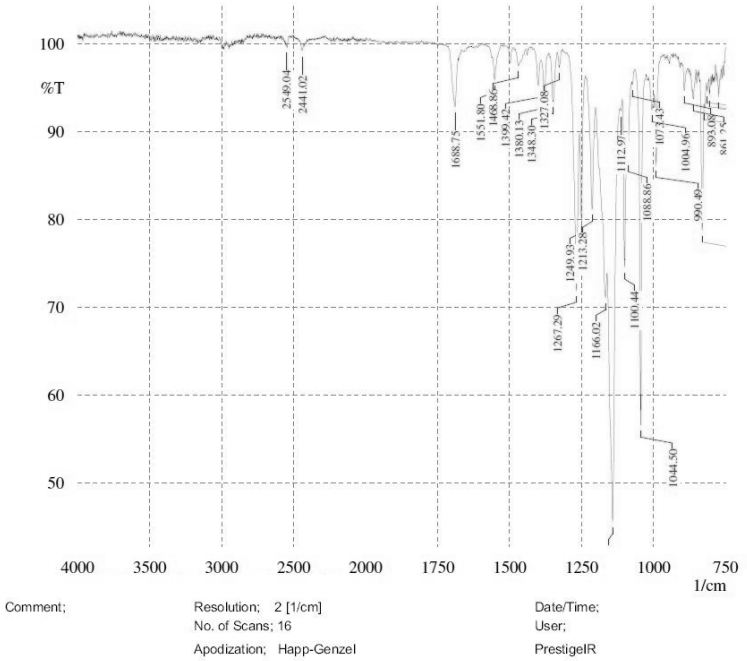

IR Spectrum of $[H_2B(3,5\text{-}(CF_3)_2Pz)_2]Cu(Cyp\text{-}\mathbf{2})$ (**74**).

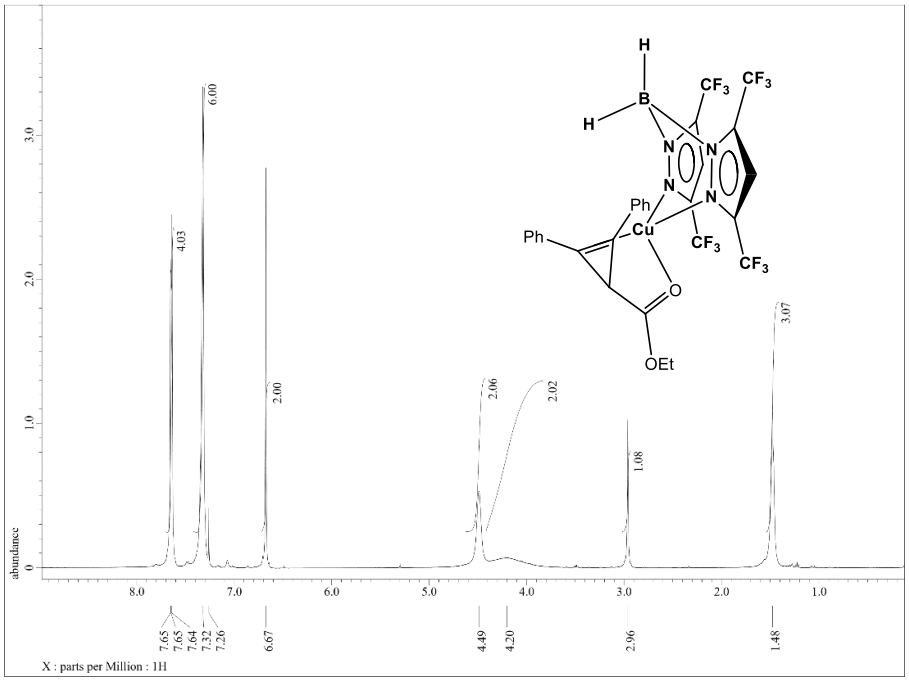

^{1}H NMR Spectrum of $[H_2B(3,5\text{-}(CF_3)_2Pz)_2]Cu(Cyp\text{-}\mathbf{3})$ (**75**).

`

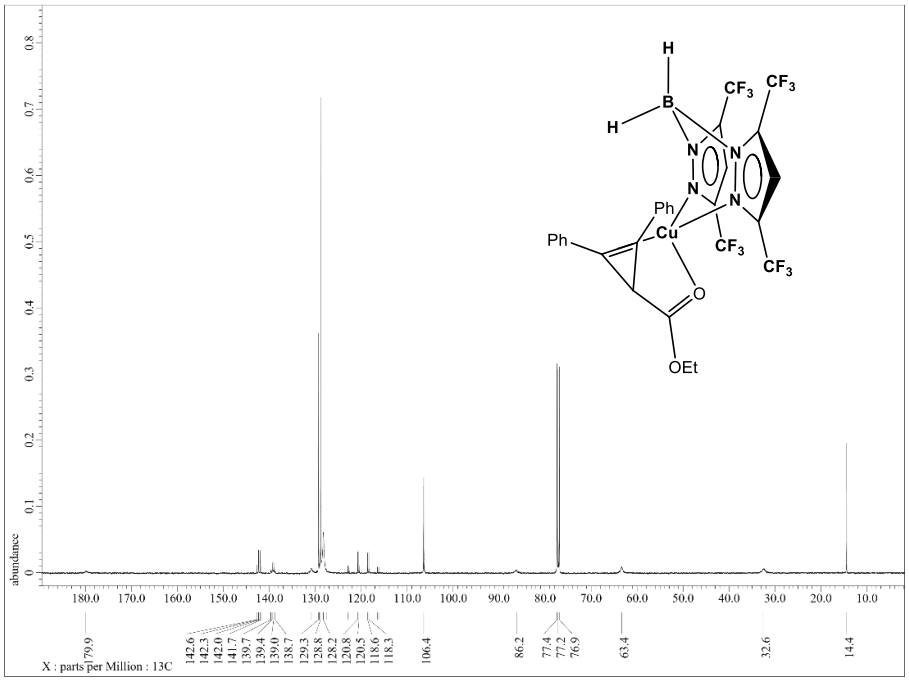

^{13}C NMR Spectrum of [$H_2B(3,5\text{-}(CF_3)_2Pz)_2$]Cu(Cyp-**3**) (**75**).

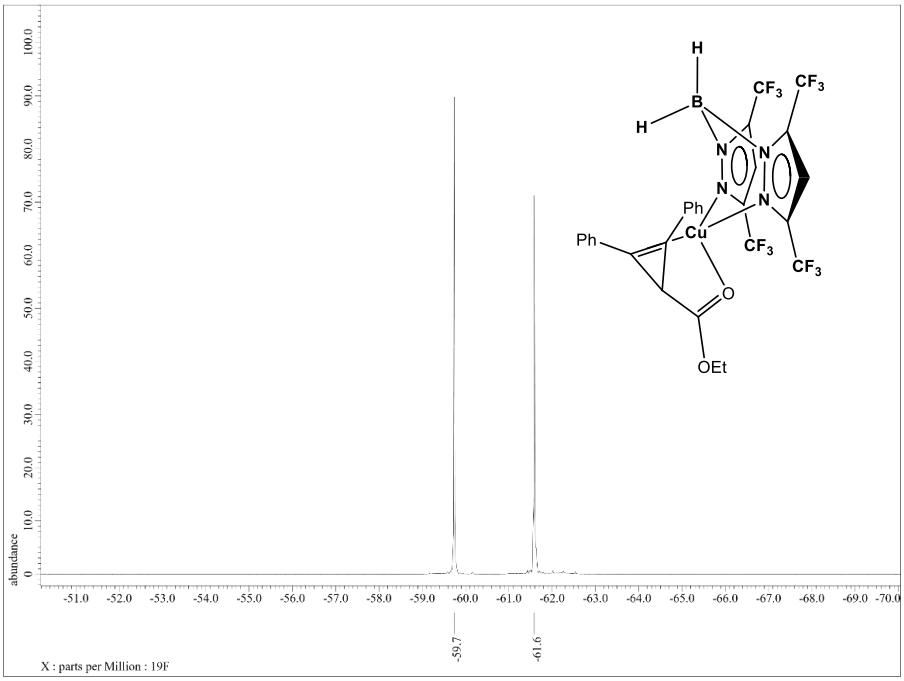

^{19}F NMR Spectrum of [$H_2B(3,5\text{-}(CF_3)_2Pz)_2$]Cu(Cyp-**3**) (**75**).

`

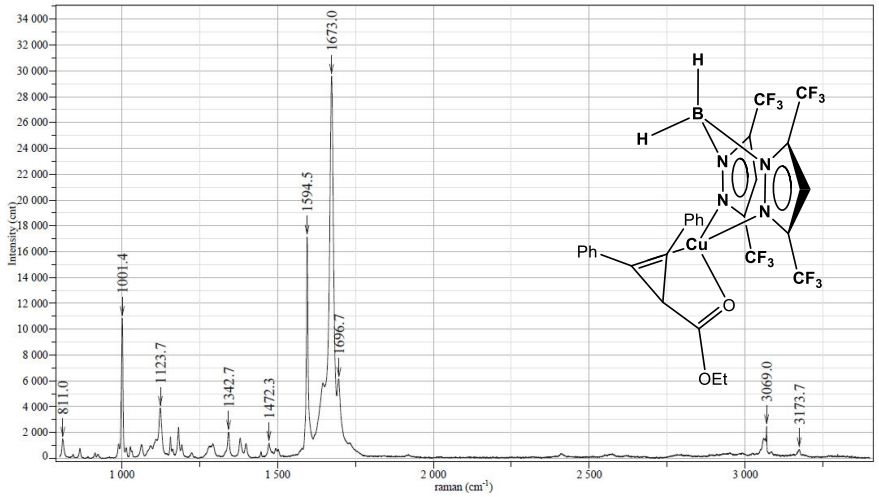

Exposition	5	Slit	100
Accumulation	1 x 21	Operator	Anurag
Laser	632.817	Sample	3,5-(CF3)2BpCu(Diphenylett
Spectro	Auto	Remark	
Hole	200	Power	

Raman Spectrum of $[H_2B(3,5\text{-}(CF_3)_2Pz)_2]Cu$(Cyp-**3**) (**75**).

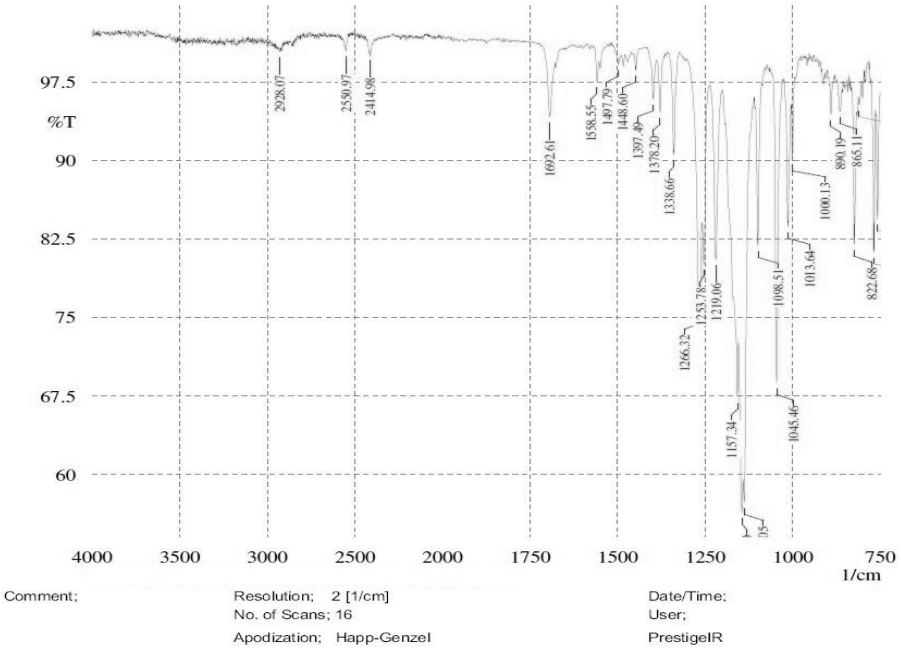

IR Spectrum of $[H_2B(3,5\text{-}(CF_3)_2Pz)_2]Cu$(Cyp-**3**) (**75**).

`

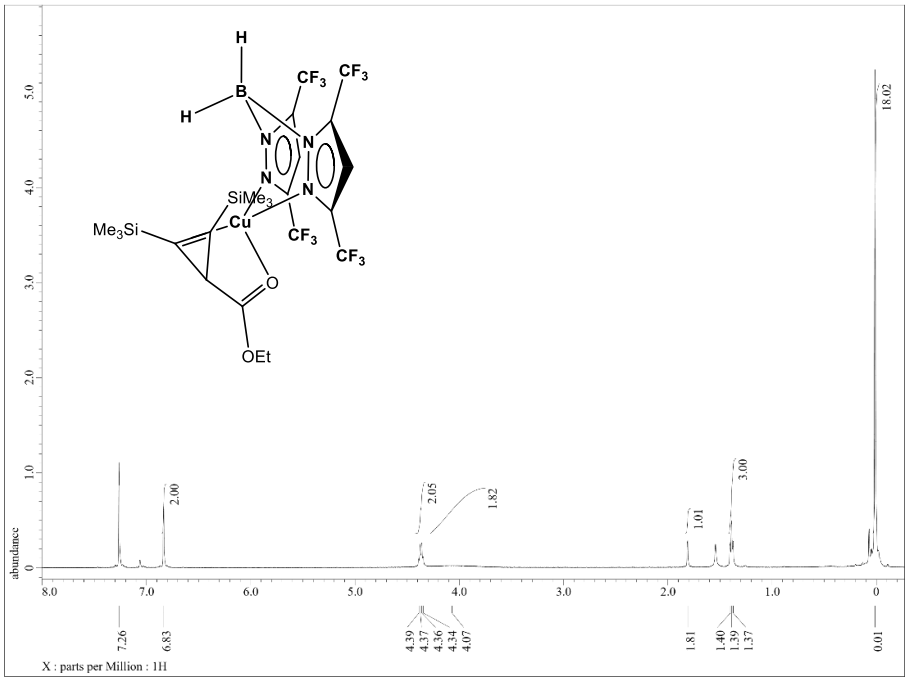

^{1}H NMR Spectrum of [$H_2B(3,5\text{-}(CF_3)_2Pz)_2$]Cu(Cyp-**4**) (**76**).

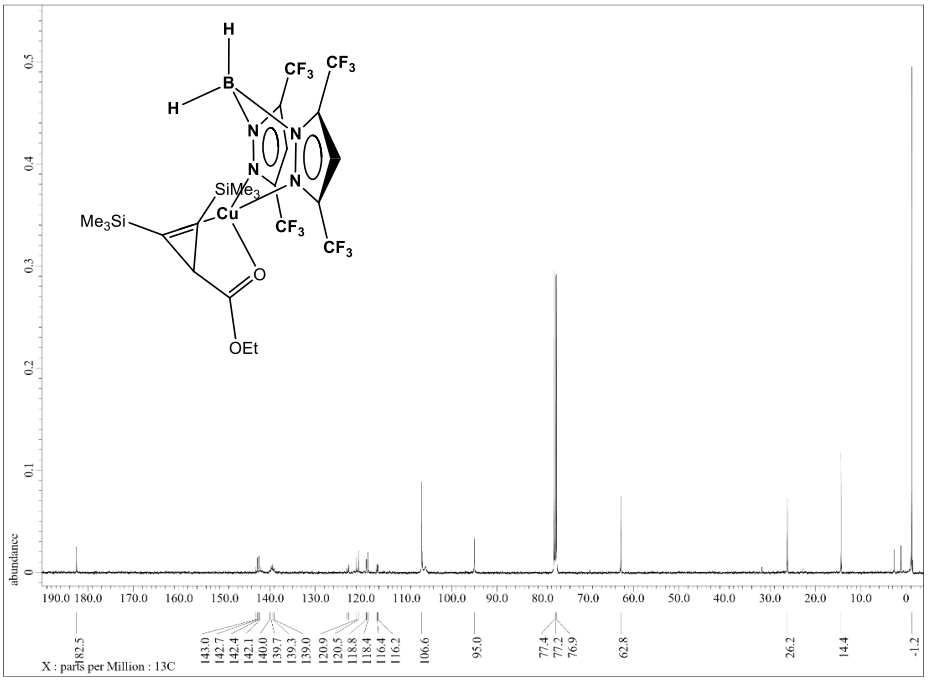

^{13}C NMR Spectrum of [$H_2B(3,5\text{-}(CF_3)_2Pz)_2$]Cu(Cyp-**4**) (**76**).

`

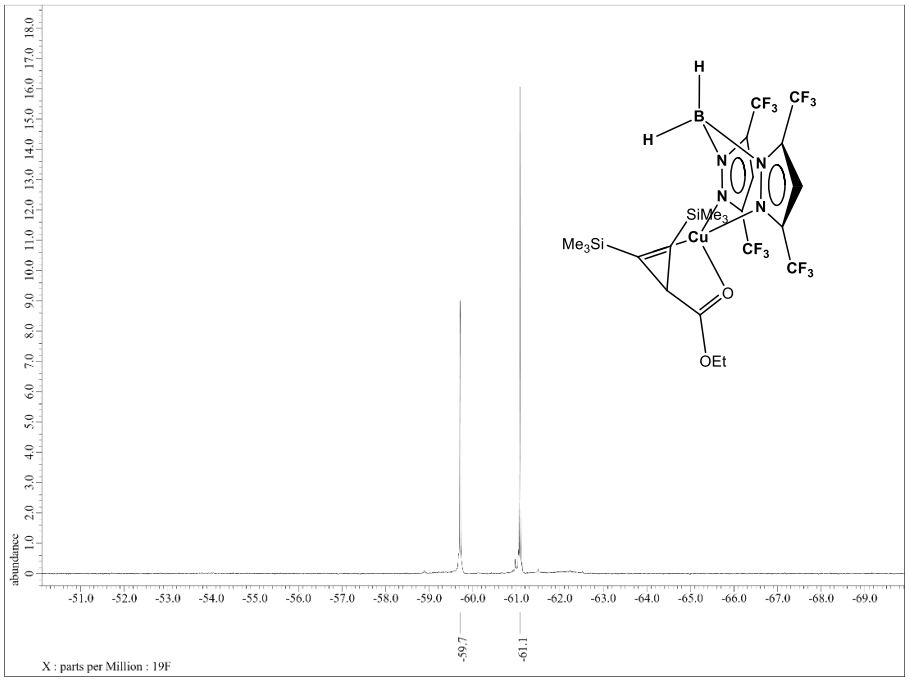

^{19}F NMR Spectrum of $[H_2B(3,5\text{-}(CF_3)_2Pz)_2]Cu$(Cyp-**4**) (**76**).

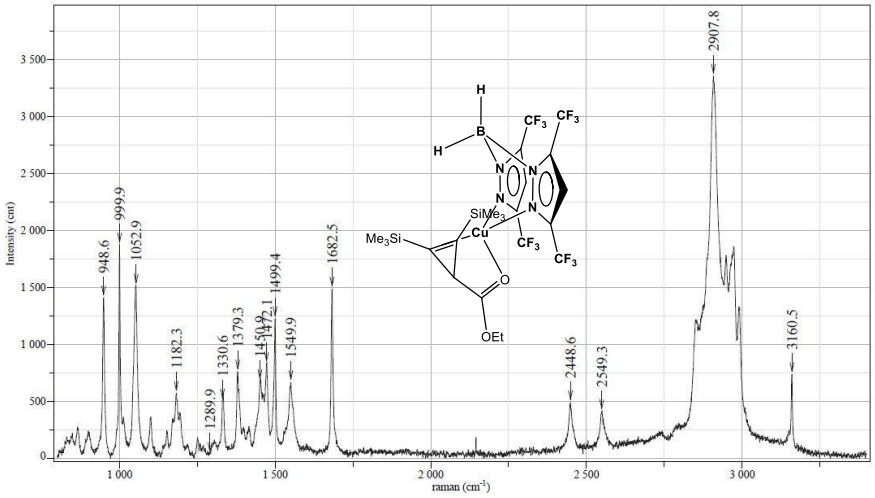

Exposition	5	Slit	100
Accumulation	1 x 21	Operator	Anurag
Laser	632.817	Sample	3,5-CF3BpCu-1,2-TMS-3-eth
Spectro	Auto	Remark	
Hole	200	Power	

Raman Spectrum of $[H_2B(3,5\text{-}(CF_3)_2Pz)_2]Cu$(Cyp-**4**) (**76**).

`

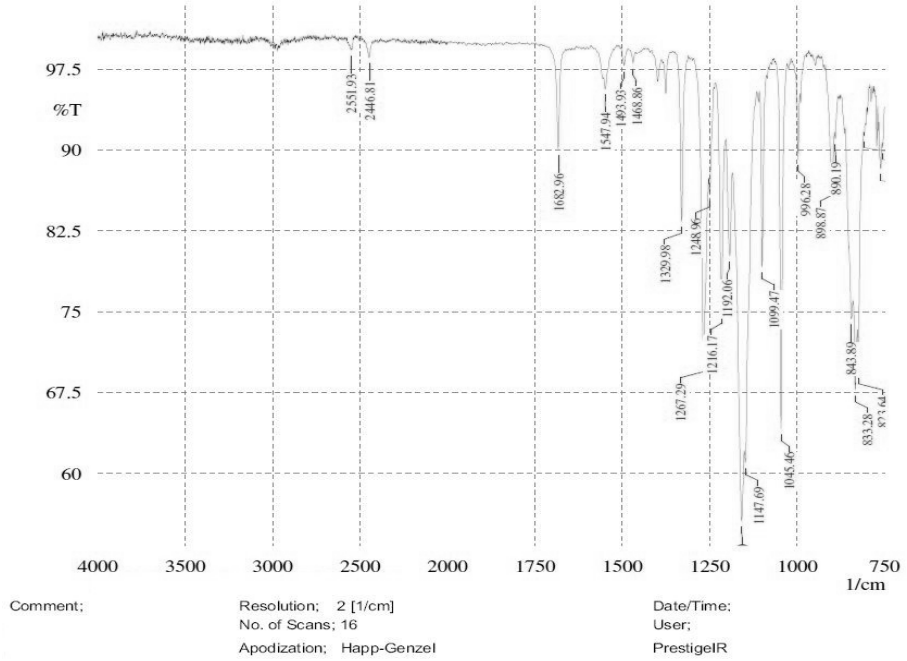

IR Spectrum of $[H_2B(3,5\text{-}(CF_3)_2Pz)_2]Cu(Cyp\text{-}\mathbf{4})$ (**76**).

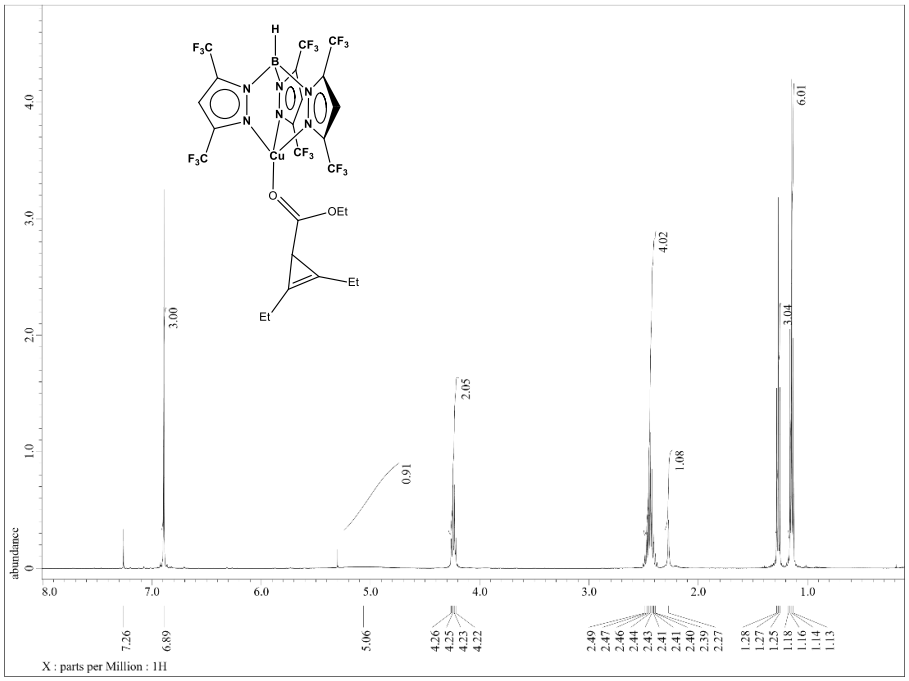

^{1}H NMR Spectrum of $[HB(3,5\text{-}(CF_3)_2Pz)_3]Cu(Cyp\text{-}\mathbf{2})$ (**77**).

`

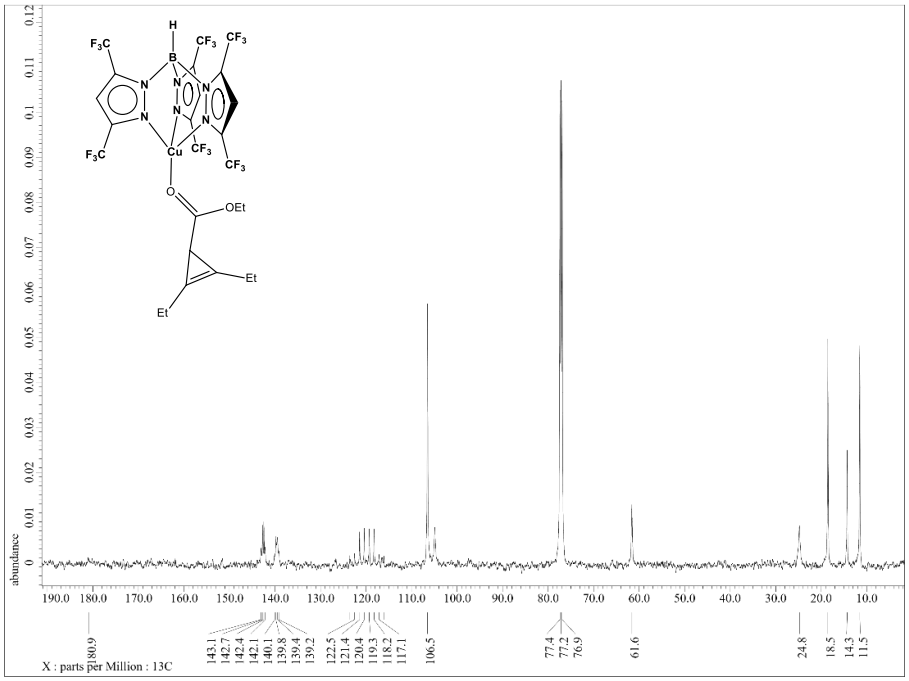

^{13}C NMR Spectrum of [HB(3,5-$(CF_3)_2$Pz)$_3$]Cu(Cyp-**2**) (**77**).

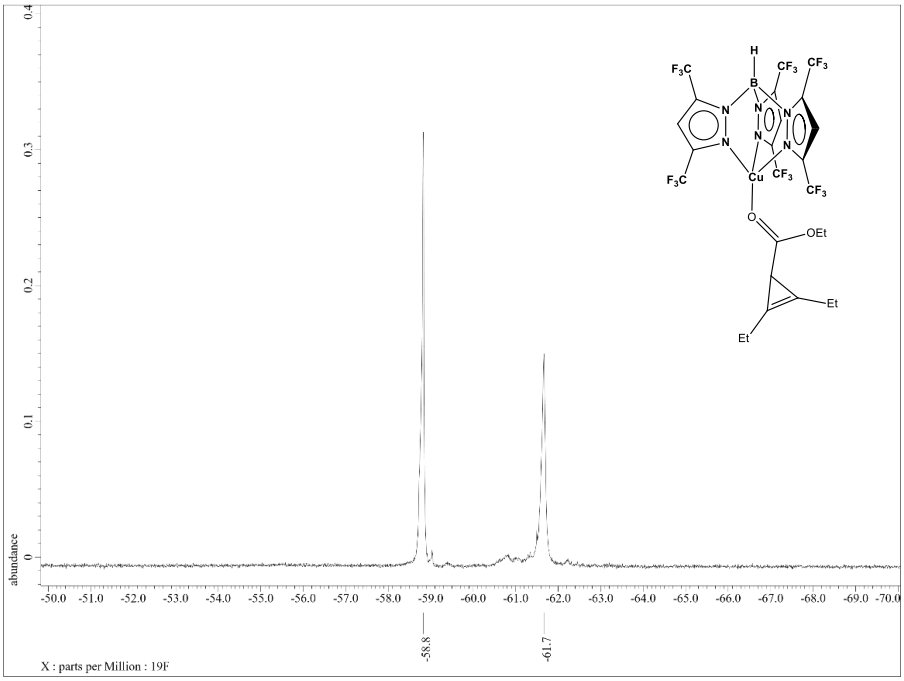

^{19}F NMR Spectrum of [HB(3,5-$(CF_3)_2$Pz)$_3$]Cu(Cyp-**2**) (**77**).

`

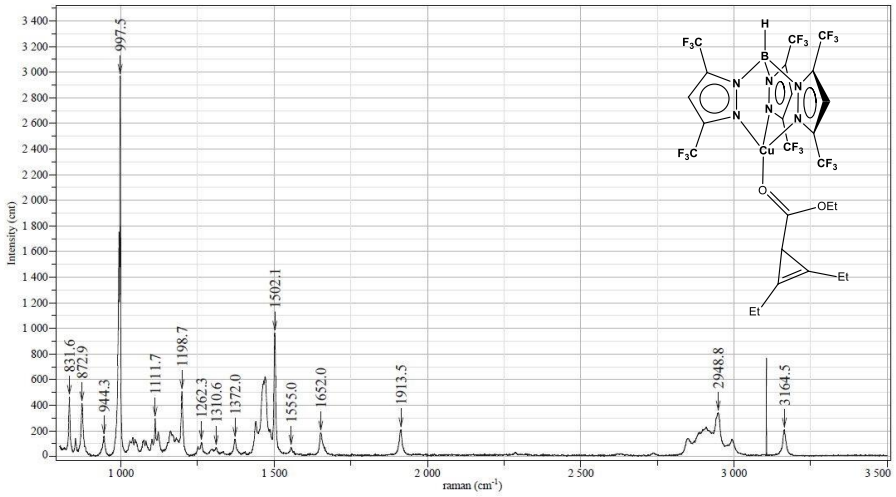

Exposition	5	Slit	100
Accumulation	1 x 40	Operator	Anurag
Laser	632.817	Sample	TpCuCyclopropene
Spectro	Auto	Remark	
Hole	200	Power	

Raman Spectrum of [HB(3,5-$(CF_3)_2Pz)_3$]Cu(Cyp-**2**) (**77**).

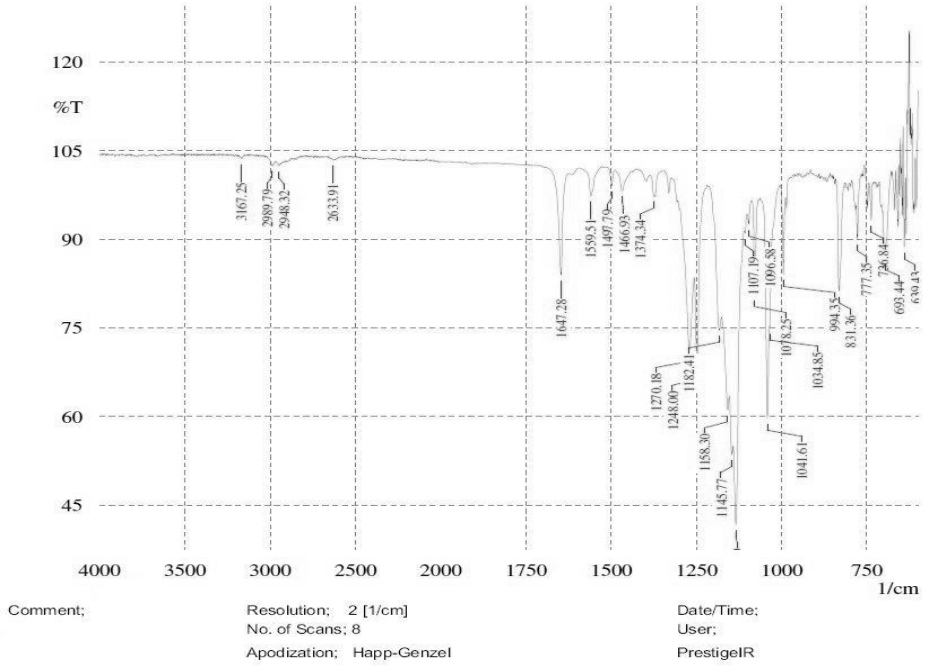

IR Spectrum of [HB(3,5-$(CF_3)_2Pz)_3$]Cu(Cyp-**2**) (**77**).

`

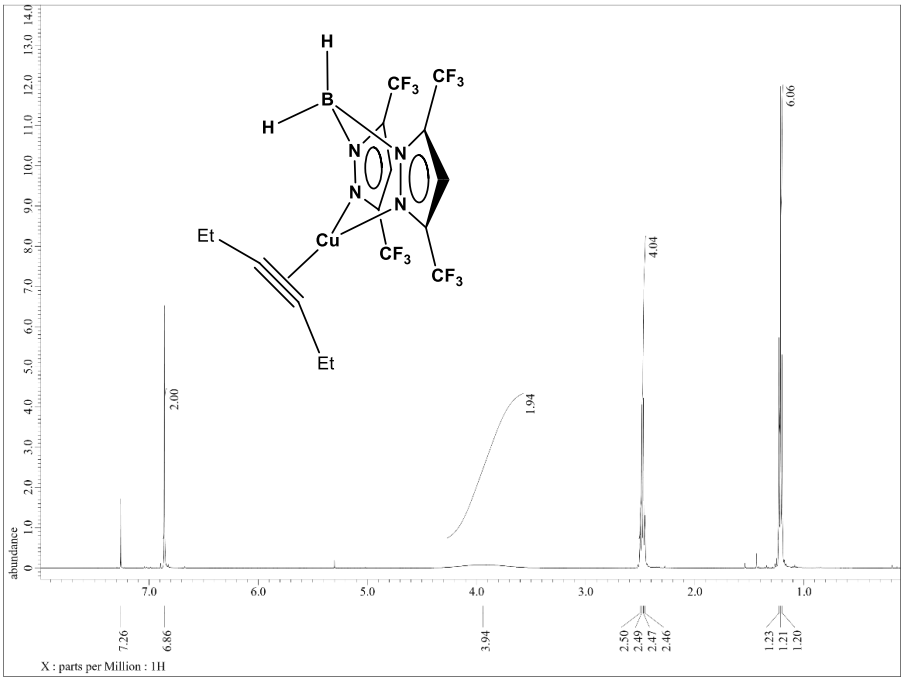

^{1}H NMR Spectrum of [$H_2B(3,5\text{-}(CF_3)_2Pz)_2$]Cu(EtC≡CEt) (**47**).

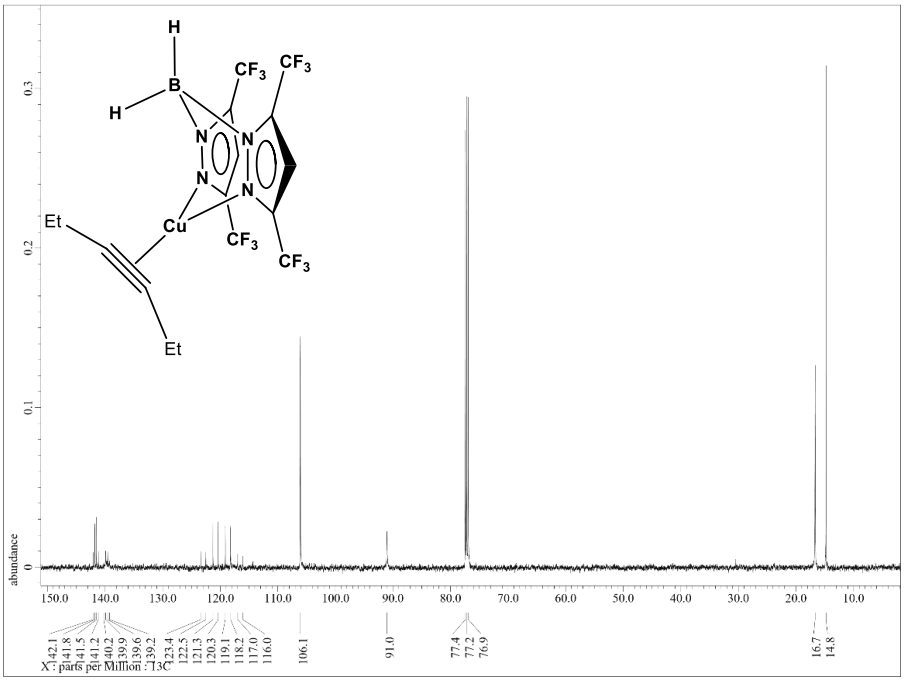

^{13}C NMR Spectrum of [$H_2B(3,5\text{-}(CF_3)_2Pz)_2$]Cu(EtC≡CEt) (**47**).

`

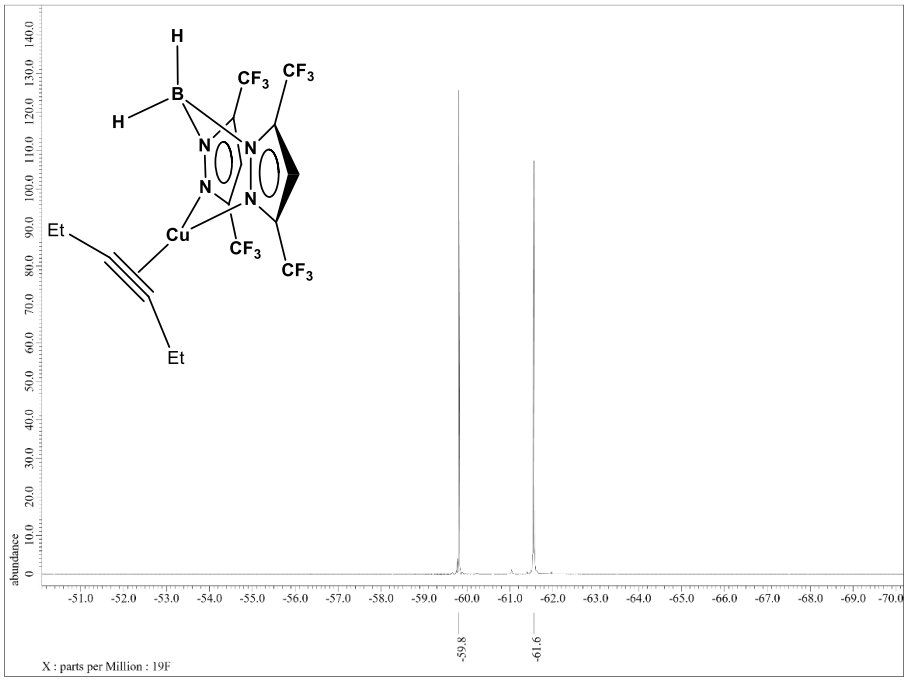

^{19}F NMR Spectrum of [$H_2B(3,5\text{-}(CF_3)_2Pz)_2$]Cu(EtC≡CEt) (**47**).

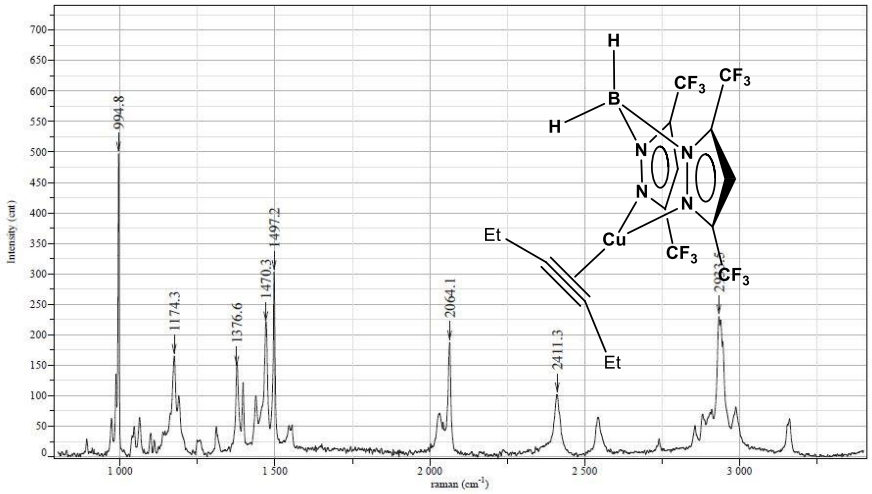

Exposition	5	Slit	100
Accumulation	1 x 21	Operator	Anurag
Laser	632.817	Sample	3,5-(CF3)2BpCu(3-hexyne)
Spectro	Auto	Remark	
Hole	200	Power	

Raman Spectrum of [$H_2B(3,5\text{-}(CF_3)_2Pz)_2$]Cu(EtC≡CEt) (**47**).

`

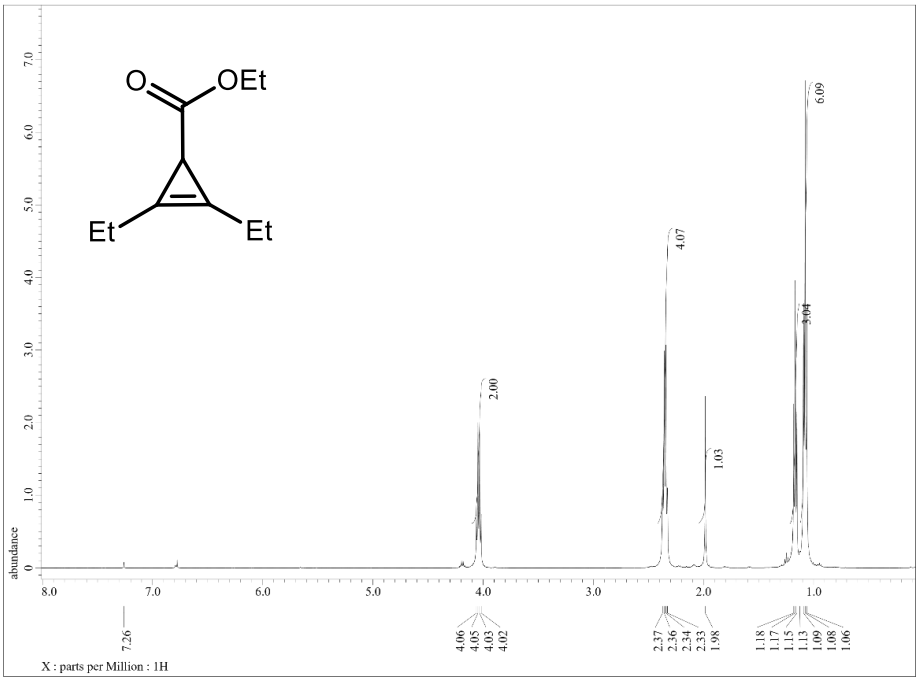

^{1}H NMR Spectrum of Cyp-**2** (**78**).

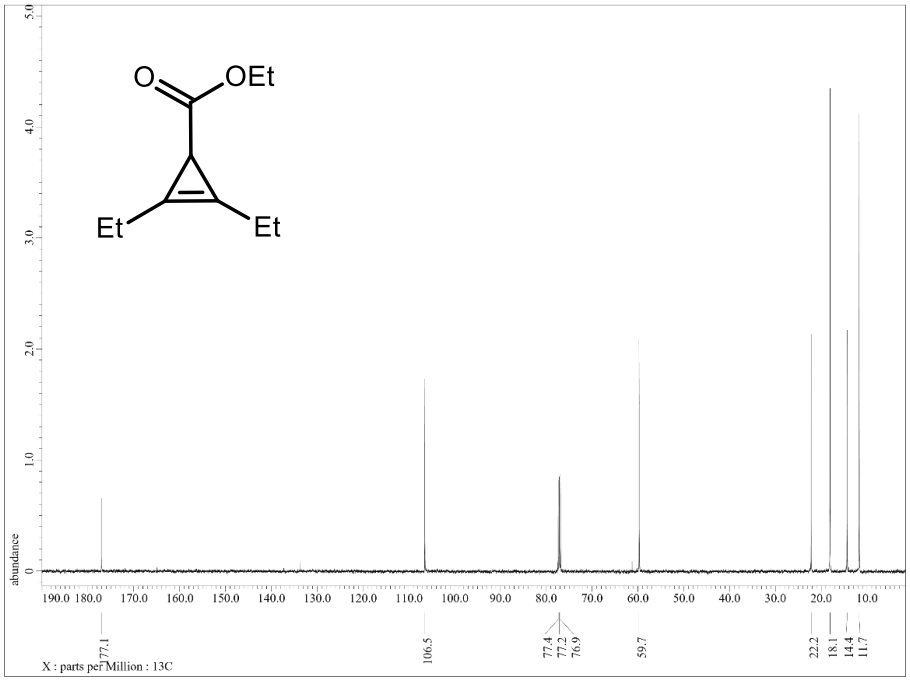

^{13}C NMR Spectrum of Cyp-**2** (**78**).

`

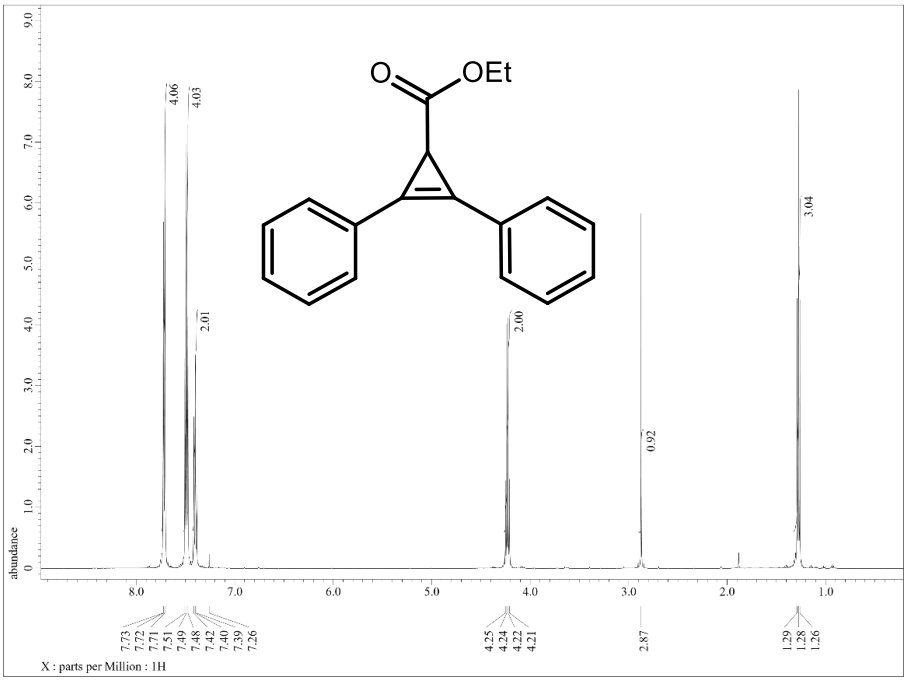

^{1}H NMR Spectrum of Cyp-**3** (**79**).

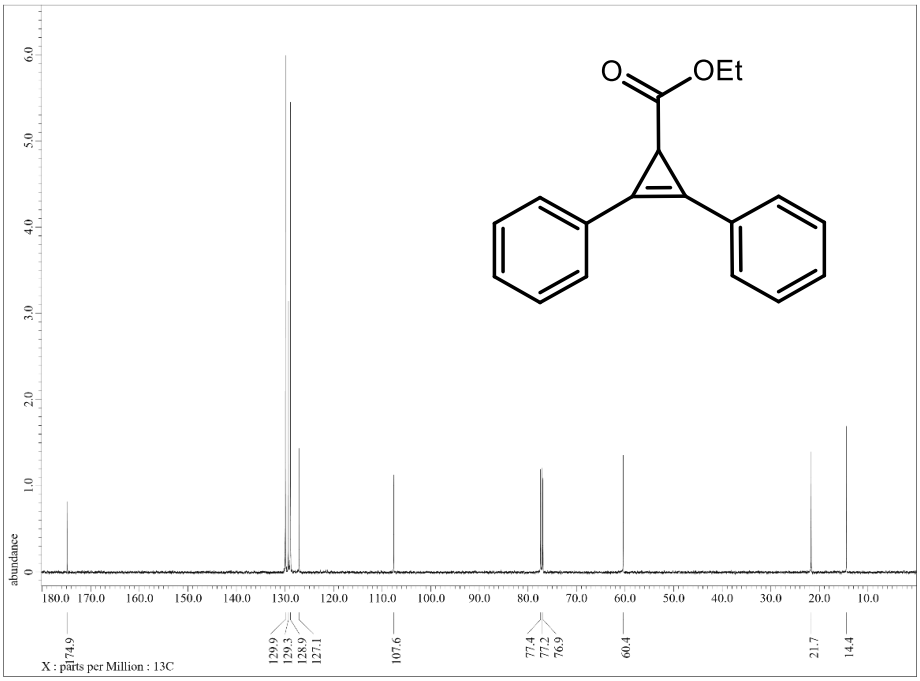

^{13}C NMR Spectrum of Cyp-**3** (**79**).

`

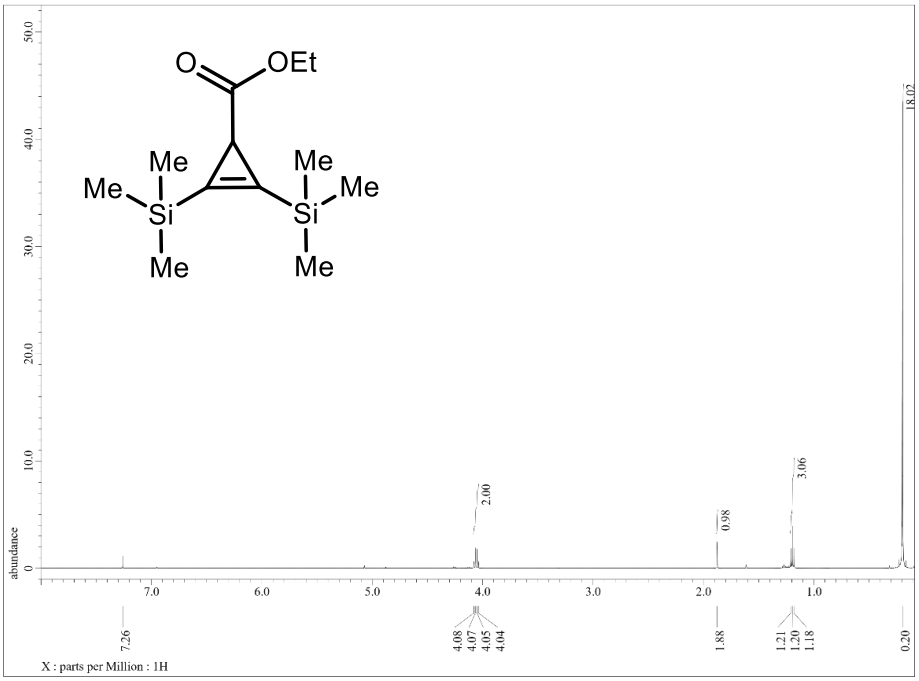

^{1}H NMR Spectrum of Cyp-**4** (**80**).

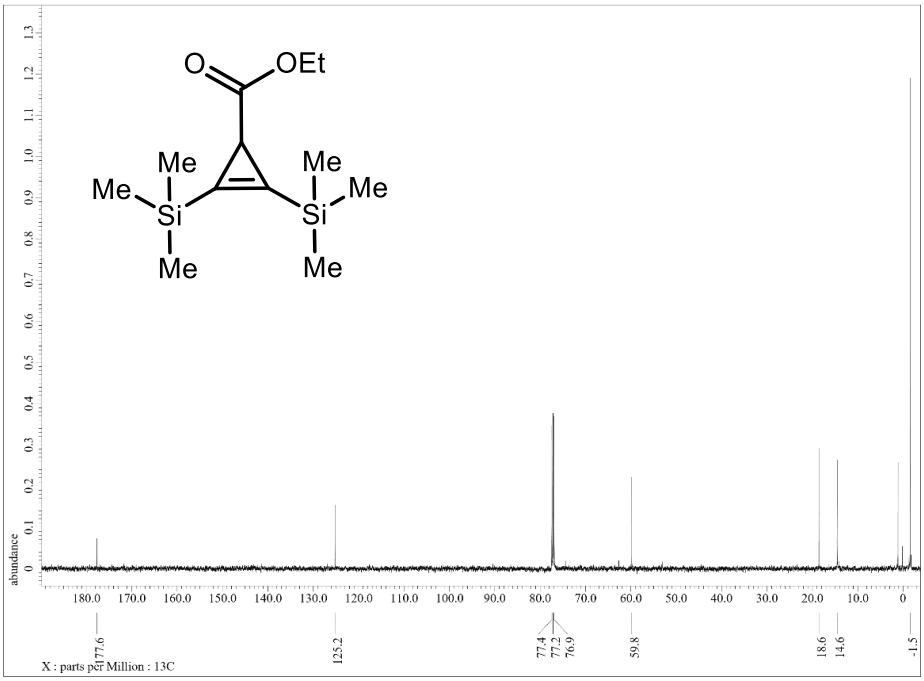

^{13}C NMR Spectrum of Cyp-**4** (**80**).

`

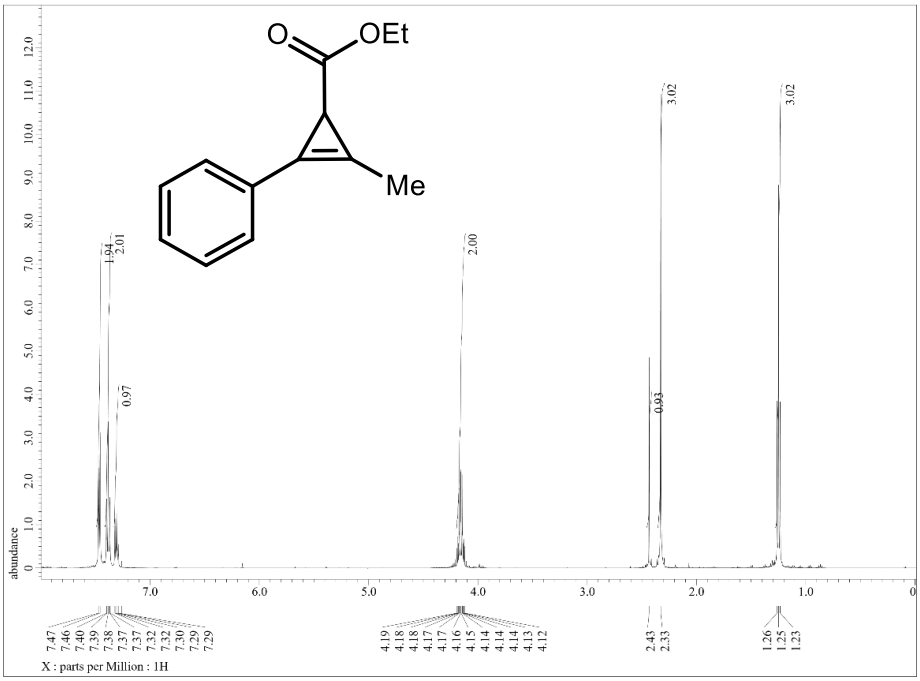

^{1}H NMR Spectrum of Cyp-**5** (**81**).

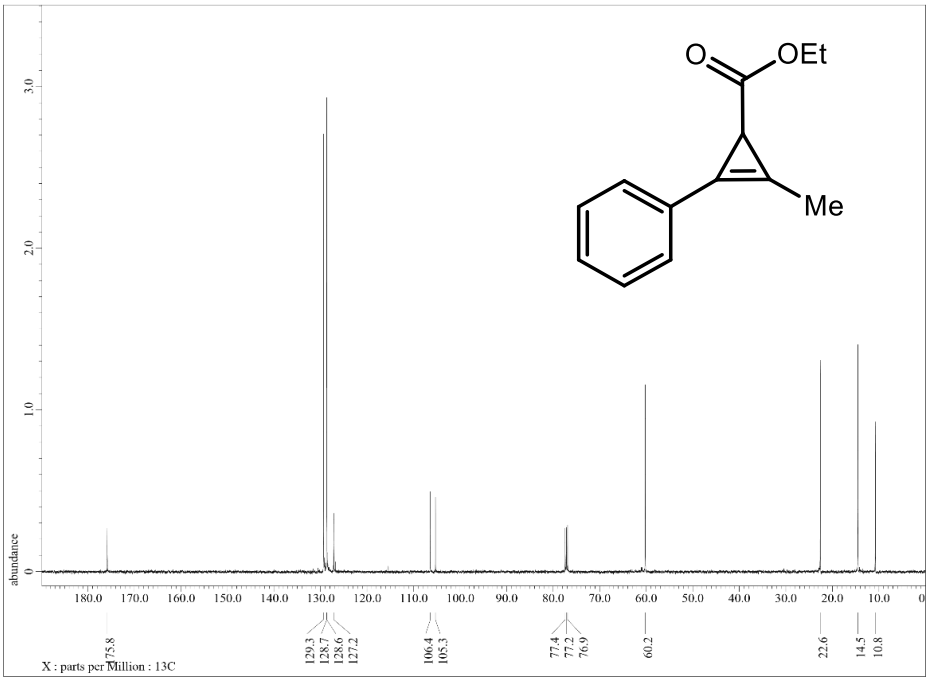

^{13}C NMR Spectrum of Cyp-**5** (**81**).

`

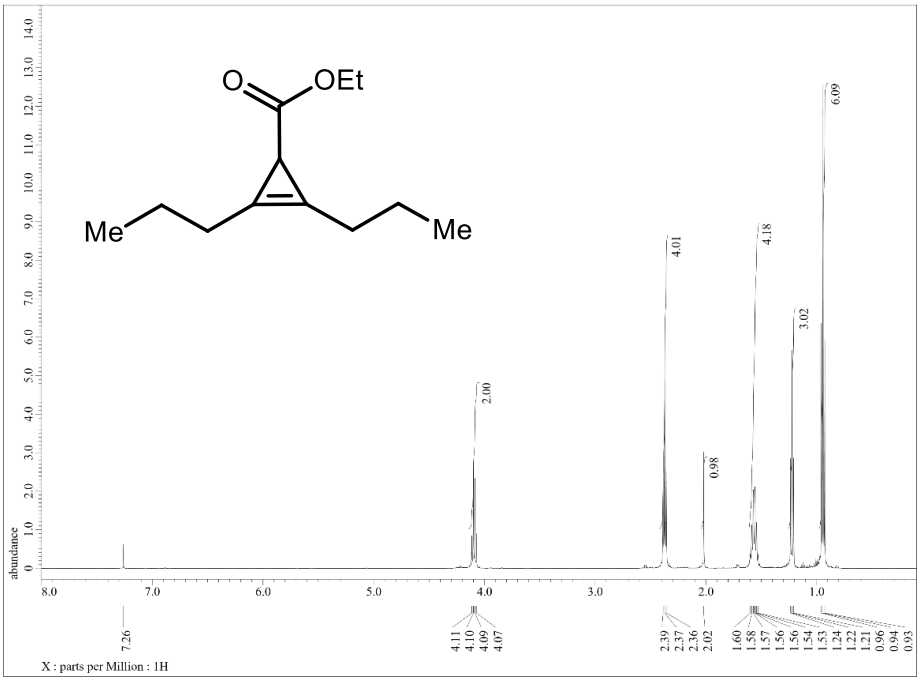

^{1}H NMR Spectrum of Cyp-**6** (**82**)

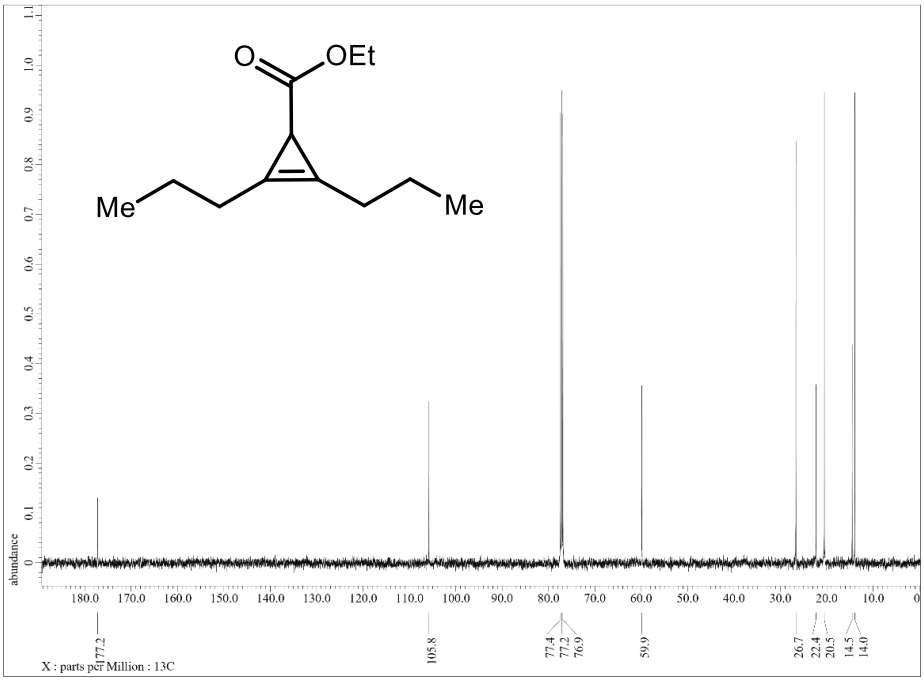

^{13}C NMR Spectrum of Cyp-**6** (**82**).

`

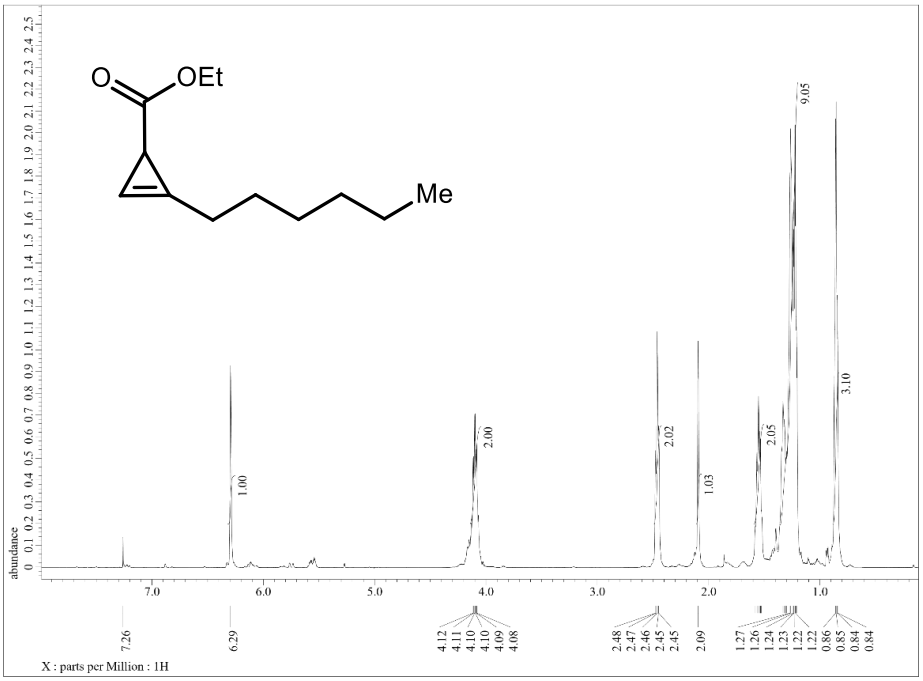

^{1}H NMR Spectrum of Cyp-**8** (**84**).

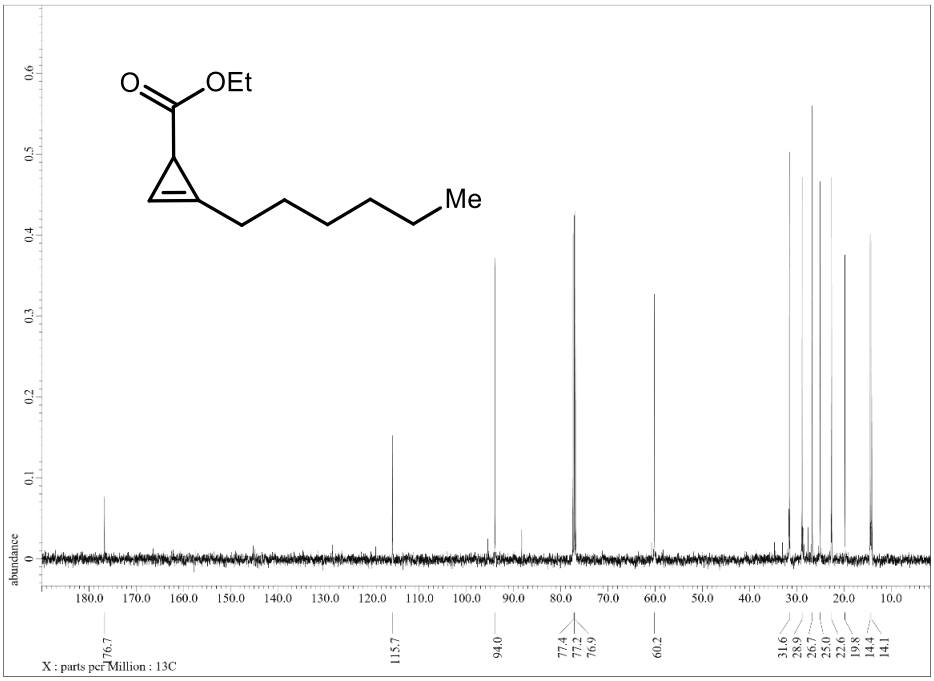

^{1}H NMR Spectrum of Cyp-**8** (**84**).

`

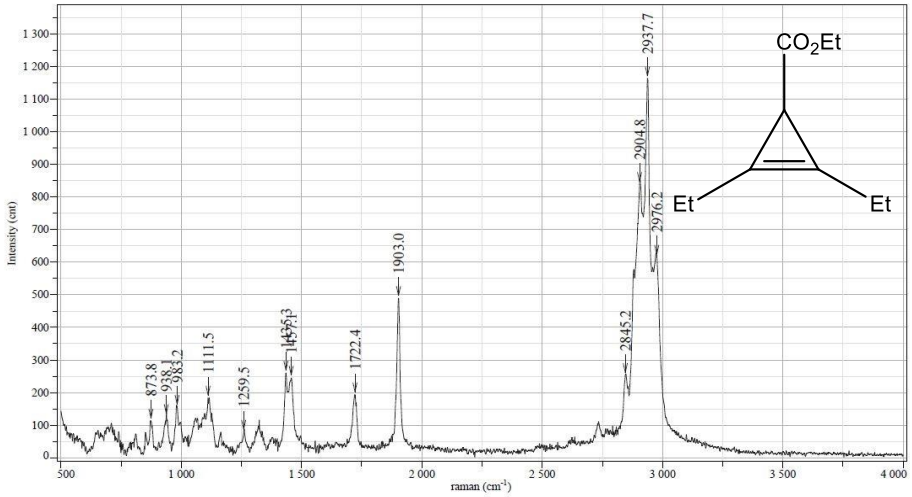

Exposition	5	Slit	100
Accumulation	1 x 28	Operator	Anurag
Laser	632.817	Sample	Et_Et_cyclopropene
Spectro	Auto	Remark	
Hole	200	Power	

Raman NMR Spectrum of Cyp-**2** (7**8**).

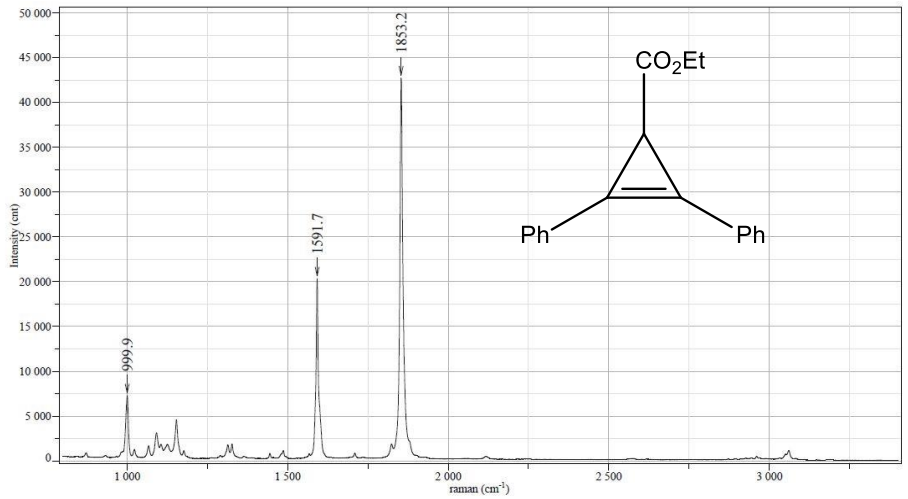

Exposition	5	Slit	100
Accumulation	1 x 21	Operator	Anurag
Laser	632.817	Sample	1,2-(diphenyl)-3-ethylcarboxy
Spectro	Auto	Remark	
Hole	200	Power	

Raman NMR Spectrum of Cyp-**3** (**79**).

`

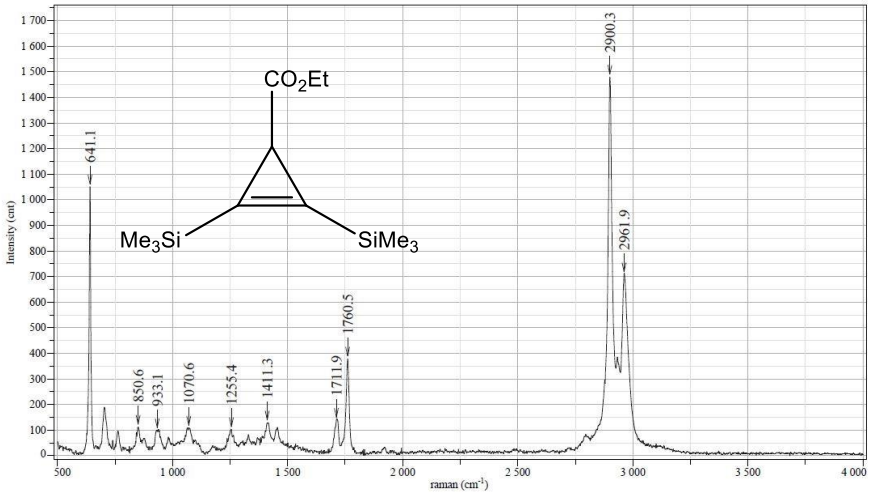

Exposition	5	Slit	100
Accumulation	1 x 28	Operator	Anurag
Laser	632.817	Sample	TMS_TMS_cyclopropene
Spectro	Auto	Remark	
Hole	200	Power	

Raman NMR Spectrum of Cyp-**4** (**80**).

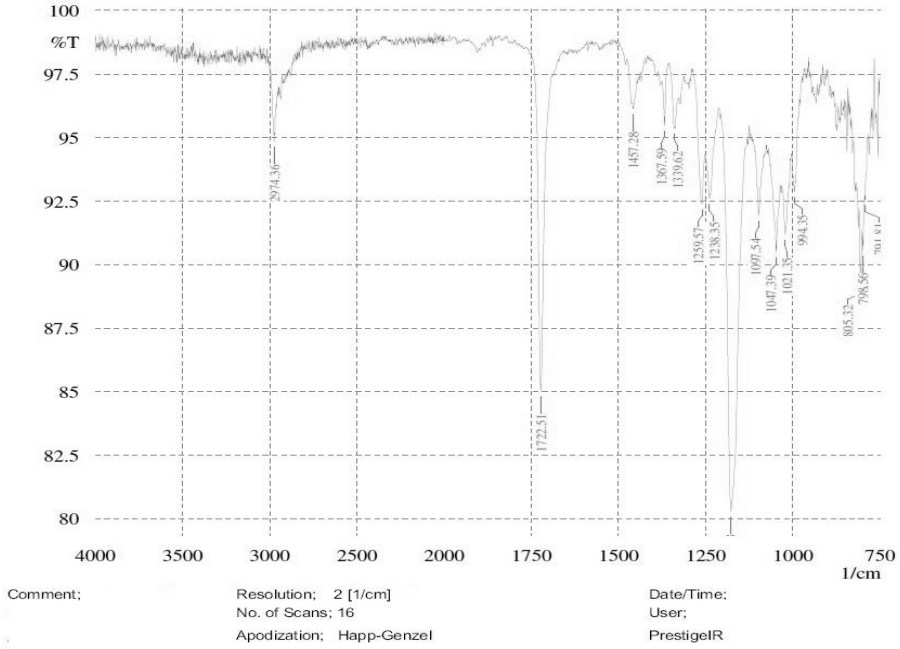

IR Spectrum of Cyp-**2** (7**8**).

`

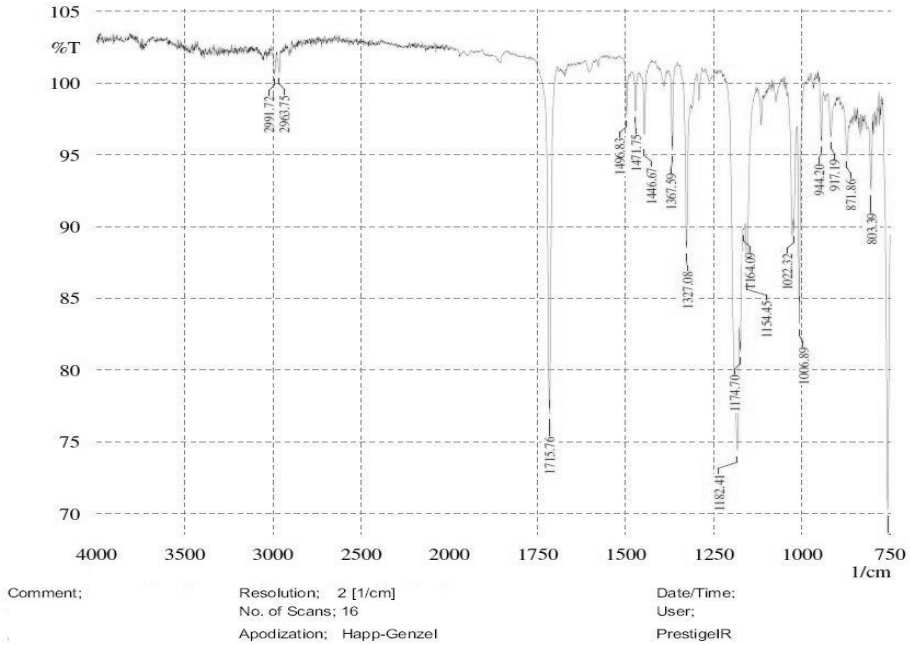

IR Spectrum of Cyp-**3** (**79**).

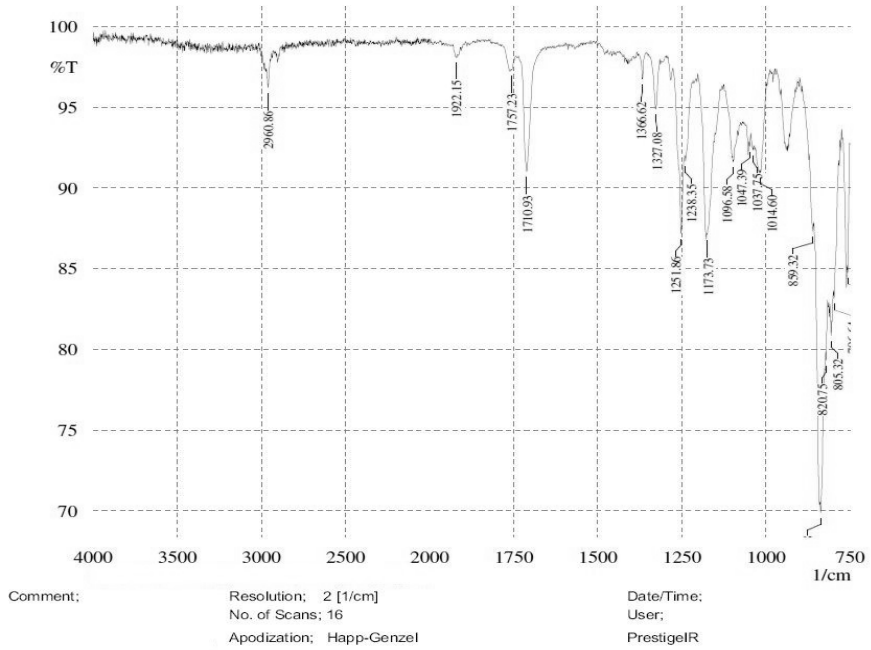

IR Spectrum of Cyp-**4** (**80**).

`

References

1. S. Trofimenko, *Journal of the American Chemical Society*, 2002, **88**, 1842-1844.
2. S. Trofimenko, *Chemical Reviews*, 2002, **93**, 943-980.
3. J. C. Calabrese, S. Trofimenko and J. S. Thompson, *Journal of the Chemical Society, Chemical Communications*, 1986, DOI: 10.1039/c39860001122, 1122.
4. D. L. Reger, J. R. Gardinier, S. BakbakCurrent address: School of Ch, R. F. Semeniuc, U. H. F. Bunz and M. D. Smith, *New Journal of Chemistry*, 2005, **29**, 1035.
5. C. Pettinari, *Angewandte Chemie International Edition*, 2007, **46**, 5652-5652.
6. S. Trofimenko, *Scorpionates : the coordination chemistry of polypyrazolylborate ligands*, Imperial College Press, London, 1999.
7. C. Pettinari, *Scorpionates II : chelating borate ligands*, Imperial College Press ; Distributed by World Scientific Pub., London; Singapore; Hackensack, NJ, 2008.
8. J. S. Thompson, R. L. Harlow and J. F. Whitney, *Journal of the American Chemical Society*, 2002, **105**, 3522-3527.
9. H. V. R. Dias, H.-L. Lu, H.-J. Kim, S. A. Polach, T. K. H. H. Goh, R. G. Browning and C. J. Lovely, *Organometallics*, 2002, **21**, 1466-1473.
10. A. Caballero, M. M. Díaz-Requejo, T. R. Belderraín, M. C. Nicasio, S. Trofimenko and P. J. Pérez, *Journal of the American Chemical Society*, 2003, **125**, 1446-1447.
11. M. M. Díaz-Requejo, T. R. Belderraín, S. Trofimenko and P. J. Pérez, *Journal of the American Chemical Society*, 2001, **123**, 3167-3168.
12. H. V. R. Dias, H.-L. Lu, R. E. Ratcliff and S. G. Bott, *Inorganic Chemistry*, 2002, **34**, 1975-1976.
13. H. V. R. Dias and J. D. Gorden, *Inorganic Chemistry*, 1996, **35**, 318-324.
14. H. V. R. Dias, G. Gioia Lobbia, G. Papini, M. Pellei and C. Santini, *European Journal of Inorganic Chemistry*, 2009, **2009**, 3935-3941.

`

15. R. G. Bergman, T. R. Cundari, A. M. Gillespie, T. B. Gunnoe, W. D. Harman, T. R. Klinckman, M. D. Temple and D. P. White, *Organometallics*, 2003, **22**, 2331-2337.
16. B. E. Smart, *Journal of Fluorine Chemistry*, 2001, **109**, 3-11.
17. H. V. R. Dias and H.-L. Lu, *Inorganic Chemistry*, 2002, **34**, 5380-5382.
18. C. Mealli, C. S. Arcus, J. L. Wilkinson, T. J. Marks and J. A. Ibers, *Journal of the American Chemical Society*, 2002, **98**, 711-718.
19. H. V. R. Dias, H.-J. Kim, H.-L. Lu, K. Rajeshwar, N. R. de Tacconi, A. Derecskei-Kovacs and D. S. Marynick, *Organometallics*, 1996, **15**, 2994-3003.
20. H. V. R. Dias and M. Fianchini, *Comments on Inorganic Chemistry*, 2007, **28**, 73-92.
21. H. V. R. Dias and J. Wu, *Angewandte Chemie International Edition*, 2007, **46**, 7814-7816.
22. H. V. R. Dias, R. G. Browning, S. A. Polach, H. V. K. Diyabalanage and C. J. Lovely, *Journal of the American Chemical Society*, 2003, **125**, 9270-9271.
23. S. T. Handy and M. Czopp, *Organic Letters*, 2001, **3**, 1423-1425.
24. H. V. R. Dias and C. J. Lovely, *Chemical Reviews (Washington, DC, United States)*, 2008, **108**, 3223-3238.
25. H. V. R. Dias and J. Wu, *European Journal of Inorganic Chemistry*, 2008, **2008**, 509-522.
26. H. V. R. Dias, Z. Wang and W. Jin, *Inorganic Chemistry*, 1997, **36**, 6205-6215.
27. W. C. Zeise, *Annalen der Physik und Chemie*, 1831, **97**, 497-541.
28. J. Dewar, *Bulletin de la Societe Chimique de France*, 1951, **18**, C71-C79.
29. J. Chatt and L. A. Duncanson, *Journal of the Chemical Society*, 1953, DOI: 10.1039/jr9530002939, 2939-2947.
30. G. E. Schaller and A. B. Bleecker, *Science (Washington, D. C.)*, 1995, **270**, 1809-1811.
31. H. Lebel, J.-F. Marcoux, C. Molinaro and A. B. Charette, *Chemical Reviews*, 2003, **103**, 977-1050.

`

32. H. Pellissier, *Tetrahedron*, 2008, **64**, 7041-7095.
33. W. Wu, Z. Lin and H. Jiang, *Organic & Biomolecular Chemistry*, 2018, **16**, 7315-7329.
34. H. Pellissier, *Advanced Synthesis & Catalysis*, 2014, **356**, 1899-1935.
35. R. A. Van Santen and H. P. C. E. Kuipers, 1987, **35**, 265-321.
36. R. M. Lambert, R. L. Cropley, A. Husain and M. S. Tikhov, *Chemical Communications*, 2003, DOI: 10.1039/b302620e, 1184-1185.
37. S. Linic, H. Piao, K. Adib and M. A. Barteau, *Angewandte Chemie*, 2004, **116**, 2978-2981.
38. M. M. Diaz-Requejo, M. A. Mairena, T. R. Belderrain, M. C. Nicasio, S. Trofimenko and P. J. Perez, *Chemical Communications (Cambridge, United Kingdom)*, 2001, DOI: 10.1039/b105020f, 1804-1805.
39. J. F. Briones and H. M. L. Davies, *Organic Letters*, 2011, **13**, 3984-3987.
40. E. Haldón, M. C. Nicasio and P. J. Pérez, *Organic & Biomolecular Chemistry*, 2015, **13**, 9528-9550.
41. A. M. Thomas, A. Sujatha and G. Anilkumar, *RSC Adv.*, 2014, **4**, 21688-21698.
42. G. Fang and X. Bi, *Chemical Society Reviews*, 2015, **44**, 8124-8173.
43. I.-T. Trotuş, T. Zimmermann and F. Schüth, *Chemical Reviews*, 2013, **114**, 1761-1782.
44. A. Noonikara-Poyil, H. Cui, A. A. Yakovenko, P. W. Stephens, R.-B. Lin, B. Wang, B. Chen and H. V. R. Dias, *Angewandte Chemie, International Edition*, 2021, DOI: 10.1002/anie.202109338, Ahead of Print.
45. D. S. Sholl and R. P. Lively, *Nature*, 2016, **532**, 435-437.
46. S. Chu, N. Liu, S. Chu, Y. Cui, N. Liu and Y. Cui, *Nature materials*, 2016, **16**, 16-22.
47. H. Li, L. Li, R.-B. Lin, W. Zhou, Z. Zhang, S. Xiang and B. Chen, *EnergyChem*, 2019, **1**, 100006.
48. R.-B. Lin, S. Xiang, W. Zhou and B. Chen, *Chem*, 2020, **6**, 337-363.
49. E. D. Bloch, W. L. Queen, R. Krishna, J. M. Zadrozny, C. M. Brown and J. R. Long, *Science (Washington, D. C.)*, 2012, **335**, 1606-1610.

`

50. Y. He, R. Krishna and B. Chen, *Energy & Environmental Science*, 2012, **5**, 9107-9120.
51. S. Yang, A. J. Ramirez-Cuesta, R. Newby, V. Garcia-Sakai, P. Manuel, S. K. Callear, S. I. Campbell, C. C. Tang and M. Schroder, *Nature Chemistry*, 2015, **7**, 121-129.
52. B. Li, Y. Zhang, R. Krishna, K. Yao, Y. Han, Z. Wu, D. Ma, Z. Shi, T. Pham, B. Space, J. Liu, P. K. Thallapally, J. Liu, M. Chrzanowski and S. Ma, *Journal of the American Chemical Society*, 2014, **136**, 8654-8660.
53. S. Aguado, G. Bergeret, C. Daniel and D. Farrusseng, *Journal of the American Chemical Society*, 2012, **134**, 14635-14637.
54. P. J. Bereciartua, Á. Cantín, A. Corma, J. L. Jordá, M. Palomino, F. Rey, S. Valencia, E. W. Corcoran, P. Kortunov, P. I. Ravikovitch, A. Burton, C. Yoon, Y. Wang, C. Paur, J. Guzman, A. R. Bishop and G. L. Casty, *Science (Washington, D. C.)*, 2017, **358**, 1068-1071.
55. L. Li, R.-B. Lin, R. Krishna, H. Li, S. Xiang, H. Wu, J. Li, W. Zhou and B. Chen, *Science (Washington, D. C.)*, 2018, **362**, 443-446.
56. R.-B. Lin, L. Li, H.-L. Zhou, H. Wu, C. He, S. Li, R. Krishna, J. Li, W. Zhou and B. Chen, *Nat. Mater.*, 2018, **17**, 1128-1133.
57. B. M. Binder, *Journal of Biological Chemistry*, 2020, **295**, 7710-7725.
58. F. I. Rodriguez, J. J. Esch, A. E. Hall, B. M. Binder, G. E. Schaller and A. B. Bleeckert, *Science (Washington, D. C.)*, 1999, **283**, 996-998.
59. S. Schott-Verdugo, L. Müller, E. Classen, H. Gohlke and G. Groth, *Sci. Rep.*, 2019, **9**, 8869.
60. S. Trofimenko, *Chemical Reviews (Washington, DC, United States)*, 1993, **93**, 943-980.
61. M. Munakata, S. Kitagawa, S. Kosome and A. Asahara, *Inorg. Chem.*, 1986, **25**, 2622-2627.
62. B. F. Straub, F. Eisentrager and P. Hofmann, *Chemical Communications (Cambridge, United Kingdom)*, 1999, DOI: 10.1039/a907928i, 2507-2508.

`

63. D. Parasar, A. H. Elashkar, A. A. Yakovenko, N. B. Jayaratna, B. L. Edwards, S. G. Telfer, H. V. R. Dias and M. G. Cowan, *Angewandte Chemie, International Edition*, 2020, **59**, 21001-21006.

64. N. B. Jayaratna, M. G. Cowan, D. Parasar, H. H. Funke, J. Reibenspies, P. K. Mykhailiuk, O. Artamonov, R. D. Noble and H. V. R. Dias, *Angewandte Chemie, International Edition*, 2018, **57**, 16442-16446.

65. M. G. Cowan, W. M. McDanel, H. H. Funke, Y. Kohno, D. L. Gin and R. D. Noble, *Angewandte Chemie, International Edition*, 2015, **54**, 5740-5743.

66. H. V. R. Dias, S. A. Richey, H. V. K. Diyabalanage and J. Thankamani, *Journal of Organometallic Chemistry*, 2005, **690**, 1913-1922.

67. E. Maslowsky, Jr., *Vibrational Spectra of Organometallics: Theoretical and Experimental Data*, Wiley, Hoboken, NJ 07030, USA, 2019.

68. G. Mezei, C. M. Zaleski and V. L. Pecoraro, *Chemical Reviews (Washington, DC, United States)*, 2007, **107**, 4933-5003.

69. C. R. Groom, I. J. Bruno, M. P. Lightfoot and S. C. Ward, *Acta Crystallographica, Section B: Structural Science, Crystal Engineering and Materials*, 2016, **72**, 171-179.

70. S. J. Geier, J. A. Mason, E. D. Bloch, W. L. Queen, M. R. Hudson, C. M. Brown and J. R. Long, *Chemical Science*, 2013, **4**, 2054-2061.

71. A. Whyte, A. Torelli, B. Mirabi, A. Zhang and M. Lautens, *ACS Catalysis*, 2020, **10**, 11578-11622.

72. Z. Bao, J. Wang, Z. Zhang, H. Xing, Q. Yang, Y. Yang, H. Wu, R. Krishna, W. Zhou, B. Chen and Q. Ren, *Angewandte Chemie, International Edition*, 2018, **57**, 16020-16025.

73. P. Li, Y. He, H. D. Arman, R. Krishna, H. Wang, L. Weng and B. Chen, *Chemical Communications (Cambridge, United Kingdom)*, 2014, **50**, 13081-13084.

74. R. Faiz and K. Li, *Chem. Eng. Sci.*, 2012, **73**, 261-284.

75. A. Noonikara-Poyil, A. Muñoz-Castro, A. Boretskyi, P. K. Mykhailiuk and H. V. R. Dias, *Chemical Science*, 2021, **12**, 14618-14623.

76. O. A. Tomashenko and V. V. Grushin, *Chemical Reviews (Washington, DC, United States)*, 2011, **111**, 4475-4521.

`

77. T. Furuya, A. S. Kamlet and T. Ritter, *Nature*, 2011, **473**, 470-477.
78. C. Alonso, E. Martinez de Marigorta, G. Rubiales and F. Palacios, *Chemical Reviews (Washington, DC, United States)*, 2015, **115**, 1847-1935.
79. X. Liu, C. Xu, M. Wang and Q. Liu, *Chemical Reviews (Washington, DC, United States)*, 2015, **115**, 683-730.
80. J. Wang, M. Sanchez-Rosello, J. L. Acena, C. del Pozo, A. E. Sorochinsky, S. Fustero, V. A. Soloshonok and H. Liu, *Chemical Reviews (Washington, DC, United States)*, 2014, **114**, 2432-2506.
81. P. K. Mykhailiuk, *Chemical Reviews (Washington, DC, United States)*, 2021, **121**, 1670-1715.
82. P. R. Savoie and J. T. Welch, *Chemical Reviews (Washington, DC, United States)*, 2015, **115**, 1130-1190.
83. J. M. W. Chan, *Journal of Materials Chemistry C: Materials for Optical and Electronic Devices*, 2019, **7**, 12822-12834.
84. N. M. Shavaleev, G. Xie, S. Varghese, D. B. Cordes, A. M. Z. Slawin, C. Momblona, E. Ortí, H. J. Bolink, I. D. W. Samuel and E. Zysman-Colman, *Inorg. Chem.*, 2015, **54**, 5907-5914.
85. S. Garg and J. n. M. Shreeve, *Journal of Materials Chemistry*, 2011, **21**, 4787-4795.
86. S. Altomonte and M. Zanda, *J. Fluorine Chem.*, 2012, **143**, 57-93.
87. M. Herder, B. M. Schmidt, L. Grubert, M. Paetzel, J. Schwarz and S. Hecht, *Journal of the American Chemical Society*, 2015, **137**, 2738-2747.
88. M. F. Sowaileh, R. A. Hazlitt and D. A. Colby, *ChemMedChem*, 2017, **12**, 1481-1490.
89. H. Qianzhu, A. P. Welegedara, H. Williamson, A. E. McGrath, M. C. Mahawaththa, N. E. Dixon, G. Otting and T. Huber, *Journal of the American Chemical Society*, 2020, **142**, 17277-17281.
90. P. Liebing, C. R. Pitts, M. Reimann, N. Trapp, D. Rombach, D. Bornemann, M. Kaupp and A. Togni, *Chemistry - A European Journal*, 2021, **27**, 6086-6093.

`

91. T. Umemoto, L. M. Garrick and N. Saito, *Beilstein Journal of Organic Chemistry*, 2012, **8**, 461-471, No 453.

92. B. Cui, M. Kosobokov, K. Matsuzaki, E. Tokunaga and N. Shibata, *Chemical Communications (Cambridge, United Kingdom)*, 2017, **53**, 5997-6000.

93. O. S. Kanishchev and W. R. Dolbier, Jr., *Angewandte Chemie, International Edition*, 2015, **54**, 280-284.

94. C. R. Pitts, D. Bornemann, P. Liebing, N. Santschi and A. Togni, *Angewandte Chemie, International Edition*, 2019, **58**, 1950-1954.

95. J.-Y. Shou, X.-H. Xu and F.-L. Qing, *Angewandte Chemie, International Edition*, 2021, **60**, 15271-15275.

96. P. Kenyon and S. Mecking, *Journal of the American Chemical Society*, 2017, **139**, 13786-13790.

97. M. Talavera, S. Hinze, T. Braun, R. Laubenstein and R. Herrmann, *Molecules*, 2020, **25**, 3977.

98. R. D. W. Kemmitt, R. D. Peacock and J. Stocks, *Journal of the Chemical Society [Section] D: Chemical Communications*, 1969, DOI: 10.1039/c2969000554a, 554.

99. W. A. Sheppard, *Journal of the American Chemical Society*, 1960, **82**, 4751-4752.

100. D. Langford, I. Goettker-Schnetmann, F. P. Wimmer, L. A. Casper, P. Kenyon, R. F. Winter and S. Mecking, *Organometallics*, 2019, **38**, 2710-2713.

101. X.-F. Ma, X.-F. Luo, Z.-P. Yan, Z.-G. Wu, Y. Zhao, Y.-X. Zheng and J.-L. Zuo, *Organometallics*, 2019, **38**, 3553-3559.

102. P. Gautam, Y. Wang, G. Zhang, H. Sun and J. M. W. Chan, *Chemistry of Materials*, 2018, **30**, 7055-7066.

103. H. R. A. Golf, H.-U. Reissig and A. Wiehe, *J. Org. Chem.*, 2015, **80**, 5133-5143.

104. L. M. Groves, C. Schotten, J. Beames, J. A. Platts, S. J. Coles, P. N. Horton, D. L. Browne and S. J. A. Pope, *Chemistry - A European Journal*, 2017, **23**, 9407-9418.

`

105. A. K. Pal, A. F. Henwood, D. B. Cordes, A. M. Z. Slawin, I. D. W. Samuel and E. Zysman-Colman, *Inorg. Chem.*, 2017, **56**, 7533-7544.
106. C. Pettinari and C. Santini, *Comprehensive Coordination Chemistry II*, 2004, **1**, 159-210.
107. K.-C. Chan, S.-C. Cheng, L. T.-L. Lo, S.-M. Yiu and C.-C. Ko, *European Journal of Inorganic Chemistry*, 2018, **2018**, 897-903.
108. H. V. R. Dias, H. V. K. Diyabalanage, M. G. Eldabaja, O. Elbjeirami, M. A. Rawashdeh-Omary and M. A. Omary, *Journal of the American Chemical Society*, 2005, **127**, 7489-7501.
109. A. Noonikara-Poyil, S. G. Ridlen and H. V. R. Dias, *Inorganic Chemistry*, 2020, **59**, 17860-17865.
110. B. Esser, J. M. Schnorr and T. M. Swager, *Angewandte Chemie, International Edition*, 2012, **51**, 5752-5756.
111. F. W. Hoover and D. D. Coffman, *J. Org. Chem.*, 1964, **29**, 3567-3570.
112. T. F. van Dijkman, M. A. Siegler and E. Bouwman, *Dalton Transactions*, 2015, **44**, 21109-21123.
113. P. O. Oguadinma and F. Schaper, *Organometallics*, 2009, **28**, 6721-6731.
114. C. Hansch, A. Leo and R. W. Taft, *Chemical Reviews (Washington, DC, United States)*, 1991, **91**, 165-195.
115. L. Falivene, Z. Cao, A. Petta, L. Serra, A. Poater, R. Oliva, V. Scarano and L. Cavallo, *Nature Chemistry*, 2019, **11**, 872-879.
116. T. Ziegler and A. Rauk, *Inorg. Chem.*, 1979, **18**, 1558-1565.
117. M. P. Mitoraj, A. Michalak and T. Ziegler, *J. Chem. Theory Comput.*, 2009, **5**, 962-975.
118. G. Pampaloni, R. Peloso, D. Belletti, C. Graiff and A. Tiripicchio, *Organometallics*, 2007, **26**, 4278-4286.
119. S. G. Ridlen, N. V. Kulkarni and H. V. R. Dias, *Inorg. Chem.*, 2017, **56**, 7237-7246.
120. H. V. R. Dias and S. Singh, *Inorg. Chem.*, 2004, **43**, 5786-5788.
121. D. Parasar, N. B. Jayaratna, A. Muñoz-Castro, A. E. Conway, P. K. Mykhailiuk and H. V. R. Dias, *Dalton Transactions*, 2019, **48**, 6358-6371.

`

122. K. Huse, H. Weinert, C. Wölper and S. Schulz, *Dalton Transactions*, 2020, **49**, 9773-9780.

123. R. A. Peralta, M. T. Huxley, J. Albalad, C. J. Sumby and C. J. Doonan, *Inorg. Chem.*, 2021, DOI: 10.1021/acs.inorgchem.1c00849, in press; DOI: 10.1021/acs.inorgchem.1021c00849.

124. M. M. Diaz-Requejo, A. Caballero, T. R. Belderrain, M. C. Nicasio, S. Trofimenko and P. J. Perez, *Journal of the American Chemical Society*, 2002, **124**, 978-983.

125. P. K. Mykhailiuk, S. Afonin, A. S. Ulrich and I. V. Komarov, *Synthesis*, 2008, **2008**, 1757-1760.

126. M. P. Doyle, V. Bagheri, T. J. Wandless, N. K. Harn, D. A. Brinker, C. T. Eagle and K. L. Loh, *Journal of the American Chemical Society*, 1990, **112**, 1906-1912.

127. A. Noonikara-Poyil, A. Muñoz-Castro and H. V. R. Dias, *Molecules*, 2021, **27**, 16.

128. C. W. Tornøe, C. Christensen and M. Meldal, *J. Org. Chem.*, 2002, **67**, 3057-3064.

129. V. V. Rostovtsev, L. G. Green, V. V. Fokin and K. B. Sharpless, *Angewandte Chemie, International Edition*, 2002, **41**, 2596-2599.

130. F. Amblard, J. H. Cho and R. F. Schinazi, *Chemical Reviews (Washington, DC, United States)*, 2009, **109**, 4207-4220.

131. J. S. S. Neto and G. Zeni, *Coordination Chemistry Reviews*, 2020, **409**, 213217pp.

132. P. Leophairatana, S. Samanta, C. C. De Silva and J. T. Koberstein, *Journal of the American Chemical Society*, 2017, **139**, 3756-3766.

133. L. Chen, D. Leslie, M. G. Coleman and J. Mack, *Chemical Science*, 2018, **9**, 4650-4661.

134. P. Li, X. Zhang and M. Shi, *Chemical Communications (Cambridge, United Kingdom)*, 2020, **56**, 5457-5471.

135. L. R. Redfern, W.-S. Lo, I. J. Dillingham, J. G. Eatman, M. R. Mian, C.-K. Tsung and O. K. Farha, *ACS Applied Materials & Interfaces*, 2020, **12**, 31496-31502.

`

136. F. Alonso, I. P. Beletskaya and M. Yus, *Chemical Reviews (Washington, DC, United States)*, 2004, **104**, 3079-3159.

137. T. Fujihara, T. Xu, K. Semba, J. Terao and Y. Tsuji, *Angewandte Chemie, International Edition*, 2011, **50**, 523-527.

138. C. Zhao, X. Zhang, Z. He, Q. Guan and W. Li, *Inorganic Chemistry Frontiers*, 2020, **7**, 3204-3216.

139. A. Dondoni and A. Marra, *European Journal of Organic Chemistry*, 2014, **2014**, 3955-3969.

140. A. Grirrane, E. Alvarez, H. Garcia and A. Corma, *Chemistry - A European Journal*, 2020, **26**, 8810-8818.

141. P. Siemsen, R. C. Livingston and F. Diederich, *Angewandte Chemie, International Edition*, 2000, **39**, 2632-2657.

142. N. Chernyak and V. Gevorgyan, *Angewandte Chemie, International Edition*, 2010, **49**, 2743-2746, S2743/2741-S2743/2738.

143. L. Su, J. Dong, L. Liu, M. Sun, R. Qiu, Y. Zhou and S.-F. Yin, *Journal of the American Chemical Society*, 2016, **138**, 12348-12351.

144. X.-Y. Dong, Y.-F. Zhang, C.-L. Ma, Q.-S. Gu, F.-L. Wang, Z.-L. Li, S.-P. Jiang and X.-Y. Liu, *Nature Chemistry*, 2019, **11**, 1158-1166.

145. T. Hamada, X. Ye and S. S. Stahl, *Journal of the American Chemical Society*, 2008, **130**, 833-835.

146. A. S. Hay, *J. Org. Chem.*, 1962, **27**, 3320-3321.

147. D. Yu and Y. Zhang, *P. Nat. Acad. Sci. USA*, 2010, **107**, 20184-20189.

148. F. Manjolinho, M. Arndt, K. Goossen and L. J. Goossen, *ACS Catalysis*, 2012, **2**, 2014-2021.

149. T. Tachiyama, M. Yoshida, T. Aoyagi and S. Fukuzumi, *Applied Organometallic Chemistry*, 2008, **22**, 205-210.

150. A. Bakhoda, O. E. Okoromoba, C. Greene, M. R. Boroujeni, J. A. Bertke and T. H. Warren, *Journal of the American Chemical Society*, 2020, **142**, 18483-18490.

151. C. Deraedt, N. Pinaud and D. Astruc, *Journal of the American Chemical Society*, 2014, **136**, 12092-12098.

`

152. Y. Fang, K. Bao, P. Zhang, H. Sheng, Y. Yun, S.-X. Hu, D. Astruc and M. Zhu, *Journal of the American Chemical Society*, 2021, **143**, 1768-1772.

153. P. Thirumurugan, D. Matosiuk and K. Jozwiak, *Chemical Reviews (Washington, DC, United States)*, 2013, **113**, 4905-4979.

154. J. Chen, K. Li, S. E. Bonson and S. C. Zimmerman, *Journal of the American Chemical Society*, 2020, **142**, 13966-13973.

155. S. Neumann, M. Biewend, S. Rana and W. H. Binder, *Macromol. Rapid Commun.*, 2020, **41**, 1900359.

156. A. K. Agrahari, P. Bose, M. K. Jaiswal, S. Rajkhowa, A. S. Singh, S. Hotha, N. Mishra and V. K. Tiwari, *Chemical Reviews (Washington, DC, United States)*, 2021, **121**, 7638-7956.

157. S. Liu, X. Han, Y. Chai, G. Wu, W. Li, J. Li, I. da Silva, P. Manuel, Y. Cheng, L. L. Daemen, A. J. Ramirez-Cuesta, W. Shi, N. Guan, S. Yang and L. Li, *Angewandte Chemie, International Edition*, 2021, DOI: 10.1002/anie.202014680, Ahead of Print.

158. S. Chen, N. Behera, C. Yang, Q. Dong, B. Zheng, Y. Li, Q. Tang, Z. Wang, Y. Wang and J. Duan, *Nano Research*, 2020, DOI: 10.1007/s12274-020-2935-1, Ahead of Print.

159. Y. He, Z. Zhang, S. Xiang, H. Wu, F. R. Fronczek, W. Zhou, R. Krishna, M. O'Keeffe and B. Chen, *Chemistry - A European Journal*, 2012, **18**, 1901-1904, S1901/1901-S1901/1925.

160. Y. Hu, S. Xiang, W. Zhang, Z. Zhang, L. Wang, J. Bai and B. Chen, *Chem. Commun. (Cambridge, U. K.)*, 2009, DOI: 10.1039/b917046d, 7551-7553.

161. J.-W. Zhang, M.-C. Hu, S.-N. Li, Y.-C. Jiang, P. Qu and Q.-G. Zhai, *Chem. Commun. (Cambridge, U. K.)*, 2018, **54**, 2012-2015.

162. H. Lang, A. Jakob and B. Milde, *Organometallics*, 2012, **31**, 7661-7693.

163. P. J. Perez and M. M. Dias-Requejo, *Copper Organometallics, in Comprehensive Organometallic Chemistry III*, Elsevier, Amsterdam, 2007.

164. K. Koehler, J. Eichhorn, F. Meyer and D. Vidovic, *Organometallics*, 2003, **22**, 4426-4432.

`

165. P. Doppelt and T. H. Baum, *Journal of Organometallic Chemistry*, 1996, **517**, 53-62.

166. H. V. R. Dias, S. A. Polach and Z. Wang, *J. Fluorine Chem.*, 2000, **103**, 163-169.

167. D. Parasar, T. T. Ponduru, A. Noonikara-Poyil, N. B. Jayaratna and H. V. R. Dias, *Dalton Transactions*, 2019, **48**, 15782-15794.

168. D. Parasar, R. M. Almotawa, N. B. Jayaratna, Y. S. Ceylan, T. R. Cundari, M. A. Omary and H. V. R. Dias, *Organometallics*, 2018, **37**, 4105-4118.

169. H. Lang, K. Koehler and S. Blau, *Coordination Chemistry Reviews*, 1995, **143**, 113-168.

170. L. Liang and D. Astruc, *Coordination Chemistry Reviews*, 2011, **255**, 2933-2945.

171. H. Bauer, J. Faust, F. Rolf, F. Johannes, U. Krüerke, M. Kunz and H. M. Somer, eds., *Cu Organocopper Compounds: Compounds with Ligands Bonded by Two C. Atoms*, Springer, Berlin, Heidelberg, 1987.

172. F. H. Jardine, in *Adv. Inorg. Chem. Radiochem.*, eds. H. J. Emeléus and A. G. Sharpe, Academic Press, 1975, vol. 17, pp. 115-163.

173. J. S. Thompson and J. F. Whitney, *Inorganic Chemistry*, 1984, **23**, 2813-2819.

174. M. Munakata, S. Kitagawa, I. Kawada, M. Maekawa and H. Shimono, *Journal of the Chemical Society, Dalton Transactions*, 1992, DOI: 10.1039/dt9920002225, 2225.

175. B. M. Mykhalichko, M. G. Mys'kiv and V. N. Davydov, *Zhurnal Neorganicheskoi Khimii*, 1999, **44**, 411-414.

176. B. M. Mykhalichko, M. G. Mys'kiv and L. G. Aksel'rud, *Koordinatsionnaya Khimiya*, 1993, **19**, 722-726.

177. S. I. Osechkin, M. G. Mys'kiv, P. Y. Zavalii and A. N. Sobolev, *Metalloorganicheskaya Khimiya*, 1991, **4**, 997-1003.

178. M. R. Hyman and D. J. Arp, *Appl Environ Microbiol*, 1987, **53**, 298-303.

179. I.-T. Trotuş, T. Zimmermann and F. Schüth, *Chemical Reviews (Washington, DC, United States)*, 2014, **114**, 1761-1782.

`

180. ACS, Spectroscopy Resources, ACS Division of Organic Chemistry, https://organicchemistrydata.org/links/#spectroscopy_resources, 2021).
181. H. Fast and H. L. Welsh, *Journal of Molecular Spectroscopy*, 1972, **41**, 203-221.
182. N. L. Wieder, P. J. Carroll and D. H. Berry, *Organometallics*, 2011, **30**, 2125-2136.
183. E. Bustelo, J. J. Carbó, A. Lledós, K. Mereiter, M. C. Puerta and P. Valerga, *Journal of the American Chemical Society*, 2003, **125**, 3311-3321.
184. K. R. Pörschke, Y.-H. Tsay and C. Krüger, *Angew. Chem. Int. Ed.*, 1985, **24**, 323-324.
185. R. K. McMullan, Å. Kvick and P. Popelier, *Acta Crystallogr. Sect. B*, 1992, **48**, 726-731.
186. J. S. Thompson and J. F. Whitney, *Journal of the American Chemical Society*, 2002, **105**, 5488-5490.
187. T. A. Albright, R. Hoffmann, J. C. Thibeault and D. L. Thorn, *Journal of the American Chemical Society*, 1979, **101**, 3801-3812.
188. F. H. Allen, O. Kennard, D. G. Watson, L. Brammer, A. G. Orpen and R. Taylor, *J. Chem. Soc., Perkin Trans. 2*, 1987, DOI: 10.1039/P298700000S1, S1-S19.
189. H. Yasuda, H. Yamamoto, T. Arai, A. Nakamura, J. Chen, Y. Kai and N. Kasai, *Organometallics*, 1991, **10**, 4058-4066.
190. A. F. Hill, N. Tshabang and A. C. Willis, *European Journal of Inorganic Chemistry*, 2007, DOI: 10.1002/ejic.200700471, 3781-3785.
191. J. L. Kiplinger, A. M. Arif and T. G. Richmond, *Organometallics*, 1997, **16**, 246-254.
192. A. A. Titov, V. A. Larionov, A. F. Smolyakov, M. I. Godovikova, E. M. Titova, V. I. Maleev and E. S. Shubina, *Chemical Communications (Cambridge, United Kingdom)*, 2019, **55**, 290-293.
193. R. Huisgen, G. Szeimies and L. Moebius, *Chemische Berichte*, 1967, **100**, 2494-2507.
194. T.-H. Wang, F.-L. Wu, G.-R. Chiang, S.-T. He and Y.-H. Lo, *Journal of Organometallic Chemistry*, 2014, **774**, 57-60.

`

195. J. M. Munoz-Molina, T. R. Belderrain and P. J. Perez, *Coordination Chemistry Reviews*, 2019, **390**, 171-189.

196. I. Cano, M. C. Nicasio and P. J. Perez, *Organic & Biomolecular Chemistry*, 2010, **8**, 536-538.

197. L. Bahsis, H. Ben El Ayouchia, H. Anane, C. Ramirez de Arellano, A. Bentama, E. M. El Hadrami, M. Julve, L. R. Domingo and S.-E. Stiriba, *Catalysts*, 2019, **9**, 687pp.

198. V. A. Larionov, A. R. Stashneva, A. A. Titov, A. A. Lisov, M. G. Medvedev, A. F. Smol'yakov, A. M. Tsedilin, E. S. Shubina and V. I. Maleev, *Journal of Catalysis*, 2020, **390**, 37-45.

199. M. Patterson and H. V. R. Dias, *Dalton Transactions*, 2021, DOI: 10.1039/D1DT04026J, DOI: 10.1039/D1031DT04026J.

200. V. V. Voronin, M. S. Ledovskaya, A. S. Bogachenkov, K. S. Rodygin and V. P. Ananikov, *Molecules*, 2018, **23**, 2442.

201. H. Schobert, *Chemical Reviews*, 2013, **114**, 1743-1760.

202. K. S. Rodygin, G. Werner, F. A. Kucherov and V. P. Ananikov, *Chemistry - An Asian Journal*, 2016, **11**, 965-976.

203. R. Buschbeck, P. J. Low and H. Lang, *Coordination Chemistry Reviews*, 2011, **255**, 241-272.

204. P. Johnston, N. Carthey and G. J. Hutchings, *Journal of the American Chemical Society*, 2015, **137**, 14548-14557.

205. L. Zhang, M. Zhou, A. Wang and T. Zhang, *Chemical Reviews*, 2019, **120**, 683-733.

206. G. X. Pei, X. Y. Liu, A. Wang, A. F. Lee, M. A. Isaacs, L. Li, X. Pan, X. Yang, X. Wang, Z. Tai, K. Wilson and T. Zhang, *ACS Catalysis*, 2015, **5**, 3717-3725.

207. M. R. Ball, K. R. Rivera-Dones, E. B. Gilcher, S. F. Ausman, C. W. Hullfish, E. A. Lebrón and J. A. Dumesic, *ACS Catalysis*, 2020, **10**, 8567-8581.

208. X.-T. Li, L. Chen, C. Shang and Z.-P. Liu, *Journal of the American Chemical Society*, 2021, **143**, 6281-6292.

209. J. Bu, Z. Liu, W. Ma, L. Zhang, T. Wang, H. Zhang, Q. Zhang, X. Feng and J. Zhang, *Nature Catalysis*, 2021, **4**, 557-564.

`

210. X. Shi, Y. Lin, L. Huang, Z. Sun, Y. Yang, X. Zhou, E. Vovk, X. Liu, X. Huang, M. Sun, S. Wei and J. Lu, *ACS Catalysis*, 2020, **10**, 3495-3504.

211. A. Sárkány and Z. Révay, *Applied Catalysis A: General*, 2003, **243**, 347-355.

212. L. Zhang, Z. Chen, Z. Liu, J. Bu, W. Ma, C. Yan, R. Bai, J. Lin, Q. Zhang, J. Liu, T. Wang and J. Zhang, *Nature Communications*, 2021, **12**.

213. T. G. Back and K. R. Muralidharan, *The Journal of Organic Chemistry*, 2002, **56**, 2781-2787.

214. H. Díaz Velázquez, Z.-X. Wu, M. Vandichel and F. Verpoort, *Catalysis Letters*, 2017, **147**, 463-471.

215. A. S. M. Iftekhar Uddin, D.-T. Phan and G.-S. Chung, *Sensors and Actuators B: Chemical*, 2015, **207**, 362-369.

216. L. Zhang, K. Jiang, L. Yang, L. Li, E. Hu, L. Yang, K. Shao, H. Xing, Y. Cui, Y. Yang, B. Li, B. Chen and G. Qian, *Angewandte Chemie International Edition*, 2021, **60**, 15995-16002.

217. O. Daugulis, J. Roane and L. D. Tran, *Accounts of Chemical Research*, 2015, **48**, 1053-1064.

218. T. C. Merkel, R. Blanc, I. Ciobanu, B. Firat, A. Suwarlim and J. Zeid, *Journal of Membrane Science*, 2013, **447**, 177-189.

219. A. Roy, S. R. Venna, G. Rogers, L. Tang, T. C. Fitzgibbons, J. Liu, H. McCurry, D. J. Vickery, D. Flick and B. Fish, *Proceedings of the National Academy of Sciences*, 2021, **118**.

220. D. J. Safarik and R. B. Eldridge, *Industrial & Engineering Chemistry Research*, 1998, **37**, 2571-2581.

221. O. Makowka, *Berichte der deutschen chemischen Gesellschaft*, 2006, **41**, 824-829.

222. J. A. Mathews and L. L. Watters, *Journal of the American Chemical Society*, 2002, **22**, 108-111.

223. F. H. Allen, *Acta Crystallographica Section B Structural Science*, 2002, **58**, 380-388.

`

224. A. Reisinger, N. Trapp, I. Krossing, S. Altmannshofer, V. Herz, M. Presnitz and W. Scherer, *Angewandte Chemie International Edition*, 2007, **46**, 8295-8298.

225. A. D. Brathwaite, T. B. Ward, J. H. Marks and M. A. Duncan, *The Journal of Physical Chemistry A*, 2020, **124**, 8562-8573.

226. A. D. Brathwaite, T. B. Ward, R. S. Walters and M. A. Duncan, *The Journal of Physical Chemistry A*, 2015, **119**, 5658-5667.

227. S. L. Stephens, D. M. Bittner, V. A. Mikhailov, W. Mizukami, D. P. Tew, N. R. Walker and A. C. Legon, *Inorganic Chemistry*, 2014, **53**, 10722-10730.

228. S. L. Stephens, W. Mizukami, D. P. Tew, N. R. Walker and A. C. Legon, *The Journal of Chemical Physics*, 2012, **137**, 174302.

229. J. Mehara, B. T. Watson, A. Noonikara-Poyil, A. O. Zacharias, J. Roithová and H. V. Rasika Dias, *Chemistry – A European Journal*, 2022, **28**.

230. M. Vanga, A. Muñoz-Castro and H. V. R. Dias, *Dalton Transactions*, 2022, **51**, 1308-1312.

231. *Proceedings of the Chemical Society*, 1961, DOI: 10.1039/ps9610000273, 273.

232. J. Liévin, J. Demaison, M. Herman, A. Fayt and C. Puzzarini, *The Journal of Chemical Physics*, 2011, **134**, 064119.

233. N. C. Craig, P. Groner and D. C. McKean, *The Journal of Physical Chemistry A*, 2006, **110**, 7461-7469.

234. G. J. H. van Nes and F. van Bolhuis, *Acta Crystallographica Section B Structural Crystallography and Crystal Chemistry*, 1979, **35**, 2580-2593.

235. S. Alvarez, *Dalton Transactions*, 2013, **42**, 8617.

236. A. Bondi, *The Journal of Physical Chemistry*, 2002, **68**, 441-451.

237. B. Cordero, V. Gómez, A. E. Platero-Prats, M. Revés, J. Echeverría, E. Cremades, F. Barragán and S. Alvarez, *Dalton Transactions*, 2008, DOI: 10.1039/b801115j, 2832.

`

238. M. A. Omary, M. A. Rawashdeh-Omary, M. W. A. Gonser, O. Elbjeirami, T. Grimes, T. R. Cundari, H. V. K. Diyabalanage, C. S. P. Gamage and H. V. R. Dias, *Inorganic Chemistry*, 2005, **44**, 8200-8210.
239. S. G. Ridlen, J. Wu, N. V. Kulkarni and H. V. R. Dias, *European Journal of Inorganic Chemistry*, 2016, **2016**, 2573-2580.
240. A. Reisinger, N. Trapp, C. Knapp, D. Himmel, F. Breher, H. RÃ¼egger and I. Krossing, *Chemistry - A European Journal*, 2009, **15**, 9505-9520.
241. E. R. Johnson, S. Keinan, P. Mori-Sánchez, J. Contreras-García, A. J. Cohen and W. Yang, *Journal of the American Chemical Society*, 2010, **132**, 6498-6506.
242. E. D. Glendening, C. R. Landis and F. Weinhold, *Journal of Computational Chemistry*, 2013, **34**, 1429-1437.
243. F. L. Carter and V. L. Frampton, *Chemical Reviews*, 1964, **64**, 497-525.
244. M. Rubin, M. Rubina and V. Gevorgyan, *Chemical Reviews (Washington, DC, United States)*, 2007, **107**, 3117-3179.
245. R. Vicente, *Chemical Reviews (Washington, DC, United States)*, 2020, **1**, 162-226.
246. Z.-B. Zhu, Y. Wei and M. Shi, *Chemical Society Reviews*, 2011, **40**, 5534-5563.
247. M. M. Meloni, S. Barton, J. C. Kaski, W. Song and T. He, *Journal of Applied Biomaterials & Functional Materials*, 2019, **17**, 1-6.
248. U. P. N. Tran, R. Hommelsheim, Z. Yang, C. Empel, K. J. Hock, T. V. Nguyen and R. M. Koenigs, *Chemistry*, 2020, **26**, 1254-1257.
249. E. C. Sisler and M. Serek, *Physiologia Plantarum*, 1997, **100**, 577-582.
250. S. M. Blankenship and J. M. Dole, *Postharvest Biology and Technology*, 2003, **28**, 1-25.
251. R. D. Row and J. A. Prescher, *Accounts of Chemical Research*, 2018, **51**, 1073-1081.
252. J. Salaun and M. S. Baird, *Current Medicinal Chemistry*, 1995, **2**, 511-542.
253. R. D. Bach and O. Dmitrenko, *Journal of the American Chemical Society*, 2004, **126**, 4444-4452.

`

254. J. M. J. M. Ravasco, C. M. Monteiro and A. F. Trindade, *Organic Chemistry Frontiers*, 2017, **4**, 1167-1198.

255. J. Yang, J. Seckute, C. M. Cole and N. K. Devaraj, *Angewandte Chemie, International Edition*, 2012, **51**, 7476-7479.

256. Y. Lou, M. Horikawa, R. A. Kloster, N. A. Hawryluk and E. J. Corey, *Journal of the American Chemical Society*, 2004, **126**, 8916-8918.

257. J. F. Briones, J. Hansen, K. I. Hardcastle, J. Autschbach and H. M. L. Davies, *Journal of the American Chemical Society*, 2010, **132**, 17211-17215.

258. A. DeAngelis, R. Panish and J. M. Fox, *Accounts of Chemical Research*, 2016, **49**, 115-127.

259. P. J. Perez, M. Brookhart and J. L. Templeton, *Organometallics*, 1993, **12**, 261-262.

260. H. Martinez-Garcia, D. Morales, J. Perez, M. Puerto and D. Miguel, *Inorg. Chem.*, 2010, **49**, 6974-6985.

261. A. K. Swenson, K. E. Higgins, M. G. Brewer, W. W. Brennessel and M. G. Coleman, *Organic & Biomolecular Chemistry*, 2012, **10**, 7483-7486.

262. T. J. Thomas, B. A. Merritt, B. E. Lemma, A. M. McKoy, T. Nguyen, A. K. Swenson, J. L. Mills and M. G. Coleman, *Organic & Biomolecular Chemistry*, 2016, **14**, 1742-1747.

263. X. Cui, X. Xu, H. Lu, S. Zhu, L. Wojtas and X. P. Zhang, *Journal of the American Chemical Society*, 2011, **133**, 3304-3307.

264. M. J. Gonzalez, L. A. Lopez and R. Vicente, *Organic Letters*, 2014, **16**, 5780-5783.

265. M. Uehara, H. Suematsu, Y. Yasutomi and T. Katsuki, *Journal of the American Chemical Society*, 2011, **133**, 170-171.

266. J. F. Briones and H. M. L. Davies, *Journal of the American Chemical Society*, 2012, **134**, 11916-11919.

267. K. Chen and F. H. Arnold, *Journal of the American Chemical Society*, 2020, **142**, 6891-6895.

268. M. Rubin, M. Rubina and V. Gevorgyan, *Synthesis*, 2006, DOI: 10.1055/s-2006-926404, 1221-1245.

`

269. C. Martin, M. Sierra, E. Alvarez, T. R. Belderrain and P. J. Perez, *Dalton Transactions*, 2012, **41**, 5319-5325.

270. S. Ma and J. Zhang, *Journal of the American Chemical Society*, 2003, **125**, 12386-12387.

271. V. Gettwert, F. Krebs and G. Maas, *European Journal of Organic Chemistry*, 1999, DOI: 10.1002/(sici)1099-0690(199905)1999:5<1213::Aid-ejoc1213>3.0.Co;2-u, 1213-1221.

272. Y. V. Tomilov, E. A. Shapiro, M. N. Protopopova, A. I. Ioffe, I. E. Dolgii and O. M. Nefedov, *Izvestiya Akademii Nauk SSSR, Seriya Khimicheskaya*, 1985, 631-639.

273. J. Chen and S. Ma, *Chemistry - An Asian Journal*, 2010, **5**, 2415-2421.

274. D. S. Müller and I. Marek, *Chemical Society Reviews*, 2016, **45**, 4552-4566.

275. M. C. Pirrung, A. B. Bleecker, Y. Inoue, F. I. Rodriguez, N. Sugawara, T. Wada, Y. Zou and B. M. Binder, *Chemistry & Biology (Cambridge, MA, United States)*, 2008, **15**, 313-321.

276. R. P. Hughes, J. W. Reisch and A. L. Rheingold, *Organometallics*, 1985, **4**, 241-244.

277. C. Boulho, P. Oulie, L. Vendier, M. Etienne, V. Pimienta, A. Locati, F. Bessac, F. Maseras, A. Pantazis Dimitrios and E. McGrady John, *J Am Chem Soc*, 2010, **132**, 14239-14250.

278. L. K. Johnson, R. H. Grubbs and J. W. Ziller, *Journal of the American Chemical Society*, 1993, **115**, 8130-8145.

279. M. S. Baird, K. Spencer, S. V. Krasnoshchiokov, Y. N. Panchenko, N. F. Stepanov and G. R. De Maré, *J. Phys. Chem. A*, 1998, **102**, 2363-2371.

280. J. J. De Boer and D. Bright, *Journal of the Chemical Society, Dalton Transactions: Inorganic Chemistry (1972-1999)*, 1975, 662-665.

281. M. W. Day, T. E. Wilhelm and R. H. Grubbs, *Acta Crystallographica, Section C: Crystal Structure Communications*, 1996, **C52**, 2460-2462.

282. G. R. Clark, L. G. Raymond, W. R. Roper, D. M. Tonei and L. J. Wright, *Inorganica Chimica Acta*, 2006, **359**, 3763-3768.

`

283. H.-P. Wu, T. J. R. Weakley and M. M. Haley, *Organometallics*, 2002, **21**, 4320-4322.

284. H.-P. Wu, D. H. Ess, S. Lanza, T. J. R. Weakley, K. N. Houk, K. K. Baldridge and M. M. Haley, *Organometallics*, 2007, **26**, 3957-3968.

285. H. Weiss, F. Hampel, W. Donaubauer, M. A. Grundl, J. W. Bats, A. S. K. Hashmi and S. Schindler, *Organometallics*, 2001, **20**, 1713-1715.

286. H. Schwager, C. Krüger, R. Neidlein and G. Wilke, *Angewandte Chemie*, 1987, **99**, 72-73.

287. R. T. Li, S. T. Nguyen, R. H. Grubbs and J. W. Ziller, *Journal of the American Chemical Society*, 1994, **116**, 10032-10040.

288. D. L. Hughes, G. J. Leigh and C. N. McMahon, *Journal of the Chemical Society, Dalton Transactions: Inorganic Chemistry (1972-1999)*, 1997, 1301-1307.

289. R. D. Gilbertson, T. J. R. Weakley and M. M. Haley, *Chemistry - A European Journal*, 2000, **6**, 437-441.

290. R. D. Gilbertson, T. L. S. Lau, S. Lanza, H.-P. Wu, T. J. R. Weakley and M. M. Haley, *Organometallics*, 2003, **22**, 3279-3289.

291. G. Maier, M. Hoppe, H. P. Reisenauer and C. Krüger, *Angew. Chem., Int. Ed. Engl.*, 1982, **21**, 437-437.

292. J. Thomas, J. John, N. Parekh and W. Dehaen, *Angew. Chem.*, 2014, **126**, 10319-10323.

293. S. Hyde, J. Veliks, B. Liégault, D. Grassi, M. Taillefer and V. Gouverneur, *Angewandte Chemie International Edition*, 2016, **55**, 3785-3789.

294. S. P. Green, K. M. Wheelhouse, A. D. Payne, J. P. Hallett, P. W. Miller and J. A. Bull, *Organic Process Research & Development*, 2019, **24**, 67-84.

295. L. Krause, R. Herbst-Irmer, G. M. Sheldrick and D. Stalke, *Journal of Applied Crystallography*, 2015, **48**, 3-10.

296. G. M. Sheldrick, *Acta Crystallographica Section A Foundations and Advances*, 2015, **71**, 3-8.

297. G. M. Sheldrick, *Acta Crystallographica Section C Structural Chemistry*, 2015, **71**, 3-8.

`

298. O. V. Dolomanov, L. J. Bourhis, R. J. Gildea, J. A. K. Howard and H. Puschmann, *Journal of Applied Crystallography*, 2009, **42**, 339-341.
299. P. J. Chupas, K. W. Chapman, C. Kurtz, J. C. Hanson, P. L. Lee and C. P. Grey, *Journal of Applied Crystallography*, 2008, **41**, 822-824.
300. B. H. Toby and R. B. Von Dreele, *Journal of Applied Crystallography*, 2013, **46**, 544-549.
301. A. P. Hammersley, S. O. Svensson, M. Hanfland, A. N. Fitch and D. Hausermann, *High Pressure Research*, 1996, **14**, 235-248.
302. C. W. Tullock, D. D. Coffman and E. L. Muetterties, *Journal of the American Chemical Society*, 1964, **86**, 357-361.
303. S. Grimme, *WIREs Computational Molecular Science*, 2011, **1**, 211-228.
304. L. Versluis and T. Ziegler, *The Journal of Chemical Physics*, 1988, **88**, 322-328.
305. E. van Lenthe, E. J. Baerends and J. G. Snijders, *The Journal of Chemical Physics*, 1994, **101**, 9783-9792.
306. M. v. Hopffgarten and G. Frenking, *WIREs Computational Molecular Science*, 2011, **2**, 43-62.
307. T. Ziegler and A. Rauk, *Theoretica Chimica Acta*, 1977, **46**, 1-10.
308. M. P. Mitoraj, A. Michalak and T. Ziegler, *Journal of Chemical Theory and Computation*, 2009, **5**, 962-975.
309. G. A. Chesnokov, M. A. Topchiy, P. B. Dzhevakov, P. S. Gribanov, A. A. Tukov, V. N. Khrustalev, A. F. Asachenko and M. S. Nechaev, *Dalton Transactions*, 2017, **46**, 4331-4345.
310. J. T. Fletcher, J. M. Sobczyk, S. C. Gwazdacz and A. J. Blanck, *Bioorganic & Medicinal Chemistry Letters*, 2018, **28**, 3320-3323.
311. F. Kloss, U. Köhn, B. O. Jahn, M. D. Hager, H. Görls and U. S. Schubert, *Chemistry - An Asian Journal*, 2011, **6**, 2816-2824.
312. S. Grimme, *Journal of Computational Chemistry*, 2004, **25**, 1463-1473.
313. S. Grimme, *Journal of Computational Chemistry*, 2006, **27**, 1787-1799.
314. S. Grimme, J. Antony, S. Ehrlich and H. Krieg, *The Journal of Chemical Physics*, 2010, **132**, 154104.

`

315. E. R. Johnson and A. D. Becke, *The Journal of Chemical Physics*, 2005, **123**, 024101.

316. S. Grimme, S. Ehrlich and L. Goerigk, *Journal of Computational Chemistry*, 2011, **32**, 1456-1465.

317. R. Ahlrichs, M. Bär, M. Häser, H. Horn and C. Kölmel, *Chemical Physics Letters*, 1989, **162**, 165-169.

318. J. P. Perdew, *Physical Review B*, 1986, **33**, 8822-8824.

319. F. Weigend and R. Ahlrichs, *Physical Chemistry Chemical Physics*, 2005, **7**, 3297.

320. K. Eichkorn, O. Treutler, H. Öhm, M. Häser and R. Ahlrichs, *Chemical Physics Letters*, 1995, **242**, 652-660.

321. G. te Velde, F. M. Bickelhaupt, E. J. Baerends, C. Fonseca Guerra, S. J. A. van Gisbergen, J. G. Snijders and T. Ziegler, *Journal of Computational Chemistry*, 2001, **22**, 931-967.

322. J. G. Snijders, P. Vernooijs and E. J. Baerends, *Atomic Data and Nuclear Data Tables*, 1981, **26**, 483-509.

323. E. v. Lenthe, E. J. Baerends and J. G. Snijders, *The Journal of Chemical Physics*, 1993, **99**, 4597-4610.

324. E. van Lenthe, A. Ehlers and E.-J. Baerends, *The Journal of Chemical Physics*, 1999, **110**, 8943-8953.

325. H. G. Richey and R. M. Bension, *The Journal of Organic Chemistry*, 2002, **45**, 5036-5042.

326. C. Li, Y. Zeng, H. Zhang, J. Feng, Y. Zhang and J. Wang, *Angewandte Chemie International Edition*, 2010, **49**, 6413-6417.

327. A. G. Dalling, T. Yamauchi, N. G. McCreanor, L. Cox and J. F. Bower, *Angewandte Chemie International Edition*, 2019, **58**, 221-225.

328. M. A. Drew, S. Arndt, C. Richardson, M. Rudolph, A. S. K. Hashmi and C. J. T. Hyland, *Chemical Communications*, 2019, **55**, 13971-13974.

`

Biographical Information

Anurag Noonikara Poyil was born in Calicut, Kerala, India. He completed his high school education at Government Vocational Higher Secondary School, Atholi, Calicut. After high school, he attended the Indian Institute of Science Education and Research (IISER) Kolkata where he received both Bachelor of Science and Master of Science (Integrated BS-MS) in Chemical Sciences in 2015. He joined the Ph.D. graduate program in Chemistry at the University of Texas at Arlington in Fall 2016.